UNIVERSITY OF CALIFORNIA
RIVERSIDE

Identification of Novel Mechanisms that Regulate the Activities of ARGONAUTE1 in *Arabidopsis thaliana*

A Dissertation submitted in partial satisfaction
of the requirements for the degree of

Doctor of Philosophy

in

Plant Pathology

by

Ye Xu

March 2022

Dissertation Committee:
Dr. Xuemei Chen, Chairperson
Dr. Katayoon Dehesh
Dr. Shou-wei Ding
Dr. Meng Chen

The Dissertation of Ye Xu is approved:

Committee Chairperson

University of California, Riverside

Acknowledgements

First and foremost, I would like to express my heartfelt gratitude to my advisor Dr. Xuemei Chen for allowing me to join her lab and participate in the field of small RNA research. I appreciate her guidance, patience, and continuous encouragement that drive me to keep thinking, exploring, and having an open mind throughout this endeavor. Without her immense support, this dissertation would not be possible.

I would also like to extend my gratitude to my guidance committee members Drs. Katayoon Dehesh, Meng Chen, Shou-wei Ding, and the former committee member Dr. Wenbo Ma for their time, advice, inspiration, and critical inputs on my dissertation work, and for generously sharing lab material and equipment with me. I also thank Dr. Philip Roberts who was on my qualifying examination committee and who is a wonderful teacher in nematology.

Furthermore, I would like to thank all of the past and present members of the Chen lab whose time overlapped with mine. I appreciate all the discussions that helped shape my research. I want to acknowledge Drs. Yong Zhang, Yuan Wang, Brandon Le, Yu Yu, Wenrong He, Lusheng Fan, and Yonghui Zhao for being fantastic lab mates as well as good friends, whose support and companionship in the lab and friendship outside the lab brought me joy and warmth and helped me overcome stressful times during this journey. I would especially like to thank Drs. Chenjiang You and Brandon Le for being willing to sit

down and discuss with me, on countless occasions, the details of bioinformatics analysis.

I am also grateful to the people who contributed to my dissertation projects and other collaborative projects. Drs. Yong Zhang and Haiyan Zheng contributed to the proteomic analysis; Dr. Hiro-oki Iwakawa performed the *in vitro* RISC assembly assay; Dr. Lusheng Fan generated the *35S::MIR165A* construct; Dr. Zhenfang Li, Alyssa Soloria, and Savannah Potter assisted in transgenic line characterization; Dr. Yingnan Hou contributed to bacterial infection assays not shown in the dissertation. I also thank Dr. Wenwei Lin for his advice on protein phosphorylation studies and Dr. Jingzhe Guo for helping me with mitochondria staining assays.

I am thankful to all my friends for their company and support that make this journey more colorful.

And last but not least, my gratitude goes to my family. I would like to thank my parents, Ping Li and Jianhua Xu, and my grandparents, Shuhan Li and Fushan Li, for their unconditional love and continued support throughout my entire life. This dissertation would not have been possible without them.

Author Contributions

Chapter 1 Introduction: biogenesis, mode of action, and degradation of plant microRNAs

Ye Xu wrote the chapter and prepared figures. Xuemei Chen provided conceptual guidance and edited the chapter.

Chapter 2 The N-terminal extension of Arabidopsis ARGONAUTE 1 is essential for microRNA activities

Ye Xu constructed sequencing libraries and analyzed sequencing data, performed RNA gel blot analyses, conducted structure prediction and sequence alignments of AGOs; Ye Xu, Zhenfang Li, Alyssa Soloria, and Savannah Potter generated and characterized the transgenic lines; Ye Xu and Xuemei Chen analyzed data; Ye Xu prepared the figures and tables. Ye Xu wrote the chapter and Xuemei Chen edited it.

Chapter 3 Phosphorylation regulates the activities of the microRNA and small interfering RNA effector ARGONAUTE1 in Arabidopsis

Ye Xu generated and characterized the transgenic lines, prepared sequencing libraries, performed bioinformatic analysis, conducted AGO1 structure prediction and AGO sequence alignments; Ye Xu and Yong Zhang performed IP for MS/MS; Haiyan Zheng and Caifeng Zhao performed MS/MS; Hiro-oki Iwakawa

performed *in vitro* RISC assembly assays; Lusheng Fan generated the *35S::MIR165A* plasmid; Ye Xu, Hiro-oki Iwakawa and Xuemei Chen analyzed data; Ye Xu and Hiro-oki Iwakawa prepared the figures; Ye Xu made the tables. Ye Xu wrote the chapter and Xuemei Chen edited it.

ABSTRACT OF THE DISSERTATION

Identification of Novel Mechanisms that Regulate the Activities of ARGONAUTE1 in *Arabidopsis thaliana*

by

Ye Xu

Doctor of Philosophy, Graduate Program in Plant Pathology
University of California, Riverside, March 2022
Dr. Xuemei Chen, Chairperson

RNA silencing mediated by 19-to-24 nucleotide-long small RNAs is a central mechanism regulating gene expression. In plants, the two major types of small RNAs are microRNAs (miRNAs) and small interfering RNAs (siRNAs). miRNAs are derived from long hairpin RNA precursors while siRNAs are derived from long double-stranded RNAs. In plants, the majority of miRNAs and certain siRNAs associate with the ARGONAUTE1 (AGO1) protein to exert their regulatory effects by forming an RNA-induced silencing complex (RISC). Even though many studies have been done to characterize Arabidopsis AGO1 and AGO1 activities, little is known about the mechanisms that regulate AGO1 RISC formation. In my dissertation research, two mechanisms that regulate AGO1 RISC formation were identified and reported in chapters two and three. In the second chapter, we found that the long structurally unresolved N-terminal extension (NTE) is essential for the functions of AGO1, as an AGO1 mutant

lacking this region is unable to rescue the developmental and molecular phenotypes of an *ago1* null allele. RNA sequencing of total small RNAs and AGO1-associated small RNAs showed that amino acids (a.a.) 91-189 of the NTE are required for RISC formation, thus crucial for the activities of AGO1 in gene silencing. Furthermore, a.a. 1-90 and a.a. 91-189 regions of the NTE redundantly promote the activities of AGO1 in the biogenesis of trans-acting siRNAs (ta-siRNAs). This work provides a new understanding of the AGO1 NTE region in RISC assembly and ta-siRNA biogenesis. In the third chapter, through immunoprecipitation-mass spectrometry, we found that AGO1 is phosphorylated *in vivo*. Analysis of AGO1-associated small RNAs *in vivo* and RISC formation assays *in vitro* showed that phospho-mimetic AGO1 is compromised in the loading of both miRNA and siRNA duplexes and in passenger strand ejection of siRNA but not miRNA duplexes. Non-phosphorylatable AGO1 is compromised in target RNA repression. This work revealed a regulatory role of phosphorylation and dephosphorylation in the small RNA association and target repression activities of AGO1. Taken together, my dissertation research provided new insights into mechanisms regulating the activities of plant AGO1 and these insights have implications beyond plant AGO1.

Table of Content

List of Figures

List of Tables

Chapter 1

Introduction: biogenesis, mode of action, and degradation of plant microRNAs

Abstract

MicroRNAs (miRNAs) are short endogenous non-coding RNAs that regulate gene expression at the post-transcriptional level in a broad range of eukaryotic species. In animals, it is estimated that more than 60% of mammalian genes are targets of miRNAs, with miRNAs regulating cellular processes such as differentiation and proliferation. In plants, miRNAs regulate gene expression and play essential roles in diverse biological processes, including growth, development, and stress responses. Arabidopsis mutants with defective miRNA biogenesis are lethal, and abnormal expression or accumulation of miRNAs can also be fatal to plants. It is therefore crucial that the homeostasis of miRNAs is tightly regulated. In this chapter, I summarize the key mechanisms of plant miRNAs' biogenesis and their homeostatic regulation. In addition, I provide an update on nuclear proteins with novel functions in miRNA biogenesis and proteins linking miRNA homeostasis to environmental triggers. I also discuss emerging roles of liquid-liquid phase separation in facilitating miRNA biogenesis and action.

1. Introduction

microRNAs (miRNAs) are ~19-to-24 nucleotide (nt) long endogenous non-coding RNAs that play an essential role in regulating gene expression in plants and animals. In 1993, lin-4, the first miRNA ever characterized, was identified as a regulator of developmental timing in *Caenorhabditis elegans* in a forward genetics screen[1]. In 2000, the second miRNA, let-7, was discovered in *C. elegans* through a similar approach[2]. lin-4 and let-7 are endogenous short RNAs that are 21 nt and 22 nt long, respectively. Both are partially complementary to the 3′ untranslated regions of their target protein-coding genes and cause translational inhibition of the messenger RNAs (mRNAs). Phylogenetic analysis of the let-7 RNA sequence revealed its conservation among bilaterian animals, such as human and the fly *Drosophila melanogaster*, suggesting that similar gene expression regulatory mechanisms could be adopted by diverse species[3]. In 2001, in a multimodal approach involving bioinformatics and cDNA cloning, many small endogenous RNAs with shared features to lin-4 and let-7 RNA were reported in multiple species, including *C. elegans*, Drosophila and human, and thereafter officially named as miRNAs[4–6]. With the application of high-throughput sequencing in the past decade, our ability to identify new species of miRNAs has dramatically expanded. According to miRBase (v.22.1), the number of mature miRNAs is more than 2600 in human, 430 in *C. elegans*, 460 in *D. melanogaster*, 420 in *Arabidopsis thaliana*, 320 in *Zea mays*, 730 in *Oryza sativa*, and these numbers continue to grow. In addition to eukaryotic species, miRNAs have also been found in viruses[7].

In plants, *MIRNA* (*MIR*) genes encoding miRNAs are transcribed into long primary miRNA (pri-miRNA) transcripts by RNA POLYMERASE II (Pol II)[8]. Pri-miRNAs are capable of folding into stem-loop structures that harbor mismatches and are recognized and cleaved by the RNase III family enzyme DICER-LIKE 1 (DCL1) and accessory proteins to produce miRNA duplexes[9]. One strand of the miRNA duplex is selected as the miRNA and incorporated into an ARGONAUTE (AGO) protein to form a miRNA-induced silencing complex (miRISC), while the other strand called miRNA* or passenger strand is removed[10]. The majority of the plant miRNAs are preferentially loaded into AGO1, which preferentially binds miRNAs with a 5' uridine (U)[11]. miRISC then binds to the target messenger RNAs that contain sequences complementary to the miRNA, thus inducing degradation or translational repression of the target transcripts. In addition to regulating gene expression post-transcriptionally, certain 22-nt plant miRNAs are also capable of triggering the biogenesis of secondary small interfering RNAs (siRNAs) from protein-coding genes or long non-coding RNAs in a phased pattern. siRNAs produced through this pathway are referred to as phasiRNAs[12].

miRNA-mediated post-transcriptional gene silencing regulates critical biological processes in plants, including growth, development, hormone synthesis, and biotic and abiotic stress responses, thus it is vital to tightly control the abundance of miRNAs. The steady-state level of a miRNA reflects the constant balance between its biogenesis, stabilization, and turnover.

2. Plant miRNA biogenesis and regulation

Tens to hundreds of miRNAs have been identified in various plant species, and the vast majority of them are encoded by *MIR* genes located in the intergenic regions[13]. In Arabidopsis the 420 *MIR* genes belong to ~200 families (miRbase, v22.1), with most families being represented by a single member. Unlike their counterparts in metazoans, plant *MIR* genes are rarely clustered in the genome[13].

The biogenesis of plant miRNAs constitutes three major steps. A *MIR* gene is first transcribed by Pol II into a long pri-miRNA, which folds into a stem-loop structure (Figure 1.1 A)[8]. The pri-miRNA is then recognized and processed by the dicing complex into a miRNA/miRNA* duplex with 2-nt overhangs at the 3′ ends. Next, the miRNA/miRNA* duplex undergoes 2'-O methylation at the 3' ends by HUA ENHANCER1 (HEN1) (Figure 1.1 B)[14]. The nuclear endonuclease DCL1, double-stranded RNA binding protein HYPONASTIC LEAVES 1 (HYL1), also known as double-stranded RNA-binding protein1 (DRB1), and the zinc finger protein SERRATE (SE) form the core component of the dicing complex. In this section, we will review the miRNA biogenesis pathway and summarize the recent findings.

2.1 *MIR* gene transcription and pri-miRNA stabilization

The transcription of *MIR* genes into pri-miRNAs is by Pol II, thus the pri-miRNA transcripts are co-transcriptionally capped and poly-A tailed[8]. While most *MIR* genes that reside in the non-coding regions between genes are independently transcribed, others are found within introns of protein-coding or non-coding genes,

such as *MIR400* and *MIR402*, and are co-transcribed with their host genes by Pol II and regulated by RNA splicing activities[15,16].

As with protein-coding genes, the transcription of *MIR* genes is regulated by both cis- and trans-regulatory modules, and general regulatory mechanisms that control protein-coding gene transcription might also apply to *MIR* gene transcription. For instance, general cis- regulators, such as the TATA box, are located upstream of the transcription start sites of *MIR* genes[8]. Binding sites for the transcription factors MYC2, ARF, SORLREP3, and LFY are overrepresented in *MIR* promoters[17]. In addition, phosphorylation of Pol II C-terminal domain (CTD) is governed by CYCLIN-DEPENDENT KINASE F;1 (CDKF;1) and CYCLIN-DEPENDENT KINASE Ds (CDKDs)[18]. Inhibition of CTD phosphorylation causes defects in pri-miRNA capping, polyadenylation and splicing. A panel of trans-regulatory modules promotes the transcription of *MIR* genes by regulating Pol II occupancy at the *MIR* loci. Trans-regulatory module mutants show reduced levels of pri-miRNAs, including those of the Mediator complex subunit MED20a[19], the Elongator complex members ELP2 and ELP5[20], two intron-lariat spliceosome (ILS) complex disassembly factors POLYPLOIDY1-1D (ILP1) and NTC-Related protein 1 (NTR1)[21], the transcription factor NEGATIVE ON TATA LESS 2 (NOT2)[22], the MOS4-ASSOCIATED COMPLEX (MAC) subunit CELL DIVISION CYCLE 5 (CDC5)[23], the chromatin-associated protein REGULATORY SUBUNIT 3A (PP4R3A) of the PROTEIN PHOSPHATASE4 (PP4) complex[24], the Three PRIME REPAIR EXONUCLEASE 2 (TREX-2) complex core components THO/HRP1

PHENOTYPE 1 (THP1) and SUPPRESSOR OF ACTIN 3A (SAC3A)[25], the splicing factor SMALL1 (SMA1)[26], and the ribosomal protein SHORT VALVE 1 (STV1)[27].

It is important to note that many *MIR* gene transcriptional regulators also interact with the dicing complex members, indicating they might have dual roles and/or promote the co-transcriptional processing of the pri-miRNAs. For example, NOT2, TREX-2 complex, ILP1, and NTR1 are found to interact with both Pol II and the dicing complex[21,22,25]. PP4 and the MAC subunit CDC5 are associated with *MIR* promoters, Pol II, and the dicing complex[23,24].

2.2 Developmental stages affect the transcription of *MIR* genes

While some transcription factors have a general impact on the transcription of *MIR* genes, others positively and/or negatively regulate individual *MIR* genes at a specific developmental stage. Two B3 domain family transcription factors FUSCA3 (FUS3) and ABSCISIC ACID INSENSETIVE3 (ABI3) directly promote *MIR156* transcription during the embryo-to-seedling transition and early stages of seed development, respectively[28,29]. Unlike FUS3, which functions primarily as a transcriptional activator, ABI3 represses *MIR156D* during later seed development and downregulates *MIR160B,* which regulates *AUXIN RESPONSE FACTOR* (*ARF*)*10* and *ARF16* that participate in seed dormancy[29]. Besides FUS3 and ABI3, the expression levels of *MIR156A* are stabilized through a feedback loop - the *SQUAMOSA PROMOTER BINDING PROTEIN-LIKE* (*SPL*) *9* and *SPL10* genes are both targets of miR156 and encode transcriptional activators of *MIR156A*[30].

Some miRNAs can act upstream to regulate the expression of other *MIR* genes. For example, SPL9 and SPL10, targets of miR156, are found to be enriched at the *MIR172B* locus to promote its transcription[30]. miR172b is critical for the juvenile-to-adult transition in Arabidopsis and maize, and during the transition, miR165 levels decline while miR172 levels increase[30]. As with *MIR156*, the transcription of *MIR172* is subject to multiple layers of regulation. The SANT-domain-containing protein POWERDRESS (PWR) was found to enhance the transcription of only three of the five *MIR172* members, *MIR172A*, *B*, and *C*, by increasing Pol II occupancy at the promoters[31]. The transcription factor APETALA2 (AP2) plays a complex role in *MIR172* regulation. AP2 was found to be enriched at two *MIR* gene loci, *MIR156* and *MIR172*[32]. AP2 positively regulates *MIR156* expression, which indirectly dampens the expression of *MIR172*[32]. Meanwhile, together with the transcriptional co-repressors LEUNIG (LUG) and SEUSS (SEU), AP2 represses the expression of *MIR172*[33]. As a regulator of *MIR172*, *AP2* is also subject to the regulation by its cognate miRNA to form a feedback loop[32,33]. The expression of *AP2* is restricted to the outer floral whorls as its mRNA translation is repressed in the inner whorls by miR172[34]. In another case, during leaf polarity development, class II homeodomain leucine zipper (HD-ZIPs) transcriptional factors HAT3 and ATHB4 interact with the class III HD-ZIP protein REVOLUTA (REV) to directly repress the transcription of *MIR165/166* genes via a conserved cis-element in their promoters[35].

2.3 Epigenetic marks affect *MIR* gene transcription

Histone modification epigenetically regulates gene expression, and studies have shown that such mechanisms also affect *MIR* gene transcription. For instance, GENERAL CONTROL NON-REPRESSED PROTEIN 5 (GCN5) promotes the expression of a subset of *MIR* genes through the addition of acetylation marks on H3K14 at the *MIR* loci[36]. By increasing H3K27me3 marks at the *MIR156A/MIR156C* loci, POLYCOMB REPRESSIVE COMPLEX 2 (PRC2) subunits CURLY LEAF (CLF) and SWINGER (SWN) redundantly mediate their transcriptional repression during vegetative phase change[37]. CHROMOSOME REMODELING2 (CHR2), also known as BRAHMA (BRM), is the ATPase subunit of the large switch/sucrose non-fermentable (SWI/SNF) complex, and a defect in CHR2/BRM reduces *MIR* gene transcription[38]. In addition, chromatin modification can affect *MIR* genes differently, for example the SWR1 chromatin remodeling complex (SWR1-C) alters the nucleosome occupancy at *MIR* gene promoters to regulate their expression positively or negatively[39]. It remains unclear how some transcription regulators distinguish one group of *MIR* genes from another.

2.4 Stabilization of pri-miRNAs

During transcription, pri-miRNAs are co-transcriptionally protected by 5' capping and 3' poly(A) tailing from nuclear RNA exosome-mediated degradation[40,41]. Additional regulation has also been reported to mediate pri-miRNA stability - mutations in specific proteins cause reduced accumulation of pri- and mature miRNA without compromising *MIR* gene transcription. Proteins in this

group include the RNA binding protein DAWDLE (DDL) [42] and MAC subunits PLEIOTROPIC REGULATORY LOCUS1 (PRL1)[43], MAC3[44] and MAC5A[45], with all four proteins showing a direct interaction with pri-miRNA transcripts and the dicing complex. MAC5A interacts with the stem-loop of pri-miRNAs and SE[45]. The reduced accumulation of pri-miRNAs in *mac5a* is partially rescued by introducing *xrn2* or *xrn3*, mutations in two nuclear 5′-to-3′ exoribonucleases that degrade aberrant RNAs, suggesting that MAC5A binds to the pri-miRNA stem-loop to prevent it from XRN2- and XRN3-mediated degradation[45]. Interestingly, an *se* mutation also suppresses the molecular defect of *mac5a*, indicating that the reduced accumulation of pri-miRNAs in *mac5a* is SE-dependent[45]. The direct interaction between SE and XRN2, identified in the same study, suggests a possible link between SE and pri-miRNA degradation, in addition to its role in pri-miRNA processing[45]. In line with this hypothesis, a recent study found that SE interacts with the NUCLEAR EXOSOME TARGETING (NEXT) complex subunits ZCCHC8A and ZCCHC8B and a subset of pri-miRNAs is increased in abundance when the NEXT complex lacks the HEN2 component while mature miRNA levels are not affected[40]. Interestingly, another study shows that loss of functions in HEN2 or SUPPRESSORS OF THE PAS2 1 (SOP1), which is also a component of the nuclear exosome that co-localizes with HEN2, preferentially increases the accumulation of a subset of pri-miRNAs in the *hyl1* mutant, and subsequently restores the levels of these miRNAs in *hyl1*[41,46]. Together, these studies suggest that pri-miRNAs might be subject to exosome surveillance.

3 Dicing complex assembly and pri-miRNA processing

Maturation of miRNAs requires the precise processing of pri-miRNAs. Pri-miRNAs vary largely in stem-loop shape and length. The dicing complex relies on structural features of the long miRNA precursors to distinguish them from other dsRNA species and define the position for the initial cut. In most cases, DCL1 processes the pri-miRNA in a base-to-loop mode, with the dicing complex recognizing a 15-17bp dsRNA stem below the miRNA/miRNA* and above an internal loop to perform the initial cut that defines one end of the miRNA[47]. In other cases, such as pri-miR159a and pri-miR319a, the first cut is generated at the distal region of the pri-miRNA in a loop-to-base mode, where DCL1 recognizes a 15-17bp dsRNA stem above the miRNA/miRNA* duplex and below a small terminal loop to perform the initial cut[48]. In either case, after the initial cut, DCL1 acts as a molecular ruler and generates a second cut ~21nt away from the first cut to release the miRNA/miRNA*[49]. While most miRNA precursors are substrates of DCL1, a few young miRNAs including miR822 and miR839 are processed by DCL4 in Arabidopsis[50]. In addition, a class of 24-nt miRNAs require DCL3 for biogenesis in rice[51].

3.1 Secondary structures of pri-miRNAs

The secondary structures of pri-miRNAs are not all alike, with differing features such as GC content, branched terminal loops, intron position, and flexible internal base-pairing having been shown to affect the efficiency of DCL1-mediated pri-miRNA processing. GC bias and signatures play a role in determining the

precision of pri-miRNA processing and the abundance of miRNAs[52]. G/C enrichment at positions 8–9, 18–19 and A/U enrichment at positions 5, 7 and 10 within miRNA regions positively correlate with miRNA abundance, with one possible explanation being that these signatures influence the structure of pri-miRNAs to promote HYL1 recruitment and binding[52].

Alternative secondary structures of miRNA precursors, such as a terminal branched loop, have been observed to affect the processing of several pri-miRNAs. Pri-miR165 and pri-166 possess a terminal branched loop, which is recognized by the dicing complex and leads to bi-directional processing[53]. The canonical base-to-loop mode promotes miRNA production whereas the non-canonical loop-to-base mode leads to unproductive cuts that diminish miRNA biogenesis[53]. For pri-miR157c, the terminal branched loop followed by an ~18 bp dsRNA segment can be recognized by the dicing complex to generate mature miRNAs, albeit the loop-to-base mode of processing is relatively slow[54].

Many pri-miRNAs possess introns, and certain introns residing in the stem-loop region can disrupt the secondary structure of pri-miRNAs and thus must be removed by splicing, such as those in pri-miR842 and pri-miR846[55]. In contrast, pri-miR161, pri-miR163 and pri-miR172b possess introns downstream of the stem-loop that play a positive role in miRNA maturation, possibly due to the 5' splice site of these introns being recognized by U1 snRNP, which in turn recruits these pri-miRNAs to the dicing complex for processing[16,56,57].

While most miRNA precursors generate only one miRNA, some can produce multiple miRNAs due to their unique sequence features. The miR168/miR168* duplex undergoes flexible internal base-pairing enabling three alternative structural configurations, which promote the production of isomeric miRNAs (isomiRs)[58]. isomiR168s vary in length and 5' terminal nucleotides hence leading to distinct AGO sorting outcomes[58]. In particular, a 22-nt miR168 isoform is enriched in AGO10 instead of AGO1, and AGO10-miR168 promotes the repression of *AGO1* by triggering the production of secondary siRNAs from the *AGO1* mRNA[58]. In addition, certain miRNA precursors can be sequentially processed by DCL1 multiple times to produce several small RNA duplexes[59].

Protein factors are capable of regulating pri-miRNA processing by altering the pri-miRNA secondary structure. In addition to promoting *MIR* gene transcription, CHR2/BRM directly binds to pri-miRNAs and alters their secondary structure thereby inhibiting processing[38]. This inhibition requires the interaction of CHR2/BRM with SE[38]. Interestingly, the association with SE is not necessary for CHR2/BRM to promote *MIR* gene transcription[38]. A recent study reports extensive cytidylation and uridylation on the 3' termini of pre-miRNAs processed through the base-to-loop mode, with the nucleotidyl transferase HEN1 SUPPRESSOR1 (HESO1), NTP6 and NTP7 contributing to a portion of the cytidine addition on pre-miRNAs[60]. HESO1 is responsible for the majority of uridine addition[60]. This untemplated tailing can restore trimmed pre-miRNAs to their intact length thereby promoting processing[60]. pri-miRNA structures can also be altered by post-

transcriptional modification. The mRNA adenosine methylase (MTA) introduces N6-methyladenosine (m6A) in pri-miRNAs[61]. A deficiency in MTA leads to less structured stem-loop regions, which hampers the association of HYL1 with these precursors and results in decreased miRNA levels[61]. MTA also interacts with Pol II and TOUGH (TGH), which are required in the early stages of miRNA biogenesis, suggesting that MTA might also act at early steps[61].

3.2 Assembly of the dicing complex

Although many proteins have been found to assist with pri-miRNA processing, the two main dicing complex components promoting the functions of DCL1 are HYL1 and SE, with these three components forming the core of the dicing complex and are colocalized in nuclear loci termed ‘dicing bodies’ (D-bodies)[62,63]. SE and HYL1 interact with each other, and both interact with DCL1[62]. HYL1 functions as a dimer to bind the stem region of pri-miRNAs and partner with SE, a C2H2 zinc finger protein that also binds pri-miRNAs, to ensure the precise cleavage of miRNA precursors by DCL1[64–68]. A lack of HYL1 or SE causes reduced accumulation of mature miRNAs globally and increases levels of pri-miRNAs[65–68]. Dicing complex formation is regulated by multiple factors. MAC subunits have been shown to be involved in dicing complex formation, including MAC7 and MAC3, which are associated with the dicing complex and promote the recruitment of HYL1[44,69]. Interestingly, the RNA binding protein MODIFIEROFSNC1,2 (MOS2)[70] and the DEAH-box helicase PHYTOPHTHORA SUPPRESSOR OF RNA SILENCING 1 (PINP1)[71] promote the assembly of the dicing complex without

interacting with it. In the absence of MOS2, the association between pri-miRNA and HYL1 is reduced and localization of HYL1 in the D-bodies is compromised[70]. A recent study shows that D-bodies are phase-separated condensates, and the phase separation property of SE drives the formation of D-body[72]. Truncation of the intrinsically disordered regions (IDRs) of SE abrogates D-body formation and results in reduced miRNA processing[72]. Moreover, the TREX-2 complex interacts with SE and promotes D-body formation in addition to its role in *MIR* gene transcription[25]. To date, it is unknown where pri-miRNA processing takes place. One possibility is that pri-miRNA processing takes place in D-bodies as many processing complex components are localized there. However, considering that the number of D-bodies in each nucleus is limited and a certain number of dicing complex cofactors are not associated with the D-bodies, miRNA processing might not exclusively take place in D-bodies[62].

3.3 Regulation of pri-miRNA processing

Efficient loading of pri-miRNAs to the dicing complex is facilitated by MOS2[70], the RNA binding protein TGH[73], the ribosomal protein STV1[27], and the THO/TREX complex[74] that mediates mRNA shuttling between the nucleus and the cytoplasm. TGH is a component of the dicing complex, it binds pri- and pre-miRNAs *in vivo*, and is required for the interaction between HYL1 and pri-miRNAs[73]. In addition, a lack of TGH reduced the activity of DCL1 *in vitro*[73]. STV1 binds pri-miRNAs and facilitates the recruitment of pri-miRNAs to the dicing complex[27]. The THO/TREX complex promotes the association of pri-miRNAs with

HYL1, however, it does not appear to interact with any miRNA biogenesis pathway factors[74].

Pri-miRNA processing might occur co-transcriptionally. First, DCL1 is associated with the chromatin regions of *MIR* genes[20]. In addition, the Elongator complex[20], CDC5[23], NOT2[22], and TREX-2[25] interact with both Pol II and the dicing complex and might act to recruit the dicing complex to *MIR* loci during *MIR* transcription. In accordance with this assumption, mutants of Elongator and NOT2 show impaired DCL1 localization in D-bodies or defects in D-body formation[20,22]. In addition, TREX-2 interacts with SE and promotes D-body formation[25]. It is unclear whether D-body formation is coupled with dicing complex component's recruitment to the *MIR* loci. A recent study suggests HASTY (HST), the plant homolog of animal EXPORTIN 5 (EXP5/XPO5), facilitates miRNA biogenesis independently of its proposed, yet unproven, role in miRNA nuclear export in Arabidopsis. HST could act as a scaffold to stabilize the DCL1-MED37 complex which in turn enhances the recruitment of DCL1 to *MIR* loci[75].

The activities of the dicing complex are modulated by specific factors. For example, RECEPTOR FOR ACTIVATED C KINASE1 (RACK1) promotes pri-miRNA processing through interaction with SE[76]. As it also interacts with AGO1, RACK 1 might be bridging pri-miRNA processing with AGO1 loading or playing a separate role downstream[76]. Some factors regulate the dicing complex in a spatiotemporal manner. The DEAD-BOX RNA HELICASE 27 (RH27) is associated

with pri-miRNAs and interacts with HYL1, SE and DDL to promote pri-miRNA processing in embryos, shoot apical meristems and root apical meristems[77].

3.4 Roles of splicing in pri-miRNA processing

A number of proteins modulating both pri-miRNA processing and splicing have been identified, suggesting these two processes might be coupled. These proteins include the dicing complex core components HYL1[78] and SE[79,80], CAP-BINDING PROTEIN 20 (CBP20) and CBP80[79,81], the splicing factor SMA1[26], HIGH OSMOTIC STRESS GENE EXPRESSION 5 (HOS5), ARGININE/SERINE-RICH SPLICING FACTOR 40 (RS40) and RS41[82], the pre-mRNA processing factor 6 homolog STABILIZED1 (STA1)[83], GLYCINE-RICH RBP 7 (GRP7) [84], SICKLE (SIC)[85], THO2 of the THO/TREX complex[74], the U1 snRNP subunit LETHAL UNLESS CBC 7 RL (LUC7rl), and the PRE-MRNA-PROCESSING PROTEIN (PRP)39b, PRP40a, PRP40b[16] are positive regulators of pri-miRNA processing and are involved in splicing. In addition, the MAC complex has been shown to associate with the spliceosome[86]. Furthermore, recent studies found that intronic lariat RNAs, the by-products of pre-mRNA splicing, inhibit pri-miRNA processing by acting as a decoy to sequester the dicing complex to prevent its binding to pri-miRNAs[87]. The two intron-lariat spliceosome (ILS) complex subunits ILP1 and NTR interact with DCL1 and SE and facilitate the degradation of lariat RNAs which in turn promote miRNA processing[21].

3.5 Regulation of the dicing complex components DCL1, HYL1 and SE

The expression and function of the dicing complex core components DCL, HYL1 and SE are regulated at transcriptional, post-transcriptional, and post-translational levels.

The transcription of *DCL1* is promoted by XAP5 CIRCADIAN TIMEKEEPER (XCT) [88] and STA1[83]. The splicing factor SMA1 facilitates the splicing of the ninth intron of *DCL1* pre-mRNA to promote miRNA processing[26]. DELAY OF GERMINATION1 (DOG1) promotes the expression of *DCL1*, *HYL1*, *SE*, *TGH*, and *CDC5*[89], while the histone acetyltransferase GCN5 indirectly represses the expression of *DCL1*, *HYL1*, and *SE*[36], and the *AGO1* gene encoding the miRNA effector[90], to negatively regulate miRNA maturation. In addition, the levels of *DCL1* mRNA are subjected to the negative feedback regulation by miR162[91] and miR838, the latter residing in intron 14 of *DCL1* pre-mRNA[50]. Furthermore, *SE* RNA is targeted and negatively regulated by miR863 during bacterial infection[92].

At the post-transcriptional level, KARYOPHERIN ENABLING THE TRANSPORT OF THE CYTOPLASMIC HYL1 (KETCH1), an importin beta protein, enhances miRNA processing by promoting the translocation of HYL1 from the cytoplasm to the nucleus[93]. In addition, pri-miRNA-like SHORT INTERSPERSED ELEMENTS (SINEs) RNAs can act as a decoy and sequester HYL1 to reduce its participation in pri-miRNA processing[94]. A recent study shows that the 20S core proteasome α subunit G1 (PAG1) promotes pri-miRNA processing by recruiting the SE protein for degradation in a ubiquitin-independent manner[95]. Presumably

the degraded SE is disordered and non-functional[95]. In the *pag1* mutant, SE is distributed in both the cytoplasm and the nucleus, while it is predominantly detected in the nucleus in the wild type[95].

The activity of the dicing complex is subjected to phosphorylation. The phosphorylation of DCL1 is required for its interaction with DDL, with this interaction being necessary for pri-miRNA processing[96,97]. HYL1 activity is also regulated by its phosphorylation states with phosphorylation inhibiting HYL1 function[98,99]. C-TERMINAL DOMAIN PHOSPHATASE-LIKE 1 (CPL1)/FIERY2 and CPL2 dephosphorylate HYL1 and facilitate its localization to D-bodies[100]. HOS5, also known as REGULATOR OF CBF GENE EXPRESSION 3 (RCF3) and SHINY1, interacts with CPL1 and CPL2 to assist HYL1 dephosphorylation in a tissue specific manner[101]. In addition, SUPPRESSOR OF MEK 1 (SMEK1) partners with PROTEIN PHOSPHATASE 4 (PP4) to dephosphorylate and stabilize HYL1, thus enhancing pri-miRNA processing[102]. MITOGEN-ACTIVATED PROTEIN KINASE 3 (MPK3) and SNF1-RELATED PROTEIN KINASE 2 (SnRK2) can phosphorylate HYL1 *in vitro*, to inactivate it, and furthermore both kinases interact with HYL1 *in vivo*[98,99]. Besides, SnRK2 also associates with and phosphorylates SE *in vitro*, although the physiological role of this modification remains unclear[99].

3.6 Regulation of miRNA biogenesis by environmental cues

As plants are sessile organisms, effective responses to environmental changes are essential. *MIR* gene expression and the activity and subcellular

localization of the dicing complex components are regulated by environmental cues in a tissue and developmental stage specific manner.

3.6.1 Regulation of *MIR* gene transcription and pri-miRNA processing by environmental cues

A growing number of *MIR* gene transcription and processing factors have been reported as being subject to the regulation by environmental changes. For example, in Arabidopsis, red light treatment and white light treatment of etiolated seedlings can alter the expression of a group of miRNAs. During shade avoidance response, the level of PHYTOCHROME-INTERACTING FACTORS (PIFs) is highly induced, and the PIFs bind to the promoters of multiple *MIR156* genes and repress their expression[103]. Another light signaling transcription factor ELONGATED HYPOCOTYL 5 (HY5) directly regulates the expression of several *MIR* genes[104]. Partnering with HY5-HOMOLOG (HYH), HY5 mediates light-induced expression of HEN1, which protects miRNAs from degradation[105]. The transcription of *MIR395*, *MIR399*, and *MIR398* genes is specifically induced upon sulfur, phosphate and copper deprivation, respectively[106–111]. In addition to copper deprivation, miR398 has also been reported to respond to heat[112,113]. Tocopherols (vitamin E) facilitate the accumulation of 3'-phosphoadenosine 5'-phosphate (PAP), which inhibits the activity of nuclear exoribonucleases XRN2 and XRN3 to promote miRNA biogenesis, possibly by protecting pri-miRNAs from being degraded[113]. The induction of tocopherols and PAP by heat is required for the increased accumulation of miR398[113]. MiR402, an intronic miRNA, is induced by heat

stress[114]. In contrast to miR402, pri-miR400 is retained in the host RNA upon heat stress, which results in reduced accumulation of miR400[15]. In cold temperatures, the expression of *STA1* is highly induced, which facilitates pri-miRNA splicing and promotes *DCL1* transcription[83,115]. The *sic* mutant is hypersensitive to cold and salt stresses[85]. SIC participates in pre-mRNA splicing, colocalizes with HYL1 and positively regulates pri-miRNA processing[85]. The cycling DOF transcription factor CDF2, which participates in photoperiodic flowering, binds to the promoter of some *MIR* genes and activates or represses their transcription[116,117]. CDF2 also interacts with DCL1 and suppresses pri-miRNA processing[117]. Under salt stress, the transcription of *MIR163* and *MIR829* genes is increased, while the transcription of *MIR161* and *MIR173* genes is repressed by AGO1[90]. Furthermore, pathogen responses can affect miRNA biogenesis. The nuclear localized disease resistance protein SNC1 partners with its interacting protein TPR1 to represses the transcription of *MIR* genes[118].

3.6.2 Regulation of the dicing complex by environmental cues

Among the abiotic and biotic stimuli affecting pri-miRNA processing, light plays the most influential role. In the light, CONSTITUTIVE PHOTOMORPHOGENIC 1 (COP1), an E3 ubiquitin ligase, translocates from the nucleus to the cytoplasm, where it stabilizes HYL1 by preventing its degradation by an unknown protease, which would otherwise degrade HYL1 by cleaving its N-terminal region[119]. Consistent with this observation, during de-etiolation, pri-miRNAs and the dicing complex components DCL1, HYL1, and SE were observed

to accumulate to higher levels[120]. However, the accumulation of most miRNAs did not change; this discrepancy suggests an unknown suppressor hampers pri-miRNA processing during de-etiolation[120]. A recent study shows that FORHEAD-ASSOCIATED DOMAIN 2 (FHA2), a light stabilized protein, might be the suppressor. FHA2 associates with DCL1, HYL1, and SE to suppress their pri-miRNA processing activity[121]. In the dark, the levels of HYL1 are reduced, and the ratio between active (dephosphorylated) and inactive (phosphorylated) HYL1 is also strongly diminished during extended periods of darkness or shade[122]. Interestingly, although inactive phosphorylated HYL1 is stabilized in the nucleus in the dark, HYL1 can be quickly activated (dephosphorylated) on plants' exposure to light[122]. During a dark to red light transition, PHYTOCHROME-INTERACTING FACTOR 4 (PIF4), a basic helix-loop-helix (bHLH) transcription factor, interacts with and destabilizes DCL1 in a ubiquitin-proteasome (UPS) independent pathway[123]. PIF4 also interacts with HYL1, and acts as a transcription activator of a group of miRNA genes[123].

Besides light, ABA treatment and other environmental stresses could activate SnRK2s, thereby phosphorylating HYL1 and SE. SnRK2s-mediated phosphorylation promotes HYL1 stability during ABA treatment[99]. In contrast to SnRK2s, MPK3-mediated phosphorylation promotes HYL1 degradation[98]. ABA treatments induce SMEK1 to antagonize HYL1 degradation mediated by MPK3[102]. In addition, the expression levels of HOS5/RCF3/SHINY are reduced by salt and ABA treatments[82,124]. Furthermore, multiple MAC subunits such as CDC5, PRL1,

and MAC7, which promote miRNA biogenesis, are responsive to different environmental cues[23,43,69].

4. miRNA stabilization and RISC assembly

The miRNA/miRNA* duplexes are 2'-O- methylated by the methyltransferase HEN1 at the 3′ terminus of each strand to protect miRNAs from degradation[14,125]. Mutations in *HEN1* lead to reduced levels of nearly all miRNAs[14,125,126]. Recent studies show that HEN1 interacts with DCL1 and HYL1 but not SE, suggesting HEN1 might replace SE in the dicing complex after pri-miRNA processing[127]. Next, the methylated miRNA/miRNA* duplex is loaded into AGO to form a miRISC. Upon loading, AGO unwinds the miRNA/miRNA* duplex and selectively retains one strand (guide strand or miRNA), which directs AGOs for target gene inhibition, whereas the other strand (passenger strand or miRNA*) is ejected[10].

4.1 miRNA strand selection

The thermodynamic differences in the base-pairing stabilities and/or the identity of the first nucleotide of the miRNA are key features for strand selection and AGO sorting. Usually, the strand with lower 5' thermostability in the duplex is selected as the guide strand and retained by AGOs[128,129]. In Arabidopsis, most miRNA guide strands start with a 5' uridine and are preferentially incorporated into AGO1, the major miRNA effector of the AGO family[11]. Small RNAs that start with a 5' adenosine are predominantly associated with AGO2 and AGO4, whereas those starting with a 5' cytosine are mainly associated with AGO5[11]. In addition,

the miRNA duplex structure has also been shown to affect their sorting. For instance, AGO1 prefers miRNA duplexes with central mismatches, while AGO2 prefers duplexes with no middle mismatches[130]. miRNAs can be loaded into more than one AGO protein. Indeed, in Arabidopsis, miR165/166 is associated with both AGO1 and AGO10[131,132]. While most miRNA* strands are degraded, some are loaded into AGO proteins and function as the guide strand in gene repression. For instance, miR393b* starts with a 5' adenosine, and is enriched in AGO2, while miR393 starts with a 5' uridine, and is mainly loaded into AGO1[133]. AGO2-miR393b* targets a Golgi-localized receptor protein MEMB12 thereby promoting the secretion of PR1, an antimicrobial pathogenesis-related protein[133]. In 2013, the miRBase database ceased using the miR/miR* nomenclature, instead, miR-5p and miR-3p naming formats are assigned for small RNA sequences derived from the 5' and 3' arm of the miRNA precursor, respectively[134]. Furthermore, protein cofactors such as HYL1[128], CPL1[100], HOS5, RS40, and RS41[82] have also been reported to assist with strand selection.

The assembly of AGO1 containing RISC requires the assistance of the molecular chaperone HEAT SHOCK PROTEIN 90 (HSP90), which binds AGO1 in an ATP-dependent manner and triggers a conformational change of AGO1 to allow sRNA duplex loading[135,136]. Following ATP hydrolysis, HSP90 dissociates from and likely prompts a second conformational change of AGO1, which results in the proper removal of the passenger strand[135,136]. The unwinding and removal of miRNA* strands from AGO1 do not require cleavage[135,137]. The AGO1-miRISC

assembly is also facilitated by CYCLOPHILIN 40/SQUINT (CYP40/SQN) and inhibited by PROTEIN PHOSPHATASE 5 (PP5) in an HSP90-dependent manner[138]. In addition, two importin-beta family proteins, ENHANCED MIRNA ACTIVITY 1 (EMA1) and TRANSPORTIN 1 (TRN1), interact with AGO1 and negatively and positively regulate AGO1-miRISC formation, respectively[139,140].

4.2 Regulation of AGO1 stability

AGO1 is subjected to post-transcriptional and post-translational regulation. At the post-transcriptional level, *AGO1* transcripts are targeted by AGO1-bound miR168, forming a negative feedback regulatory loop[141]. At the post-translational level, the F-box protein F-BOX WITH WD-40 2 (FBW2) negatively regulates AGO1 protein levels, with the overexpression of *FBW2* decreasing the accumulation of AGO1 protein but not *AGO1* mRNA, whereas a lack of FBW2 increases AGO1 protein levels[142]. Several studies show that AGO1 is also targeted by viral F-box RNA silencing suppressors. Polerovirus-encoded F-box protein (P0) and Enamovirus-encoded P0 destabilize host AGO1 upon viral infection[143,144]. Although F-box proteins are known for tethering poly-ubiquitins to mark proteins for degradation through the uUPS, treatment with proteasome inhibitor does not prevent AGO1 from FBW2-, Polerovirus P0-, and Enamovirus P0-mediated destabilization, suggesting AGO1 is not degraded via the UPS pathway in these cases[142–144]. Interestingly, AGO1 levels were significantly increased in P0-expressing transgenic plants treated with an autophagy inhibitor[145]. In addition, AGO1 co-localizes with AUTOPHAGY 8 (ATG8), a ubiquitin-like autophagosome

membrane protein[145]. Taken together, the data imply that FBW2 and P0 might mediate the degradation of ubiquitinated AGO1 through an autophagy-dependent pathway. Another study shows that AGO1 could also be degraded through the UPS pathway depending on a viral RNA silencing suppressor. Potato virus X protein P25 interacts with and destabilizes AGO1 through the UPS pathway, as MG132 significantly promotes the accumulation of AGO1 despite the presence of P25[146]. A recent study shows when under UV exposure, CLF, a methyltransferase subunit of the PRC2, inhibits *FBW2* expression thereby enhancing AGO1 stability[147].

4.3 The cell biology of RISC assembly

Animal pre-miRNAs are exported to the cytosol by EXPORTIN5 (EXP5/XPO5), a RanGTP-dependent dsRNA-binding protein, for final processing and RISC formation[148–150]. Unlike animals, plant miRNA maturation takes place exclusively in the nucleus. It has been proposed that plant miRNAs are exported from the nucleus to the cytoplasm by HASTY (HST), the plant ortholog of EXP5/XPO5, and loaded into AGO1 in the cytoplasm. However, this assumption is not supported by experimental data, as the nucleo-cytosolic partitioning of miRNAs is not altered in the *hst* loss-of-function mutant[151,152]. A recent study proposed a revised model, in which AGO1 protein shuttles between the nucleus and the cytoplasm, and nuclear miRNAs are translocated to the cytoplasm as AGO1-miRNA complexes through the CRM1/EXPORTIN1 (EXPO1) pathway (Figure 1.1 C)[153]. A nuclear localization signal (NLS) and a putative nuclear export

signal (NES) residing in the N terminal extension of AGO1 are proposed to direct the nucleo-cytosolic shuttling of AGO1[153]. Upon treatment with Leptomycin-B, a compound that inhibits EXPO1-mediated NES-dependent protein nuclear export, the ratio between cytoplasmic and nuclear AGO1 significantly decreased, suggesting AGO1 could be exported to the cytoplasm in an EXPO1/NES-dependent manner[153]. In addition, AGO1 with a mutated NES sequence associated with the same miRNAs as its intact counterpart, indicating that miRNAs' loading into AGO1 could take place in the nucleus[153]. However, it is possible there are other yet unidentified NES or nuclear export pathways that transport AGO1mNES from the nucleus to the cytoplasm. Indeed, it was recently found that the TREX-2 complex core subunit THP1 interacts with the nucleoporin protein NUP1 at the nuclear envelope, together promoting the nuclear export of AGO1 or AGO1-miRISC (Figure 1.1 C)[25]. Further studies need to be done to determine whether miRNAs are loaded into AGO1 exclusively in the nucleus or cytoplasm, or both.

5. miRNAs' modes of action

Plant miRISCs repress target gene expression via transcript cleavage or translational repression (Figure 1.2 A). Transcript cleavage leads to reduced levels of mRNA, while translational repression results in unchanged levels of mRNA but reduced accumulation of translated protein. Most plant miRNAs possess nearly perfect complementarity to their target transcripts, which results in cleavage of the target. However, there are some exceptions: miR172, miR171, miR398, miR395,

miR834, miR159, miR164, miR165/166, miR156/157 and probably miR167 regulate target expression through translational repression regardless of a high degree of complementarity[34,154–158]. This raises the question of how a miRISC chooses between cleavage and translational inhibition. One hypothesis is that this choice depends on the subcellular localization of AGO1, the core effector of miRNA-mediated gene silencing. Fluorescence microscopy analysis shows that AGO1 is mainly distributed in the cytoplasm, around the nuclear envelope[145], and co-localized with the endoplasmic reticulum (ER)[157,159] and processing bodies (P bodies)[160]. When subjected to Leptomycin-B treatment, a chemical blocking NES-dependent protein nuclear export, the AGO1 signal was enriched in the nucleus, suggesting AGO1 is a nucleo-cytosolic shuttling protein that transiently exists in the nucleus[153]. Subcellular fractionation assays revealed that AGO1 and miRNAs are associated with polysomes[157]. Further assays showed both AGO1 and miRNAs can be detected in the membrane-bound polysomes (MBPs) fraction, and all miRNAs are preferably associated with MPBs instead of polysomes in general, suggesting miRISC-mediated gene repression might take place on the ER[161]. Indeed, an ER membrane protein, ALTERED MERISTEM PROGRAM1 (AMP1), interacts with AGO1 and is required for translational repression but is dispensable for transcript cleavage, implying that miRNA-mediated translational inhibition occurs on the ER[157]. However, some studies argue that the membrane association of AGO1 might not be the key to determining the regulatory mode of miRISC. Li *et al.* found that the 3’ cleavage products of miRISCs are associated with the MBPs

fraction[161]. In addition, a mutant of 3-HYDROXY-3-METHYLGLUTARYL COA REDUCTASE (HMG1), an enzyme required for the synthesis of essential membrane constituents, showed reduced levels of membrane-bound AGO1 and is compromised in target mRNA cleavage[159]. Together these findings suggest membrane-associated AGO1 could perform both target cleavage and translational repression, and thus the selection of miRISC action might depend on other factors. AGO1 also localizes in P bodies, the cytoplasmic ribonucleoprotein granules comprised of mRNAs and proteins involved in 5′-to-3′ mRNA decay and translational repression[160,162,163]. DRB2, the paralog of HYL1/DRB1, was found to assist in translational repression and repress the expression of *HYL1/DRB1* [164]. A recent study shows that the cytoplasmically localized HYL1 plays an unexpected role in miRNA-mediated translation repression. The authors found that HYL1 is associated with both AGO1 and AMP1, an ER membrane protein[165]. Fluorescence microscopy detection further shows that HYL1 is co-localized with ER[165]. And polysome profiling showed that cytoplasmic HYL1 promotes the distribution of AGO1 on polysomes [165]. Strikingly, cytoplasmic HYL1 binds to miRNA target transcripts, and miRNA-mediated translational repression, but not target mRNA cleavage, is impaired without cytoplasmic HYL1[165].

5.1 Cleave of target transcripts

Plant miRNA-induced target transcript cleavage, also known as slicing, occurs specifically between the 10th and 11th nucleotide from the 5’ end of the miRNA within the region of miRNA-target complementarity[166]. The cleavage

produces a 5’ cleavage fragment and a 3’ cleavage fragment with a 5’ monophosphate, and high-throughput sequencing of RNA with a 5’ monophosphate revealed that most miRNA targets are subject to cleavage[167]. The PIWI domain of AGO1 harbors an RNase H like motif that possesses endonuclease activity[168]. Besides AGO1[10,169], Arabidopsis AGO2[169], AGO4[170], AGO7[169,171], and AGO10[172] have been shown to be capable of cleavage.

After miRISC-mediated cleavage, the 5’ and 3’ cleavage fragments of target mRNA are degraded by exonucleases. In Arabidopsis, the uncapped 3’ cleavage fragments are degraded by the 5’-to-3’ exoribonuclease EXORIBONUCLEASE 4 (XRN4), mutants of which have a higher level of 3’ cleavage fragments[173]. For the 5’ cleavage fragments, an untemplated oligo-uridine or oligo-adenine tail is first added by a nucleotidyltransferase and then degraded by 3'-5' exoribonucleases. In the green alga *Chlamydomonas reinhardtii*, oligo-adenylation by the nucleotidyltransferase MUT68 triggers the degradation of 5’ cleavage fragments by the cytoplasmic exosome[174]. HESO1, the Arabidopsis homolog of *C. reinhardtii* MUT68 and its paralog UTP:RNA URIDYLYL TRANSFERASE 1 (URT1) uridylate 5′ cleavage fragments to trigger their degradation by RISC-INTERACTING CLEARING 3’–to-5’ EXORIBONUCLEASE 1 (RICE1)[175–177]. The cytoplasmic exosome might also participate in 5’ cleavage fragment degradation, as SUPERKILLER2 (SKI2), SKI3, and SKI8, three co-factors of the exosome, are required for this process[178].

5.2 Biogenesis of secondary siRNAs

Some miRISCs do not trigger the immediate degradation of cleaved transcripts. Instead, the 5’ or 3’ cleavage product is converted to dsRNA by RNA-DEPENDENT RNA POLYMERASE 6 (RDR6), and the dsRNA is then cleaved by a Dicer protein, usually DCL4, from the 5’ end of the 3’ cleavage product (or the 3’ end of the 5’ cleavage product) producing siRNAs in a phased configuration, namely phasiRNAs (Figure 1.2 B)[179,180]. RDR6 is recruited by AGO-RISC with the assistance of the dsRNA binding protein SUPPRESSOR OF GENE SILENCING3 (SGS3), which binds directly to the 3’ end of the AGO-loaded miRNA on the target[179,181]. The role of SGS3 is not well understood, it was proposed that SGS3 stabilizes the 3’ cleavage product to protect it from degradation[181]. A recent study shows that the SGS3-miRNA-AGO complex can interrupt ribosome movement resulting in ribosome stalling, which correlates positively with phasiRNA biogenesis[182]. In addition, a recent study shows that SGS3 exhibits liquid–liquid phase separation through its prion-like domains, although it remains unclear whether this property of SGS3 is required for phasiRNA biogenesis[183]. An epigenetic factor FLOWERING LOCUS VE (FVE) has been recently reported to coordinate phasiRNA biogenesis[184]. FVE interacts with and promotes the homodimerization of SGS3 that is required for its function[184]. Furthermore, truncated FVE shows increased binding activity to dsRNA, which affects the association and routing of SGS3-RNA to downstream processing[184].

As in miRNA loading, phasiRNA duplexes are sorted into AGO proteins based on their sequence features[11]. As a result of RDR6 activity, phasiRNA duplexes are perfectly matched and require the cleavage activity of AGO for passenger strand removal[135,137]. As phasiRNA biogenesis occurs in the cytoplasm, it is likely that phasiRNA loading also takes place there. Indeed, an AGO1 mutant retained inside the nucleus showed reduced association with phasiRNAs[153].

In plants, *PHAS* loci can be either non-coding regions or protein-coding genes such as nucleotide binding leucine-rich repeat (*NBS-LRR*) genes and *PENTA-TRICOPEPTIDE REPEAT* (*PPR*) genes[12,185–190]. A subset of phasiRNAs derived from the non-coding *TAS* loci are named trans-acting siRNAs (ta-siRNAs) - they are so called as these 21-nt phasiRNAs target transcripts from other loci for silencing[12,185,191]. In the Arabidopsis Columbia-0 genome, there are 4 *TAS* families comprising eight loci, *TAS1a/b/c*, *TAS2*, *TAS3a/b/c*, and *TAS4*[171,179,185,191,192]. There are two approaches adopted by plants for phasiRNA biogenesis, the “one-hit model” and the “two-hit model”. Most phasiRNAs are produced via the “one-hit model”, for instance, *TAS1a/b/c*- and *TAS2*-derived ta-siRNAs triggered by the AGO1-miR173 complex, and *TAS4*-derived ta-siRNAs triggered by the AGO1-miR828 complex[179,185,192]. In the “one-hit model”, a single 22-nt miRNA directs the cleavage of the target RNA triggering ta-siRNA biogenesis from the 3’ cleavage fragments[179,185,192]. So far, the “two-hit model” is only observed for AGO7-miR390-initiated production of *TAS3a/b/c*-derived ta-siRNAs[193]. In the “two-hit model”, miR390, a 21-nt miRNA trigger, is associated with AGO7 and targets the *TAS3*

transcripts at two distinct locations[193]. The cleavage only occurs at the 3' miR390 binding site, triggering ta-siRNA biogenesis from the 5' cleavage fragments[193]. The 5' binding site of miR390 is not cleaved but remains essential for ta-siRNA biogenesis[193].

5.3 Translational inhibition

mRNA subjected to the regulation of miRNA-mediated translational inhibition show reduced accumulation of protein translated from the mRNA without noticeable changes in the levels of the mRNA itself. Studies in animals suggest mismatched miRNA/target sequences are more prone to translational inhibition, whereas mRNA with a high degree of complementarity to a miRNA is often degraded via cleavage[194]. However, the selection of regulatory mechanisms between plant miRNA and its target does not follow this rule. For instance, Arabidopsis miR172, miR171, miR398, and miR156 translationally inhibit the expression of *APETALA2* (*AP2*), *SCARECROW-LIKE PROTEIN 4* (*SCL4*), *COPPER/ZINC SUPEROXIDE DISMUTASE 2* (*CSD2*), and *SQUAMOSA PROMOTER BINDING PROTEIN-LIKE 3* (*SPL3*), respectively, although there is a high degree of complementarity between the miRNA and its target[34,154–156]. In plants, translational inhibition is not as commonly observed as transcript cleavage, this might be partially due to the lack of specific antibodies to detect the level of target proteins.

Multiple factors have been identified to affect miRNA-mediated translational inhibition including the microtubule-severing enzyme KATANIN 1 (KTN1)[156], the

de-capping component VARICOSE (VCS)[156], the GW-repeat protein SUO[195], and the ER membrane protein AMP1[157]. AMP1 is required for miRNA-mediated translational inhibition but not mRNA cleavage activity[157]. In addition, lack of *AMP1* leads to miRNA target transcripts being significantly increased in the MBP fraction, whereas nontarget transcripts remain unchanged[157]. AMP1 interacts with AGO1, however, this interaction is not required for the membrane association of the AGO1 protein[157]. Together the data indicate miRNA-mediated translational inhibition takes place on the ER. The de-capping component VCS positively impacts translational inhibition; it is localized in the P bodies and is required for the 5'-to-3' degradation of mRNA[156]. SUO colocalizes with the P body component DCP1, which forms a complex with DCP2 and VCS to promote mRNA de-capping, suggesting mRNA de-capping in the P body is involved in miRNA-mediated translational inhibition[195]. The requirement of KTN1, a subunit of the microtubule-severing enzyme that is involved in cortical microtubule array organization, indicates that cytoskeleton dynamics assist miRNA-mediated translational repression[156]. Disruption of the microtubule organization might affect the integrity of cellular compartments required for translational repression.

5.4 Regulation of miRISC activity

Target mimicry has been observed in plants and animals and serves as a mechanism to negatively regulate miRISC activities. In Arabidopsis, miR399 is sequestered by a non-coding transcript from the *IPS1* (*INDUCED BY PHOSPHATE STARVATION 1*) locus, which prevents it from cleaving

PHOSPHATE 2 (*PHO2*) mRNA[196]. *IPS1* is complementarity to miR399, but a 3-nt mismatch at the miRNA cleavage site prevents miR399-mediated cleavage and sequesters miR399 from its other targets, thereby making *IPS1* transcripts a target mimic (TM)[196]. Genome-wide bioinformatic analyses indicate that many long non-coding RNAs and protein-coding transcripts could potentially serve as endogenous target mimics to regulate miRNA activity[197,198].

5.5 Nuclear functions of miRNAs and AGO1

Emerging evidence suggests miRNA and AGO1 can mediate gene expression inside the nucleus at the transcriptional level in addition to their role in miRNA-mediated post-transcriptional gene silencing. In *Oryza sativa*, a group of 24-nt miRNAs processed by DCL3 from pri-miRNAs is loaded into AGO4 based on their size and 5' end nucleotide[51]. These 24-nt miRNA-AGO4 complexes can direct DNA methylation to regulate gene expression in cis and trans, possibly through base-pairing with RNA transcribed from these target loci[51]. Under salinity stress conditions, Arabidopsis AGO1 co-transcriptionally regulates the expression of *MIR161* and *MIR173* in the nucleus[90]. Chromatin Immunoprecipitation (ChIP) revealed that the AGO1 protein accumulates at *MIR161* and *MIR173* loci, and an increased association between AGO1 protein and the stem-loop encoding region was observed under salt treatment[90]. This association negatively regulates the expression of *MIR161* and *MIR173* genes, probably by disassembling the Pol II complex from the DNA template[90]. The authors also showed that the association of AGO1 with chromatin is reduced in *hyl1* mutants in response to salt stress[90]. As

HYL1 is a key factor in miRNA biogenesis, this result suggests that AGO1's chromatin association depends on HYL1 and/or miRNAs. Indeed, AGO1 was detected on *TAS1a/b/c* and *TAS2* transcripts but not on *TAS3*, a target of AGO7-miR390 but not AGO1-miRNA, which implies the involvement of miRNAs in the AGO1-chromatin association[90].

The AGO1-miRNA complex can also positively regulate gene expression via binding to chromatin. Using the ChIP assay, Liu *et al.* showed that under hormone and stress stimuli, Arabidopsis AGO1 binds to actively transcribed gene loci and enhances their transcription in an sRNA- and SWI/SNF (chromatin remodeling complex)-dependent manner[199]. Interestingly, the authors found that nuclear AGO1 associated with a lower ratio of miRNAs and a higher ratio of ta-siRNAs compared with total AGO1, whereas the proportions of other AGO1-associated sRNA species did not show a noticeable change between the two[199]. This observation seems contradictory to the model that miRNA loading occurs inside the nucleus. It is possible that miRNA loading also takes place in the cytoplasm, or AGO1-ta-siRNA complexes are actively transported to the nucleus from the cytoplasm for an unknown reason.

6. miRNA stabilization and turnover

Like miRNA biogenesis, miRNA stabilization and miRNA turnover are crucial for maintaining miRNA homeostasis. During developmental transitions or in response to environmental stresses, fast and efficient degradation of unwanted miRNAs may be essential. In addition, misprocessed isomiRNAs also need to be

properly removed. Processes affecting miRNA stabilization include 2'-O methylation at the 3' ends of miRNAs by HEN1, AGO association[14,200], and 3'-to-5' truncation of free and AGO1-bound miRNAs by the exoribonucleases[201,202]. In addition, non-templated tailing of miRNAs at the 3' end promotes miRNA degradation[126].

6.1 miRNA stabilization

HEN1methylates the miRNA/miRNA* duplex on the 3′ terminus of each strand to protect the miRNA from degradation[14]. The *hen1* mutant shows reduced accumulation of all miRNAs but increased variation in miRNA sizes, which is caused by 3' end truncation and 3' end tailing[14,125,126,201].

It has been shown that AGO-bound miRNAs are less prone to degradation, as a large group of miRNAs (guide strand) show reduced accumulation in *ago1* null mutants[203]. Certain AGO-miRNA pairs can also destabilize miRNA. For instance, Arabidopsis AGO10 shows a higher binding affinity to miR165 and miR166 compared to AGO1, and the association of miR165/166 with AGO10 promotes their degradation by SMALL RNA DEGRADING NUCLEASE 1 (SDN1) and SDN2 *in vivo*[131,132,202]. This competition between AGO10 and AGO1 toward miR165 and miR166 is essential for stem cell homeostasis in the shoot apical meristem (SAM) and leaf polarity[204,205].

6.2 Exonucleases in miRNA degradation

In Arabidopsis, miRNA 3' end truncation is carried out by the SDN family, which comprises four exoribonuclease members with redundant functions in

miRNA destabilization[201]. The *sdn1 sdn2 sdn3* triple mutant causes pleiotropic developmental defects and higher levels of miRNA accumulation[201]. *In vitro* assays showed that SDN1 specifically degrades short single-strand RNA and yields a product 8- to 9-nt long, whereas it has no effects on miRNA/miRNA* duplexes, an oligo-uridine tailed miRNA, or long single-stranded RNAs[201]. The exonuclease activity of SDN1 on miRNA is inhibited by 2′-O-methylation at the 3' end of the miRNA[201]. SDN1 can truncate miRNAs with or without 3' end methylation. Small RNA sequencing of the *sdn1 sdn2* double mutant shows that 3' truncated miRNAs are reduced compared to wild-type[202]. Similarly, the *sdn1 sdn2 hen1* mutant shows a reduced level of 3' truncated miRNAs compared to the *hen1* mutant, in which miRNAs lose 3' end methylation[202]. A further *in vitro* study shows that SDN1 can act on methylated, AGO1-bound miRNAs to trigger their truncation[202].

In addition to SDNs, miRNAs and miRNA*s that lose 2'-O-methylation-dependent protection are partially degraded by ATRIMMER 2 (ATRM2), a DEDDy-type 3′-to-5′ exoribonuclease[206]. Lack of ATRM2 restores the level of a subset of miRNAs in the *hen1* mutant without affecting the truncation and tailing profile, suggesting ATRM2 acts downstream of HEN1-mediated methylation but likely upstream of miRNA 3' end uridylation[206]. As ATRM2 interacts with AGO1, it is possible ATRM2 acts on miRISC or during miRISC assembly[206].

So far, the exonucleases responsible for the degradation of oligo-uridine tailed miRNA or the 5'-to-3' miRNA truncation is still unknown in plants. In animals, DIS3-LIKE 2 (DIS3L2), a 3'-to-5' exonuclease, degrades oligo-uridine tailed RNA,

such as uridylated mouse pre-let-7[207]. In the alga *C. reinhardtii*, the exosome subunit RIBOSOMAL RNA-PROCESSING PROTEIN 6 (RRP6) is capable of degrading oligo-uridine tailed miRNA. SUPPRESSOR OF VARICOSE (SOV) [208] and three RIBOSOMAL RNA-PROCESSING PROTEIN 6-LIKE (RRP6L)[206] genes are the Arabidopsis orthologs of DIS3L2 and RRP6, respectively, making them potential candidates for the degradation of oligo-uridine tailed miRNA. In the nematode *C. elegans*, the 5'-to-3' exonuclease XRN-2 is involved in miRNA degradation[209]. However, XRN2 and XRN3, the Arabidopsis ortholog of *C. elegans* XRN-2, are involved in pri-miRNA degradation without affecting the mature miRNA level[45]. In addition, a study in human cell line shows that the endonuclease TUDOR-SN (TSN) initiates the degradation of both free miRNA and AGO2-loaded miRNA[210].

6.3 miRNA tailing

Non-templated nucleotide addition to the 3′ end of RNA, also known as RNA tailing, is a common and conserved RNA modification that determines the fate of the modified RNA. In Arabidopsis, 3' tailed miRNAs are very low in abundance in the wild-type due to the methyl group protecting miRNAs from being tailed[14]. In Arabidopsis, rice, and maize, levels of oligo-uridine tailed miRNAs are significantly increased in the *hen1* mutant, due to the lack of protection at the 3' end[14,125,126,211,212]. In the Arabidopsis *hen1* mutant, the nucleotidyl transferase HESO1 and its paralog URT1 catalyze the uridylation of unmethylated miRNAs, which leads to their degradation[175,176]. *In vitro* assays show that both HESO1 and

URT1 interact with AGO1 and can tail free unmethylated miRNAs and AGO1-bound unmethylated miRNAs but fail to act on 3' methylated miRNAs[176]. Loss of function in HESO1 or URT1 suppresses the *hen1* phenotype and partially rescues the accumulation of a subset of miRNAs[176]. Loss of function in both HESO1 and URT1 globally abolished miRNA tailing in *hen1*[176]. URT1 acts on only a few miRNAs in the presence of HESO1, however, it plays a more prominent role in miRNA uridylation when HESO1 is missing[176,213]. Interestingly, the majority of 3' tailed miRNAs possess mono uridine in the *hen1 heso1* double mutant, and HESO1 prefers miRNAs with a 3' uridine while URT1 favors 3' adenine[176]. It is possible that URT1 first mono-uridylates miRNAs that possess a 3' adenine that is unfavored by HESO1, and the added uridine could then promote recruitment of HESO1 to produce a long tail.

6.4 Target RNA-directed miRNA degradation

As discussed above, a target mimic RNA could sequester a miRNA from its other targets[196]. Interestingly, animal studies show that a high degree of base pairing between miRNAs and artificial target RNAs results in miRNA destabilization through 3' end truncation and tailing, and this phenomenon is named target RNA-directed miRNA degradation (TDMD)[214]. Similarly, in Arabidopsis, transgenic lines expressing Short Tandem Target Mimic (STTM), an artificially designed RNA composed of two tandem miRNA targeting sites, leads to miRNA destabilization[215,216]. This process requires the activity of SDN1 and SDN2, as in the *sdn1sdn2* double mutant the level of STTM-targeted miRNA is increased[215].

Crystal structure analysis of a *Thermus thermophilus* AGO suggests that extensive base pairing between the guide DNA and its target transcript induces a conformational change of the AGO protein exposing the 3' end of the guide from the binding pocket of AGO[217]. It is possible that target transcripts with a high degree of complementarity to miRNAs could expose the miRNA 3' ends to SDN1, SDN2, HESO1, or URT1 for truncation and tailing.

7. Concluding remarks

Our knowledge of miRNA-mediated gene silencing has greatly increased in the past two decades. Many factors involved in the regulation of miRNA biogenesis, action, and degradation have been identified, however, there are still many unanswered questions regarding when, where, and how are these factors contribute to miRNA processing and activities.

Figures

Figure 1.1. Mechanisms for the biogenesis and loading of plant miRNAs.

(A) *MIR* gene transcription. RNA polymerase II (Pol II)-mediated *MIR* gene transcription is regulated positively and/or negatively by transcription factors. Phosphorylation of Pol II at the C-terminal domain (CTD) of its largest subunit by CDKF;1 and CDKDs promotes *MIR* gene transcription. Phosphorylation is indicated by “P” in the purple circle. Histone acetylation by GCN5 and methylation by PRC2 of *MIR* loci are indicated by “A” in a black circle and “M” in a red circle, respectively.

(B) Pri-miRNA processing in the base-to-loop mode. The capped and poly-A tailed pri-miRNA folds into a stem-loop structure that harbors mismatches, and is cleaved by the dicing complex into precursor miRNA (pre-miRNA). The pre-miRNA is further cleaved by the dicing complex to release an approximately 21-nt long miRNA/miRNA* duplex with a 2-nt 3’ overhang on each strand. The duplex is 2’-O methylated at the 3’ ends by HEN1 (the methyl group is marked with “M” in a green square). miRNA strand is highlighted in red color.

(C) miRNA-induced silencing complex (miRISC) formation. The miRNA/miRNA* duplex is loaded into AGO1 and following unwinding, the miRNA strand is selectively retained with AGO1, while the miRNA* strand is ejected. The miRISCs are exported to the cytoplasm through the nuclear pore in the CRM1/EXPO1-dependent pathway. Whether other mechanisms underlie AGO1 and/or miRISC nucleo-cytosolic shuttling is still unknown. The miRNA and miRNA* strands are

highlighted in red and blue color, respectively. The methyl group at the 3’ end is marked with “M” in a green rectangle.

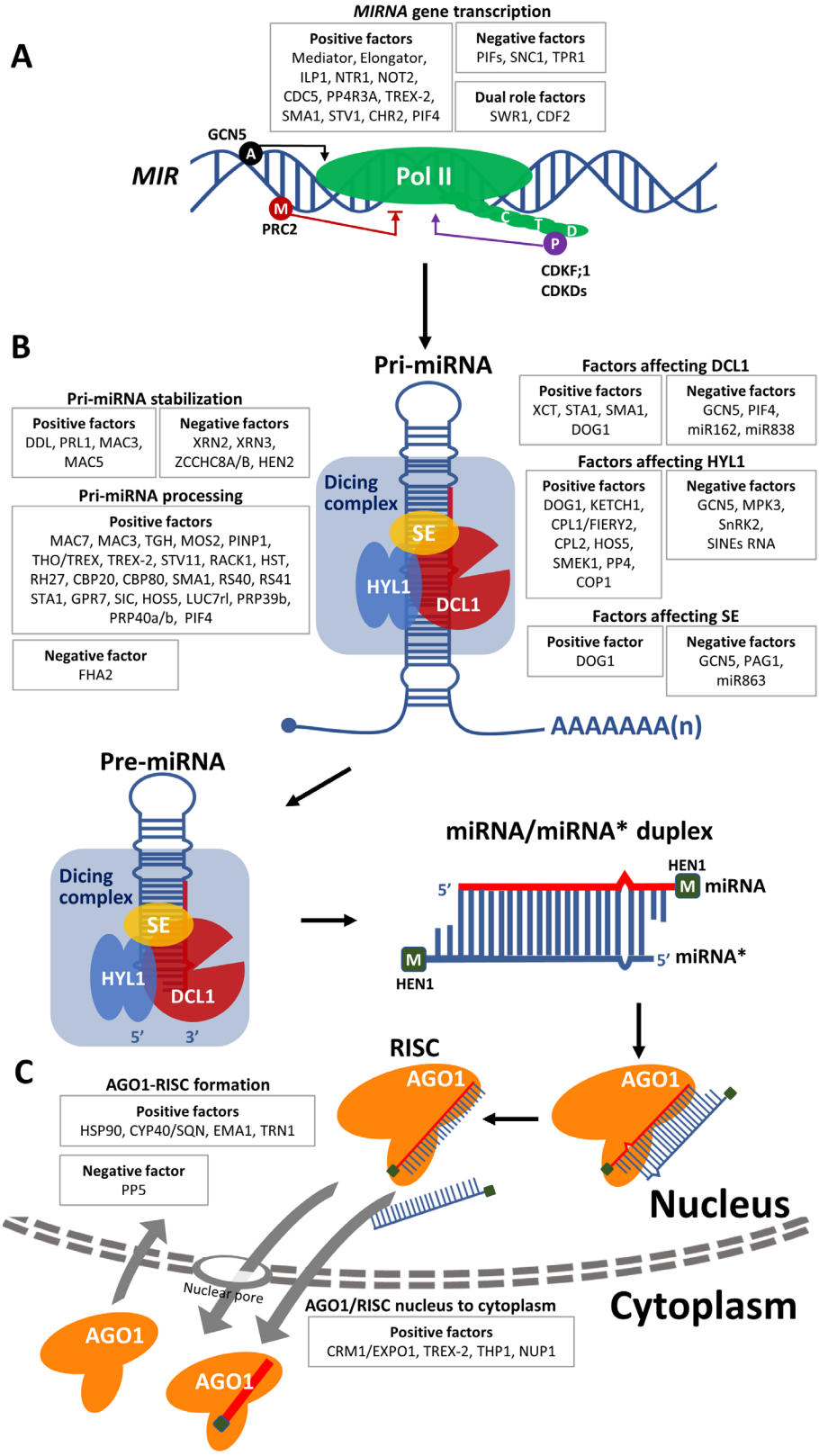
A
MIRNA gene transcription
Positive factors
Mediator, Elongator, ILP1, NTR1, NOT2, CDC5, PP4R3A, TREX-2, SMA1, STV1, CHR2, PIF4
Negative factors
PIFs, SNC1, TPR1
Dual role factors
SWR1, CDF2
GCN5
A
MIR
Pol II
M
PRC2
C
T
D
P
CDKF;1
CDKDs
B
Pri-miRNA
Pri-miRNA stabilization
Positive factors
DDL, PRL1, MAC3, MAC5
Negative factors
XRN2, XRN3, ZCCHC8A/B, HEN2
Pri-miRNA processing
Positive factors
MAC7, MAC3, TGH, MOS2, PINP1, THO/TREX, TREX-2, STV11, RACK1, HST, RH27, CBP20, CBP80, SMA1, RS40, RS41 STA1, GPR7, SIC, HOS5, LUC7rl, PRP39b, PRP40a/b, PIF4
Negative factor
FHA2
Dicing complex
SE
HYL1
DCL1
AAAAAAA(n)
Factors affecting DCL1
Positive factors
XCT, STA1, SMA1, DOG1
Negative factors
GCN5, PIF4, miR162, miR838
Factors affecting HYL1
Positive factors
DOG1, KETCH1, CPL1/FIERY2, CPL2, HOS5, SMEK1, PP4, COP1
Negative factors
GCN5, MPK3, SnRK2, SINEs RNA
Factors affecting SE
Positive factor
DOG1
Negative factors
GCN5, PAG1, miR863
Pre-miRNA
Dicing complex
SE
HYL1
DCL1
5′
3′
miRNA/miRNA* duplex
HEN1
M
miRNA
5′
5′ miRNA*
M
HEN1
C
RISC
AGO1
AGO1
AGO1-RISC formation
Positive factors
HSP90, CYP40/SQN, EMA1, TRN1
Negative factor
PP5
Nucleus
Nuclear pore
Cytoplasm
AGO1/RISC nucleus to cytoplasm
Positive factors
CRM1/EXPO1, TREX-2, THP1, NUP1
AGO1
AGO1

Figure 1.2. Modes of action of miRISCs in plants.

(A) miRNA-mediated post-transcriptional gene silencing. After miRISC formation, miRNAs direct post-transcriptional gene silencing through transcript cleavage and translation repression on the ER. The translation repression by miRISC on the ER requires the assistance of AMP1, an ER membrane protein. miRNA methylation at the 3' end is indicated with a green rectangle. Ribosomes are indicated by yellow circles. Both cleavage and translation repression probably also occur in the cytoplasm.

(B) Models of the ta-siRNA biogenesis in Arabidopsis. In the "one-hit" model, as exemplified by Arabidopsis *TAS1A/B/C*, *TAS2,* and *TAS4* transcripts, a single site in the target transcripts is cleaved by a 22-nt miRNA-containing RISCs. In the "two-hits" model, as exemplified by Arabidopsis *TAS3* transcripts, two sites in the target transcripts are targeted by a 21-nt miRNA-containing RISC, with only the 3' target site being cleaved. RDR6 is recruited by miRISCs with the assistance of SGS3 to convert the single-stranded target transcripts into double-stranded RNAs, which are then processed by DCL4 into multiple 21-nt ta-siRNAs in a phased pattern. The double-stranded RNAs are processed from the 5' and the 3' end of the target RNA in the "one-hit" model and the "two-hits" model, respectively. The ta-siRNAs are loaded into an AGO protein to direct target RNA cleavage and/or trigger the biogenesis of phasiRNAs. miRNA, miRNA target transcript, and RDR6-transcribed RNA are in red, blue, and brown color, respectively. miRNA methylation at the 3' end is marked with a green rectangle. Ribosomes are indicated by yellow circles.

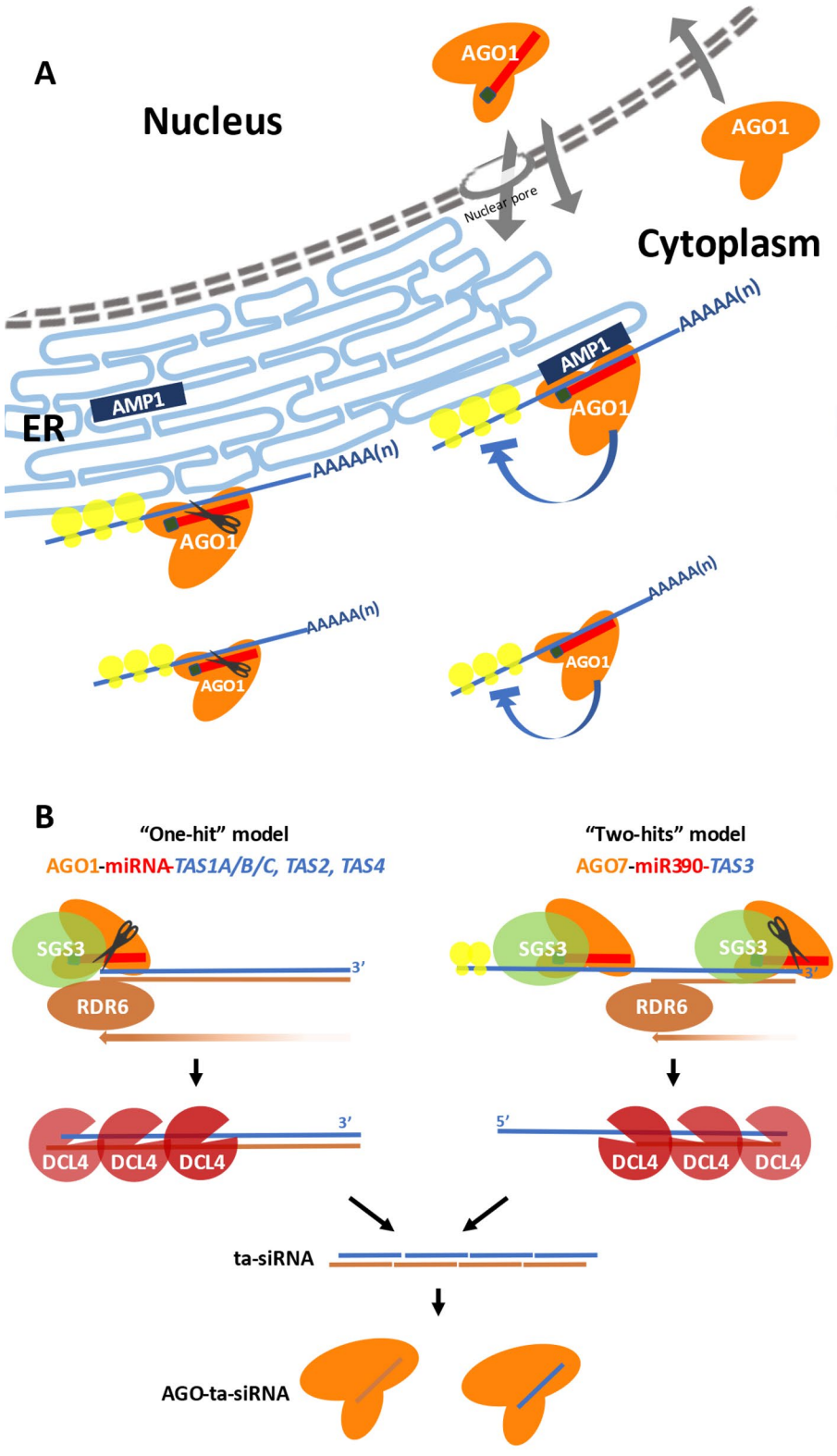
A
Nucleus
AGO1
AGO1
Nuclear pore
Cytoplasm
AAAAA(n)
AMP1
AMP1
AGO1
ER
AAAAA(n)
AGO1
AAAAA(n)
AGO1
AAAAA(n)
AGO1
B
"One-hit" model
AGO1-miRNA-TAS1A/B/C, TAS2, TAS4
"Two-hits" model
AGO7-miR390-TAS3
SGS3
RDR6
3'
SGS3
SGS3
RDR6
3'
DCL4
DCL4
DCL4
3'
5'
DCL4
DCL4
DCL4
ta-siRNA
AGO-ta-siRNA

References

1. Lee, R., Feinbaum, R. & Ambros, V. The C. elegans heterochronic gene lin-4 encodes small RNAs with antisense complementarity to lin-14. Cell 75, 843–854 (1993).
2. Reinhart, B. et al. The 21-nucleotide let-7 RNA regulates developmental timing in Caenorhabditis elegans. Nature 403, 901–906 (2000).
3. Pasquinelli, A. E. et al. Conservation of the sequence and temporal expression of let-7 heterochronic regulatory RNA. Nature 408, 86–89 (2000).
4. Lee, R. C. & Ambros, V. An extensive class of small RNAs in Caenorhabditis elegans. Science 294, 862–864 (2001).
5. Lagos-Quintana, M., Rauhut, R., Lendeckel, W. & Tuschl, T. Identification of novel genes coding for small expressed RNAs. Science 294, 853–858 (2001).
6. Lau, N. C., Lim, L. P., Weinstein, E. G. & Bartel, D. P. An abundant class of tiny RNAs with probable regulatory roles in Caenorhabditis elegans. Science 294, 858–862 (2001).
7. Pfeffer, S. et al. Identification of virus-encoded microRNAs. Science 304, 734–737 (2004).
8. Xie, Z. et al. Expression of Arabidopsis MIRNA genes. Plant Physiol. 138, 2145–2154 (2005).
9. Park, W., Li, J., Song, R., Messing, J. & Chen, X. CARPEL FACTORY, a Dicer homolog, and HEN1, a novel protein, act in microRNA metabolism in Arabidopsis thaliana. Curr. Biol. 12, 1484–1495 (2002).
10. Baumberger, N. & Baulcombe, D. C. Arabidopsis ARGONAUTE1 is an RNA slicer that selectively recruits microRNAs and short interfering RNAs. Proc. Natl. Acad. Sci. U. S. A. 102, 11928–33 (2005).
11. Mi, S. et al. Sorting of small RNAs into Arabidopsis Argonaute complexes is directed by the 5’ terminal nucleotide. Cell 133, 116–127 (2008).
12. Liu, Y., Teng, C., Xia, R. & Meyers, B. C. PhasiRNAs in plants: their biogenesis, genic sources, and roles in stress responses, development, and reproduction. Plant Cell 32, 3059–3080 (2020).
13. Nozawa, M., Miura, S. & Nei, M. Origins and evolution of microRNA genes in plant species. Genome Biol. Evol. 4, 230–239 (2012).
14. Yu, B. et al. Methylation as a crucial step in plant microRNA biogenesis. Science 307, 932–935 (2005).

15. Yan, K. et al. Stress-induced alternative splicing provides a mechanism for the regulation of microRNA processing in Arabidopsis thaliana. Mol. Cell 48, 521–531 (2012).

16. Knop, K. et al. Active 5' splice sites regulate the biogenesis efficiency of Arabidopsis microRNAs derived from intron-containing genes. Nucleic Acids Res. 45, 2757–2775 (2017).

17. Megraw, M. et al. MicroRNA promoter element discovery in Arabidopsis. RNA 12, 1612–1619 (2006).

18. Hajheidari, M., Farrona, S., Huettel, B., Koncz, Z. & Koncz, C. CDKF;1 and CDKD protein kinases regulate phosphorylation of serine residues in the C-terminal domain of arabidopsis RNA polymerase II. Plant Cell 24, 1626–1642 (2012).

19. Kim, Y. J. et al. The role of Mediator in small and long noncoding RNA production in Arabidopsis thaliana. EMBO J. 30, 814–822 (2011).

20. Fang, X., Cui, Y., Li, Y. & Qi, Y. Transcription and processing of primary microRNAs are coupled by Elongator complex in Arabidopsis. Nat. Plants 1, 1–9 (2015).

21. Wang, J. et al. Spliceosome disassembly factors ILP1 and NTR1 promote miRNA biogenesis in Arabidopsis thaliana. Nucleic Acids Res. 47, 7886–7900 (2019).

22. Wang, L. et al. NOT2 proteins promote polymerase II-dependent transcription and interact with multiple microRNA biogenesis factors in Arabidopsis. Plant Cell 25, 715–727 (2013).

23. Zhang, S., Xie, M., Ren, G. & Yu, B. CDC5, a DNA binding protein, positively regulates posttranscriptional processing and/or transcription of primary microRNA transcripts. Proc. Natl. Acad. Sci. U. S. A. 110, 17588–17593 (2013).

24. Wang, S. et al. The PROTEIN PHOSPHATASE4 complex promotes transcription and processing of primary microRNAs in Arabidopsis. Plant Cell 31, 486–501 (2019).

25. Zhang, B. et al. Linking key steps of microRNA biogenesis by TREX-2 and the nuclear pore complex in Arabidopsis. Nat. Plants 6, 957–969 (2020).

26. Li, S. et al. SMA1, a homolog of the splicing factor Prp28, has a multifaceted role in miRNA biogenesis in Arabidopsis. Nucleic Acids Res. 46, 9148–9159 (2018).

27. Li, S. et al. STV1, a ribosomal protein, binds primary microRNA transcripts to promote their interaction with the processing complex in Arabidopsis. Proc. Natl. Acad. Sci. U. S. A. 114, 1424–1429 (2017).

28. Wang, F. & Perry, S. E. Identification of direct targets of FUSCA3, a key regulator of Arabidopsis seed development. Plant Physiol. 161, 1251–1264 (2013).

29. Tian, R. et al. Direct and indirect targets of the arabidopsis seed transcription factor ABSCISIC ACID INSENSITIVE3. Plant J. 103, 1679–1694 (2020).

30. Wu, G. et al. The sequential action of miR156 and miR172 regulates developmental timing in Arabidopsis. Cell 138, 750–759 (2009).

31. Yumul, R. E. et al. POWERDRESS and diversified expression of the MIR172 gene family bolster the floral stem cell network. PLoS Genet. 9, (2013).

32. Yant, L. et al. Orchestration of the floral transition and floral development in arabidopsis by the bifunctional transcription factor APETALA2. Plant Cell 22, 2156–2170 (2010).

33. Grigorova, B. et al. LEUNIG and SEUSS co-repressors regulate miR172 expression in Arabidopsis flowers. Development 138, 2451–2456 (2011).

34. Chen, X. A microRNA as a translational repressor of APETALA2 in Arabidopsis flower development. Science 303, 2022–2025 (2004).

35. Merelo, P. et al. Regulation of MIR165/166 by class II and class III homeodomain leucine zipper proteins establishes leaf polarity. Proc. Natl. Acad. Sci. U. S. A. 113, 11973–11978 (2016).

36. Kim, W. et al. Histone acetyltransferase GCN5 interferes with the miRNA pathway in Arabidopsis. Cell Res. 19, 899–909 (2009).

37. Xu, M., Hu, T., Smith, M. R. & Poethig, R. S. Epigenetic regulation of vegetative phase change in Arabidopsis. Plant Cell 28, 28–41 (2016).

38. Wang, Z. et al. SWI2/SNF2 ATPase CHR2 remodels pri-miRNAs via Serrate to impede miRNA production. Nature 557, 516–521 (2018).

39. Choi, K. et al. Regulation of microRNA-mediated developmental changes by the SWR1 chromatin remodeling complex. Plant Physiol. 171, 1128–1143 (2016).

40. Bajczyk, M. et al. SERRATE interacts with the nuclear exosome targeting (NEXT) complex to degrade primary miRNA precursors in Arabidopsis. Nucleic Acids Res. 48, 6839–6854 (2020).

41. Gao, S. et al. Hyponastic Leaves 1 protects pri-miRNAs from nuclear exosome attack. Proc. Natl. Acad. Sci. U. S. A. 117, 17429–17437 (2020).

42. Yu, B. et al. The FHA domain proteins DAWDLE in Arabidopsis and SNIP1 in humans act in small RNA biogenesis. Proc. Natl. Acad. Sci. U. S. A. 105, 10073–10078 (2008).

43. Zhang, S., Liu, Y. & Yu, B. PRL1, an RNA-binding protein, positively regulates the accumulation of miRNAs and siRNAs in Arabidopsis. PLoS Genet. 10, (2014).

44. Li, S. et al. MAC3A and MAC3B, two core subunits of the MOS4-associated complex, positively influence miRNA biogenesis. Plant Cell 30, 481–494 (2018).

45. Li, S. et al. MAC5, an RNA-binding protein, protects pri-miRNAs from SERRATE-dependent exoribonuclease activities. Proc. Natl. Acad. Sci. U. S. A. 117, 23982–23990 (2020).

46. Hématy, K. et al. The zinc-finger protein SOP1 is required for a subset of the nuclear exosome functions in Arabidopsis. PLoS Genet. 12, 1–22 (2016).

47. Song, L., Axtell, M. J. & Fedoroff, N. V. RNA secondary structural determinants of miRNA precursor processing in Arabidopsis. Curr. Biol. 20, 37–41 (2010).

48. Bologna, N. G., Mateos, J. L., Bresso, E. G. & Palatnik, J. F. A loop-to-base processing mechanism underlies the biogenesis of plant microRNAs miR319 and miR159. EMBO J. 28, 3646–3656 (2009).

49. Qi, Y., Denli, A. M. & Hannon, G. J. Biochemical specialization within Arabidopsis RNA silencing pathways. Mol. Cell 19, 421–428 (2005).

50. Rajagopalan, R., Vaucheret, H., Trejo, J. & Bartel, D. P. A diverse and evolutionarily fluid set of microRNAs in Arabidopsis thaliana. Genes Dev. 20, 3407–3425 (2006).

51. Wu, L. et al. DNA methylation mediated by a microRNA pathway. Mol. Cell 38, 465–475 (2010).

52. Narjala, A., Nair, A., Tirumalai, V., Vivek Hari Sundar, G. & Shivaprasad, P. V. A conserved sequence signature is essential for robust plant miRNA biogenesis. Nucleic Acids Res. 48, 3103–3118 (2020).

53. Zhu, H. et al. Bidirectional processing of pri-miRNAs with branched terminal loops by Arabidopsis Dicer-like1. Nat. Struct. Mol. Biol. 20, 1106–1115 (2013).

54. Moro, B. et al. Efficiency and precision of microRNA biogenesis modes in plants. Nucleic Acids Res. 46, 10709–10723 (2018).

55. Jia, F. & Rock, C. D. MIR846 and MIR842 comprise a cistronic MIRNA pair that is regulated by abscisic acid by alternative splicing in roots of Arabidopsis. Plant Mol. Biol. 81, 447–460 (2013).

56. Bielewicz, D. et al. Introns of plant pri-miRNAs enhance miRNA biogenesis. EMBO Rep. 14, 622–628 (2013).

57. Schwab, R., Speth, C., Laubinger, S. & Voinnet, O. Enhanced microRNA accumulation through stemloop-adjacent introns. EMBO Rep. 14, 615–621 (2013).

58. Iki, T. et al. Structural flexibility enables alternative maturation, ARGONAUTE sorting and activities of miR168, a global gene silencing regulator in plants. Mol. Plant 11, 1008–1023 (2018).

59. Zhang, W. et al. Multiple distinct small RNAs originate from the same microRNA precursors. Genome Biol. 11, R81 (2010).

60. Song, J. et al. Prevalent cytidylation and uridylation of precursor miRNAs in Arabidopsis. Nat. Plants 5, 1260–1272 (2019).

61. Bhat, S. S. et al. mRNA adenosine methylase (MTA) deposits m6A on pri-miRNAs to modulate miRNA biogenesis in Arabidopsis thaliana. Proc. Natl. Acad. Sci. U. S. A. 117, 21785–21795 (2020).

62. Fang, Y. & Spector, D. L. Identification of nuclear dicing bodies containing proteins for microRNA biogenesis in living Arabidopsis plants. Curr. Biol. 17, 818–823 (2007).

63. Song, L., Han, M. H., Lesicka, J. & Fedoroff, N. Arabidopsis primary microRNA processing proteins HYL1 and DCL1 define a nuclear body distinct from the Cajal body. Proc. Natl. Acad. Sci. U. S. A. 104, 5437–5442 (2007).

64. Yang, S. W. et al. Structure of Arabidopsis HYPONASTIC LEAVES1 and its molecular implications for miRNA processing. Structure 18, 594–605 (2010).

65. Dong, Z., Han, M. H. & Fedoroff, N. The RNA-binding proteins HYL1 and SE promote accurate in vitro processing of pri-miRNA by DCL1. Proc Natl Acad Sci U S A 105, 9970–9975 (2008).

66. Kurihara, Y., Takashi, Y. & Watanabe, Y. The interaction between DCL1 and HYL1 is important for efficient and precise processing of pri-miRNA in plant microRNA biogenesis. RNA 12, 206–212 (2006).

67. Yang, X. et al. Homodimerization of HYL1 ensures the correct selection of cleavage sites in primary miRNA. Nucleic Acids Res. 42, 12224–12236 (2014).

68. Iwata, Y., Takahashi, M., Fedoroff, N. V. & Hamdan, S. M. Dissecting the interactions of SERRATE with RNA and DICER-LIKE 1 in Arabidopsis microRNA precursor processing. Nucleic Acids Res. 41, 9129–9140 (2013).

69. Jia, T. et al. The Arabidopsis MOS4-associated complex promotes microRNA biogenesis and precursor messenger RNA splicing. Plant Cell 29, 2626–2643 (2017).

70. Wu, X. et al. A role for the RNA-binding protein MOS2 in microRNA maturation in Arabidopsis. Cell Res. 23, 645–657 (2013).

71. Hou, Y. et al. A Phytophthora Effector suppresses trans-kingdom RNAi to promote disease susceptibility. Cell Host Microbe 25, 153-165.e5 (2019).

72. Xie, D. et al. Phase separation of SERRATE drives dicing body assembly and promotes miRNA processing in Arabidopsis. Nat. Cell Biol. 23, 32–39 (2021).

73. Ren, G. et al. Regulation of miRNA abundance by RNA binding protein TOUGH in Arabidopsis. Proc. Natl. Acad. Sci. U. S. A. 109, 12817–12821 (2012).

74. Francisco-Mangilet, A. G. et al. THO2, a core member of the THO/TREX complex, is required for microRNA production in Arabidopsis. Plant J. 82, 1018–1029 (2015).

75. Cambiagno, D. A. et al. HASTY modulates miRNA biogenesis by linking pri-miRNA transcription and processing. Mol. Plant 14, 426–439 (2021).

76. Speth, C., Willing, E., Rausch, S., Schneeberger, K. & Laubinger, S. RACK1 scaffold proteins influence miRNA abundance in Arabidopsis. Plant J. 76, 433–445 (2013).

77. Hou, X. L. et al. DEAD-BOX RNA HELICASE 27 regulates microRNA biogenesis, zygote division, and stem cell homeostasis. Plant Cell 33, 66–84 (2021).

78. Szarzynska, B. et al. Gene structures and processing of Arabidopsis thaliana HYL1-dependent pri-miRNAs. Nucleic Acids Res. 37, 3083–3093 (2009).

79. Laubinger, S. et al. Dual roles of the nuclear cap-binding complex and SERRATE in pre-mRNA splicing and microRNA processing in Arabidopsis thaliana. Proc. Natl. Acad. Sci. U. S. A. 105, (2008).

80. Raczynska, K. D. et al. The SERRATE protein is involved in alternative splicing in Arabidopsis thaliana. Nucl 42, 1224–1244 (2014).

81. Kim, S. et al. Two cap-binding proteins CBP20 and CBP80 are involved in processing primary microRNAs. Plant Cell Physiol. 49, 1634–1644 (2008).

82. Chen, T., Cui, P. & Xiong, L. The RNA-binding protein HOS5 and serine/arginine-rich proteins RS40 and RS41 participate in miRNA biogenesis in Arabidopsis. Nucleic Acids Res. 43, 8283–8298 (2015).

83. Chaabane, S. Ben et al. STA1, an Arabidopsis pre-mRNA processing factor 6 homolog , is a new player involved in miRNA biogenesis. Nucleic Acids Res. 41, 1984–1997 (2013).

84. Köster, T. et al. Regulation of pri-miRNA processing by the hnRNP-like protein AtGRP7 in Arabidopsis. Nucleic Acids Res. 42, 9925–9936 (2014).

85. Zhan, X. et al. Arabidopsis proline-rich protein important for development and abiotic stress tolerance is involved in microRNA biogenesis. Proc. Natl. Acad. Sci. U. S. A. 109, 18198–18203 (2012).

86. Monaghan, J. et al. Two Prp19-Like U-Box proteins in the MOS4-associated complex play redundant roles in plant innate immunity. PLoS Pathog. 5, e1000526 (2009).

87. Li, Z. et al. Intron lariat RNA inhibits microRNA biogenesis by sequestering the dicing complex in Arabidopsis. PLoS Genet. 12, 1–25 (2016).

88. Fang, X., Shi, Y., Lu, X., Chen, Z. & Qi, Y. CMA33/XCT regulates small RNA production through modulating the transcription of Dicer-Like genes in Arabidopsis. Mol. Plant 8, 1227–1236 (2015).

89. Huo, H., Wei, S. & Bradford, K. J. DELAY OF GERMINATION1 (DOG1) regulates both seed dormancy and flowering time through microRNA pathways. PNAS 1, 2199–2206 (2016).

90. Dolata, J. et al. Salt stress reveals a new role for ARGONAUTE1 in miRNA biogenesis at the transcriptional and posttranscriptional levels. Plant Physiol. 172, 297–312 (2016).

91. Xie, Z., Kasschau, K. D. & Carrington, J. C. Negative feedback regulation of Dicer-Like1 in Arabidopsis by microRNA-guided mRNA degradation. Curr. Biol. 13, 784–789 (2003).

92. Niu, D. et al. miRNA863-3p sequentially targets negative immune regulator ARLPKs and positive regulator SERRATE upon bacterial infection. Nat. Commun. 7, (2016).

93. Zhang, Z. et al. KETCH1 imports HYL1 to nucleus for miRNA biogenesis in Arabidopsis. Proc. Natl. Acad. Sci. U. S. A. 201619755 (2017). doi:10.1073/pnas.1619755114

94. Pouch-Pélissier, M. N. et al. SINE RNA induces severe developmental defects in Arabidopsis thaliana and interacts with HYL1 (DRB1), a key member of the DCL1 complex. PLoS Genet. 4, e1000096 (2008).

95. Li, Y. et al. Degradation of SERRATE via ubiquitin-independent 20S proteasome to survey RNA metabolism. Nat. Plants 6, 970–982 (2020).

96. Machida, S. & Yuan, Y. A. Crystal structure of Arabidopsis thaliana dawdle forkhead-associated domain reveals a conserved phospho-threonine recognition cleft for Dicer-like 1 binding. Mol. Plant 6, 1290–1300 (2013).

97. Zhang, S. et al. DAWDLE interacts with DICER-LIKE proteins to mediate small RNA biogenesis. Plant Physiol. 177, 1142–1151 (2018).

98. Raghuram, B., Sheikh, A. H., Rustagi, Y. & Sinha, A. K. MicroRNA biogenesis factor DRB1 is a phosphorylation target of mitogen activated protein kinase MPK3 in both rice and Arabidopsis. FEBS J. 282, 521–536 (2015).

99. Yan, J. et al. The SnRK2 kinases modulate miRNA accumulation in Arabidopsis. PLoS Genet. 13, 1–21 (2017).

100. Manavella, P. A. et al. Fast-forward genetics identifies plant CPL phosphatases as regulators of miRNA processing factor HYL1. Cell 151, 859–870 (2012).

101. Karlsson, P. et al. KH domain protein RCF3 is a tissue-biased regulator of the plant miRNA biogenesis cofactor HYL1. Proc. Natl. Acad. Sci. U. S. A. 112, 14096–14101 (2015).

102. Su, C. et al. The protein phosphatase 4 and SMEK1 complex dephosphorylates HYL1 to promote miRNA biogenesis by antagonizing the MAPK cascade in Arabidopsis. Dev. Cell 41, 527-539.e5 (2017).

103. Xie, Y. et al. Phytochrome-interacting factors directly suppress MIR156 expression to enhance shade-avoidance syndrome in Arabidopsis. Nat. Commun. 8, (2017).

104. Zhang, H. et al. Genome-wide mapping of the HY5-mediated gene networks in Arabidopsis that involve both transcriptional and post-transcriptional regulation. Plant J. 65, 346–358 (2011).

105. Tsai, H. L. et al. HUA ENHANCER1 is involved in posttranscriptional regulation of positive and negative regulators in Arabidopsis photomorphogenesis. Plant Cell 26, 2858–2872 (2014).

106. Jagadeeswaran, G., Li, Y. F. & Sunkar, R. Redox signaling mediates the expression of a sulfate-deprivation-inducible microRNA395 in Arabidopsis. Plant J. 77, 85–96 (2014).

107. Kawashima, C. G. et al. Sulphur starvation induces the expression of microRNA-395 and one of its target genes but in different cell types. Plant J. 57, 313–321 (2009).

108. Hsieh, L. C. et al. Uncovering small RNA-mediated responses to phosphate deficiency in Arabidopsis by deep sequencing. Plant Physiol. 151, 2120–2132 (2009).

109. Fujii, H., Chiou, T. J., Lin, S. I., Aung, K. & Zhu, J. K. A miRNA involved in phosphate-starvation response in Arabidopsis. Curr. Biol. 15, 2038–2043 (2005).

110. Beauclair, L., Yu, A. & Bouche, N. microRNA-directed cleavage and translational repression of the copper chaperone for superoxide dismutase mRNA in Arabidopsis. Plant J. 62, 454–462 (2010).

111. Yamasaki, H. et al. Regulation of copper homeostasis by micro-RNA in Arabidopsis. J. Biol. Chem. 282, 16369–16378 (2007).

112. Guan, Q., Lu, X., Zeng, H., Zhang, Y. & Zhu, J. Heat stress induction of miR398 triggers a regulatory loop that is critical for thermotolerance in Arabidopsis. Plant J. 74, 840–851 (2013).

113. Fang, X. et al. Chloroplast-to-nucleus signaling regulates microRNA biogenesis in Arabidopsis. Dev. Cell 48, 371-382.e4 (2019).

114. Baev, V. et al. Insight into small RNA abundance and expression in high- and low-temperature stress response using deep sequencing in Arabidopsis. Plant Physiol. Biochem. 84, 105–114 (2014).

115. Lee, B., Kapoor, A., Zhu, J. & Zhu, J. STABILIZED1, a stress-upregulated nuclear protein , is required for pre-mRNA splicing , mRNA turnover , and stress tolerance in Arabidopsis. Plant Cell 18, 1736–1749 (2006).

116. Fornara, F. et al. Arabidopsis DOF transcription factors act redundantly to reduce CONSTANS expression and are essential for a photoperiodic flowering response. Dev. Cell 17, 75–86 (2009).

117. Sun, Z., Guo, T., Liu, Y., Liu, Q. & Fang, Y. The roles of Arabidopsis CDF2 in transcriptional and posttranscriptional regulation of primary microRNAs. PLoS Genet. 11, 1–19 (2015).

118. Cai, Q. et al. The disease resistance protein SNC1 represses the biogenesis of microRNAs and phased siRNAs. Nat. Commun. 9, 1–14 (2018).

119. Cho, S. K., Chaabane, S. Ben, Shah, P., Poulsen, C. P. & Yang, S. W. COP1 E3 ligase protects HYL1 to retain microRNA biogenesis. Nat. Commun. 1–10 (2014). doi:10.1038/ncomms6867

120. Choi, S. W. et al. Light triggers the miRNA-biogenetic inconsistency for de-etiolated seedling survivability in Arabidopsis thaliana. Mol. Plant 13, 431–445 (2020).

121. Park, S. J. et al. Light-stabilized FHA2 suppresses miRNA biogenesis through interactions with DCL1 and HYL1. Mol. Plant 14, 647–663 (2021).

122. Achkar, N. P. et al. A quick HYL1-dependent reactivation of microRNA production is required for a proper developmental response after extended periods of light deprivation. Dev. Cell 46, 236-247.e6 (2018).

123. Sun, Z. et al. Coordinated regulation of Arabidopsis microRNA biogenesis and red light signaling through Dicer-like 1 and phytochrome-interacting factor 4. PLoS Genet. 14, 1–21 (2018).

124. Jiang, J. et al. The Arabidopsis RNA binding protein with K homology motifs, SHINY1, interacts with the C-terminal domain Phosphatase-like 1 (CPL1) to repress stress-inducible gene expression. PLoS Genet. 9, (2013).

125. Yang, Z., Ebright, Y. W., Yu, B. & Chen, X. HEN1 recognizes 21-24 nt small RNA duplexes and deposits a methyl group onto the 2′ OH of the 3′ terminal nucleotide. Nucleic Acids Res. 34, 667–675 (2006).

126. Li, J., Yang, Z., Yu, B., Liu, J. & Chen, X. Methylation protects miRNAs and siRNAs from a 3′-end uridylation activity in Arabidopsis. Curr. Biol. 15, 1501–1507 (2005).

127. Baranauske, S. et al. Functional mapping of the plant small RNA methyltransferase: HEN1 physically interacts with HYL1 and DICER-LIKE 1 proteins. Nucleic Acids Res. 43, 2802–2812 (2015).

128. Eamens, A. L., Smith, N. A., Curtin, S. J., Wang, M.-B. & Waterhouse, P. M. The Arabidopsis thaliana double-stranded RNA binding protein DRB1 directs guide strand selection from microRNA duplexes. RNA 15, 2219–35 (2009).

129. Tomari, Y., Matranga, C., Haley, B., Martinez, N. & Zamore, P. D. A protein sensor for siRNA asymmetry. Science 306, 1377–1380 (2004).

130. Zhang, X. et al. ARGONAUTE PIWI domain and microRNA duplex structure regulate small RNA sorting in Arabidopsis. Nat. Commun. 5, 5468 (2014).

131. Zhu, H. et al. Arabidopsis Argonaute10 specifically sequesters miR166/165 to regulate shoot apical meristem development. Cell 145, 242–256 (2011).

132. Zhou, Y. et al. Spatiotemporal sequestration of miR165/166 by arabidopsis argonaute10 promotes shoot apical meristem maintenance. Cell Rep. 10, 1819–1827 (2015).

133. Zhang, X. et al. Arabidopsis Argonaute 2 regulates innate immunity via miRNA393*-mediated silencing of a Golgi-localized SNARE gene, MEMB12. Mol. Cell 42, 356–366 (2011).

134. Kozomara, A. & Griffiths-Jones, S. MiRBase: Annotating high confidence microRNAs using deep sequencing data. Nucleic Acids Res. 42, 68–73 (2014).

135. Iki, T. et al. In vitro assembly of plant RNA-induced silencing complexes facilitated by molecular chaperone HSP90. Mol. Cell 39, 282–291 (2010).

136. Iwasaki, S. et al. Hsc70/Hsp90 chaperone machinery mediates ATP-dependent RISC loading of small RNA duplexes. Mol. Cell 39, 292–299 (2010).

137. Arribas-Hernández, L. et al. The slicer activity of ARGONAUTE1 is required specifically for the phasing, not production, of trans-acting short interfering RNAs in Arabidopsis. Plant Cell 28, 1563–1580 (2016).

138. Iki, T., Yoshikawa, M., Meshi, T. & Ishikawa, M. Cyclophilin 40 facilitates HSP90-mediated RISC assembly in plants. EMBO J. 31, 267–278 (2012).

139. Wang, W. et al. An importin beta protein negatively regulates microRNA activity in Arabidopsis. Plant Cell 23, 3565–3576 (2011).

140. Cui, Y., Fang, X. & Qi, Y. TRANSPORTIN1 promotes the association of microRNA with ARGONAUTE1 in Arabidopsis. Plant Cell 28, 2576–2585 (2016).

141. Vaucheret, H., Mallory, A. C. & Bartel, D. P. AGO1 homeostasis entails coexpression of MIR168 and AGO1 and preferential stabilization of miR168 by AGO1. Mol. Cell 22, 129–136 (2006).

142. Earley, K., Smith, M. R., Weber, R., Gregory, B. D. & Poethig, R. S. An endogenous F-box protein regulates ARGONAUTE1 in Arabidopsis thaliana. Silence 1, 1–10 (2010).

143. Baumberger, N., Tsai, C. H., Lie, M., Havecker, E. & Baulcombe, D. C. C. The Polerovirus silencing suppressor P0 targets ARGONAUTE proteins for degradation. Curr. Biol. 17, 1609–1614 (2007).

144. Fusaro, A. F. et al. The Enamovirus P0 protein is a silencing suppressor which inhibits local and systemic RNA silencing through AGO1 degradation. Virology 426, 178–187 (2012).

145. Derrien, B. et al. Degradation of the antiviral component ARGONAUTE1 by the autophagy pathway. Proc. Natl. Acad. Sci. U. S. A. 109, 15942–15946 (2012).

146. Chiu, M. H., Chen, I. H., Baulcombe, D. C. & Tsai, C. H. The silencing suppressor P25 of Potato virus X interacts with Argonaute1 and mediates its degradation through the proteasome pathway. Mol. Plant Pathol. 11, 641–649 (2010).

147. Ré, D. A. et al. CURLY LEAF regulates microRNA activity by controlling ARGONAUTE 1 degradation in plants. Mol. Plant 13, 72–87 (2020).

148. Lund, E., Güttinger, S., Calado, A., Dahlberg, J. E. & Kutay, U. Nuclear export of microRNA precursors. Science 303, 95–98 (2004).

149. Bohnsack, M. T., Czaplinski, K. & Görlich, D. Exportin 5 is a RanGTP-dependent dsRNA-binding protein that mediates nuclear export of pre-miRNAs. RNA 10, 185–191 (2004).

150. Yi, R., Qin, Y., Macara, I. G. & Cullen, B. R. Exportin-5 mediates the nuclear export of pre-microRNAs and short hairpin RNAs. Genes Dev. 17, 3011–3016 (2003).

151. Mee Yeon, P., Wu, G., Gonzalez-Sulser, A., Vaucheret, H. & Poethig, R. S. Nuclear processing and export of microRNAs in Arabidopsis. Proc. Natl. Acad. Sci. U. S. A. 102, 3691–3696 (2005).

152. Zhu, J. et al. CRD1, an Xpo1 domain protein, regulates miRNA accumulation and crown root development in rice. Plant J. 100, 328–342 (2019).

153. Bologna, N. G. et al. Nucleo-cytosolic shuttling of ARGONAUTE1 prompts a revised model of the plant microRNA pathway. Mol. Cell 69, 709-719.e5 (2018).

154. Gandikota, M. et al. The miRNA156/157 recognition element in the 3′ UTR of the Arabidopsis SBP box gene SPL3 prevents early flowering by translational inhibition in seedlings. Plant J. 49, 683–693 (2007).

155. Aukerman, M. J. & Sakai, H. Regulation of flowering time and floral organ identity by a microRNA and its Apetala2-Like target genes. Plant Cell 15, 2730–3741 (2004).

156. Brodersen, P. et al. Widespread translational inhibition by plant miRNAs and siRNAs. Science 320, 1185–1190 (2008).

157. Li, S. et al. MicroRNAs inhibit the translation of target mRNAs on the endoplasmic reticulum in Arabidopsis. Cell 153, 562–574 (2013).

158. Alonso-Peral, M. M. et al. The microRNA159-regulated GAMYB-like genes inhibit growth and promote programmed cell death in Arabidopsis. Plant Physiol. 154, 757–771 (2010).

159. Brodersen, P. et al. Isoprenoid biosynthesis is required for miRNA function and affects membrane association of ARGONAUTE 1 in Arabidopsis. Proc. Natl. Acad. Sci. U. S. A. 109, 1778–1783 (2012).

160. Pomeranz, M. C. et al. The Arabidopsis tandem zinc finger protein AtTZF1 traffics between the nucleus and cytoplasmic foci and binds both DNA and RNA. Plant Physiol. 152, 151–165 (2010).

161. Li, S. et al. Biogenesis of phased siRNAS on membrane-bound polysomes in Arabidopsis. Elife 5, e22750 (2016).

162. Xu, J. & Chua, N. H. Processing bodies and plant development. Curr. Opin. Plant Biol. 14, 88–93 (2011).

163. Hubstenberger, A. et al. P-Body purification reveals the condensation of repressed mRNA regulons. Mol. Cell 68, 144-157.e5 (2017).

164. Reis, R. S., Hart-Smith, G., Eamens, A. L., Wilkins, M. R. & Waterhouse, P. M. Gene regulation by translational inhibition is determined by Dicer partnering proteins. Nat. Plants 1, 1–6 (2015).

165. Yang, X. et al. Cytoplasmic HYL1 modulates miRNA-mediated translational repression. Plant Cell 33, 1980–1996 (2021).

166. Kasschau, K. D. et al. P1/HC-Pro, a viral suppressor of RNA silencing, interferes with Arabidopsis development and miRNA function. Dev. Cell 4, 205–217 (2003).

167. German, M. A. et al. Global identification of microRNA-target RNA pairs by parallel analysis of RNA ends. Nat. Biotechnol. 26, 941–946 (2008).

168. Song, J. J., Smith, S. K., Hannon, G. J. & Joshua-Tor, L. Crystal structure of argonaute and its implications for RISC slicer activity. Science 305, 1434–1437 (2004).

169. Carbonell, A. et al. Functional analysis of three Arabidopsis ARGONAUTES using slicer-defective mutants. Plant Cell 24, 3613–3629 (2012).

170. Qi, Y. et al. Distinct catalytic and non-catalytic roles of ARGONAUTE4 in RNA-directed DNA methylation. Nature 443, 1008–1012 (2006).

171. Montgomery, T. A. et al. Specificity of ARGONAUTE7-miR390 Interaction and Dual Functionality in TAS3 Trans-Acting siRNA Formation. Cell 133, 128–141 (2008).

172. Ji, L. et al. ARGONAUTE10 and ARGONAUTE1 regulate the termination of floral stem cells through two microRNAs in Arabidopsis. PLoS Genet. 7, 1–14 (2011).

173. Souret, F. F., Kastenmayer, J. P. & Green, P. J. AtXRN4 degrades mRNA in Arabidopsis and its substrates include selected miRNA targets. Mol. Cell 15, 173–183 (2004).

174. Ibrahim, F. et al. Uridylation of mature miRNAs and siRNAs by the MUT68 nucleotidyltransferase promotes their degradation in Chlamydomonas. Proc. Natl. Acad. Sci. U. S. A. 107, 3906–3911 (2010).

175. Ren, G. et al. Methylation protects microRNAs from an AGO1-associated activity that uridylates 5' RNA fragments generated by AGO1 cleavage. Proc. Natl. Acad. Sci. U. S. A. 111, 6365–6370 (2014).

176. Tu, B. et al. Distinct and cooperative activities of HESO1 and URT1 nucleotidyl transferases in microRNA turnover in Arabidopsis. PLOS Genet. 11, e1005119 (2015).

177. Zhang, Z. et al. RISC-interacting clearing 3'- 5' exoribonucleases (RICES) degrade uridylated cleavage fragments to maintain functional RISC in Arabidopsis thaliana. Elife 6, 1–29 (2017).

178. Branscheid, A. et al. SKI2 mediates degradation of RISC 5'-cleavage fragments and prevents secondary siRNA production from miRNA targets in Arabidopsis. Nucleic Acids Res. 43, 10975–10988 (2015).

179. Yoshikawa, M., Peragine, A., Park, M. Y. & Poethig, R. S. A pathway for the biogenesis of trans-acting siRNAs in Arabidopsis. Genes Dev. 19, 2164–75 (2005).

180. Gasciolli, V., Mallory, A. C., Bartel, D. P. & Vaucheret, H. Partially redundant functions of arabidopsis DICER-like enzymes and a role for DCL4 in producing trans-acting siRNAs. Curr. Biol. 15, 1494–1500 (2005).

181. Yoshikawa, M. et al. 3′ fragment of miR173-programmed RISC-cleaved RNA is protected from degradation in a complex with RISC and SGS3. Proc. Natl. Acad. Sci. U. S. A. 110, 4117–4122 (2013).

182. Iwakawa, H. oki et al. Ribosome stalling caused by the Argonaute-microRNA-SGS3 complex regulates the production of secondary siRNAs in plants. Cell Rep. 35, 109300 (2021).

183. Kim, E. Y. et al. Ribosome stalling and SGS3 phase separation prime the epigenetic silencing of transposons. Nat. Plants 7, 303–309 (2021).

184. Sun, D. et al. The epigenetic factor FVE orchestrates cytoplasmic SGS3-DRB4-DCL4 activities to promote transgene silencing in Arabidopsis. Sci. Adv. 7, eabf3898 (2021).

185. Chen, H. M. et al. 22-Nucleotide RNAs trigger secondary siRNA biogenesis in plants. Proc. Natl. Acad. Sci. U. S. A. 107, 15269–15274 (2010).

186. Zhai, J. et al. MicroRNAs as master regulators of the plant NB-LRR defense gene family via the production of phased, trans-acting siRNAs. Genes Dev. 25, 2540–2553 (2011).

187. Fei, Q., Li, P., Teng, C. & Meyers, B. C. Secondary siRNAs from Medicago NB-LRRs modulated via miRNA-target interactions and their abundances. Plant J. 83, 451–465 (2015).

188. Howell, M. D. et al. Genome-wide analysis of the RNA-DEPENDENT RNA POLYMERASE6/DICER-LIKE4 pathway in Arabidopsis reveals dependency on miRNA- and tasiRNA-directed targeting. Plant Cell 19, 926–942 (2007).

189. Xia, R. et al. MicroRNA superfamilies descended from miR390 and their roles in secondary small interfering RNA biogenesis in eudicots. Plant Cell 25, 1555–1572 (2013).

190. Xia, R., Xu, J., Arikit, S. & Meyers, B. C. Extensive families of miRNAs and PHAS loci in Norway spruce demonstrate the origins of complex phasiRNA networks in seed plants. Mol. Biol. Evol. 32, 2905–2918 (2015).

191. Cuperus, J. T. et al. Unique functionality of 22-nt miRNAs in triggering RDR6-dependent siRNA biogenesis from target transcripts in Arabidopsis. Nat. Struct. Mol. Biol. 17, 997–1003 (2010).

192. Allen, E., Xie, Z., Gustafson, A. M. & Carrington, J. C. microRNA-directed phasing during trans-acting siRNA biogenesis in plants. Cell 121, 207–221 (2005).

193. Axtell, M. J., Jan, C., Rajagopalan, R. & Bartel, D. P. A Two-Hit trigger for siRNA biogenesis in plants. Cell 127, 565–577 (2006).

194. Fabian, M. R., Sonenberg, N. & Filipowicz, W. Regulation of mRNA translation and stability by microRNAs. Annu. Rev. Biochem. 79, 351–379 (2010).

195. Yang, L., Wu, G. & Poethig, R. S. Mutations in the GW-repeat protein SUO reveal a developmental function for microRNA-mediated translational repression in Arabidopsis. Proc. Natl. Acad. Sci. U. S. A. 109, 315–320 (2012).

196. Franco-Zorrilla, J. M. et al. Target mimicry provides a new mechanism for regulation of microRNA activity. Nat. Genet. 39, 1033–1037 (2007).

197. Ivashuta, S. et al. Regulation of gene expression in plants through miRNA inactivation. PLoS One 6, (2011).

198. Wu, H. J., Wang, Z. M., Wang, M. & Wang, X. J. Widespread long noncoding RNAs as endogenous target mimics for microRNAs in plants. Plant Physiol. 161, 1875–1884 (2013).

199. Liu, C. et al. Arabidopsis ARGONAUTE1 binds chromatin to promote gene transcription in response to hormones and stresses. Dev. Cell 44, 348-361.e7 (2018).

200. Vaucheret, H., Vazquez, F., Crété, P. & Bartel, D. P. The action of ARGONAUTE1 in the miRNA pathway and its regulation by the miRNA pathway are crucial for plant development. Genes Dev. 18, 1187–1197 (2004).

201. Ramachandran, V. & Chen, X. Degradation of microRNAs by a family of exoribonucleases in Arabidopsis. Science 321, 1490–1492 (2008).

202. Yu, Y. et al. ARGONAUTE10 promotes the degradation of miR165/6 through the SDN1 and SDN2 exonucleases in Arabidopsis. PLoS Biol. 15, 1–26 (2017).

203. Bohmert, K. et al. AGO1 defines a novel locus of Arabidopsis controlling leaf development. EMBO J. 17, 170–180 (1998).

204. Lynn, K. et al. The PINHEAD/ZWILLE gene acts pleiotropically in Arabidopsis development and has overlapping functions with the ARGONAUTE1 gene. Development 126, 469–481 (1999).

205. Moussian, B., Schoof, H., Haecker, A., Jürgens, G. & Laux, T. Role of the ZWILLE gene in the regulation of central shoot meristem cell fate during Arabidopsis embryogenesis. EMBO J. 17, 1799–1809 (1998).

206. Wang, X. et al. Degradation of unmethylated miRNA/miRNA*s by a DEDDy-type 3′ to 5′ exoribonuclease Atrimmer 2 in Arabidopsis. Proc. Natl. Acad. Sci. U. S. A. 115, E6659–E6667 (2018).

207. Chang, H. M., Triboulet, R., Thornton, J. E. & Gregory, R. I. A role for the Perlman syndrome exonuclease Dis3l2 in the Lin28-let-7 pathway. Nature 497, 244–248 (2013).

208. Zhang, W., Murphy, C. & Sieburth, L. E. Conserved RNaseII domain protein functions in cytoplasmic mRNA decay and suppresses Arabidopsis decapping mutant phenotypes. Proc. Natl. Acad. Sci. U. S. A. 107, 15981–15985 (2010).

209. Chatterjee, S. & Großhans, H. Active turnover modulates mature microRNA activity in Caenorhabditis elegans. Nature 461, 546–549 (2009).

210. Elbarbary, R. A. et al. Tudor-SN-mediated endonucleolytic decay of human cell microRNAs promotes G1/S phase transition. Science 356, 859–862 (2017).

211. Zhai, J. et al. Plant microRNAs display differential 3’ truncation and tailing modifications that are ARGONAUTE1 dependent and conserved across species. Plant Cell 25, 2417–2428 (2013).

212. Abe, M. et al. WAVY LEAF1, an ortholog of arabidopsis HEN1, regulates shoot development by maintaining microRNA and trans-acting small interfering RNA accumulation in rice. Plant Physiol. 154, 1335–1346 (2010).

213. Zuber, H., Scheer, H., Joly, A. C. & Gagliardi, D. Respective contributions of URT1 and HESO1 to the uridylation of 5′ fragments produced from RISC-Cleaved mRNAs. Front. Plant Sci. 9, 1–14 (2018).

214. la Mata, M. et al. Potent degradation of neuronal mi RNA s induced by highly complementary targets. EMBO Rep. 16, 500–511 (2015).

215. Yan, J. et al. Effective small RNA destruction by the expression of a short tandem target mimic in Arabidopsis. Plant Cell 24, 415–427 (2012).

216. Todesco, M., Rubio-Somoza, I., Paz-Ares, J. & Weigel, D. A collection of target mimics for comprehensive analysis of MicroRNA function in Arabidopsis thaliana. PLoS Genet. 6, 1–10 (2010).

217. Sheng, G. et al. Structure-based cleavage mechanism of Thermus thermophilus argonaute DNA guide strand-mediated DNA target cleavage. Proc. Natl. Acad. Sci. U. S. A. 111, 652–657 (2014).

Chapter 2

The N-terminal extension of Arabidopsis ARGONAUTE 1 is essential for microRNA activities

Abstract

microRNAs (miRNAs) regulate target gene expression through their ARGONAUTE (AGO) effector protein, mainly AGO1 in *Arabidopsis thaliana*. In addition to the highly conserved N, PAZ, MID and PIWI domains with known roles in RNA silencing, AGO1 contains a long, unstructured N-terminal extension (NTE) of little known function. Here, we show that the NTE is indispensable for the functions of Arabidopsis AGO1, as a lack of the NTE leads to seedling lethality. Within the NTE, the region containing amino acids (a.a.) 91 to 189 is essential for rescuing an *ago1* null mutant. Through global analyses of small RNAs, AGO1-associated small RNAs, and miRNA target gene expression, we show that the region containing a.a. 91-189 is required for the loading of miRNAs into AGO1. Furthermore, we show that the 1-to-90a.a. and 91-to-189a.a. regions of the NTE redundantly promote the activities of AGO1 in the biogenesis of trans-acting siRNAs. Together, we report novel roles of the NTE of Arabidopsis AGO1.

Introduction

In eukaryotes, microRNAs (miRNAs) are ~19-to-24 nucleotide (nt) long endogenous non-coding RNAs that regulate gene expression at the post-transcriptional level through sequence complementarity with target transcripts. In plants, miRNA-mediated gene silencing is essential for a broad range of biological processes, including growth, development, and responses to abiotic and biotic stresses[1,2]. The *MIRNA* (*MIR*) genes are transcribed into long primary miRNA (pri-miRNA) transcripts by RNA POLYMERASE II in a manner similar to that of protein-coding genes[3]. The imperfect stem-loop structures of pri-miRNAs are recognized and cropped to produce pre-miRNAs by DICER-LIKE 1 (DCL1), an RNase III family enzyme, which further processes pre-miRNAs to produce miRNA duplexes with 2-nt overhangs at the 3′ ends of each strand[4]. The miRNA duplexes are 2'-O-methylated by the methyltransferase HEN1 at the 3′ terminus of each strand[5]. The duplex is loaded into an ARGONAUTE (AGO) protein to form a miRNA-induced silencing complex (miRISC). During miRISC formation, the duplex is unwound and one strand of the duplex is selected as the miRNA (or the guide strand), while the other strand called miRNA* (or the passenger strand) is ejected[6]. Most plant miRNAs are preferentially loaded into AGO1, which prefer miRNAs with a 5' uridine (U)[7]. A miRISC binds to a target messenger RNA (mRNA) with sequence complementary to the miRNA, leading to the degradation or translational repression of the target transcript.

In plants, certain miRISCs, such as AGO1-miR173 and AGO7-miR390, can trigger the biogenesis of small interfering RNAs (siRNAs) from their target transcripts[8]. Upon cleavage of the target transcripts by these miRISCs, the cleaved products are converted to double-stranded RNAs (dsRNAs) by RNA-DEPENDENT RNA POLYMERASE 6 (RDR6) and the dsRNAs are processed by a Dicer protein, usually DCL4, to produce 21-nt siRNAs in a phased pattern[9,10]. Those siRNAs derived from the non-coding *TAS* loci are called trans-acting siRNAs (ta-siRNAs). In the Arabidopsis Columbia-0 (Col-0) genome, there are four families of *TAS* genes, *TAS1a/b/c*, *TAS2*, *TAS3a/b/c*, and *TAS4*[9,11–14]. The biogenesis of *TAS1a/b/c*- and *TAS2*-derived ta-siRNAs requires the AGO1-miR173 complex, and that of *TAS4*-derived ta-siRNAs requires the AGO1-miR828 complex[9,11,13]. However, for ta-siRNAs derived from the *TAS3a/b/c* loci, an AGO7-containing miRISC, AGO7-miR390, is required[15]. As in miRNA loading, ta-siRNA duplexes are selectively loaded into AGO proteins based on their sequence features[7]. The ta-siRNA-containing RISCs can direct target RNA cleavage and/or trigger the biogenesis of secondary siRNAs[8].

Eukaryotic AGO protein family members are highly conserved. An AGO protein contains four conserved domains: the N-terminal domain (N), which is required for small RNA duplex unwinding[16]; the PIWI/Argonaute/Zwille (PAZ) domain, which anchors the 3’ end of the miRNA guide strand[17,18]; the Middle (MID) domain, which binds the 5’ phosphate of the miRNA guide strand[19,20]; and the P-element-induced wimpy-testis (PIWI) domain, which in some AGOs, harbors an

RNase H like motif that cleaves target RNA transcripts[21,22]. In Arabidopsis, AGO1, AGO2, AGO4, AGO7, and AGO10 have been shown to possess cleavage activity[6,12,23–25]. Structural studies of human AGO2 and prokaryotic AGOs show that the four domains of AGO form a two-lobed structure with a central cleft that cradles guide and target RNAs, with the N-PAZ domains composing one lobe and the MID-PIWI domains constituting the other[21,26]. The N and PAZ domain are directly connected by the L1 linker, while the MID and PIWI domain are directly connected by the L2 linker, which also connects the N-PAZ lobe and the MID-PIWI lobe[26–29].

In addition to the N, PAZ, MID and PIWI domains that are highly conserved, AGO proteins may harbor an N-terminal extension (NTE) of varying lengths and sequences, and the molecular or biological functions of this region are less understood. The NTE of AGOs is also referred as the N-terminal coil in some studies as it was predicted to possess coil-like structures. A recent study shows that a nuclear localization signal (NLS) and a nuclear export signal (NES) are present in the NTE (1-189a.a.) of Arabidopsis AGO1[30]. As inhibition of the EXPO1/NES-dependent protein nuclear export pathway significantly increases the ratio between nuclear and cytoplasmic AGO1, it was proposed that these signals direct the nucleo-cytosolic shuttling of AGO1[30]. Strikingly, AGO1 with the NES sequence mutated (AGO1mNES) associated with the same miRNA cohorts as its intact counterpart, suggesting that miRNAs' loading into AGO1 takes place in the nucleus[30]. However, it remains unclear whether there are other nuclear export

pathways that transport AGO1mNES from the nucleus to the cytoplasm. Indeed, it was recently shown that the TREX-2 complex core component THP1 partners with the nucleoporin protein NUP1 at the nuclear envelope, together promoting the nuclear export of AGO1 or AGO1-miRISC[31]. 56 mutant alleles of Arabidopsis AGO1 have been reported in the literature, with 20 of the 56 being missense mutations, however only one of the 20 alleles resides in the NTE[32]. *ago1-38*, a weak allele of *AGO1*, harbors a Gly-to-Arg mutation at the very end of the NTE region[33]. One study reported that the AGO1 protein abundance is similar between *ago1-38* and wild-type (WT), but the membrane association of AGO1 in the inflorescence tissue is reduced in *ago1-38*[34]. Other studies revealed that AGO1 and miRNAs are associated with membrane-bound polysomes, and the membrane-associated AGO1 could cause both target cleavage and translational repression[35,36]. Furthermore, *AGO1* is under feedback regulation - *AGO1* RNA is targeted by AGO1-bound miR168 at the NTE region[37]. Studies in animal AGOs show diverse functions of the NTE region, In *Caenorhabditis elegans*, WAGO-1 (worm ARGONAUTE 1) and WAGO-3 are processed at their NTE by DPF-3, a dipeptidase[38]. Proteolytic activity of DPF-3 on the third and second a.a. of WAGO-1 and WAGO-3, respectively, promotes correct sorting of 22G siRNAs into those AGOs and thus safeguard genome integrity[38]. *Drosophila melanogaster* AGO2 contains a ~400 a.a. long N-terminal glutamine-rich repeat (GRR) region, reduced copy numbers of GRRs result in defected RNAi responses and embryonic development[39].

Here, through analyzing the miRNA-related defects manifested by the Arabidopsis AGO1 NTE truncation lines, we uncover novel roles of the NTE in miRNA-mediated gene silencing. We show that loss of the entire NTE leads to a seedling-lethal phenotype resembling that of an *ago1* null allele, suggesting that the NTE is essential for the functions of AGO1. Additionally, we find that the 91-to-189a.a. region of the AGO1 NTE is essential for rescuing the morphological defects of the *ago1* null allele. Global analyses of miRNAs and their association with AGO1 revealed that the NTE, and particularly the 91-189 region, facilitates miRNAs' loading into AGO1. Furthermore, we show that the biogenesis of ta-siRNAs requires the presence of either the 1-to-90a.a. or the 91-to-189a.a. region of AGO1. Taken together, our results reveal novel roles of the NTE of Arabidopsis AGO1.

Results

Truncation of the AGO1 N-terminal extension causes severe morphological defects

In *Arabidopsis thaliana*, the ten AGO family members can be grouped into three clades based on their phylogenetic relationship (Supplementary Fig. 2.1a). All members of the AGO1/5/10 and AGO2/3/7 clades possess NTEs longer than 130 a.a., whereas members of the AGO4/6/8/9 clade contain NTEs less than 70 a.a. long (Supplementary Fig. 2.1a). Protein sequence alignment of the NTE region of all Arabidopsis AGOs shows extremely low similarity (Supplementary Fig. 2.1b). Even AGO10, the most closely related paralog of AGO1, shares little similarity in

its NTE region to that of AGO1. Furthermore, phylogenetic analysis using only the NTE regions of the ten AGOs shows that the AGO10 NTE is the most distantly related to that of AGO1 (Supplementary Fig. 2.1c). Together, the sequence analyses suggest that the NTE region of AGOs might serve AGO-specific functions.

To investigate the functions of the NTE (1-189a.a.) region of Arabidopsis AGO1, we searched for potential domains and functional motifs of this region employing protein databases including Pfam, InterPro, and NCBI Conserved Domains Database. The 75-to-172 a.a region of Arabidopsis AGO1 was annotated as a glycine-rich_AGO1 domain by multiple protein databases. This domain is appeared in 117 species, all within the Magnoliopsida class (flowering plants), suggesting a plant unique function. Sequence alignment of the AGO1 NTE from six Magnoliopsida species, including *Arabidopsis thaliana* (*At*), *Arabidopsis lyrate* (*Al*), *Brassica napus* (*Bn*), *Glycine max* (*Gm*), *Oryza sativa* (*Os*), and *Zea mays* (*Zm*), shows that this glycine-rich_AGO1 domain is evolutionally conserved (Supplementary Fig. 2.2). In addition, six RGG/RG repeats are found within the NTE region. The RGG/RG motif, which may undergo arginine methylation, is known for mediating RNA binding, protein localization, and protein-protein interactions [40]. Three of the six RGG/RG motifs are clustered at a.a. 83 to 103 in the glycine-rich_AGO1 domain, with two of them being conserved in AGO1s of the six species mentioned above except for *Oryza sativa*. One RGG/RG motif, ^{59}RGGRG^{63}, is conserved in all six species. Furthermore, glutamine (Q) content is particularly high in the NTE, with 30 Qs scattered along the region and accounting

for 15.9% of the total amino acids in the NTE. This feature is conserved in the NTEs of all six inspected plant AGO1s. Next, we predicted sorting signals within the NTE that might facilitate the sub-cellular localization of AGO1. In addition to an NLS (^{2}VRKRR^{6}) and NES (^{149}LAQQFEQLSV^{158}) that were previously reported for Arabidopsis AGO1[30], a putative NLS (^{102}GGGPSSGPPQ^{111}) was predicted by SeqNLS with a score of 0.737 out of 1.

To understand how these features of the NTE affect the functions of AGO1, we tried to predict the structure of the NTE region by searching for similar protein sequences with available structural information in the Protein Data Bank using the SWISS-MODEL server. However, no protein template with significant similarity to AGO1 NTE was found. Next, we utilized AlphaFold, a machine learning tool that predicts protein structures, to get insights into the 3D structure of the NTE region (Fig. 2.1a). The N-terminal segment (a.a 1-90) of the NTE is mostly unstructured and loosely attached to the rest of the AGO1 protein. The C-terminal segment (a.a. 91-189) of the NTE is more structured and could potentially interact with the PIWI domain of AGO1. The very C-terminus of the AGO1 NTE together with the L2 Linker is tucked in between the N and PIWI domains, and thus could potentially assist with the connection and movement between the N-PAZ lobe and the MID-PIWI lobe. The rest of the NTE C-terminus protrudes from the two lobes of AGO1, with a.a. 145-175 adopting an L shape that is close to the PIWI domain.

To further investigate how the NTE region affects the function of Arabidopsis AGO1 *in vivo*, we introduced N-terminal HA-tagged, wild-type (WT) or

truncation mutants of AGO1 without the NTE region (AGO1Δ1-189), without the unstructured N-terminal segment of the NTE (AGO1Δ1-90), or without the more structured C-terminal segment of the NTE (AGO1Δ91-90) into the *ago1-36* mutant background (Fig. 2.1b). The *ago1-36* allele contains a T-DNA insertion in the AGO1 gene at a position within the encoded the PAZ domain, and produces a truncated AGO1 protein lacking the MID and PIWI domains[6]. The phenotype of *ago1-36* resembles *ago1* null alleles, such as *ago1-3*[41,42]. We found that both *HA-AGO1 ago1-36* and *HA-AGO1Δ1-90 ago1-36* had a WT phenotype, suggesting that the N-terminal half of the NTE is largely dispensable, at least under laboratory growth conditions. *HA-AGO1Δ91-90* partially rescued the developmental phenotypes of *ago1-36* plants, whereas *HA-AGO1Δ1-189 ago1-36* seedlings resembled *ago1-36* except that the hypocotyl hook was straightened, and the cotyledons were expanded at early developmental stages (Fig. 2.1c). This suggests that the NTE, and particularly the region of a.a. 91-189, is essential for the functions of AGO1.

The a.a. 91-189 region of the AGO1 NTE is crucial for miRNA accumulation

To determine the effects of AGO1 NTE truncation on miRNA accumulation, we performed RNA gel blot assays to determine the levels of miRNAs in seedling of *ago1-3*, *ago1-36,* and *ago1-36* expressing HA-tagged wild-type or truncated forms of AGO1. We found that compared to wild-type AGO1, the levels of three tested miRNAs were decreased in *AGO1Δ91-189* and *AGO1Δ1-189* to levels similar to those of *ago1-36* and *ago1-3*, whereas their levels remained unchanged

in *AGO1Δ1-90* (Fig. 2.2a). Next, we used small RNA sequencing to examine the effects of AGO1 NTE truncation on miRNA accumulation. Principal component analysis (PCA) of the small RNA sequencing data showed that the three biological replicates of each genotype were highly reproducible (Supplementary Fig. 2.3a). The size distribution of both total small RNAs and miRNAs was similar in *ago1-36* and *ago1-36* expressing wild-type or NTE-truncated AGO1s (Supplementary Fig. 2.3b). Consistent with previous findings, total small RNAs showed a 21 nucleotides (nt) peak and a more abundant 24-nt peak, while the majority of miRNAs were 21-nt long[24,36].

Detailed analyses were carried out to compare the abundance of individual miRNAs between AGO1 NTE truncation lines. Among a total of 428 Arabidopsis miRNAs, 104 miRNAs and 53 miRNA*s with an average level > 2 RPM (reads per million) in the small RNA-seq samples were included in the analyses. Few differentially accumulated miRNAs and miRNA* were found between *AGO1Δ1-90 ago1-36* and *AGO1 ago1-36*, whereas more than 36% of miRNAs were decreased and over 34% of miRNA*s were increased in *AGO1Δ91-189*, *AGO1Δ1-189*, and *ago1-36* when compared to *AGO1 ago1-36* (Fig. 2.2b). This result was consistent with miRNA quantification using RNA gel blot assays (Fig. 2.2a). In accordance with the previous report on *ago1-3*[42], a null allele of AGO1, around 50% (48 out of 104) of miRNAs were significantly decreased in *ago1-36* compared to *AGO1 ago1-36*; it is likely that failure of these miRNAs to load into an AGO protein made them more vulnerable to degradation. In contrast, 9 miRNAs were upregulated in *ago1-*

36 compared to *AGO1 ago1-36*, for example, miR172a;b;c;d, miR866, and miR5026. These upregulated miRNAs might be preferentially sorted into and stabilized by AGO2, as 6 out of 9 upregulated miRNAs possess a 5' adenine (A), the preferred 5' nucleotide by Arabidopsis AGO2[7]. In addition, 18 miRNA* accumulated to a higher level in *ago1-36* compared to *AGO1 ago1-36*, for example, miR391* and miR393b*, both of which containing a 5' adenine (A) and shown to preferentially associate with AGO2[7]. As the majority of the upregulated miRNA*s in *ago1-36* contain a 5' adenine (A) or guanine (G), they might be selectively loaded and protected by other AGOs when AGO1 is absent.

Comparison showed that the differentially accumulated miRNAs and miRNA*s (i.e. reduced levels of miRNAs and increased levels of miRNA*s) in *ago1-36* were highly correlated with those in *AGO1Δ1-189 ago1-36*, and with those in *AGO1Δ91-189 ago1-36*, although to a lesser extent (Fig. 2.2c). No correlation was found for the differentially accumulated miRNAs and miRNA*s in *ago1-36* and *AGO1Δ1-90 ago1-36* (Fig. 2.2c). These findings suggest that the AGO1 NTE (1-189a.a.), particularly the 91-189 region, is required for restoring miRNA and miRNA* levels in *ago1-36*. And as the differential accumulation of a small number of miRNAs and miRNA*s between *AGO1Δ1-189 ago1-36* and *AGO1Δ91-189 ago1-36* was not correlated, the a.a 1-90 region of the NTE might also play a minor role in miRNA accumulation.

We further assessed the effects of NTE truncations on miRISC formation by examining the abundance of miRNAs and their corresponding miRNA*s. During

miRISC formation, AGO1 unwinds the miRNA/miRNA* duplex and selectively retains one strand (miRNA), whereas the other strand (miRNA*) is ejected[6]. A total of 31 miRNA species with both miRNA and miRNA* detected in the small RNA sequencing were evaluated. The levels of most miRNAs and their miRNA*s in *ago1-36* showed a reversed trend - while the majority of the miRNAs were downregulated, their corresponding miRNA*s were up-regulated, likely due to association with other AGOs (Fig. 2.2d). Only a few miRNAs showed the same trend in changes in *ago1-36* to that of their corresponding miRNA*s, such as miR172a;b;c;d and miR390a;b (Fig. 2.2d). A similar pattern was observed in *AGO1Δ1-189 ago1-36* and *AGO1Δ91-189 ago1-36*, indicating miRISC formation was likely defective for both forms of AGO1, and the a.a 91-189 region of AGO1 plays a major role in this miRISC formation (Fig. 2.2d).

The a.a. 91-189 region of the AGO1 NTE is essential for miRNA and ta-siRNA loading

To test our hypothesis that the NTE region of AGO1 affects miRISC formation, we examined whether the association between miRNAs and ta-siRNAs with the NTE-truncated AGO1 is compromised. Small RNAs associated with the HA-tagged AGO1 and AGO1 mutants were immunoprecipitated (IP-ed) and sequenced. The AGO1Δ91-189 and AGO1Δ1-189 were in the *ago1-36* heterozygous background to ensure a similar cellular small RNA profile and morphological phenotypes across all tested plants. PCA analysis showed that the two biological replicates for each sample were highly reproducible, and AGO1Δ91-

189 IP and AGO1Δ1-189 IP samples were clustered together and separate from the other samples, suggesting they had small RNA binding profiles similar to each other yet different from AGO1 IP and AGO1Δ1-90 IP (Supplementary Fig. 2.4a). Similar to total small RNA profiles (Supplementary Fig. 2.3a), AGO1Δ1-90 IP clustered with AGO1 IP on the PC1 level, suggesting a similar small RNA binding preference between the two (Supplementary Fig. 2.4a).

Consistent with previous findings[7], the size distribution of wild-type AGO1 associated total small RNAs, miRNAs, and ta-siRNAs showed an enrichment of the 21-nt peak (Fig. 2.3a). Like AGO1, AGO1Δ1-90 predominantly associated 21-nt small RNAs, however, a minor reduced preference toward 21-nt miRNAs and an increased association with 20-nt miRNAs was observed (Fig. 2.3a). As the sequenced size of small RNAs was used in the size distribution analysis, the 20-nt miRNAs could represent a pool of annotated 20-nt miRNAs, truncated miRNAs from a larger size, and misprocessed miRNAs. We specifically analyzed the association of miRNAs with various annotated sizes with AGO1. Annotated 20-nt miRNAs constituted a slightly higher proportion in AGO1Δ1-90-associated miRNAs as compared to wild-type AGO1, suggesting that the a.a. 1-90 region of the NTE might facilitate size selection of miRNAs (Supplementary Fig. 2.4b). Strikingly, AGO1Δ91-189 and AGO1Δ1-189 completely lacked the preference toward 21-nt small RNAs, and their association with miRNAs and ta-siRNAs was almost depleted, suggesting that the a.a. 91-189 region of AGO1 is essential for miRNA and ta-siRNA loading (Fig. 2.3a).

We next examined the differential association of individual miRNAs between AGO1 NTE mutants and wild-type AGO1. A total of 76 miRNAs and 24 miRNA*s were at an average level of > 2 RPM in the IP small RNA-seq samples and were included in the differential expression analysis. The association of miRNAs and miRNA*s with AGO1Δ1-90 was unaffected compared to wild-type AGO1, suggesting that a.a 1-90 of AGO1 have negligible effects on miRNAs loading. On the contrary, more than 88% of miRNAs and 87% of miRNA*s showed reduced association with both AGO1Δ91-189 and AGO1Δ1-189 (Fig. 2.3b), and the miRNAs and miRNA*s downregulated in the two mutants were highly correlated (and Supplementary Fig. 2.4c), suggesting that a.a 91-189 of AGO1 affect miRNA association globally. Furthermore, both the miRNA strand and its corresponding miRNA* strand showed reduced association with AGO1Δ91-189 and AGO1Δ1-189 (Supplementary Fig. 2.4d), implying that the reduced miRNA loading is unlikely due to defects in stand selection or miRNA* ejection. As AGO protein stabilizes its associated miRNAs, this compromised miRNA loading could explain the severe phenotypes and the reduced abundance of miRNAs in *AGO1Δ91-189 ago1-36* and *AGO1Δ1-189 ago1-36*. The reduced association of miRNA*s with AGO1Δ91-189 and AGO1Δ1-189 also suggests that the increased accumulation of miRNA*s in *AGO1Δ91-189 ago1-36* and *AGO1Δ1-189 ago1-36* is likely due to the loading of miRNA*s into other AGOs. Similar to miRNAs, most 21-nt ta-siRNAs showed reduced levels in AGO1Δ91-189 IP and AGO1Δ1-189 IP, but not in AGO1Δ1-90 IP (Fig. 2.3c).

The 91-to-189 a.a region of AGO1 facilitates miRNA loading independently of its role in nuclear-cytoplasmic shuttling

AGO1 was previously reported to shuttle between the cytoplasm and the nucleus in an NLS (a.a. 2-6)- and NES (a.a. 149-158)- dependent manner[30]. The AGO1Δ1-90 protein lacks the NLS (a.a. 2-6), and the NES (a.a. 149-158) was removed from AGO1Δ91-189, while the AGO1Δ1-189 lacks both the NLS and the NES. To investigate whether the reduced loading of miRNAs and ta-siRNAs into AGO1 NTE mutants was due to defects in nuclear-cytoplasmic shuttling, we further examined the nucleocytoplasmic distribution of AGO1 in these mutants. In addition to the NTE truncation mutants generated in this study, we also included an NES mutated AGO1 (AGO1mNES) allele that was reported before, which showed enhanced nuclear localization, intact miRNA association, and reduced ta-siRNA binding[30]. Consistent with previous findings[30,31], the cytoplasm/nucleus ratio of wild-type AGO1 was around 3:1, and this ratio was reduced to 0.3:1 for the AGO1mNES protein (Fig. 2.3d). In comparison to wild-type AGO1, the levels of cytoplasmic AGO1Δ1-90 increased, supporting the nucleus-importing role of NLS (a.a. 2-6) that resides within the 1-to-90 a.a. region of the NTE. However, the reduced levels of nuclear AGO1Δ1-90 did not affect its profiles of miRNA and ta-siRNA association (Fig. 2.3b). Interestingly, the cytoplasm/nucleus ratio of the AGO1Δ1-189 protein lacking both NLS (a.a. 2-6) and NES (a.a. 149-158) was similar to that of wild-type AGO1, suggesting that there exist mechanisms to affect the nuclear-cytoplasm shuttling of AGO1 in an NTE-independent manner.

Compared to wild-type AGO1, AGO1Δ91-189 showed increased nuclear accumulation, which is consistent with the role of the NES (a.a. 149-158) in directing AGO1's nuclear export (Fig. 2.3d). However, the truncation of a.a. 91-189 caused weaker effects in AGO1's nuclear enrichment compared to the deletion of the NES. One possible explanation is that an unidentified motif in a.a. 91-189 of AGO1 facilitates the nuclear import. In this study, we identified a putative NLS (^{102}GGGPSSGPPQ^{111}) that resides in this region of AGO1, but its role in nuclear import has yet to be tested. It is worth noting that, unlike AGO1mNES, which predominantly resides in the nucleus and shows a wild-type-like miRNA-binding profile, miRNA association is depleted for AGO1Δ91-189 even though its nuclear accumulation is increased compared to wild-type AGO1, suggesting that a.a. 91-189 of AGO1 regulate miRNA loading independently of its role in the nuclear-cytoplasmic partitioning of AGO1 (Fig. 2.3d).

The a.a. 1-90 and a.a. 91-198 regions of the AGO1 NTE function redundantly in ta-siRNA biogenesis

To test whether the NTE region of AGO1 affects the activity of miRISC, we performed RNA-seq to examine the expression of miRNA target genes. The same RNA samples that were used in the total small RNA sequencing analysis were also used here for the RNA-seq analysis, including *ago1-36* and *ago1-36* expressing wild-type *AGO1* or *AGO1* NTE truncated mutants driven by the *AGO1* promoter. Three biological replicates gave highly reproducible results (Supplementary Fig. 2.5). 130 experimentally verified miRNA target genes were investigated to identify

differentially expressed genes between wild-type *AGO1* and *AGO1* NTE mutants. In comparison to *AGO1 ago1-36*, gene expression in *AGO1Δ1-90 ago1-36* was largely unaffected (Fig. 2.4a and 2.4b). Around 35% of miRNA target genes were derepressed in ago*1-36* and *AGO1Δ1-189 ago1-36* (Fig. 2.4a), and the two genotypes were highly correlated in terms of the miRNA target genes affected (Fig. 2.4c. Interestingly, only 25% of miRNA target genes were derepressed in *AGO1Δ91-189 ago1-36* (Fig. 2.4a), and the levels of change were lesser than their counterparts in *ago1-36* and *AGO1Δ1-189 ago1-36* (Fig. 2.4d). The less severe molecular phenotype of *AGO1Δ91-189 ago1-36* is consistent with their better seedling phenotype compared to *AGO1Δ1-189 ago1-36*, suggesting that a.a. 1-90 of AGO1 can partially rescue *AGO1Δ1-189 ago1-36*. Since miRNA association is reduced to a similar level in AGO1Δ91-189 and AGO1Δ1-189, it is possible that a.a. 1-90 of AGO1 facilitate target repression after miRNA loading.

In addition to target gene repression, certain miRNAs can trigger the biogenesis of secondary siRNAs from target loci such as *TAS1a/b/c* and *TAS2*, which produce ta-siRNAs in an AGO1-miR173 dependent manner. To determine whether the NTE of AGO1 affects ta-siRNA biogenesis, we compared 21-nt small RNAs derived from the *TAS* loci. *TAS3a/b* ta-siRNAs, which require AGO7-miR390 for biogenesis, were included as a control. Strikingly, we found that ta-siRNA levels from the four AGO1-dependent loci were largely unchanged in *AGO1Δ1-90 ago1-36* or *AGO1Δ91-189 ago1-36* while significantly reduced in *AGO1Δ1-189 ago1-36* (Fig. 2.4e). The levels of *TAS3* ta-siRNAs were unaffected

in *AGO1Δ1-189 ago1-36* (Fig. 2.4e), consistent with expectations. We further confirmed that the reduced ta-siRNA levels from *TAS1* and *TAS2* loci in *AGO1Δ1-189 ago1-36* were not due to reduced accumulation of miR173, as the levels of miR173 were largely unaffected in all NTE truncation alleles of AGO1 (Fig. 2.4f). Both AGO1Δ91-189 and AGO1Δ1-189 showed reduced association with miR173 (Fig. 2.4g), which raised the possibility that miR173 triggered the biogenesis of ta-siRNAs in association with another AGO. However, this cannot explain the lack of ta-siRNA biogenesis in AGO1Δ1-189. A more likely scenario is that AGO1Δ91-189, despite reduced miR173 association, is sufficient to trigger ta-siRNAs production, while AGO1Δ1-189 cannot, which would suggest that a.a. 1-90 play a role in ta-siRNA biogenesis. However, ta-siRNA accumulation was not affected in *AGO1Δ1-90 ago1-36*, implying that a.a. 91-189 can also facilitate ta-siRNA biogenesis. It is likely that a.a. 1-90 and a.a. 91-189 of AGO1 redundantly enable the activities of AGO1 in ta-siRNA biogenesis.

Discussion

In this study, we show that the NTE (1-to-189 a.a.) region of AGO1 is essential for rescuing the developmental and molecular phenotypes of *ago1-36*. We further show that a.a. 91-189 are required for the association with miRNAs and ta-siRNAs *in vivo*, and are thus essential for miRNA-mediated gene silencing. On the other hand, a.a 1-90 are dispensable for the association with miRNAs and ta-siRNAs *in vivo*. While the NTE is essential for ta-siRNA biogenesis, the presence

of neither a.a. 1-90 nor a.a. 91-189 of the NTE is required for ta-siRNA biogenesis, suggesting a redundant function of these two regions in ta-siRNA biogenesis.

Proper loading into an AGO protein is essential for miRNAs to exert their roles in target gene repression. We show that miRNA association is severely and similarly compromised for AGO1Δ91-189 and AGO1Δ1-189 (Fig. 2.3a, 2.3b, and Supplementary Fig. 2.4c), suggesting a.a. 91-189 of AGO1 are required for miRNA loading. Whereas AGO1Δ1-90 IP shows a similar miRNA association profile to wild-type AGO1 IP, suggesting that a.a. 1-90 of AGO1 are not required for miRNA loading (Fig. 2.3a and 2.3b). A previous study shows that an NLS (a.a. 2-6) in AGO1 promotes the nuclear localization of a reporter protein (GFP-GUS) when a section of the AGO1 NTE (a.a. 1-148) was fused to the reporter protein, while mutating an NES (a.a. 149-158) prevents the nuclear export of AGO1[30]. A similar finding was made in this study, we show that compared to wild-type AGO1, the cytoplasmic/nuclear ratio of AGO1Δ1-90 and AGO1Δ91-189 was increased and decreased, respectively (Fig 2.3d). It was proposed that miRNA loading into AGO1 occurs inside the nucleus, as AGO1mNES, which predominantly resides in the nucleus, shows a similar miRNA binding profile to that of wild-type AGO1[30]. In this study we show that AGO1Δ91-189, which shows increased nuclear localization, does not manifest a wild-type-like miRNA-binding profile as does AGO1mNES, suggesting that a.a. 91-189 of AGO1 are critical to miRNA loading independently of its role in the nuclear-cytoplasmic shuttling of the protein (Fig 2.3b and 2.3d). It is possible that a.a. 91-189 of AGO1 are required for the interaction with HSP90,

which is essential for miRNA loading[43]. Furthermore, we show that the reduced nuclear localization of AGO1Δ1-90 does not affect its miRNA loading or target transcripts repression, suggesting that the residual nuclear localization was sufficient to allow for miRNA loading or that miRNA loading can also occur in the cytoplasm (Fig 2.3b, 2.3d and 2.4a). To test whether miRNA loading can occur in the cytoplasm, an AGO1 mutant exclusively residing in the cytoplasm is required. Unlike AGO1mNES, which almost exclusively resides in the nucleus, 30% of the AGO1Δ91-189 protein is in the cytoplasm, suggesting a motif that promotes nuclear import could be in this region (Fig 2.3d). A new NLS (^{102}GGGPSSGPPQ^{111}) that resides in the a.a. 91-189 region of AGO1 was predicted in this study. Mutating both NLS (a.a. 2-6) and NLS (a.a. 102-111) might create a cytoplasm-exclusive AGO1 that is suitable to test our hypothesis.

The 1-to-90 a.a. region of AGO1 is not required for rescuing the developmental defects of *ago1-36* or for miRNA loading, however, we found it can facilitate target repression and ta-siRNA biogenesis. We show that the association of miRNAs with AGO1Δ91-189 and AGO1Δ1-189 is almost depleted (Fig. 2.3a and 2.3b), whereas miRNA target gene repression is less affected in *AGO1Δ91-189 ago1-36* compared to *AGO1Δ1-189 ago1-36* (Fig 2.4a and 2.4d), suggesting that a.a. 1-90 of AGO1 assist in target transcript cleavage. Furthermore, although miR173, the trigger miRNA for the biogenesis of *TAS1a/b/c*- and *TAS2*-derived ta-siRNAs, was significantly reduced in AGO1Δ91-189 IP compared to wild-type AGO1 IP (Fig 2.4g), ta-siRNA biogenesis was largely unaffected in *AGO1Δ91-189*

ago1-36 (Fig 2.4e). It is unlikely that other AGOs associated with miR173 triggers ta-siRNA biogenesis when AGO1 loading is compromised, as miR173-dependent ta-siRNA biogenesis is downregulated in *ago1-36* (Fig 2.4e). Together, these observations suggest that a.a. 1-90 of the NTE are sufficient for ta-siRNA biogenesis. We hypothesize that only a small amount of AGO1-miR173 is required to trigger the biogenesis of ta-siRNAs. In addition, we noticed that phasiRNA production from protein-coding genes, such as *AGO1*, *PPR*, and *NBS-LRR* genes, which are targeted by miR168, miR161.1, and miR472, respectively, is nearly abolished in *AGO1Δ91-189 ago1-36* (Supplementary Fig. 2.6). The absence of *AGO1*-derived phasiRNAs is due to the deletion of the miR168 targeting site within the a.a. 91-189 region of the NTE. The elimination of *PPR*- and *NBS-LRR*-derived phasiRNAs in *AGO1Δ91-189 ago1-36* but not *AGO1Δ1-90 ago1-36* suggests that a.a. 91-189 are indispensable for miRNA-triggered phasiRNA biogenesis from protein-coding genes. Why is AGO1Δ91-189 capable of ta-siRNA biogenesis but not phasiRNA biogenesis from protein-coding genes? One possibility is that these two processes require different auxiliary proteins, and a.a. 91-189 are required for specific protein-protein interactions. Alternatively, these two processes might take place at distinct subcellular locations, and a.a. 91-189 are required for the localization of AGO1 to one of the subcellular compartments.

Although miRNAs and ta-siRNAs were almost depleted in AGO1Δ91-189 IP and AGO1Δ1-189 IP, these proteins are still associated with small RNAs *in vivo* (Fig. 2.3a). Wild-type AGO1 is mainly associated with 21-nt miRNAs and ta-

siRNAs, although it is also loaded with Pol IV-dependent siRNAs and small RNAs derived from coding genes, TEs, inverted-repeats, snRNA, snoRNA, rRNA, and tRNA. We found that over 80% of the 18-to-26 nt reads from the small RNA libraries from AGO1Δ91-189 and AGO1Δ1-189 IP are derived from rRNA (Fig. 2.5a). The proportion of rRNA- and tRNA-derived small RNAs are dramatically increased in AGO1Δ91-189 IP and AGO1Δ1-189 IP compared to wild-type AGO1 IP, while all other small RNA species show a corresponding decrease (Fig. 2.5a). We suspect that when lacking a.a. 91-189, AGO1 is unable to distinguish between the Dicer-dependent small RNAs and rRNA-derived small RNAs. This would be an exciting avenue for future investigation.

Methods

Plant materials and growth conditions

All *Arabidopsis thaliana* lines in this study were in the Columbia (Col) ecotype. Seeds of *ago1-36* (SALK_087076) were obtained from the ABRC collection. Seeds were surface-sterilized with 75% ethanol and stratified in water at 4°C for 2 days then transferred to 1x Murashige–Skoog (MS) medium. All plants were kept in a growth chamber at 22°C under white light and long-day conditions (16 h light / 8 h dark).

ago1-36 and *ago1-36/+* expressing *pAGO1::3XHA-AGO1*, *pAGO1::3XHA-AGO1Δ1-90, pAGO1::3XHA-AGO1Δ91-189,* and *pAGO1::3XHA-AGO1Δ1-189* were generated in this study. To construct the plasmids of the above transgenes, a 1648bp AGO1 promoter (including the 5' UTR) and the 399bp 3' UTR were

amplified from genomic DNA, the full length *AGO1* coding region and NTE-truncated *AGO1* were amplified from cDNA, and the 3xHA tag was amplified from pGWB615[44]; these fragments were then cloned into pEarleyGate 301[45] (predigested by XbaI and NcoI) using the NEBuilder HiFi DNA Assembly Cloning Kit (NEB). All clones were validated by sequencing. Sequences of the primers are listed in Supplementary Table 2.1.

Small-RNA gel blot analysis and sequencing

RNA isolation and RNA gel blot analysis of small RNAs were performed as described[36]. 5-10 μg of total RNA was isolated from 12-day-old Arabidopsis seedlings using TRI Reagent (NRC), resolved on 15% urea–PAGE gels and transferred to NX membrane (Amersham Hybond-NX). MiRNAs were detected with 5' end ^{32}P-labeled antisense DNA oligonucleotide probes. Sequences of the DNA oligonucleotide probes in this study are listed in Supplementary Table 2.1. Hybridization signals were analyzed by phosphorimager (Typhoon 9410, GE).

Small-RNA sequencing and data analysis were performed as described[36]. 25 μg of total RNA was extracted from 12-day-old Arabidopsis seedlings and resolved on a 15% urea-PAGE gel, and small RNAs of 15- to 40-nt were isolated from the gel. Small RNA libraries of gel-purified small RNA or small RNA acquired from AGO1 immunoprecipitation (as described below) were constructed using the NEBNext Multiplex Small-RNA Library Prep Set for Illumina (E7300). The libraries were sequenced on an Illumina HiSeq X Ten, and the resulting data were analyzed using an in-house pipeline pRNASeqTools v.0.8 (https://github.com/grubbybio/

pRNASeqTools). The three-prime-end adapter sequence (AGATCGGAAGAGC) was trimmed from raw reads, followed by filtering to retain 18- to 42-nt reads using cutadapt v3.0[46]. Trimmed reads were then aligned to the Arabidopsis genome (TAIR10) using ShortStack v.3.8.5[47] with parameters '-bowtie_m1000 -ranmax 50 -mmap u -mismatches 0'. For total small RNA, reads were normalized against total 18- to 42-nt reads minus 45S rRNA reads (RPM, Reads Per Million Reads). For small RNA acquired from AGO1 immunoprecipitation, reads were normalized against total 18- to 42-nt reads (RPM). Differential comparison of small RNAs was conducted by DESeq2 v1.30.0 with fold change of 1.5 and adjusted *P* value < 0.01 as the parameters[48]. Annotation of miRNA and miRNA* sequences were obtained from miRbase v21 (http://www.mirbase.org/). For miRNA length distribution and small RNA composition analysis, reads that match perfectly or with a 1-nt shift on either end from the annotated sequence were assigned to the miRNA. For miRNA differential expression analysis, only reads that match perfectly to the annotated sequence were assigned to the corresponding miRNA. For ta-siRNA, levels were quantified by summing 21-nt small RNA reads that mapped to each of the eight *TAS* loci. Sequence logo presentations were generated using WebLogo 3.7.4 (http://weblogo.threeplusone.com/)[49].

Immunoprecipitation and western blot analysis

2 g of 12-day-old seedlings were ground into fine powder in liquid nitrogen and the powder was homogenized in 3 ml lysis buffer (50 mM Tris-HCl, pH7.5, 150 mM NaCl, 10% glycerol, 0.1% CA-630, one tablet of cOmplete EDTA-free

Protease Inhibitor Cocktail /50ml (Roche)), and incubated for 30 min at 4°C with gentle rotation. The total lysate was centrifuged at 12,000 g at 4°C for 20 min twice to remove cell debris. Meanwhile, 30 μl Dynabeads™ Protein A (ThermoFisher) was incubated with 8 μg of anti-HA antibody (Sigma, H6908) for 30 min at room temperature with gentle rotation, and the beads were then washed with lysis buffer 5 times to remove the extra antibody. The lysate was incubated with the anti-HA antibody-protein A beads for 2 hours at 4°C with gentle rotation, and then beads were captured magnetically and washed with lysis buffer 5 times. Washed beads were divided for small RNA and protein analysis.

For small RNA analysis, washed beads were boiled in H_2O for 5 min under constant shaking and removed magnetically. The supernatant containing immunoprecipitated RNA was used in small RNA library construction (as described above). For western blot analysis, washed beads were boiled in 2xSDS sample buffer (50 mM Tris-HCL at pH 6.8, 10% glycerol, 2% SDS, 0.1% bromophenol blue, and 1% 2-mercaptoethanol) for 10 min with vigorous shaking. The beads were then removed magnetically, and the supernatant containing the immunoprecipitated protein was resolved on a 10% SDS-PAGE gel and detected by an anti-HA antibody (Roche, 12158167001).

RNA-seq and data analysis

Total RNA was isolated from 12-day-old Arabidopsis seedlings using TRI Reagent (NRC), and DNA was removed by DNase I (Roche) treatment. PolyA RNA was then enriched from 1 μg of DNase I-treated RNA using Oligo d(T)25

Magnetic Beads (NEB S1419S), followed by RNA-seq libraries construction using the NEBNext Ultra Directional RNA Library Prep Kit for Illumina (NEB E7420). RNA libraries were sequenced on an Illumina NovaSeq 6000 platform (PE150 bp), and the sequencing data were analyzed using the pRNASeqTools v.0.8 pipeline. Briefly, raw reads were aligned to the Arabidopsis genome (TAIR 10) using STAR v2.7.6a[50] with parameters '--alignIntronMax 5000 --outSAMmultNmax 1 --outFilterMultimapNmax 50 --outFilterMismatchNoverLmax 0.1', and counted by featureCounts v2.0.0[51]. Normalization was performed by calculating the FPKM (Fragments Per Kilobase Million) for each gene, and differential gene expression analysis was conducted by DESeq2 v1.30.0 with a fold change of 1.5 and adjusted *P* value < 0.05 as the parameters[48].

Small RNA phasing analysis

Small RNA phasing analysis was performed as previously described[36,52,53]. Small RNA reads from both the sense and antisense strands were included in the analysis. The formula used for phasing score calculation was described before[36].

Nuclear–cytoplasmic fractionation

Nuclear-cytoplasmic fractionation was performed as described[31]. 1 g of 12-day-old Arabidopsis seedlings was crosslinked in 0.5% formaldehyde/1× PBS buffer through vacuum infiltration for 15 min at room temperature, and crosslinking was stopped by vacuum infiltration in 100 mM glycine/1× PBS buffer for 5 min at room temperature. The plant material was washed with 1× PBS buffer and blotted dry, and then ground to a fine powder in liquid nitrogen. The powder was

resuspended in 2 ml lysis buffer (20 mM Tris-HCl, pH7.5, 20 mM KCl, 2.5 mM $MgCl_2$, 2 mM EDTA, 25% glycerol, 250 mM sucrose, 5 mM DTT and cOmplete Protease Inhibitor Cocktail (Roche)) and filtered through a 40 μm cell strainer (Falcon). The flow-through was centrifuged at 1,500g for 10 min at 4°C. The supernatant representing the cytoplasmic fraction was further centrifuged at 10,000g for 10 min at 4°C to remove any residual debris. The pellet from the 1,500g spin representing the nuclei was dissolved with 10 ml nuclei resuspension buffer 1 (NRB1) (20 mM Tris-HCl, pH7.4, 2.5 mM $MgCl_2$, and 0.2% Triton X-100) and centrifuged at 1,500g for 10 min to collect nuclei; this step was repeated 8 times to thoroughly wash the nuclei. After the final wash, the pellet was resuspended with 500 μl NRB2 (20 mM Tris-HCl, pH7.5, 250 mM sucrose, 10 mM $MgCl_2$, 0.5% Triton X-100, 5 mM 2-mercaptoethanol, and cOmplete Protease Inhibitor Cocktail (Roche)), and carefully loaded onto 500 μl NRB3 (20 mM Tris-HCl, pH7.5, 1.7 M sucrose, 10 mM $MgCl_2$, 0.5% Triton X-100, 5 mM 2-mercaptoethanol, and cOmplete Protease Inhibitor Cocktail (Roche)) without disturbing the bottom layer, then the sample was centrifuged at 16,000g for 45 min at 4°C. The nuclear pellet was resuspended and boiled in 1XSDS loading buffer for 10 min for protein gel blot analysis.

Multiple sequence alignment

Protein sequences of AGO1 paralogs and orthologs from *Arabidopsis thaliana* and representative species were acquired from Uniprot (https://www.uniprot.org/), including 10 *Arabidopsis thaliana* AGOs, AGO1

(O04379), AGO2 (Q9SHF3), AGO3 (Q9SHF2), AGO4 (Q9ZVD5), AGO5 (Q9SJK3), AGO6 (O48771), AGO7 (Q9C793), AGO8 (Q3E984), AGO9 (Q84VQ0), and AGO10 (Q9XGW1), *Arabidopsis lyrata* AGO1 (D7KD09), *Brassica napus* AGO1 (A0A078JMZ3), *Glycine max* AGO1a (I1MQL3), *Oryza sativa* AGO1a (Q6EU14), and *Zea mays* AGO1a (A0A096TTL7). Protein sequence alignments were conducted by MUSCLE[54] (https://www.ebi.ac.uk/Tools/msa/muscle/) with default settings, and figures were made using ESPript3[55] (https://espript.ibcp.fr).

Structure prediction

The protein sequence of *Arabidopsis thaliana* AGO1 (O04379) was obtained from Uniprot (https://www.uniprot.org/). Structure prediction was conducted by AlphaFold[56] (https://alphafold.ebi.ac.uk/) with default settings. Protein structure homology-modelling was performed by SWISS-MODEL (https://swissmodel.expasy.org/).

Protein feature analysis

Protein domain and motif analysis was performed by Pfam (http://pfam.xfam.org/), InterPro (https://www.ebi.ac.uk/interpro/), and NCBI Conserved Domains Database (https://www.ncbi.nlm.nih.gov/Structure/cdd/wrpsb.cgi). Protein subcellular localization prediction was performed by WoLFPSORT (https://wolfpsort.hgc.jp/), SeqNLS (http://mleg.cse.sc.edu/seqNLS/), cNLS Mapper (http://nls-mapper.iab.keio.ac.jp/cgi-bin/NLS_Mapper_form.cgi), and NESmapper (https://sourceforge.net/projects/nesmapper/).

Figures and Table

Figure 2.1. Arabidopsis AGO1 harbors an unstructured N-terminal extension.

(a) Front and side views of a putative Arabidopsis AGO1 structure predicted by AlphaFold. The colors represent the per-residue confidence score (pLDDT), with dark blue (pLDDT > 90), light blue (90 > pLDDT > 70), yellow (70 > pLDDT > 50), and orange (pLDDT < 50) denoting high, medium, low, and very low confidence, respectively.

(b) Schematic representation of HA-tagged Arabidopsis AGO1 and AGO1 NTE truncation forms. Blue blocks: domains; black ovals: the HA tag; solid lines: protein sequences; dashed lines: truncated protein sequences; green: NLS; purple: NES.

(c) Fourteen-day-old plants of Col, *ago1-36*, and *ago1-36* expressing *HA-AGO1*, *HA-AGO1Δ1-189*, *HA-AGO1Δ1-90,* and *HA-AGO1Δ91-189* transgenes. Scale bar, 1cm.

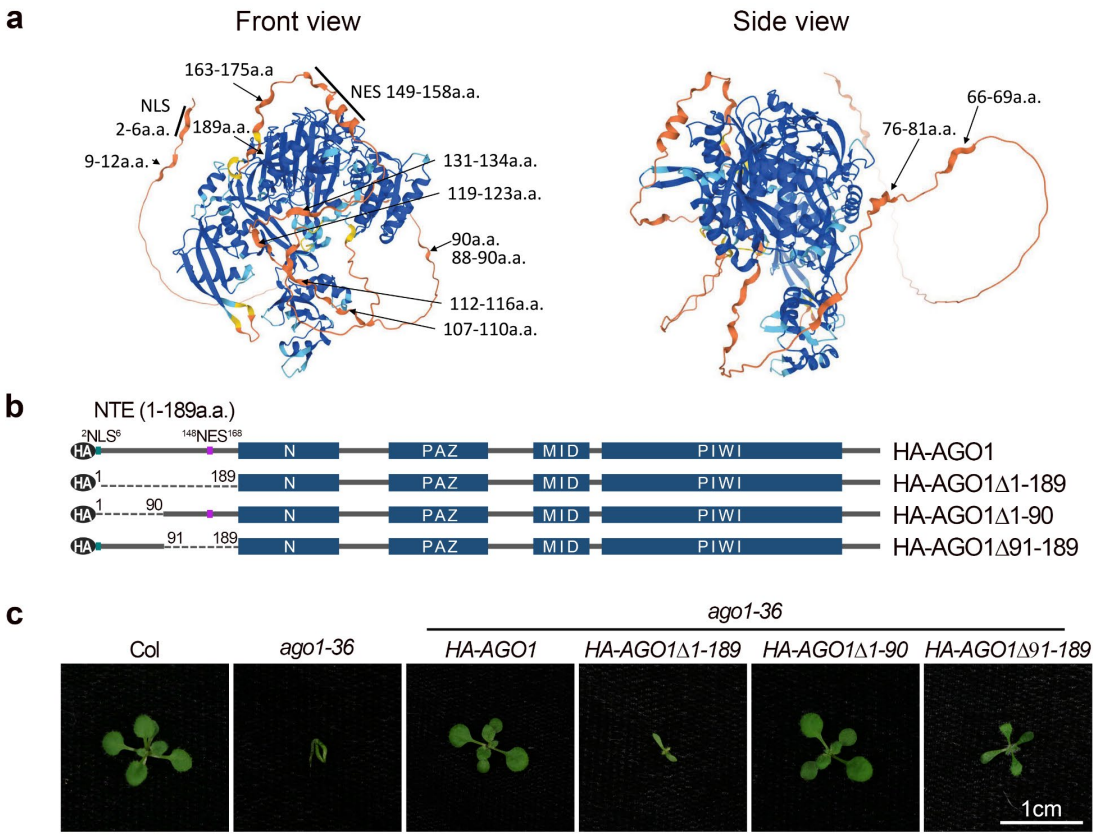
a
Front view
Side view
163-175a.a
NES 149-158a.a.
NLS
2-6a.a.
189a.a.
9-12a.a.
131-134a.a.
119-123a.a.
90a.a.
88-90a.a.
112-116a.a.
107-110a.a.
66-69a.a.
76-81a.a.
b
NTE (1-189a.a.)
2NLS6
148NES168
N
PAZ
MID
PIWI
HA-AGO1
HA-AGO1Δ1-189
HA-AGO1Δ1-90
HA-AGO1Δ91-189
c
ago1-36
Col
ago1-36
HA-AGO1
HA-AGO1Δ1-189
HA-AGO1Δ1-90
HA-AGO1Δ91-189
1cm

Figure 2.2. The AGO1 N-terminal extension is required for the miRNA accumulation.

(a) RNA gel blot analysis of miRNA abundance in 12-day-old seedlings of *ago1-3*, *ago1-36*, and *ago1-36* expressing *AGO1* full-length or various NTE-truncated forms. The numbers represent miRNA abundance in different genotypes relative to *AGO1 ago1-36*. The U6 blots serve as a loading control for the miRNA blots above.

(b to d) Small RNA-seq analysis of 12-day-old seedlings. Except for *ago1-36*, all lines contain *pAGO1:3XHA-AGO1* or *pAGO1:3XHA-AGO1* NTE-truncated forms in the *ago1-36* background. Three biological replicates of each genotype were included in the analysis.

(b) Scatter plots showing the miRNAs and miRNA*s with significantly different expression (average RPM > 2, fold change > 1.5 and adjusted *P* value < 0.01) between *AGO1* mutants and *AGO1*. Red and blue dots denote miRNAs or miRNA*s with significantly increased and decreased abundance, respectively.

(c) Scatter plots comparing the $\log_2$(fold change) of miRNAs and miRNA*s between pairs of *AGO1* mutants.

(d) Heatmap depicting the levels of miRNAs and their corresponding miRNA*s in *AGO1* mutants relative to *pAGO1:3XHA-AGO1 ago1-36*.

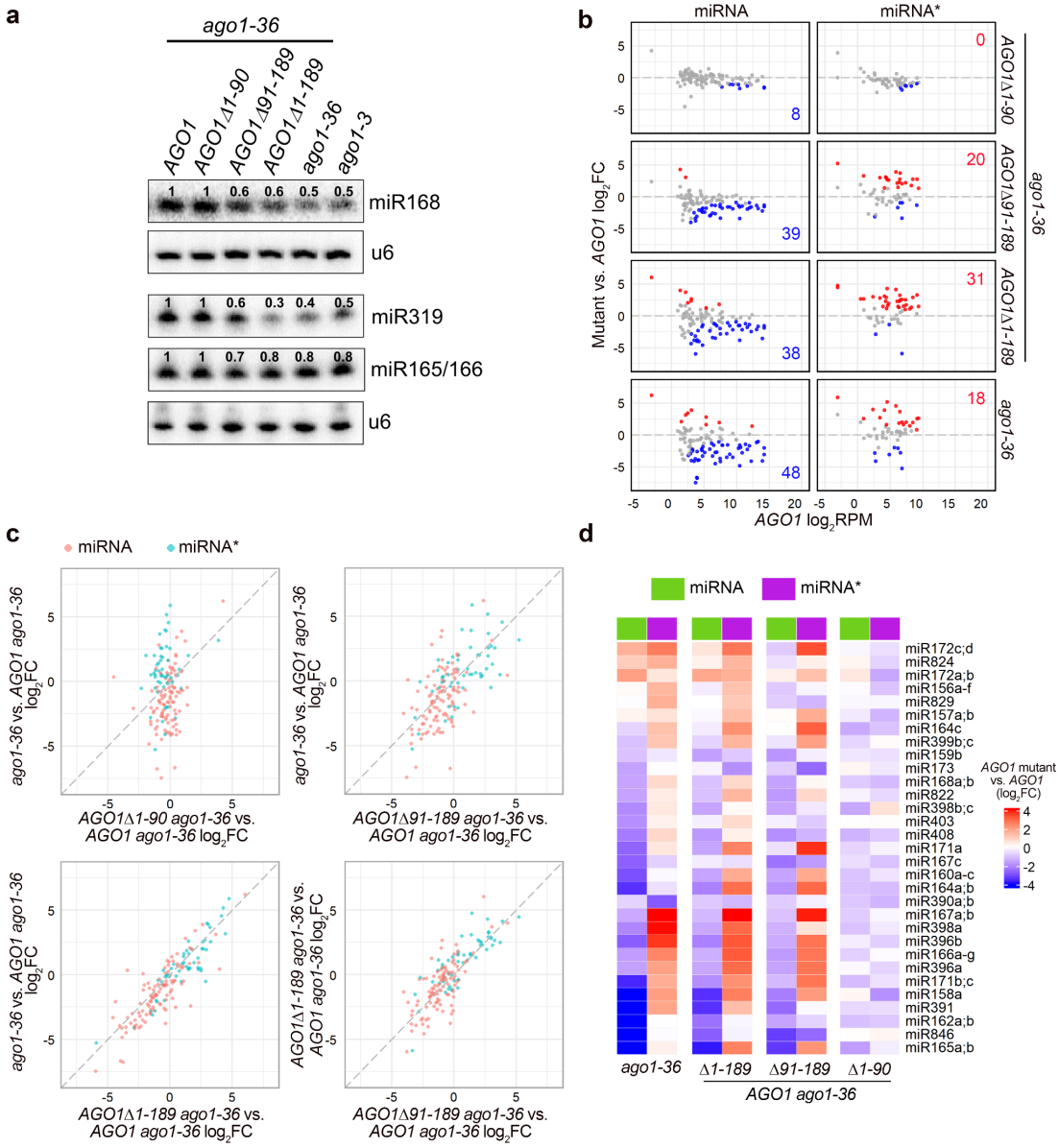
a
ago1-36
AGO1
AGO1Δ1-90
AGO1Δ91-189
AGO1Δ1-189
ago1-36
ago1-3
1 1 0.6 0.6 0.5 0.5
miR168
u6
1 1 0.6 0.3 0.4 0.5
miR319
1 1 0.7 0.8 0.8 0.8
miR165/166
u6
b
miRNA
miRNA*
AGO1Δ1-90
AGO1Δ91-189
AGO1Δ1-189
ago1-36
Mutant vs. AGO1 log2FC
AGO1 log2RPM
0
8
20
39
31
38
18
48
c
miRNA
miRNA*
ago1-36 vs. AGO1 ago1-36 log2FC
AGO1Δ1-90 ago1-36 vs. AGO1 ago1-36 log2FC
AGO1Δ91-189 ago1-36 vs. AGO1 ago1-36 log2FC
AGO1Δ1-189 ago1-36 vs. AGO1 ago1-36 log2FC
AGO1Δ91-189 ago1-36 vs. AGO1 ago1-36 log2FC
d
miRNA
miRNA*
miR172c;d
miR824
miR172a;b
miR156a-f
miR829
miR157a;b
miR164c
miR399b;c
miR159b
miR173
miR168a;b
miR822
miR398b;c
miR403
miR408
miR171a
miR167c
miR160a-c
miR164a;b
miR390a;b
miR167a;b
miR398a
miR396b
miR166a-g
miR396a
miR171b;c
miR158a
miR391
miR162a;b
miR846
miR165a;b
AGO1 mutant vs. AGO1 (log2FC)
ago1-36
Δ1-189
Δ91-189
Δ1-90
AGO1 ago1-36

Figure 2.3. The loading of miRNAs and ta-siRNAs into AGO1 is affected by truncations of the AGO1 N-terminal extension.

(a to c) Analysis of small RNA-seq data of AGO1-associated small RNAs. Wild-type AGO1 and AGO1Δ1-90 were in the *ago1-36* background, while other AGO1 NTE-truncated forms were in the *ago1-36/+* background. Two biological replicates of each genotype were included in the analysis.

(a) Size (in nt) distribution depicting the abundance of 18- to 26-nt small RNAs in IPs from plants containing AGO1 and AGO1 NTE-truncated forms. Total small RNAs, miRNAs and ta-siRNAs are shown. RPM, reads per million (see Methods).

(b) Scatter plots showing the miRNAs and miRNA*s with significantly different levels (fold change > 1.5 and adjusted *P* value < 0.01) between IP-ed AGO1 mutants and AGO1. Red dots denote miRNAs or miRNA*s with significantly higher abundance, while blue dots denote miRNAs or miRNA*s with significantly lower abundance.

(c) Bar plots depicting the $\log_2$(fold change) of 21-nt ta-siRNAs between IP-ed AGO1 NTE-truncated forms and AGO1. Blue bars denote ta-siRNAs with significantly lower levels (fold change > 1.5 and adjusted *P* value < 0.01).

(d) Bar plots depicting the cytoplasmic/nuclear ratio of AGO1 in AGO1 NTE mutants. Wild-type AGO1 and two replicates of AGO1Δ1-90 were in the *ago1-36* background, AGO1mNES was in the Col background, while other AGO1 NTE-truncated mutants and one replicate of AGO1Δ1-90 were in the *ago1-36/+* background. Error bars indicate s.d..

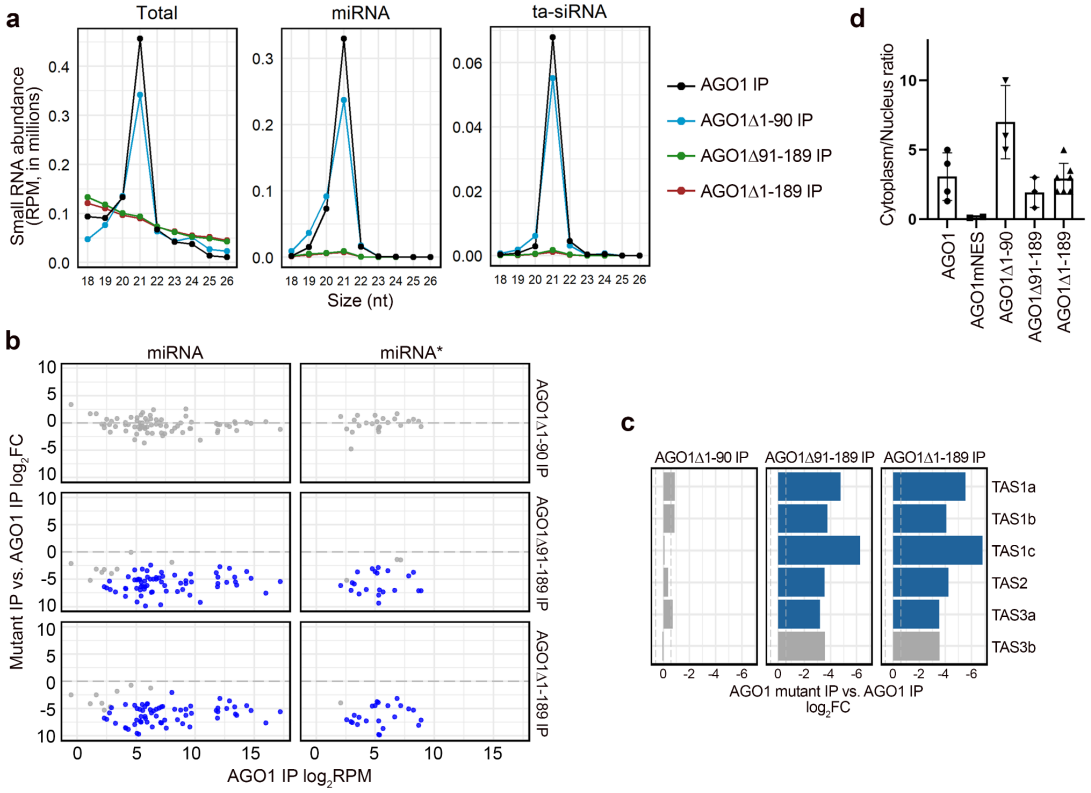
a
Total
miRNA
ta-siRNA
Small RNA abundance (RPM, in millions)
Size (nt)
AGO1 IP
AGO1Δ1-90 IP
AGO1Δ91-189 IP
AGO1Δ1-189 IP
d
Cytoplasm/Nucleus ratio
AGO1
AGO1mNES
AGO1Δ1-90
AGO1Δ91-189
AGO1Δ1-189
b
miRNA
miRNA*
Mutant IP vs. AGO1 IP log2FC
AGO1 IP log2RPM
c
AGO1Δ1-90 IP
AGO1Δ91-189 IP
AGO1Δ1-189 IP
TAS1a
TAS1b
TAS1c
TAS2
TAS3a
TAS3b
AGO1 mutant IP vs. AGO1 IP log2FC

Figure 2.4. miRNA activities are affected by truncations of the AGO1 N-terminal extension.

RNA-seq and small RNA-seq analysis of 12-day-old seedlings. Wild-type AGO1 and AGO1 NTE-truncated mutants were expressed in the *ago1-36* background. Three biological replicates of each genotype were included in the analysis.

(a) Scatter plots showing miRNA target genes with significantly different expression (fold change > 1.5 and adjusted *P* value < 0.05) between *AGO1* mutants and *AGO1*. Red and blue dots denote genes with significantly increased and decreased expression, respectively.

(b-d) Scatter plots comparing the $\log_2$(fold change) of miRNA target gene expression between pairs of *AGO1* mutants.

(e) Bar plots showing the relative levels of miR173 and miR390 in *ago1-36* expressing various *AGO1* mutants compared to *AGO1 ago1-36*.

(f) Bar plots showing the $\log_2$(fold change) of IP-ed miR173 between AGO1 NTE mutants and AGO1.

(g) Bar plots (right) showing the $\log_2$(fold change) of 21-nt ta-siRNAs between *ago1-36* expressing various *AGO1* mutants and *AGO1 ago1-36*. Blue bars and * denote miRNAs or ta-siRNAs with significantly lower levels (fold change > 1.5 and adjusted *P* value < 0.01).

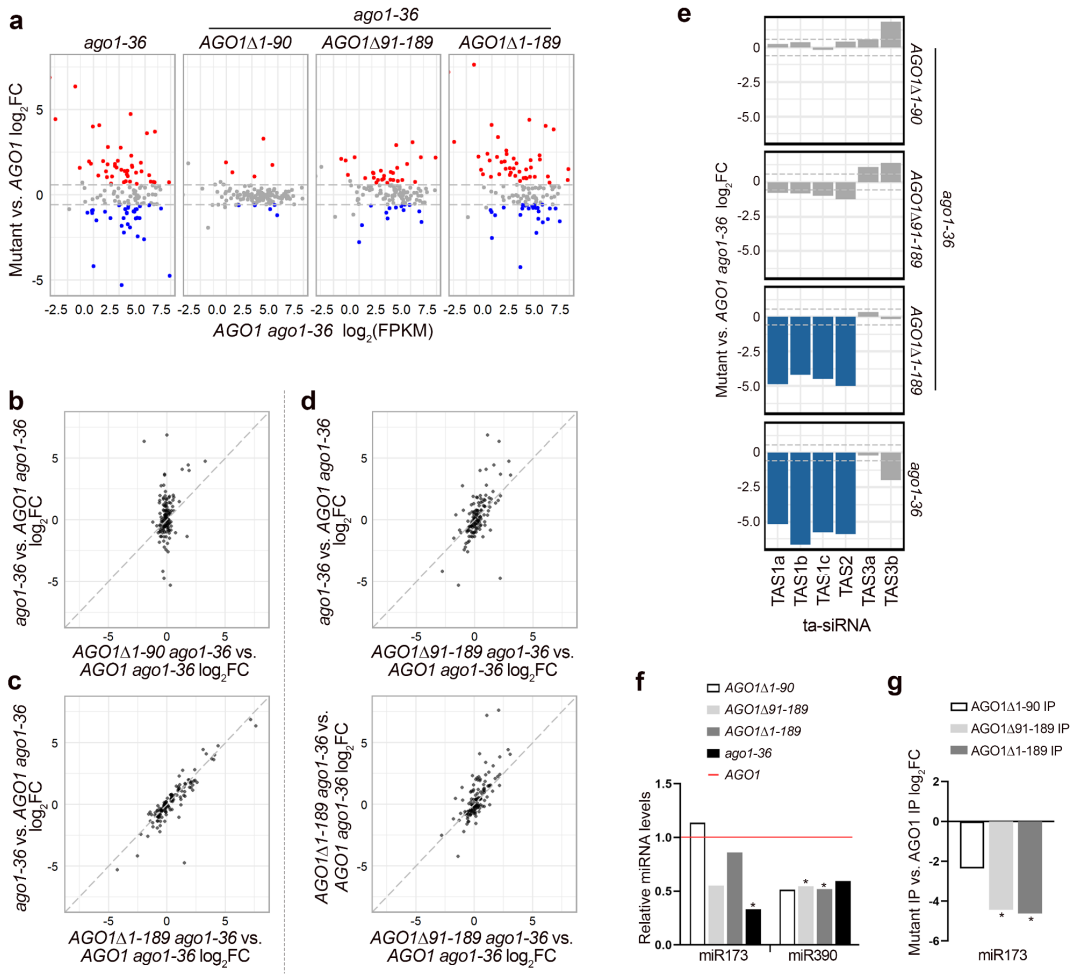
a
ago1-36
ago1-36
AGO1Δ1-90
AGO1Δ91-189
AGO1Δ1-189
Mutant vs. AGO1 log2FC
AGO1 ago1-36 log2(FPKM)
b
ago1-36 vs. AGO1 ago1-36 log2FC
AGO1Δ1-90 ago1-36 vs. AGO1 ago1-36 log2FC
c
ago1-36 vs. AGO1 ago1-36 log2FC
AGO1Δ1-189 ago1-36 vs. AGO1 ago1-36 log2FC
d
ago1-36 vs. AGO1 ago1-36 log2FC
AGO1Δ91-189 ago1-36 vs. AGO1 ago1-36 log2FC
AGO1Δ1-189 ago1-36 vs. AGO1 ago1-36 log2FC
AGO1Δ91-189 ago1-36 vs. AGO1 ago1-36 log2FC
e
Mutant vs. AGO1 ago1-36 log2FC
AGO1Δ1-90
AGO1Δ91-189
AGO1Δ1-189
ago1-36
ago1-36
TAS1a
TAS1b
TAS1c
TAS2
TAS3a
TAS3b
ta-siRNA
f
AGO1Δ1-90
AGO1Δ91-189
AGO1Δ1-189
ago1-36
AGO1
Relative miRNA levels
miR173
miR390
g
AGO1Δ1-90 IP
AGO1Δ91-189 IP
AGO1Δ1-189 IP
Mutant IP vs. AGO1 IP log2FC
miR173

Figure 2.5. The N-terminal extension of AGO1 allows AGO1 to distinguish between Dicer-dependent small RNAs and rRNA-derived small RNAs (rsRNAs).

(a to b) Analysis of small RNA-seq data of AGO1-associated small RNAs. Wild-type AGO1 and AGO1Δ1-90 were in the *ago1-36* background, while other AGO1 NTE-truncated mutants were in the *ago1-36/+* background. Two biological replicates of each genotype were included in the analysis.

(a) Size (in nt) distribution depicting the abundance of 18- to 26-nt rsRNAs in IPs from AGO1 and AGO1 NTE-truncated mutants. RPM, reads per million (see Methods).

(b) Composition of small RNAs in the 20-, 21-, 22-, and 24-nt classes in IPs from wild-type AGO1 (WT) and AGO1 NTE-truncated forms. Each column represents a biological replicate.

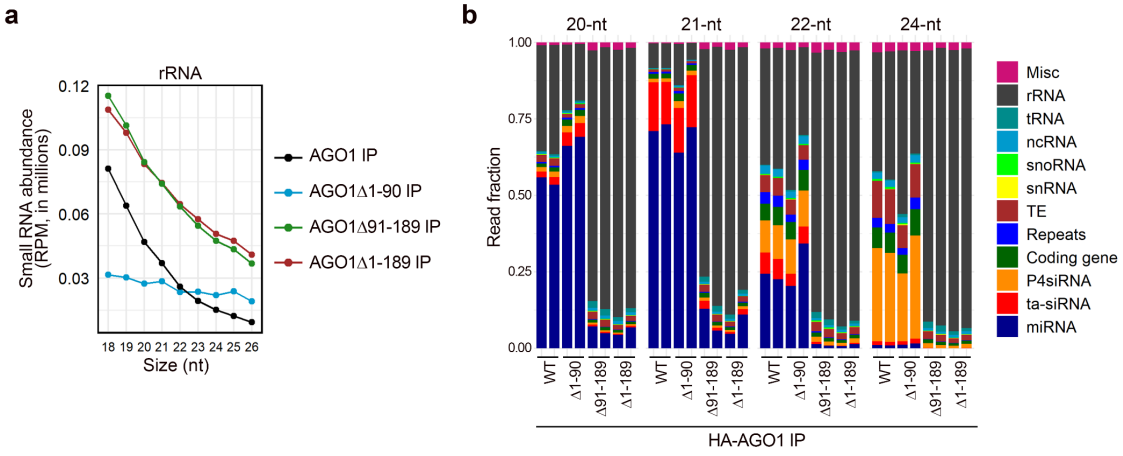
a
rRNA
Small RNA abundance (RPM, in millions)
0.12
0.09
0.06
0.03
18 19 20 21 22 23 24 25 26
Size (nt)
AGO1 IP
AGO1Δ1-90 IP
AGO1Δ91-189 IP
AGO1Δ1-189 IP
b
20-nt
21-nt
22-nt
24-nt
Read fraction
1.00
0.75
0.50
0.25
0.00
WT
Δ1-90
Δ91-189
Δ1-189
HA-AGO1 IP
Misc
rRNA
tRNA
ncRNA
snoRNA
snRNA
TE
Repeats
Coding gene
P4siRNA
ta-siRNA
miRNA

Figure S2.1. Phylogenetic analysis of Arabidopsis AGOs and Arabidopsis AGO NTEs, and alignment of Arabidopsis AGO NTEs.

(a) Phylogenetic analysis of 10 Arabidopsis AGOs. The black bars denote the lengths of the NTE regions in the AGOs.

(b) Alignments showing the conservation or lack of conservation of the NTE regions in the Arabidopsis AGO family. The red rectangle denotes identity of residues in all proteins. Yellow rectangles denote similar residues. The NLS and NES are marked by the red lines.

(c) Phylogenetic analysis of the NTE regions of 10 Arabidopsis AGOs.

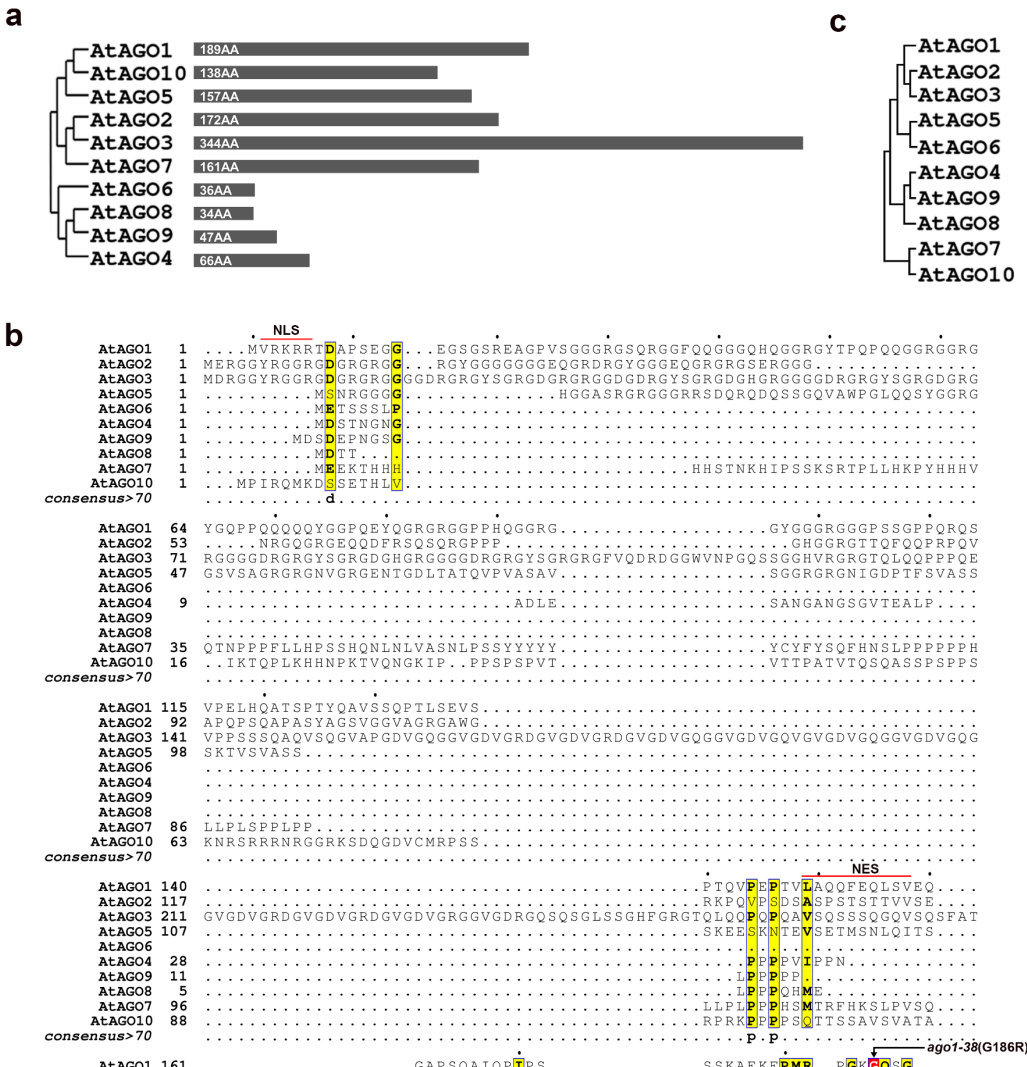
a
AtAGO1
AtAGO10
AtAGO5
AtAGO2
AtAGO3
AtAGO7
AtAGO6
AtAGO8
AtAGO9
AtAGO4
189AA
138AA
157AA
172AA
344AA
161AA
36AA
34AA
47AA
66AA
c
AtAGO1
AtAGO2
AtAGO3
AtAGO5
AtAGO6
AtAGO4
AtAGO9
AtAGO8
AtAGO7
AtAGO10
b
NLS
NES
ago1-38(G186R)
AtAGO1 1 ....MVRKRRTDAPSEGG...EGSGSREAGPVSGGGRGSQRGGFQQGGGQHQGGRGYTPQPQQGGRGGRG
AtAGO2 1 MERGGYRGGRGDGRGRGG...RGYGGGGGGGEQGRDRGYGGGEQGRGRGSERGGG
AtAGO3 1 MDRGGYRGGRGDGRGRGGGGDRGRGYSGRGDGRGRGGDGDRGYSGRGDGHGRGGGGDRGRGYSGRGDGRG
AtAGO5 1 ....MSNRGGGG.............HGGASRGRGGGRRSDQRQDQSSGQVAWPGLQQSYGGRG
AtAGO6 1 ....METSSSLP
AtAGO4 1 ....MDSTNGNG
AtAGO9 1 ....MDSDEPNGSG
AtAGO8 1 ....MDTT...
AtAGO7 1 ....MEEKTHH.....HHSTNKHIPSSKSRTPLLHKPYHHHV
AtAGO10 1 ...MPIRQMKDSSETHLV
consensus>70 ....d
AtAGO1 64 YGQPPQQQQQYGGPQEYQGRGRGGPPHQGGRG.....GYGGGRGGGPSSGPPQRQS
AtAGO2 53 .....NRGQGRGEQQDFRSQSQRGPPP.....GHGGRGTTQFQQPRPQV
AtAGO3 71 RGGGGDRGRGYSGRGDGHGRGGGGDRGRGYSGRGRGFVQDRDGGWVNPGQSSGGHVRGRGTQLQQPPPQE
AtAGO5 47 GSVSAGRGRGNVGRGENTGDLTATQVPVASAV.....SGGRGRGNIGDPTFSVASS
AtAGO6
AtAGO4 9 .....ADLE.....SANGANGSGVTEALP....
AtAGO9
AtAGO8
AtAGO7 35 QTNPPPFLLHPSSHQNLNLVASNLPSSYYYYY.....YCYFYSQFHNSLPPPPPPH
AtAGO10 16 ..IKTQPLKHHNPKTVQNGKIP..PPSPSPVT.....VTTPATVTQSQASSPSPPS
consensus>70
AtAGO1 115 VPELHQATSPTYQAVSSQPTLSEVS
AtAGO2 92 APQPSQAPASYAGSVGGVAGRGAWG
AtAGO3 141 VPPSSSQAQVSQGVAPGDVGQGGVGDVGRDGVGDVGRDGVGDVGQGGVGDVGQVGVGDVGQGGVGDVGQG
AtAGO5 98 SKTVSVASS
AtAGO6
AtAGO4
AtAGO9
AtAGO8
AtAGO7 86 LLPLSPPLPP
AtAGO10 63 KNRSRRRNRGGRKSDQGDVCMRPSS
consensus>70
AtAGO1 140 .....PTQVPEPTVLAQQFEQLSVEQ....
AtAGO2 117 .....RKPQVPSDSASPSTSTTVVSE....
AtAGO3 211 GVGDVGRDGVGDVGRDGVGDVGRGGVGDRGQSQSGLSSGHFGRGTQLQQPQPQAVSQSSSQGQVSQSFAT
AtAGO5 107 .....SKEESKNTEVSETMSNLQITS....
AtAGO6
AtAGO4 28 .....PPPPVIPPN.....
AtAGO9 11 .....LPPPPP.....
AtAGO8 5 .....LPPPQHME.....
AtAGO7 96 .....LLPLPPPHSMTRFHKSLPVSQ....
AtAGO10 88 .....RPRKPPPPSQTTSSAVSVATA....
consensus>70 .....p.p.....
AtAGO1 161 .....GAPSQAIQPIPS.....SSKAFKFPMR..PGKGQSG
AtAGO2 138 .....PVRVAEVMNLKPSVQV.....ATSDRKEPMKRPDRGGVVA
AtAGO3 281 GGVGLGAWARKPQLFSDSTVLPSSSSSNVVASHTASGSQVMTPKPSSSDKKEPVKRPDKGGNIK
AtAGO5 128 .....TETKPEMTSLPPA.....SSKAVTFPVR..PGRGTLG
AtAGO6 9 .....LSPISIEPEQP.....SHRDYDITTR..RGVGTTG
AtAGO4 37 .....VEPVRVKTELAE.....KKGPVRVPMAR.KGFGTRG
AtAGO9 17 .....FVPANLVPEVEP.....VKKNILLPMARPRGSGSKG
AtAGO8 13 .....REPL.....KSKSSLLPMTR.RGNGSKG
AtAGO7 117 .....VVERKQQHQQKKKIQVSNNKVSGSIAIEEAALVVAKRPDFGGQDG
AtAGO10 109 .....GEIVAVNHQMQMG.....VRKNSNFAPR..PGFGTLG
consensus>70 .....e.....p.....g.G..g

Figure S2.2. Protein sequence alignment of the NTE region of Arabidopsis AGO1 and AGO1s from six plant species. Alignments showing the conservation or lack of conservation of *Arabidopsis thaliana* AGO1 NTE regions in AGO1s from six plant species, including *Arabidopsis thaliana* (*At*), *Arabidopsis lyrate* (*Al*), *Brassica napus* (*Bn*), *Glycine max* (*Gm*), *Oryza sativa* (*Os*), and *Zea mays* (*Zm*). The red rectangles denote amino acid identity in all proteins. Yellow rectangles denote similar residues. The NLS and NES are marked by the red lines.

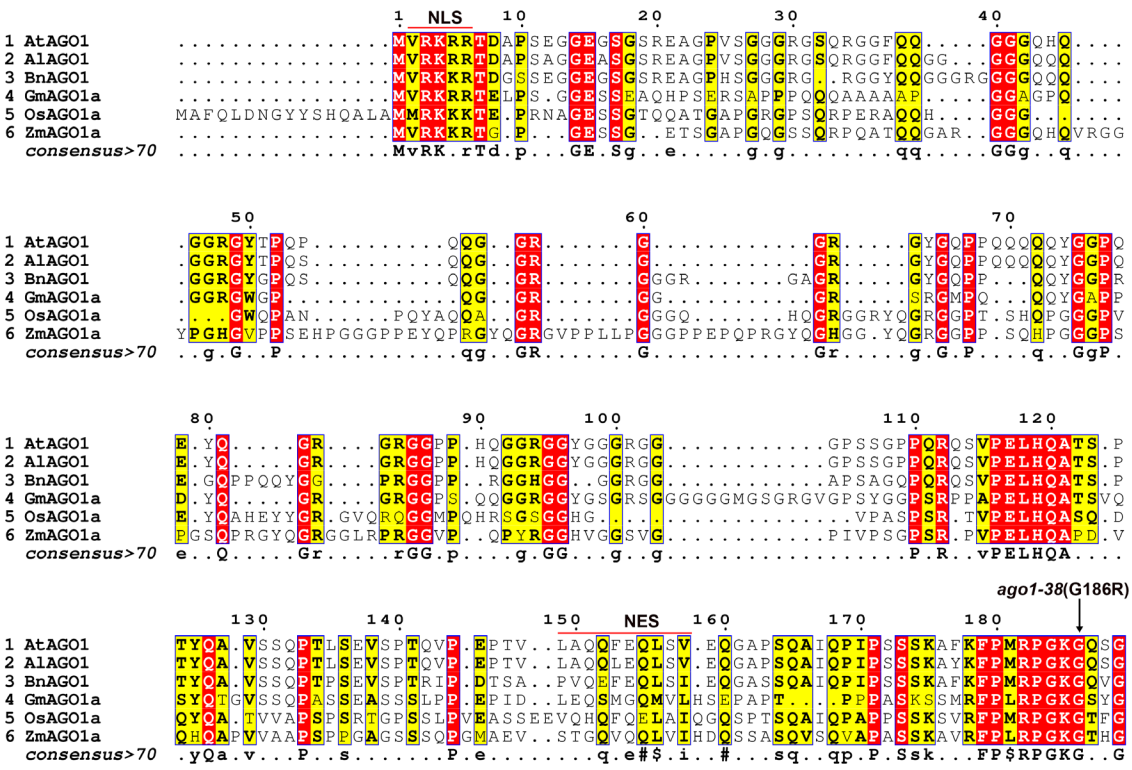
NLS
NES
ago1-38(G186R)
1 AtAGO1
2 AlAGO1
3 BnAGO1
4 GmAGO1a
5 OsAGO1a
6 ZmAGO1a
consensus>70

Figure S2.3. Analysis of small RNA-seq data of AGO1 NTE mutants.

(a) PCA showing the reproducibility of the three replicates.

(b) Size (in nt) distribution depicting the abundance of 18- to 26-nt total small RNAs and miRNAs in *ago1-36* expressing AGO1 and AGO1 NTE-truncated mutants. RPM, reads per million (see Methods).

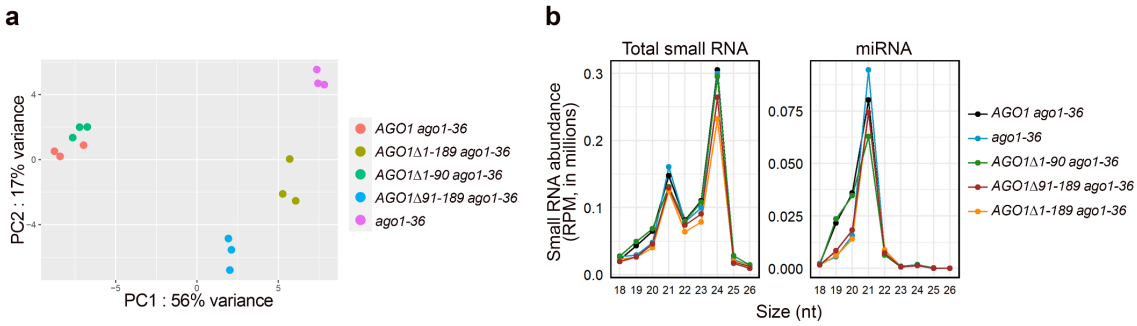
a
PC2 : 17% variance
PC1 : 56% variance
AGO1 ago1-36
AGO1Δ1-189 ago1-36
AGO1Δ1-90 ago1-36
AGO1Δ91-189 ago1-36
ago1-36
b
Total small RNA
miRNA
Small RNA abundance (RPM, in millions)
Size (nt)
AGO1 ago1-36
ago1-36
AGO1Δ1-90 ago1-36
AGO1Δ91-189 ago1-36
AGO1Δ1-189 ago1-36

Figure S2.4. Analysis of small RNA-seq data of AGO1-associated small RNAs.

(a) PCA analysis showing that the two biological replicates of each genotype were reproducible.

(b) Bar plots showing the composition of reads corresponding to annotated 19-to-24 nt miRNAs in AGO1 IPs and AGO1Δ1-90 IPs. Reads mapping to miRNA*s were excluded from this analysis. Annotated 20-nt miRNAs showed increased association with AGO1Δ1-90 as compared to wild type AGO1.

(c) Scatter plots comparing the $\log_2$(fold change) of IP-ed miRNAs and miRNA*s between pairs of AGO1 mutants.

(d) Heatmap depicting the differential levels of IP-ed miRNAs and their corresponding miRNA*s in AGO1 mutants. Note that only miRNAs for which the corresponding miRNA*s also passed the abundance filter (see Methods) are included in the heatmap.

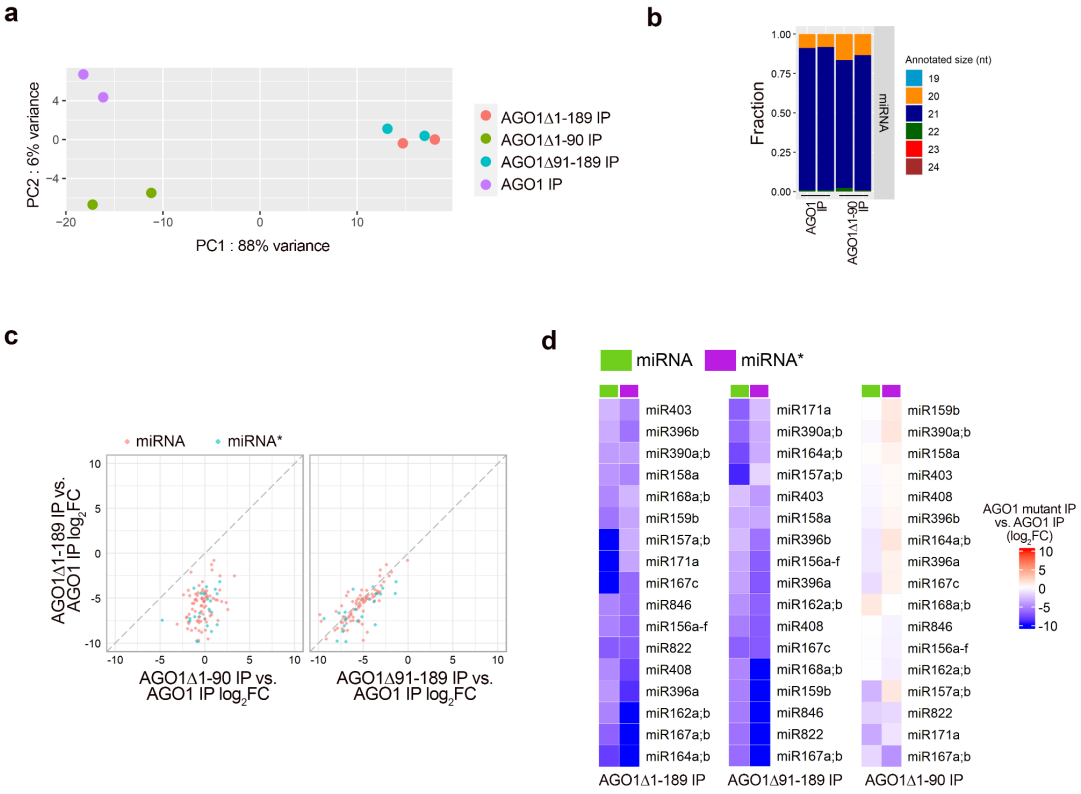
a
PC2 : 6% variance
PC1 : 88% variance
AGO1Δ1-189 IP
AGO1Δ1-90 IP
AGO1Δ91-189 IP
AGO1 IP
b
Fraction
miRNA
Annotated size (nt)
19
20
21
22
23
24
AGO1 IP
AGO1Δ1-90 IP
c
miRNA
miRNA*
AGO1Δ1-189 IP vs. AGO1 IP log2FC
AGO1Δ1-90 IP vs. AGO1 IP log2FC
AGO1Δ91-189 IP vs. AGO1 IP log2FC
d
miRNA
miRNA*
miR403
miR396b
miR390a;b
miR158a
miR168a;b
miR159b
miR157a;b
miR171a
miR167c
miR846
miR156a-f
miR822
miR408
miR396a
miR162a;b
miR167a;b
miR164a;b
AGO1Δ1-189 IP
miR171a
miR390a;b
miR164a;b
miR157a;b
miR403
miR158a
miR396b
miR156a-f
miR396a
miR162a;b
miR408
miR167c
miR168a;b
miR159b
miR846
miR822
miR167a;b
AGO1Δ91-189 IP
miR159b
miR390a;b
miR158a
miR403
miR408
miR396b
miR164a;b
miR396a
miR167c
miR168a;b
miR846
miR156a-f
miR162a;b
miR157a;b
miR822
miR171a
miR167a;b
AGO1Δ1-90 IP
AGO1 mutant IP vs. AGO1 IP (log2FC)

Figure S2.5. PCA analysis of RNA-seq data of AGO1 NTE mutants. Three biological replicates of each genotype cluster together.

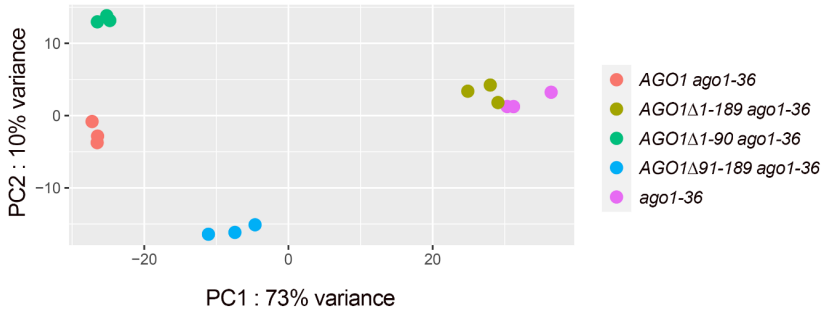
PC2 : 10% variance
10
0
−10
−20
0
20
PC1 : 73% variance
AGO1 ago1-36
AGO1Δ1-189 ago1-36
AGO1Δ1-90 ago1-36
AGO1Δ91-189 ago1-36
ago1-36

Figure S2.6. Biogenesis of phasiRNAs in NTE-truncated AGO1 mutants.

(a) The phasing of small RNAs over the *TAS* transcripts in *ago1-36* and *ago1-36* expressing wild-type *AGO1* or *AGO1* NTE mutants.

(b) The phasing of small RNAs over *AGO1*, *PPR*, and *NBS-LRR* gene transcripts in *ago1-36* and *ago1-36* expressing wild-type *AGO1* or *AGO1* NTE mutants.

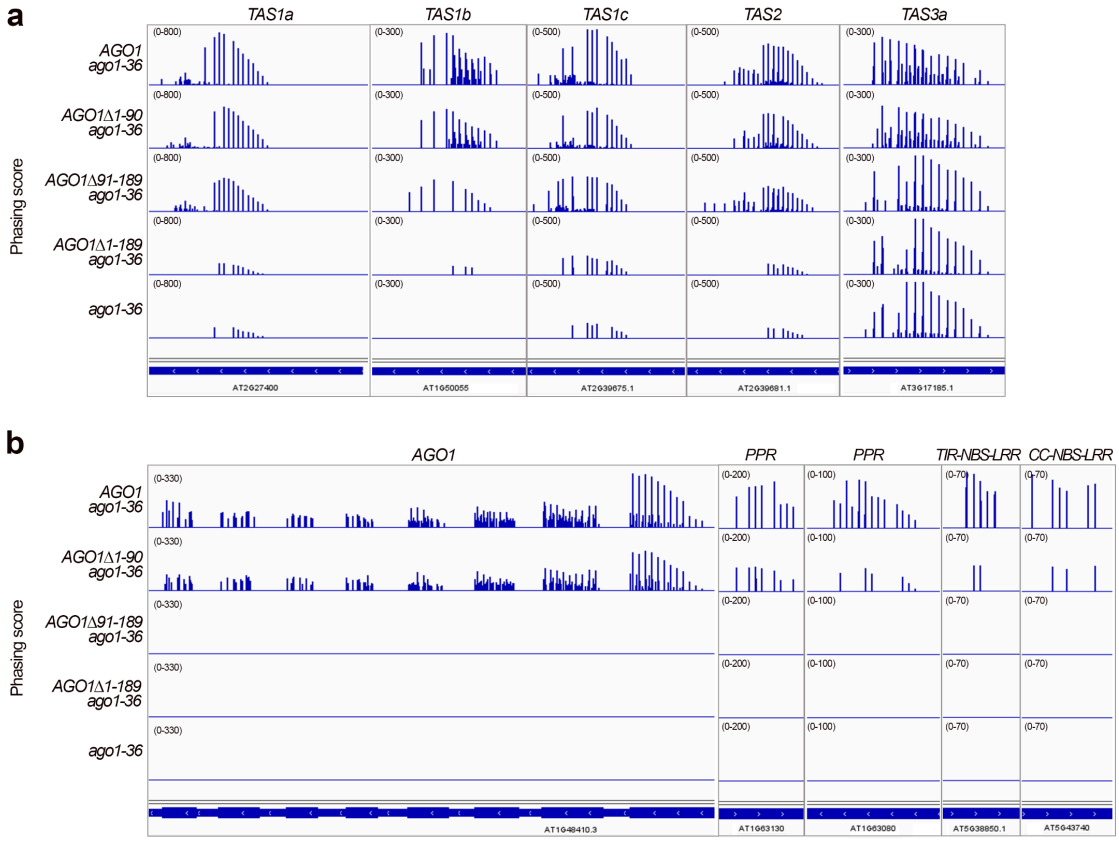
a
TAS1a
TAS1b
TAS1c
TAS2
TAS3a
Phasing score
AGO1
ago1-36
AGO1Δ1-90
ago1-36
AGO1Δ91-189
ago1-36
AGO1Δ1-189
ago1-36
ago1-36
(0-800)
(0-300)
(0-500)
(0-500)
(0-300)
AT2G27400
AT1G50055
AT2G39675.1
AT2G39681.1
AT3G17185.1
b
AGO1
PPR
PPR
TIR-NBS-LRR
CC-NBS-LRR
Phasing score
AGO1
ago1-36
AGO1Δ1-90
ago1-36
AGO1Δ91-189
ago1-36
AGO1Δ1-189
ago1-36
ago1-36
(0-330)
(0-200)
(0-100)
(0-70)
(0-70)
AT1G48410.3
AT1G63130
AT1G63080
AT5G38850.1
AT5G43740

Supplementary table 2.1. Primers and probes

Genotyping	**Sequence(5’ -> 3’)**
Y23 LBb1.3	ATTTTGCCGATTTCGGAAC
Y135 ago1-36 SALK_087076 F	AATCAGGTATATTCCGGTGGG
Y136 ago1-36 SALK_087076 R	CAATGAGGCTTTATCACCAGC
Cloning	**Sequence(5’ -> 3’)**
Y249 AGO1 NP OL 3XHA R	ttaacccgctcatGATGATTCCTGTGAAAATAACA CAAC
Y250 AGO1 NP OL 3XHA F	cacaggaatcatcATGAGCGGGTTAATTAAC
Y267 AGO1 CDS OL 3'UTR R	agggtgaatcaacTCAGCAGTAGAACATGAC
Y268 AGO1 CDS OL 3'UTR F	gttctactgctgaGTTGATTCACCCTCTATCTATCT TTATG
Y245 PEG301 NcoI OL AGO1NP 1.6K F	acaacttcttcgcccccgttttcacACGTGATGACAGCC ACCA
Y269 AGO1 3'UTR OL PEG301 XbaI R	ctagtcccgggtcttaattaactctTTTAGGCATTTTCCA CGC
Y249 AG01 NP OL 3XHA R (AGO1NP)	ttaacccgctcatGATGATTCCTGTGAAAATAACA CAAC
Y250 AG01 NP OL 3XHA F (3XHA)	cacaggaatcatcATGAGCGGGTTAATTAAC
Y528 AGO1 1-90AA OL NTD CDS R	tgcaacgcttATGAGGAGGTCCTCCTCTTC
Y529 AGO1 1-90AA OL NTD CDS F	acctcctcatAAGCGTTGCATTGTGAAG
AGO1 DEL1-189 CDS OL HA R	CTTCACAATGCAACGCTTCATGGTGAAGGG GGCGGCCGCGG
Y106 AGO1 DEL1-189 CDS OL HA F	ccgcggccgccccttcaccatgAAGCGTTGCATTGT GAAG
Y106 AGO1 DEL91-189 CDS OL HA R	GACCTCCTTGCATGGTGAAGGGGGCGGCC GCGG
Y106 AGO1 DEL91-189 CDS OL HA F	ccgcggccgccccttcaccatgcaaggaggtc
Northern blot probes	**Sequence(5’ -> 3’)**
U6 probe	AGGGGCCATGCTAATCTTCTC
miR168-AS probe	TTCCCGACCTGCACCAAGCGA
miR165/166-AS probe	GGGGAATGAAGCCTGGTCCGA
miR319-AS probe	AGGGAGCTCCCTTCAGTCCAA

References

1. Yu, Y., Zhang, Y., Chen, X. & Chen, Y. Plant noncoding RNAs: hidden players in development and stress responses. Annu. Rev. Cell Dev. Biol. 35, 407–431 (2019).
2. Song, X., Li, Y., Cao, X. & Qi, Y. MicroRNAs and their regulatory roles in plant-environment interactions. Annu. Rev. Plant Biol. 70, 489–525 (2019).
3. Xie, Z. et al. Expression of Arabidopsis MIRNA genes. Plant Physiol. 138, 2145–2154 (2005).
4. Park, W., Li, J., Song, R., Messing, J. & Chen, X. CARPEL FACTORY, a Dicer homolog, and HEN1, a novel protein, act in microRNA metabolism in Arabidopsis thaliana. Curr. Biol. 12, 1484–1495 (2002).
5. Yu, B. et al. Methylation as a crucial step in plant microRNA biogenesis. Science 307, 932–935 (2005).
6. Baumberger, N. & Baulcombe, D. C. Arabidopsis ARGONAUTE1 is an RNA slicer that selectively recruits microRNAs and short interfering RNAs. Proc. Natl. Acad. Sci. U. S. A. 102, 11928–33 (2005).
7. Mi, S. et al. Sorting of small RNAs into Arabidopsis Argonaute complexes is directed by the 5’ terminal nucleotide. Cell 133, 116–127 (2008).
8. Liu, Y., Teng, C., Xia, R. & Meyers, B. C. PhasiRNAs in plants:their biogenesis, genic sources, and roles in stress responses, development, and reproduction. Plant Cell 32, 3059–3080 (2020).
9. Yoshikawa, M., Peragine, A., Park, M. Y. & Poethig, R. S. A pathway for the biogenesis of trans-acting siRNAs in Arabidopsis. Genes Dev. 19, 2164–75 (2005).
10. Gasciolli, V., Mallory, A. C., Bartel, D. P. & Vaucheret, H. Partially redundant functions of arabidopsis DICER-like enzymes and a role for DCL4 in producing trans-acting siRNAs. Curr. Biol. 15, 1494–1500 (2005).
11. Allen, E., Xie, Z., Gustafson, A. M. & Carrington, J. C. microRNA-directed phasing during trans-acting siRNA biogenesis in plants. Cell 121, 207–221 (2005).
12. Montgomery, T. A. et al. Specificity of ARGONAUTE7-miR390 interaction and dual functionality in TAS3 trans-acting siRNA formation. Cell 133, 128–141 (2008).
13. Chen, H. M. et al. 22-nucleotide RNAs trigger secondary siRNA biogenesis in plants. Proc. Natl. Acad. Sci. U. S. A. 107, 15269–15274 (2010).

14. Cuperus, J. T. et al. Unique functionality of 22-nt miRNAs in triggering RDR6-dependent siRNA biogenesis from target transcripts in Arabidopsis. Nat. Struct. Mol. Biol. 17, 997–1003 (2010).

15. Axtell, M. J., Jan, C., Rajagopalan, R. & Bartel, D. P. A Two-hit trigger for siRNA biogenesis in plants. Cell 127, 565–577 (2006).

16. Kwak, P. B. & Tomari, Y. The N domain of Argonaute drives duplex unwinding during RISC assembly. Nat. Struct. Mol. Biol. 19, 145–152 (2012).

17. Lingel, A., Simon, B., Izaurralde, E. & Sattler, M. Nucleic acid 3′-end recognition by the Argonaute2 PAZ domain. Nat. Struct. Mol. Biol. 11, 576–577 (2004).

18. Ma, J. B., Ye, K. & Patel, D. J. Structural basis for overhang-specific small interfering RNA recognition by the PAZ domain. Nature 429, 318–322 (2004).

19. Frank, F., Sonenberg, N. & Nagar, B. Structural basis for 5′-nucleotide base-specific recognition of guide RNA by human AGO2. Nature 465, 818–822 (2010).

20. Frank, F., Hauver, J., Sonenberg, N. & Nagar, B. Arabidopsis Argonaute MID domains use their nucleotide specificity loop to sort small RNAs. EMBO J. 31, 3588–95 (2012).

21. Song, J., Smith, S. K., Hannon, G. J. & Joshua-Tor, L. Crystal structure of Argonaute and its implications for RISC slicer activity. Science 305, 1434–1437 (2004).

22. Liu, J. et al. Argonaute2 is the catalytic engine of mammalian RNAi. Science 305, 1437–1441 (2004).

23. Carbonell, A. et al. Functional analysis of three Arabidopsis ARGONAUTES using slicer-defective mutants. Plant Cell 24, 3613–3629 (2012).

24. Qi, Y. et al. Distinct catalytic and non-catalytic roles of ARGONAUTE4 in RNA-directed DNA methylation. Nature 443, 1008–1012 (2006).

25. Ji, L. et al. ARGONAUTE10 and ARGONAUTE1 regulate the termination of floral stem cells through two microRNAs in Arabidopsis. PLoS Genet. 7, 1–14 (2011).

26. Schirle, N. T. & MacRae, I. J. The crystal structure of Human Argonaute2. Science 336, 1037–1040 (2012).

27. Nakanishi, K., Weinberg, D. E., Bartel, D. P. & Patel, D. J. Structure of yeast Argonaute with guide RNA. Nature 486, 368–374 (2012).

28. Elkayam, E. et al. The structure of human argonaute-2 in complex with miR-20a. Cell 150, 100–110 (2012).

29. Wang, Y., Sheng, G., Juranek, S., Tuschl, T. & Patel, D. J. Structure of the guide-strand-containing argonaute silencing complex. Nature 456, 209–214 (2008).

30. Bologna, N. G. et al. Nucleo-cytosolic shuttling of ARGONAUTE1 prompts a revised model of the plant microRNA pathway. Mol. Cell 69, 709-719.e5 (2018).

31. Zhang, B. et al. Linking key steps of microRNA biogenesis by TREX-2 and the nuclear pore complex in Arabidopsis. Nat. Plants 6, 957–969 (2020).

32. Poulsen, C., Vaucheret, H. & Brodersen, P. Lessons on RNA silencing mechanisms in plants from eukaryotic Argonaute structures. Plant Cell 25, 22–37 (2013).

33. Gregory, B. D. et al. A link between RNA metabolism and silencing affecting Arabidopsis development. Dev. Cell 14, 854–866 (2008).

34. Brodersen, P. et al. Isoprenoid biosynthesis is required for miRNA function and affects membrane association of ARGONAUTE 1 in Arabidopsis. Proc. Natl. Acad. Sci. U. S. A. 109, 1778–1783 (2012).

35. Li, S. et al. MicroRNAs inhibit the translation of target mRNAs on the endoplasmic reticulum in Arabidopsis. Cell 153, 562–574 (2013).

36. Li, S. et al. Biogenesis of phased siRNAS on membrane-bound polysomes in Arabidopsis. Elife 5, e22750 (2016).

37. Vaucheret, H., Mallory, A. C. & Bartel, D. P. AGO1 homeostasis entails coexpression of MIR168 and AGO1 and preferential stabilization of miR168 by AGO1. Mol. Cell 22, 129–136 (2006).

38. Gudipati, R. K. et al. Protease-mediated processing of Argonaute proteins controls small RNA association. Mol. Cell 81, 2388–2402 (2021).

39. Meyer, W. J. et al. Overlapping functions of Argonaute proteins in patterning and morphogenesis of Drosophila embryos. PLoS Genet. 2, 1224–1239 (2006).

40. Thandapani, P., O'Connor, T. R., Bailey, T. L. & Richard, S. Defining the RGG/RG motif. Mol. Cell 50, 613–623 (2013).

41. Bohmert, K. et al. AGO1 defines a novel locus of Arabidopsis controlling leaf development. EMBO J. 17, 170–180 (1998).

42. Arribas-Hernández, L., Kielpinski, L. J. & Brodersen, P. mRNA decay of most Arabidopsis miRNA targets requires slicer activity of AGO1. Plant Physiol. 171, 2620–2632 (2016).

43. Iwasaki, S. et al. Hsc70/Hsp90 chaperone machinery mediates ATP-dependent RISC loading of small RNA duplexes. Mol. Cell 39, 292–299 (2010).

44. Nakamura, S. et al. Gateway binary vectors with the bialaphos resistance gene, bar, as a selection marker for plant transformation. Biosci. Biotechnol. Biochem. 74, 1315–1319 (2010).

45. Earley, K. W. et al. Gateway-compatible vectors for plant functional genomics and proteomics. Plant J. 45, 616–629 (2006).

46. Martin, M. Cutadapt removes adapter sequences from high-throughput sequencing reads. EMBnet.journal 17, 10 (2011).

47. Johnson, N. R., Yeoh, J. M., Coruh, C. & Axtell, M. J. Improved placement of multi-mapping small RNAs. G3 Genes, Genomes, Genet. 6, 2103–2111 (2016).

48. Love, M. I., Huber, W. & Anders, S. Moderated estimation of fold change and dispersion for RNA-seq data with DESeq2. Genome Biol. 15, (2014).

49. Crooks, G. E., Hon, G., Chandonia, J. & Brenner, S. E. WebLogo : A sequence logo generator. Genome Res. 14, 1188–1190 (2004).

50. Dobin, A. et al. STAR: Ultrafast universal RNA-seq aligner. Bioinformatics 29, 15–21 (2013).

51. Liao, Y., Smyth, G. K. & Shi, W. FeatureCounts: An efficient general purpose program for assigning sequence reads to genomic features. Bioinformatics 30, 923–930 (2014).

52. Paoli, E. D. E. et al. Distinct extremely abundant siRNAs associated with cosuppression in petunia. RNA 1965–1970 (2009). doi:10.1261/rna.1706109.RNA

53. Howell, M. D. et al. Genome-wide analysis of the RNA-DEPENDENT RNA POLYMERASE6/DICER-LIKE4 pathway in Arabidopsis reveals dependency on miRNA- and tasiRNA-directed targeting. Plant Cell 19, 926–942 (2007).

54. Edgar, R. C. MUSCLE : a multiple sequence alignment method with reduced time and space complexity. BMC Bioinformatics 5, (2004).

55. Robert, X. & Gouet, P. Deciphering key features in protein structures with the new ENDscript server. Nucleic Acids Res. 42, W320-4 (2014).

56. Jumper, J. et al. Highly accurate protein structure prediction with AlphaFold. Nature 596, 583–589 (2021).

Chapter 3

Phosphorylation regulates the activities of the microRNA and small interfering RNA effector ARGONAUTE1 in Arabidopsis

Abstract

ARGONAUTE1 (AGO1) is a major effector of small RNA-mediated gene silencing in plants and performs crucial functions in development and immunity. To date, little is known about whether and how post-translational modifications regulate AGO1 activities. Here, we revealed that *Arabidopsis thaliana* AGO1 is phosphorylated *in vivo*, and the phosphorylation status of AGO1 impacts RISC formation and RISC activity. We identified a highly conserved phospho-tyrosine residue Y255 residing in the N domain of AGO1. *In vivo* analysis of AGO1-associated small RNAs and *in vitro* RISC formation assays showed that phospho-mimetic AGO1 is compromised in the loading of both microRNA (miRNA) and small interfering RNA (siRNA) duplexes and in passenger strand ejection of siRNA but not miRNA duplexes. On the other hand, non-phosphorylatable AGO1 is compromised in target RNA repression. These findings implicated that phosphorylation and dephosphorylation of AGO1 regulate the efficiency of RISC formation and target repression.

Introduction

MicroRNA (miRNA)-mediated gene silencing is a central mechanism that regulates gene expression in eukaryotes. In plants, genes encoding miRNAs are transcribed by RNA polymerase II into stem-loop-containing pri-miRNAs, which are processed into duplexes with 2-nt 3' overhangs by DICER-LIKE1 (DCL1)[1–6]. The duplexes are further 2'-*O*-methylated at the 3' ends by the methyltransferase HUA ENHANCER1 (HEN1), followed by loading into ARGONAUTE1 (AGO1)[7–10]. After loading, the passenger strand (miRNA*) of the duplex is selectively ejected, while the guide strand (miRNA) remains associated with AGO1 to form a functional RNA-induced silencing complex (RISC)[10]. miRNA-loaded RISCs (miRISCs) recognize target mRNAs through base pairing and cause mRNA cleavage or translational repression to regulate target gene expression[8,11–13]. In *Arabidopsis thaliana* (*At*), most miRNAs associate with AGO1[14], one of ten AGO family members, and act in many developmental processes[15,16]. Loss-of-function mutants of *AGO1* display pleiotropic defects in plant growth and development[17]. In addition to repressing gene expression, specific miRISCs, such as Arabidopsis miR173-AGO1 and miR390-AGO7, also trigger the production of 21-nt secondary small interfering RNAs (siRNAs) from non-coding *TAS* transcripts in a phased pattern[18–22]. Some of the secondary siRNAs function similarly to miRNAs in directing the silencing of non-*TAS* transcripts and are thus named trans-acting siRNAs (ta-siRNAs)[18,23–25]. Ta-siRNAs also function through AGO1, forming siRNA-loaded RISCs (siRISCs)[8,9].

Most eukaryotic AGOs are composed of four highly conserved domains: a poorly understood N domain, a PAZ (PIWI-ARGONAUTE-ZWILLE) domain that binds and anchors the 3' end of the guide RNA[26,27], a MID (middle) domain containing a nucleotide specificity loop that determines the preference for the 5' nucleotide[28,29], and a PIWI domain that harbors an RNase H-like motif allowing some AGO proteins to cleave RNAs that are complementary to the guide RNA (the endonuclease activity is sometimes referred to as the slicer activity)[30,31]. The MID and PIWI domains also form a binding pocket that anchors the 5' phosphate (P) of the guide RNA[32,33]. Besides the highly conserved domains, Arabidopsis AGO1 contains a probably unstructured N-terminal extension that harbors a nuclear localization (NLS) signal and a nuclear export (NES) signal[34]. Mature miRNAs are thought to be loaded into AGO1 in the nucleus and then exported to the cytosol as miRISCs[34]. Some endogenous siRNAs, such as ta-siRNAs, are thought to be loaded into AGO1 in the cytoplasm[34].

RISC assembly entails at least two phases, small RNA duplex loading to form the pre-RISC and RISC maturation in which the passenger strand is ejected. *In vitro* studies showed that Heat Shock Protein 90 (HSP90) assists the loading of miRNAs and siRNAs into Arabidopsis AGO1, likely by inducing conformational changes of AGO1 to enable small RNA binding[10]. Consistent with the model of small RNA loading in plants, both Drosophila and human studies found that Hsp70 and Hsp90 chaperones together activate AGO2 into an open form that allows small RNA duplex loading[35,36]. The removal of the passenger strand occurs in either a

slicer-dependent or slicer-independent manner. Studies on plant AGO1 showed that the release of miRNAs does not require AGO1's endonuclease activity, probably because the imperfect base pairing of the duplex sufficiently lowers the energy required for strand separation[10,37]. In contrast to miRISC formation, strand separation for siRNA duplexes requires the slicer activity of AGO1[10,37]. Notably, a study of human AGO2 led to the proposal that the 3' end of the guide strand in the small RNA duplex is pried open through wedging by the N domain in preparation for passenger strand ejection, and that passenger strand cleavage in siRISC formation requires a functional N domain[38]. Moreover, a structural study of a *Thermus thermophilus* AGO suggested that the N domain blocks guide DNA-target RNA base pairing beyond position 16[39]. Thus, it is likely that the N domain plays a role in RISC maturation and RISC activity.

In addition to interacting proteins such as chaperones, the functions of AGO proteins are regulated via phosphorylation, which is a reversible post-translational modification that may alter protein activity by the addition of a phosphate group[40]. In eukaryotes, phosphorylation usually occurs on the hydroxyl group of certain serine (S), threonine (T), or tyrosine (Y) residues within the target proteins[40]. Studies in animals have reported that phosphorylation can impact RISC in several ways, including small RNA loading, target silencing activities, and subcellular localization[41–46]. For example, a phospho-mimetic mutation of human AGO2 at position 529, which substitutes a tyrosine residue located in the small RNA 5'-binding pocket for a glutamic acid to mimic the constitutively phosphorylated state,

inhibits small RNA binding[42]. Human AGO2 is thought to undergo a phosphorylation and dephosphorylation cycle at the highly conserved S824–S834 cluster, which is important for the association of miRISCs with target mRNAs[43]. Non-phosphorylated human AGO2 shows a significantly expanded target repertoire, which reduces the silencing efficiency of individual target transcripts[43]. Phospho-mimetic substitution at the same cluster of *Caenorhabditis elegans* ALG-1, a miRNA effector, impairs its binding to target mRNAs[45]. Moreover, reduced phosphorylation of human AGO2 at S387 disrupts its localization to processing bodies and interaction with GW182[44,46].

To date, knowledge of phosphorylation of plant AGOs is lacking. Using mass spectrometry analysis, we found that Arabidopsis AGO1 is phosphorylated at multiple sites *in vivo*. Among these amino acids, a tyrosine residue located in the N domain, Y255, is conserved in both land plant AGO1 proteins and some animal AGOs. Characterization of non-phosphorylatable and phospho-mimetic mutants of AGO1 at Y255 showed that neither form was able to fully rescue the developmental phenotypes of an *ago1* null mutant. Analyses of *in vivo* small RNA association and *in vitro* RISC assembly showed that the phospho-mimetic AGO1 at Y255 was defective in the loading of both miRNA and siRNA duplexes; while the ejection of passenger strand to form mature miRISCs was largely normal, strand separation to form mature siRISCs was compromised. In contrast, *in vivo* formation of miRISCs and siRISCs were largely normal for non-phosphorylatable AGO1 at Y255. However, the repression of a set of miRNA target transcripts was

impaired, suggesting a partial loss of RISC activity. Together, our findings suggest that the phosphorylation status of AGO1 at Y255 affects the efficiency of RISC formation and target repression, and that plants adopt phosphorylation as a means to regulate the activities of AGO1 in gene silencing.

Results

Arabidopsis thaliana AGO1 is phosphorylated at multiple residues *in vivo*

In several independent efforts to identify AGO1-interacting proteins, we performed AGO1 immunoprecipitation (IP) followed by mass spectrometry. In these experiments, we also noticed four phospho-peptides at discrete locations of AGO1 (Supplementary Fig. 3.1a, 3.1b, 3.1c, and 3.1d). The mass signatures pinpointed three phosphorylated serine residues: S11 in the N terminal extension region, S350 in Linker 1 between the N and PAZ domains, and S1001 in the C-terminal region close to the PIWI domain (Fig. 3.1a). In addition, a peptide from the less functionally characterized N domain, ^{253}SLYTAGPLPFNSK^{265}, was identified as a phospho-peptide containing a mono-phosphate (Supplementary Fig. 3.1d). A weak MS/MS signal corresponding to a phosphorylated fragment of ^{255}YTAGPLPFNSK^{265} was observed, while the ^{256}TAGPLPFNSK^{265} fragment did not show phosphorylation, suggesting that the phosphorylation residue was likely Y255 (Supplementary Fig. 3.1e). However, due to the weak signal, phosphorylation on S253 could not be excluded. Thus, both S253 and Y255 were included in this study.

Next, we investigated whether the amino acids that undergo phosphorylation are conserved. The AGO family has undergone expansion during plant evolution, with most species containing more than one AGO member[47]. Based on phylogenetic relationships, the 10 *Arabidopsis thaliana* AGO proteins can be grouped into three clades, AGO1/5/10, AGO2/3/7, and AGO4/6/8/9. Residues S11, S350, and S1001 are in variable regions of the AGO1 protein, and they are not conserved even within the AGO1/5/10 clade (Fig. 3.1b). AGO1 S253 and Y255 are present in all members of the AGO1/5/10 clade, and Y255 is also conserved in AGO6, 7, and 8 from the other two clades (Fig. 3.1b). This suggested that, with the exception of Y255, these residues are specific to AGO1 or the AGO1 clade. Next, we examined the conservation of these residues among plant AGO1 orthologs and non-plant AGO homologs. Multiple sequence alignment was performed with 16 AGO and PIWI proteins from 13 species, including seven monocotyledonous and dicotyledonous flowering plants, the moss *Physcomitrella patens*, the green alga *Chlamydomonas reinhardtii*, the bacterium *Thermus thermophilus*, the fission yeast *Schizosaccharomyces pombe*, the fruit fly *Drosophila melanogaster* and two mammalian species, mouse and human (Fig. 3.1c). All five residues of Arabidopsis AGO1 are also found in AGO1 proteins from two other Brassicaceae family members, *Arabidopsis lyrata* and *Brassica napus*. S253, Y255, and S1001 are conserved among the seven flowering plants and the moss *P. patens*. Y255 is not only highly conserved among all land plant AGO1s, but is also present in non-plant AGOs, such as fruit fly AGO1, mouse AGO2, and

human AGO2. The conservation of Arabidopsis AGO1 Y255 implies that this residue is important for the structure and/or function of AGO proteins across species.

As the function of the AGO N domain is little known, we were particularly interested in the potential function of the highly conserved residues S253 and Y255 in Arabidopsis AGO1. We modeled AGO1 based on the crystal structure of human AGO2 with an associated 21-nt single-stranded guide RNA (Fig. 3.1d)[48]. S253 and Y255 were found to be located on the same β-sheet facing the central cleft. As the central cleft accommodates RNA during both pre-RISC formation and target RNA binding, we suspect that the phosphorylation of S253 or Y255 might affect small RNA loading and/or small RNA-target RNA interaction.

Non-phosphorylatable or phospho-mimetic AGO1 mutations cause severe morphological and molecular defects

To evaluate whether phosphorylation at these residues (S11, S253, Y255, S350, S1001) affects the function of Arabidopsis AGO1, we mutated all five residues to alanine or aspartic acid to produce a non-phosphorylatable form (5A) or a phospho-mimetic form (5D), respectively. We then generated stable transgenic lines expressing N-terminal HA-tagged, wild-type (WT) or mutant AGO1 driven by the *AGO1* promoter in the Arabidopsis *ago1-36* background. The *ago1-36* allele is likely a null as it possesses a T-DNA insertion that is predicted to truncate the protein, such that the mutant protein would lack the MID and PIWI domains, which are essential for small RNA loading[8]. Indeed, *ago1-36* mutants are

seedling-lethal and resemble the phenotypes of *ago1-3,* an *ago1* null allele in which a premature stop codon at glycine 42 leads to a loss of AGO1 activity[17,49]. AGO1 was proposed to protect its associated miRNAs from degradation, as in *ago1-3* the accumulation of most miRNAs is reduced[49,50]. The *ago1-36* mutant was shown to have reduced levels of miRNAs[51,52]. By northern blots, we show that miRNA levels are similarly reduced in *ago1-36* and *ago1-3* seedlings (Supplementary Fig. 3.2). Taken together, these findings suggest that in *ago1-36*, the truncated AGO1 protein is compromised in miRNA loading. Thus, we introduced transgenes encoding AGO1 phosphorylation mutants into the *ago1-36* background to study their functions.

For simplicity, we refer to these transgenes as *AGO1*, *AGO1 5A* and *AGO1 5D*. We found that while WT *AGO1* fully rescued the developmental phenotypes of *ago1-36* plants, neither *AGO1 5A* nor *AGO1 5D* did (Fig. 3.2a, 3.2b and Supplementary Fig. 3.3a, 3.3b). *AGO1 5A ago1-36* plants were smaller than *AGO1 ago1-36*, had abnormal rosette leaves resembling the partial loss-of-function *ago1* mutant *ago1-27*[53] (Fig. 3.2b) and showed reduced fertility (Supplementary Fig. 3c). *AGO1 5D ago1-36* plants had more severe phenotypes, these plants could barely bolt and were infertile with darker green, long, and narrow leaves (Fig. 3.2a, 3.2b and Supplementary Fig. 3.3a, 3.3b). This implies that some, if not all, phosphoresidues are vital for the functions of *At*AGO1.

To determine the effects of the non-phosphorylatable and phospho-mimetic mutations of AGO1 on miRNA accumulation, we performed RNA gel blot analysis

with seedlings of *ago1-36* and *ago1-36* expressing *AGO1*, *AGO1 5A* and *AGO1 5D*. In *ago1-36,* the accumulation of three miRNAs, miR168, miR319, and miR165/166, was reduced to varying degrees as compared to *AGO1 ago1-36*; the reduced accumulation of these three miRNAs was fully rescued by *AGO1 5A* but only partially rescued by *AGO1 5D* (Fig. 3.3a). Next, small RNA sequencing was performed with seedlings of *ago1-36* expressing *AGO1*, *AGO1 5A* or *AGO1 5D* to determine the global profiles of small RNAs. Principal component analysis (PCA) showed that the three biological replicates of each genotype were highly reproducible (Supplementary Fig. 3.4a). The small RNA size distribution was similar for *AGO1 ago1-36*, *AGO1 5A ago1-36*, and *AGO1 5D ago1-36* (Supplementary Fig. 3.4b). Few differentially accumulated miRNAs were found between *AGO1 5A ago1-36* and *AGO1 ago1-36*, while more such miRNAs were found between *AGO1 5D ago1-36* and *AGO1 ago1-36* (Supplementary Fig. 3.4c). It was noteworthy that a number of miRNA*s accumulated to higher levels in *AGO1 5D ago1-36* than *AGO1 ago1-36* (Supplementary Fig. 3.4c). The miRISC formation process entails at least two events: 1) duplex loading, during which strand selection occurs whereby the 5' end of the miRNA is loaded into the MID-PIWI pocket of AGO, and 2) passenger strand ejection. A reduced efficiency in duplex loading results in lower levels of both miRNA and miRNA*, while defects in strand selection or passenger strand ejection results in higher levels of miRNA*. To evaluate the potential defect in miRISC formation for AGO1 5D, we examined the abundance of miRNAs and their corresponding miRNA*s. As compared to *AGO1*

ago1-36, a few miRNAs and miRNA*s had opposite changes in *AGO1 5D ago1-36* (Supplementary Fig. 3.4d). This could be due to a strand selection problem, or a combined defect in both duplex loading and passenger strand ejection. An alternative possibility for the increased abundance of miRNA*s was the loading of the miRNA*s into another AGO protein in the absence of a functional AGO1. In fact, miRNA*s accumulate to higher levels in *ago1* null mutants, consistent with their loading into another AGO protein[49].

We next determined the ability of AGO1 5A and AGO1 5D to associate with miRNAs *in vivo* by AGO1 IP followed by small RNA sequencing. To ensure that the small RNA populations were similar, the experiment was conducted with *pAGO1::HA-AGO1* in the *ago1-36* homozygous background vs. *pAGO1::HA-AGO1 5A* and *pAGO1::HA-AGO1 5D* in the *ago1-36* heterozygous background. Two replicates of AGO1 IP samples were processed, and PCA analysis showed that the replicates were reproducible (Supplementary Fig. 3.5a). All AGO1 IP samples showed a diminished 24-nt peak as compared to the input samples, suggesting that the IP was successful as AGO1 prefers to bind 21-nt rather than 24-nt small RNAs (Supplementary Fig. 3.5b)[14]. However, AGO 5D IP was different in that a 20-nt peak was more prominent (Supplementary Fig. 3.5b) and that the proportion of ta-siRNAs was reduced (Supplementary Fig. 3.5c). Consistently, RNA gel blot assays showed that AGO1 5D-associated ta-siRNAs from *TAS1* loci were reduced in abundance (Supplementary Fig. 3.5d).

We further examined the association of miRNAs and miRNA*s with AGO1 5A and AGO1 5D in comparison to AGO1. Globally, miRNA and miRNA* read counts were similar in AGO1 IP and AGO1 5A IP but drastically different between AGO1 IP and AGO1 5D IP, with AGO1 5D showing lower levels of associated miRNAs and miRNA*s (Supplementary Fig. 3.5e). As miRNAs are in general stabilized when loaded into an AGO protein, this could explain the reduction in miRNA abundance in *AGO1 5D ago1-36* (Supplementary Fig. 3.4c). Next, we determined differentially immunoprecipitated miRNAs or miRNA*s in AGO1 5A IP and AGO1 5D IP in comparison to AGO1 IP, using fold change > 1.5 and adjusted *P* value < 0.01 as the criteria. Many miRNAs and a few miRNA*s showed significantly reduced AGO1 5D association, while a few miRNA*s exhibited increased AGO1 5D association (Supplementary Fig. 3.5f). Also, a subset of miRNA*s showed increased abundance while the corresponding miRNAs showed reduced abundance in AGO1 5D IP (Supplementary Fig. 3.5g), implying that AGO1 5D might be compromised in strand selection or in both duplex loading and passenger strand ejection.

In contrast to AGO1 5D, AGO1 5A was largely similar to AGO1 in its association with miRNAs, miRNAs*, and ta-siRNAs (Supplementary Fig. 3.5d, 3.5e, and 3.5f), suggesting that the morphological phenotype of *AGO1 5A ago1-36* must result from a defect after RISC formation. We thus conducted RNA-seq with *AGO1*, *AGO1 5A* and *AGO1 5D* in the *ago1-36* background. Among the 130 experimental confirmed miRNA target genes analyzed[54], approximately 25% and 17% were

derepressed in *AGO1 5D ago1-36* and *AGO1 5A ago1-36*, respectively, as compared to *AGO1 ago1-36* (Supplementary Table 3.1).

In summary, these results suggested that phospho-mimetic AGO1 is compromised in miRISC formation, possibly in duplex loading, strand selection, or passenger strand ejection. In contrast, non-phosphorylatable AGO1 affects target RNA repression.

AGO1 phosphorylation residues S253 and Y255 are functionally important

To further investigate which phosphoresidue(s) is(are) essential for the functions of AGO1, we generated phospho-mimetic mutants of AGO1 by introducing into *ago1-36* transgenes with single or multiple mutations at amino acids that are highly conserved across flowering plants. The transgenic lines were *pAGO1::AGO1 3D (S253D/Y255D/S1001D)*, *pAGO1::AGO1 2D (S253D/Y255D)*, *pAGO1::AGO1 S253D*, and *pAGO1::AGO1 Y255D*. Similarly, transgenes encoding non-phosphorylatable forms of AGO1 at single or multiple residues were introduced into the *ago1-36* background, including *pAGO1::AGO1 2A (S253A/Y255A)*, *pAGO1::AGO1 S253A*, *pAGO1::AGO1 Y255A*, and *pAGO1::AGO1 S1001A*.

The *ago1-36* phenotype was fully rescued only in *AGO1 S1001A ago1-36* transgenic lines (Supplementary Fig. 3.3d). In addition, *AGO1 3D* and *AGO1 2D* conferred similar morphological phenotypes as *AGO1 5D* at all developmental stages (Fig. 3.2a, 3.2b and Supplementary Fig. 3.3a, 3.3b and 3.3d). This suggested that changes in the phosphorylation status of AGO1 S1001 did not

contribute to the severe morphological phenotypes of *AGO1 5A ago1-36* or *AGO1 5D ago1-36* lines. Next, we examined the phenotypes of S253 and Y255 single phospho-mutants and S253/Y255 double phospho-mutants (Fig. 3.2a, 3.2b and Supplementary Fig. 3.3a, 3.3b, and 3.3c). None of the *pAGO1::HA-AGO1* transgenes with a single mutation (S253A, S253D, Y255A, and Y255D) fully rescued *ago1-36* phenotypes (Fig. 3.2a, 3.2b and Supplementary Fig. 3.3a, 3.3b, and 3.3c). Among the transgenic lines, *AGO1 S253A ago1-36* exhibited the mildest phenotypes, with a slight reduction in seed set and ovule size (Supplementary Fig. 3.3c). Both Y255A *ago1-36* and Y255D *ago1-36* lines showed a lower seed set than S253A *ago1-36* or S253D *ago1-36* lines (Supplementary Fig. 3.3c). Meanwhile, all transgenes with single amino acid mutations showed much weaker morphological defects compared to *AGO1 2A ago1-36* and *AGO1 2D ago1-36* (Fig. 3.2a, 3.2b and Supplementary Fig. 3.3a, 3.3b, and 3.3c). These results suggested that AGO1 S253 and Y255, which are located in the N domain, were important for the functions of AGO1. Between these two sites, Y255 was more critical.

AGO1 Y255 phospho-mutants affect small RNA accumulation

To investigate the functionality of phospho-mutated AGO1 at S253 and Y255, we determined the accumulation of small RNAs by high throughput sequencing in seedlings of *ago1-36* and *ago1-36* expressing WT, single or double non-phosphorylatable (S253A/Y255A, S253A, Y255A) or phospho-mimetic (S253D/Y255D, S253D, Y255D) forms of AGO1 (Supplementary Fig. 3.6a). PCA analysis showed that the three replicates were highly reproducible (Supplementary

Fig. 3.6b). In addition, *ago1-36* was apart from all other samples, as expected, and *AGO1 2D* and *AGO1 Y255D* were apart from both WT *AGO1* and *ago1-36*, while the rest of the phospho-mutants were clustered together with *AGO1* (Supplementary Fig. 3.6b). The size distribution of small RNAs was unaffected in *ago1-36* or any of the phospho-mutant lines (Supplementary Fig. 3.6c). Next, we determined differentially accumulated miRNAs or miRNA*s in comparison to *AGO1 ago1-36*, using fold change > 1.5 and adjusted *P* value < 0.01 as the criteria. In *ago1-36*, 56 out of 149 miRNAs showed reduced levels, while 20 out of 67 miRNA*s were increased in abundance (Fig. 3.3b). As *ago1-36* is likely a null allele, certain miRNA*s and miRNAs were likely loaded into and stabilized by other AGOs and thus showed increased accumulation. We found that the AGO1 phospho-mutants could be separated into three groups based on patterns of their miRNA and miRNA* accumulation (Fig. 3.3c). The first group, including *AGO1 2D* and *AGO1 Y255D*, was similar to *ago1-36* but weaker, in that miRNA accumulation was strongly reduced (Fig. 3.3b), and levels of a subset of miRNA*s were increased (Fig. 3.3b). A heatmap depiction showed that miRNAs and miRNA*s in *AGO1 2D* and *AGO1 Y255D* were similarly affected to those in *ago1-36* (Fig. 3.3c). These results suggested that *AGO1 2D* and *AGO1 Y255D* may have defects in RISC assembly. The second group, including *AGO1 2A*, *AGO1 Y255A*, and *AGO1 S253D*, had a small number of statistically significantly affected miRNAs or miRNA*s (Fig. 3.3b), but showed an overall trend of reduced levels of miRNAs and miRNA*s (Fig. 3.3c). In fact, the reduction was found for the corresponding

miRNAs and miRNA*s (Fig. 3.3d), implying that miRNAs were still preferentially loaded into AGO1 over other AGOs, but at reduced efficiency. The third group was *AGO1 S253A*, in which the accumulation of miRNAs and miRNA*s was largely unaffected (Fig. 3.3b and 3.3c). Taken together, these results showed that all phospho-mutants affecting Y255 might be defective in RISC assembly.

Phospho-mimetic AGO1 Y255D disrupts miRNA loading

Defects in miRNA accumulation in the AGO1 S253 and Y255 mutants could be due to problems in binding miRNAs. To test our hypothesis, an *in vitro* cell-free system was adopted to investigate miRISC assembly (Fig. 3.4a), including miRNA duplex loading and passenger strand ejection. A *FLAG-AGO1* or FLAG-tagged *AGO1* phospho-mutant mRNA was translated in tobacco BY-2 cell lysate, then incubated with a miRNA duplex with a P^{32} at the 5' end of the miRNA guide strand (Fig. 3.4b). After RISC assembly, FLAG-AGO1 proteins were immunoprecipitated and the associated RNAs were analyzed by native gel electrophoresis to distinguish the double-stranded (ds) miRNA duplex from the single-stranded (ss) miRNA (Fig. 3.4c and 3.4d). Loading efficiency of the AGO1 phospho-mutant was represented by the levels of dsRNA+ssRNA normalized to that of AGO1. All four phospho-mutants, AGO1 Y255A, AGO1 Y255D, AGO1 2A and AGO1 2D showed different degrees of reduced loading efficiency with three tested miRNAs when compared to WT AGO1 (Fig. 3.4e, Supplementary Fig. 3.7a, and 3.7b). The rate of passenger strand ejection was calculated as the fraction of ssRNA in the sum of ssRNA and dsRNA. AGO1 Y255D and AGO1 2D were slightly defective in

miRNA* ejection (Fig. 3.4f and Supplementary Fig. 3.7b). The single mutations at AGO1 S253 did not affect miRISC assembly (Supplementary Fig. 3.7a and 3.7b).

To determine the *in vivo* small RNA-binding status of the AGO1 phospho-mutants, we immunoprecipitated HA-tagged AGO1 mutants and sequenced the associated small RNAs. The 2A, 2D, S253A, S253D, Y255A, and Y255D transgenes were in the *ago1-36* heterozygous background so that the cellular small RNA profiles were expected to be similar and the morphological phenotypes of all plants were similar. PCA analysis showed that the two biological replicates for each sample were reproducible (Supplementary Fig. 3.8a). In addition, AGO1 2D IP and AGO1 Y255D IP were clearly separate from other samples (Supplementary Fig. 3.8a), suggesting that they had a different small RNA binding profile. The size distribution of all IP-ed small RNAs showed an enrichment of the 21-nt peak vs. the 24-nt peak (Fig. 3.4g), consistent with AGO1's preference for 21-nt small RNAs. Notably, AGO1 2D-associated small RNAs showed a 20-nt peak, which was also observed for AGO1 2D-associated miRNAs and to a lesser extent ta-siRNAs (Fig. 3.4g and 3.5f). Analysis of the 20-nt miRNAs associated with AGO1 2D showed that most were isoforms of annotated 21-nt miRNAs and they tended to be 1-nt shorter than 21-nt miRNAs at the 3' ends (Supplementary Fig. 3.9a). Moreover, for annotated 21-nt miRNAs, more than half of the reads from these miRNAs in AGO1 2D IP showed 1-nt truncation at the 3' ends, while only ~20% of the reads from these miRNAs in AGO1 IP had truncations (Supplementary Fig. 3.9b). An analysis of all annotated 21-nt miRNA species

revealed that most had a lower 21-nt vs. 20-nt ratio in AGO1 2D IP as compared to AGO1 IP (Supplementary Fig. 3.9c).

We next examined the extent of miRNA association by various AGO1 phospho-mutants as compared to WT. Global changes were obvious only for AGO1 Y255D and AGO1 2D (Fig. 3.4h). Statistical analysis showed that differentially loaded miRNAs and miRNA*s were found mainly for AGO1 Y255D and AGO1 2D (Fig. 3.4i). A large number of miRNAs showed reduced association with AGO1 Y255D and AGO1 2D, while a few showed increased association (Fig. 3.4i). AGO1-loaded miRNA*s were either increased or decreased in AGO1 Y255D and AGO1 2D (Fig. 3.4i). By comparing the changes of miRNAs and the corresponding miRNA*s (Supplementary Fig. 3.8b), we found two major scenarios for AGO1 2D's miRNA association. First, both miRNAs and miRNA*s showed reduced association, suggesting reduced efficiency of duplex loading. Second, decreased miRNA association was accompanied by increased miRNA* association, which could reflect a defect in strand selection during duplex loading or a combination of reduced duplex loading efficiency and defect in passenger strand ejection.

Phospho-mimetic AGO1 Y255 disrupts siRNA loading

AGO1 also associates with siRNAs, such as endogenous ta-siRNAs and siRNAs from transgenes or viruses, *in vivo*. We employed BY-2 lysate to examine the effects of AGO1 phospho-mutations on siRISC assembly. Experiments were performed as in Fig. 3.4a, except that *in vitro* translated proteins were incubated

with an siRNA duplex in which the strand with a 5' U was radioactively labeled (Fig. 3.5a). AGO1 Y255A, AGO1 Y255D, AGO1 2A and AGO1 2D, showed a reduction in loading efficiency for this siRNA duplex compared to WT AGO1 (Fig. 3.5b, 3.5c). For three other siRNA duplexes, AGO1 Y255A was less affected than AGO1 Y255D (Supplementary Fig. 3.7c, 3.7d and 3.7e). In addition, both AGO1 Y255D and AGO1 2D were defective in passenger strand ejection, while the other mutants were normal (Fig. 3.5d and Supplementary Fig. 3.7f). AGO1 prefers to load small RNAs with a 5' U[14], and the AGO1 Y255A and AGO1 Y255D mutants retained this preference (Supplementary Fig. 3.7g, 3.7h, and 3.7i).

Next, we examined the *in vivo* association of AGO1 phospho-mutated proteins with ta-siRNAs. Similar to miRNAs (Fig. 3.4g), the levels of ta-siRNAs in AGO1 IP were dramatically reduced in AGO1 2D and AGO1 255D (Fig. 3.5e). Among the AGO1 2D-associated small RNAs, the proportion of ta-siRNAs was greatly reduced (Fig. 3.5f), consistent with a defect in siRISC formation. Since the passenger strand ejection defect of AGO1 Y255D was observed *in vitro*, we investigated whether the *in vivo* siRISCs reflected this defect. We examined the siRNA vs. siRNA* ratio of siR255 (*TAS1*) and siRNA 5D7 (*TAS3*) in AGO1 IP small RNA-seq. In comparison to WT AGO1 and AGO1 Y255A, the ratios were reduced in AGO1 Y255D, consistent with a defect in passenger strand removal (Fig. 3.5g).

MiRNA target repression requires AGO1 Y255 phosphorylation

The AGO1 IP small RNA-seq results showed that AGO1 2A and AGO1 Y255A were largely normal in miRNA association *in vivo*, which made us wonder

whether the lack of complete rescue of the morphological phenotype of *ago1-36* mutants by these transgenes was due to a deficiency in target repression. To examine the expression of miRNA target genes, we performed RNA-seq with *ago1-36* and *ago1-36* expressing WT *AGO1* or *AGO1* phospho-mutants driven by the *AGO1* promoter. Three biological replicates gave highly reproducible results (Supplementary Fig. 3.10a). We investigated 130 experimentally verified miRNA target genes to identify differentially expressed genes between *AGO1* phospho-mutants and WT *AGO1*. In *ago1-36*, 46 genes were derepressed, which probably represented compromised miRNA-mediated repression (Fig. 3.6a). In *AGO1 Y255D ago1-36* and *AGO1 2D ago1-36*, 26 and 30 genes were derepressed as compared to *AGO1 ago1-36* (Fig. 3.6a and Supplementary Table 3.1), which is consistent with the reduction in miRNA association by these AGO1 mutants. Intriguingly, *AGO1 Y255A ago1-36* and *AGO1 2A ago1-36* also showed a similar number of derepressed genes (Fig. 3.6a). Since these AGO1 mutants were largely normal in miRNA association *in vivo* (Fig. 3.4g, 3.4h, and 3.4i), the results suggested that AGO1 Y255A and AGO1 2A were defective in target repression. In fact, the target expression profiles of *AGO1 Y255D ago1-36* and *AGO1 Y255A ago1-36* were very similar (Fig. 3.6b and Supplementary Table 3.1). To further correlate the expression of the target genes with the levels of the corresponding miRNAs, we compiled small RNA-seq and RNA-seq data for comparison (Fig. 3.6c). In *AGO1 Y255D ago1-36*, the de-repression of miRNA target genes was correlated with the lower levels of miRNAs. However, in *AGO1 Y255A ago1-36*,

the target transcripts of miR396a, miR396b, and miR755 were derepressed even when the levels of the miRNAs were unaffected or increased (Fig. 3.6c). This observation suggests that phosphorylation of AGO1 at position Y255 is required for its activities in target gene repression.

Additional phosphorylation mutations at AGO1 Y255

To investigate the biological significance of protein phosphorylation, serine and threonine phosphorylation sites are typically mutated to alanine, a non-phosphorylatable amino acid that chemically resembles serine and threonine, while the tyrosine residue is often mutated to phenylalanine, or sometimes to alanine[55]. Phenylalanine is identical to tyrosine, except that it lacks a hydroxyl group, whereas alanine lacks the aromatic ring and the hydroxyl group of tyrosine, thus the substitution of tyrosine with alanine could potentially induce a larger conformational change of the target protein compared to the phenylalanine substitution. On the other hand, serine, threonine and tyrosine are normally mutated to aspartic or glutamic acid, which are negatively charged amino acids that mimic the constitutively phosphorylated state. Some studies prefer glutamic acid over aspartic acid as a phospho-mimetic mutation of tyrosine, mainly because glutamic acid possesses a longer side chain. However, neither glutamic acid nor aspartic acid fully resembles the size and charge of phospho-tyrosine, as both are shorter and lack the aromatic ring of tyrosine. As alanine and aspartic acid used in this study share limited similarities to tyrosine, could the effects of AGO1 Y255A and AGO1 Y255D mutations be solely due to compromised structural integrity? To

address this, we sought to compare AGO1 Y255A, Y255F, Y255D, and Y255E. GFP-tagged wild-type AGO1 as well as the four phosphorylation mutants were transiently expressed in *Nicotiana benthamiana* together with *MIR165A*. The proteins were immunoprecipitated and the levels of miR165 associated with the different AGO1 proteins were determined by RNA gel blot analyses (Supplementary Fig. 3.11). Consistent with the *in vivo* HA-AGO1 IP sRNA-sequencing data (Supplementary Fig. 8b), miR165 showed slightly increased and decreased association with GFP-AGO1 Y255A and GFP-AGO1 Y255D, respectively (Supplementary Fig. 3.11). Strikingly, Y255F resembled Y255A in slightly increased association with miR165, while Y255E was similar to Y255D, showing reduced association with miR165. This result suggests that the activity of AGO1 phospho-mutants likely depends on the charged state of Y255 rather than the size of the residue. The reduced association of AGO1 Y255D and Y255E with miR165 further strengthens our conclusion that miRISC formation is compromised in phospho-mimetic AGO1 at Y255.

Discussion

In plants, little is known about the mechanism that regulates RISC formation. In this study, we report that Arabidopsis AGO1 is phosphorylated *in vivo*, and show that the phosphorylation status of AGO1 affects the activities of miRISCs as well as two major steps in RISC formation: small RNA duplex loading into AGO1 and passenger strand ejection (Fig. 3.7a). Our experiments demonstrate that non-phosphorylatable AGO1 at Y255 is significantly compromised in target repression,

which cannot be attributed to reduced levels of miRISCs; while phospho-mimetic AGO1 at Y255 reduces the loading efficiency of both miRNA and siRNA, and have minor and severe effects on passenger strand ejection for miRNA and siRNA, respectively. Given that neither the non-phosphorylatable nor phospho-mimetic AGO1 can fully rescue the developmental and molecular phenotypes of *ago1-36*, phosphorylation and dephosphorylation of AGO1 may regulate the efficiency of RISC formation and target repression (Fig. 3.7b).

Structural studies of eukaryotic AGO proteins revealed a two-lobed structure, with the N-PAZ domains constituting one lobe, while the MID-PIWI domains forming the other[56–58]. These two lobes are connected by the linker 2 region (L2) and form a positively charged central cleft that accommodates the negatively charged guide RNA and its complementary target transcript[56]. Based on the predicted structure of Arabidopsis AGO1 (Fig. 3.1d), Y255 is located on a β-sheet of the N domain that is exposed to the inner pocket of AGO1. We found that mutating AGO1 Y255 to a negatively charged residue, aspartic acid (D), reduces the loading efficiency for both miRNA and siRNA duplexes, while mutating AGO1 Y255 to an uncharged amino acid alanine (A) does not affect small RNA loading. Since phosphorylation switches tyrosine (Y) from an uncharged amino acid to a negatively charged one, it is possible that the ability of AGO1 to bind RNA is impaired when AGO1 Y255 is phosphorylated. NMR-based investigations reveal that the tyrosine (Y) side-chain hydroxyl group can form hydrogen bonds with DNA phosphate groups[59]. It is possible that tyrosine could interact with RNA in a similar

manner. Phosphorylation on AGO1 Y255 substitutes the side-chain hydroxyl with a phosphate group, which could abolish the interaction of Y255 with small RNA or target RNA, leading to reduced association.

Phosphorylation of AGO1 Y255 may also affect the motion of the N domain. Based on the predicted structure of AGO1, the β-sheet on which AGO1 Y255 resides faces a linkage helix that connects the N domain to the rest of AGO1, and hydrogen bonds are predicted to form between the β-sheet and the helix. Phosphorylation of Y255 could affect the range of motion between the N domain and the MID-PIWI lobe by modulating the interaction between the β-sheet and the helix. Biochemical studies of human AGO2 show that the N domain is involved in passenger strand ejection of both miRNA and siRNA duplexes regardless of the slicer activity; it was proposed that the N domain pries open the 3' end of the guide strand in the small RNA duplex through wedging[38]. Plant AGO1 could adopt a similar strategy using the N domain to assist passenger strand ejection of small RNA duplexes. In the same human AGO2 study, 41 conserved amino acids in the human AGO2 N domain were systematically mutated, including tyrosine residue 101 corresponding to Arabidopsis AGO1 Y255. Mutating human AGO2 Y101 to an alanine (A) impaired the strand separation of siRNA but not miRNA duplexes[38]. Similarly, our data show that phospho-mimetic AGO1 at Y255 is severely compromised in siRNA duplex separation but is largely normal in miRNA duplex separation (Fig. 3.4f and 3.5d).

Other observed defects of AGO1 phospho-mutants, such as those in target repression and miRNA 3' nucleotide protection, may also be explained by the structural role of the N domain in AGO's interactions with the guide RNA or the target RNA. Structural studies of human AGO2 associated with a 21-nt guide RNA show that the position of the N domain is critical for the functions of RISC, as nucleotides 14 to 18 of the guide RNA pass through a narrow channel formed between the N and the PAZ domains. This precludes nucleotides 14 to 18 of the guide RNA from participating in initial target recognition[48]. Although plant miRISCs target RNA transcripts with perfect or near-perfect complementarity, it is possible that the non-phosphorylatable AGO1 at Y255 affects the narrow channel between the N and the PAZ domains leading to a deficiency in target repression. At the end of the narrow channel, nucleotides 19 to 21 of the guide strand turn and extend into the 3' binding pocket in the PAZ domain[48]. In this study, we found that most annotated 21-nt miRNAs co-immunoprecipitated with AGO1 5D and AGO1 2D were 1-nt shorter at the 3' end (Fig. 3.4g, Supplementary Fig. 3.5b and Supplementary Fig. 3.9a, 3.9b and 3.9c). It is possible the AGO1 S253D and Y255D mutations together disrupt the narrow channel even more and leave the 3' end of the guide RNA unprotected.

In addition to affecting AGO1's structure, the phosphorylation status of AGO1 Y255 could affect RISC formation by other means. HSP90 assists the loading of small RNAs for animal and plant AGOs[10,35]. The phospho-mimetic AGO1 at Y255 may affect interactions with HSP90, which we did not examine.

Alternatively, the phosphorylation status might affect the subcellular localization of AGO1. In Arabidopsis, miRNAs are likely loaded into AGO1 inside the nucleus, while the loading of ta-siRNAs into AGO1 occurs in the cytoplasm[34]. Our fractionation studies showed that the nucleo-cytoplasmic partitioning of AGO1 phospho-mutants was largely unaffected (Supplementary Fig. 3.5h).

In this study, five phosphorylation sites of Arabidopsis AGO1 were detected in 14-day-old seedlings, but it is uncertain whether these residues are phosphorylated in a tissue- and/or developmental stage-dependent manner. Given the strong developmental defects of *AGO1 2A ago1-36* and *AGO1 2D ago1-36* plants in both vegetative and reproductive stages (Fig. 3.2a, Supplementary Fig. 3.3a, 3.3b and 3.3c), it is likely that the phosphorylation/de-phosphorylation of AGO1 at S253/Y255 occurs in all tissues and developmental stages. At the subcellular level, AGO1 localizes to the nucleus, the cytosol, and the endoplasmic reticulum[34,60]. It is possible that phosphorylation/dephosphorylation of AGO1 only takes place at certain subcellular compartments, or affects AGO1's localization to or AGO1's activity at, certain subcellular compartments.

In summary, our studies show that Arabidopsis AGO1 is phosphorylated *in vivo*. Although non-phosphorylatable AGO1 at Y255 can form miRISC, it is compromised in target repression. Phospho-mimetic AGO1 at Y255 impairs both miRNA and siRNA duplex loading and siRNA passenger strand ejection. This suggests that phosphorylation and dephosphorylation regulate the activities of AGO1 in miRNA-mediated gene silencing. In addition, plant AGO1 is also essential

for antiviral immunity[53]. Virus-derived siRNAs are loaded into AGO1 to guide the cleavage of viral RNAs. As phospho-mimetic AGO1 is defective in siRNA duplex loading and passenger strand ejection, the de-phosphorylation of AGO1 is likely crucial for plant antiviral immunity. Furthermore, our studies show that the poorly understood N domain has essential roles in nearly all AGO1's activities. As Arabidopsis AGO1 Y255 is highly conserved in AGO proteins, phosphorylation could be a mechanism to regulate RISC formation and target repression in other species.

Methods

Plant materials and growth conditions

All *Arabidopsis thaliana* mutant and transgenic lines in this study were in the Col-0 accession. *ago1-36* (SALK_087076) was obtained from the Arabidopsis Biological Resource Center (ABRC) and was described previously[8]. Seeds were surface-sterilized and stratified in water for 2 days at 4°C then sown on 1x MS medium. Seedlings were collected at 12 days for molecular analyses or transferred to soil at 6-7 days to obtain adult plants. All plants were kept in a growth chamber at 22°C under long-day conditions (16 h light/8 h dark).

Transgenic lines containing *pAGO1::3XHA-AGO1*, *pAGO1::3XHA-AGO1 5A (S11A/S253A/Y255A/S350A/S1001A)*, *pAGO1::3XHA-AGO1 5D (S11D/S253D/Y255D/S350D/S1001D)*, *pAGO1::3XHA-AGO1 3D (S253D/Y255D/S1001D)*, *pAGO1::3XHA-AGO1 2A (S253A/Y255A)*, *pAGO1::3XHA-AGO1 2D (S253D/Y255D)*, *pAGO1::3XHA-AGO1 S253A*,

pAGO1::3XHA-AGO1 S253D, *pAGO1::3XHA-AGO1 Y255A*, *pAGO1::3XHA-AGO1 Y255D* and *pAGO1::3XHA-AGO1 S1001A* in the *ago1-36* background were generated in this study.

To construct *pAGO1::3XHA-AGO1*, individual parts were assembled as follows. *AGO1* cDNA was amplified from total RNA by RT-PCR, the 1648bp *AGO1* promoter+5'UTR and the 399bp 3'UTR were amplified from genomic DNA, and the 3XHA tag was amplified from pGWB615[61], and all fragments were cloned into pEarleyGate 301[62] (predigested by XbaI and NcoI) using NEBuilder HiFi DNA Assembly Cloning Kit (NEB). To generate AGO1 phospho-mutants, *AGO1* cDNA was first subcloned into pENTR/D-TOPO (Invitrogen) with pENTR Directional TOPO Cloning Kits (Invitrogen), and mutations were introduced by PCR amplification of D-TOPO-AGO1 with primers carrying the mutations. Mutated *AGO1* cDNA together with the *AGO1* promoter, 3' UTR and 3xHA were introduced into pEarleyGate 301 as described above. The plasmids were sequenced to confirm the correct fusions and to ensure the presence of the *AGO1* mutations. Sequences of the primers used in this study are listed in Supplementary Table 2. Plant transformation was performed with *ago1-36* heterozygous plants through the floral dip method using the *Agrobacterium tumefaciens* GV3101 strain[63]. Transgenic lines were genotyped to identify ones homozygous for *ago1-36* in the T2 generation. Seeds were collected from multiple T2 plants for those that were fertile in *ago1-36* and were screened on selection medium to identify lines that were also homozygous for the transgene. Seeds were also collected from multiple

T2 plants that were heterozygous for *ago1-36* and screened as described above for homozygosity for the transgene. T4 plants in *ago1-36* were used for phenotypic and molecular analyses, and T4 plants in *ago1-36/+* were used for immunoprecipitation assays.

RNA gel blot analysis

RNA gel blot analysis of small RNAs was performed as described[64]. Total RNA from 12-day-old Arabidopsis seedlings or RNA from AGO1 immunoprecipitates was isolated using TRI Reagent (NRC). 5-15μg of total RNA was resolved in 15% urea–PAGE gels and transferred to membrane (Amersham Hybond-NX), and RNA was cross-linked to the NX membrane using EDC cross-linking buffer (0.16 M EDC, 0.13 M 1-methylimidazole, pH 8.0) at 65°C for 1.5 hours. MiRNAs and ta-siRNAs were detected with antisense DNA probes labeled at the 5' end with ^{32}P. Sequences of the probes in this study are listed in Supplementary Table 2. Hybridization signals were detected using a Typhoon phosphorimager and relative expression levels of small RNAs were calculated against the internal control U6.

Immunoprecipitation and protein gel blot analysis

12-day-old seedlings of the transgenic line of *HA-AGO1* in the homozygous *ago1-36* background and transgenic lines containing HA-tagged AGO1 phospho-mutants in the heterozygous *ago1-36* background were used to immunoprecipitate AGO1. 2 g of seedlings was ground into fine powder in liquid nitrogen and the powder was homogenized in 3 ml lysis buffer for 30 min at 4°C (lysis buffer: 50

mM Tris-HCl, pH7.5, 150 mM NaCl, 10% glycerol, 0.1% CA-630, one tablet of cOmplete EDTA-free Protease Inhibitor Cocktail /50ml [Roche], and 50 units/ mL SUPERase•IN RNase Inhibitor [ThermoFisher]). Cell debris was removed from the lysate by centrifugation at 12,000 rpm at 4°C for 20 min twice. 8 μg of anti-HA antibody (Sigma, H6908) was incubated with 30 μl Dynabeads™ Protein A (ThermoFisher) for 30 min at room temperature, beads were then washed 5 times with lysis buffer to remove the extra antibody. The lysate was incubated with the anti-HA antibody-protein A beads for 2 hours at 4°C under gentle rotation. Dynabeads were captured magnetically and washed with 1 ml lysis buffer five times. Washed beads were then divided for protein and small RNA analysis. For protein gel blot analysis, the beads were resuspended in 2xSDS sample buffer (50 mM Tris-HCL at pH 6.8, 10% glycerol, 2% SDS, 0.1% bromophenol blue, and 1% 2-mercaptoethanol) and incubated at 95°C for 10 min with vigorous shaking. The tube was placed onto a magnetic stand for 2 min and the supernatant containing the immunoprecipitated AGO1 was transferred to a new tube. The protein samples were then resolved in 10% SDS-PAGE gel, transferred to a membrane and detected by an anti-HA antibody (Roche, 12158167001). For RNA analysis, Dynabeads were resuspended in H_2O and boiled for 5 min under constant shaking. The tube was placed onto a magnetic stand for 2 min, and the supernatant containing immunoprecipitated RNA was transferred to a new tube for subsequent uses in RNA gel blot analysis or small RNA library construction.

IP–MS analyses

10 g of 14-day-old Col-0 seedlings was used for AGO1 immunoprecipitation as described above, except that 20 ml lysis buffer without RNase Inhibitor was used and anti-AGO1 antibody (Agrisera, AS09527) was used to precipitate endogenous AGO1. The protein sample was then resolved in a 10% SDS-PAGE gel. After Coomassie Blue staining, the gel band corresponding to AGO1 was excised and sent to the Biological Mass Spectrometry Facility at Rutgers University for analysis. The gel band corresponding to AGO1 was subjected to reduction with 10mM DTT for 30 min at 60°C followed by alkylation with 20 mM iodoacetamide for 45 min at room temperature in the dark and then digested overnight at 37°C with MS grade trypsin protease (Thermo Scientific Cat#: 90058). Peptides were extracted twice with 5% formic acid and 60% acetonitrile, then dried under vacuum. Proteolytic digests of purified samples were loaded onto a self-packed 100 µm x 2 cm trap (Magic C18AQ, 5µm 200 Å, Michrom Bioresources, Inc.) and desalted for 5 min with Buffer A (0.2% formic acid) at a flow rate of 10 µl/min. The trap was brought in-line with the analytical column (Magic C18AQ, 3 µm 200 Å, 75 µm x 50 cm) and peptides were fractionated at 300 nL/min using segmented linear gradients: 4-15% B (0.2% formic acid in acetonitrile) 35 min, 15-25%B 55 min, and 25-50%B 65 min. Peptides were solubilized in 0.1% trifluoroacetic acid and analyzed by Nano LC-MS/MS (Dionex Ultimate 3000 RLSCnano System interfaced with a QExactive HF (Thermofisher) or Velos-LTQ-Orbitrap (ThermoFisher). Mass spectrometry data were acquired using a data-dependent

acquisition procedure with a cyclic series of a full scan acquired with a resolution of 60,000 (Velos, in Orbitrap) or 120,000 (QE) followed by MS/MS of the 20 most intense ions and a dynamic exclusion duration of 30 sec for both instruments. For QExactive HF, the parent ions were collected in C-trap and fragmented with higher-energy C-trap dissociation at a relative collision energy of 27%. The fragments were scanned in orbitrap with a resolution of 15,000. For Velos Oribitrap, the parent ions were fragmented in ion trap with collision induced dissociation with a relative collision energy of 35% and the MS/MS were scanned in CID with unit resolution.

Peak lists in MASCOT Generic Format (.mgf) were generated using Proteome Discover 1.3 (ThermoFisher). Data were searched using an in-house version of X!Tandem (GPM Fury[65]) against Arabidopsis TAIR v. 10, plus a database composed of common lab contaminants to assign spectral data[66,67]. Search parameters are as follows: fragment mass error: ±20 ppm for QE and ±0.4 Da for Velos; parent mass error: ±7 ppm for QE and ±10 ppm for Velos; fixed modification: carbamidomethylation on cysteine; flexible modifications: methionine oxidation, deamination on asparagine and glutamine residues and phosphorylation on serine, threonine and tyrosine; protease specificity: trypsin (C-terminal of R/K unless followed by P), with 1 miss-cut during preliminary search and 5 miss-cut during refinement. Only spectra with $\log_e$ <-2 were included in the final report. The identified phosphorylation sites were examined manually for confirmation.

Small RNA-seq and data analysis

Small RNA-seq library construction and data analysis were performed as described[51]. 25 μg of total RNA was resolved in a 15% urea-PAGE gel, and the 15- to 40-nt region was excised from the gel. The gel piece was smashed and soaked in 0.3 M NaCl overnight at 4°C, and small RNA in the supernatant was precipitated with ethanol. Gel-purified small RNA or small RNA acquired from AGO1 immunoprecipitation (as described above) was used for library construction using the NEBNext Multiplex Small-RNA Library Prep Set for Illumina (E7300). The libraries were sequenced on a HiSeq X Ten platform, and the resulting sequencing data were analyzed using an in-house plant high-throughput sequencing data analysis pipeline pRNASeqTools v.0.8 (https://github.com/grubbybio/pRNASeqTools). Raw reads from small RNA sequencing were processed to trim off the 3' adapter sequence (AGATCGGAAGAGC) and retain 18- to 42-nt reads using cutadapt v3.0[68]. Trimmed reads were aligned to the Arabidopsis genome (TAIR10) using ShortStack v.3.8.5[69] with parameters '-bowtie_m1000 -ranmax 50 -mmap u -mismatches 0'. Reads were normalized to total 18- to 42-nt reads minus 45S rRNA reads (RPM, Reads Per Million Reads). Differentially accumulated small RNAs were calculated by DESeq2 v1.30.0 with fold change of 1.5 and adjusted *P* value < 0.01 as the parameters[70]. Annotated miRNA and miRNA* sequences were obtained from miRbase v21 (http://www.mirbase.org/). TAS1_siR255 and TAS3_5D7 sequences were reported previously[71]. Reads that match perfectly or with a 1-nt shift on either the 5' or 3' end from the annotated small RNAs were

assigned to the small RNAs. Ta-siRNA levels were quantified by summing up 21-nt small RNA reads at each of the eight *TAS* loci.

RNA-seq and data analysis

Total RNA from 12-day-old Arabidopsis seedlings was isolated using TRI Reagent (NRC), and DNA was removed by DNase I (Roche) treatment. PolyA RNA was enriched from 1 μg of DNase I-treated RNA with Oligo d(T)25 Magnetic Beads (NEB S1419S) and subjected to RNA-seq library construction using NEBNext Ultra Directional RNA Library Prep Kit for Illumina (NEB E7420). Libraries were sequenced on an Illumina NovaSeq 6000 platform (PE150 bp). The RNA sequencing data were analyzed using the pRNASeqTools v.0.8 pipeline. Briefly, raw reads were mapped against the Arabidopsis genome (TAIR 10) using STAR v2.7.6a[72] with parameters '--alignIntronMax 5000 --outSAMmultNmax 1 --outFilterMultimapNmax 50 --outFilterMismatchNoverLmax 0.1', and counted by featureCounts v2.0.0[73]. Mapped reads were normalized using FPKM (Fragments Per Kilobase Million), and differentially expressed genes were identified by DESeq2 v1.30.0 with fold change of 1.5 and adjusted *P* value < 0.05 as the parameters.

Nuclear–cytoplasmic fractionation

1 g of 12-day-old Arabidopsis seedlings was crosslinked with 0.5% formaldehyde in 1× PBS buffer by vacuum infiltration for 15 min at room temperature. Crosslinking was stopped by vacuum infiltration in 1XPBS buffer in the presence of 100 mM glycine for 5 min at room temperature. The plant material

was washed one time with 1× PBS buffer and blotted dry, and then ground into fine powder in liquid nitrogen. The powder was resuspended in 2 ml lysis buffer (20 mM Tris-HCl, pH7.5, 20 mM KCl, 2.5 mM $MgCl_2$, 2 mM EDTA, 25% glycerol, 250 mM sucrose, 5 mM DTT and cOmplete Protease Inhibitor Cocktail (Roche)). The slurry was filtered through a 40 μm cell strainer (Falcon), and the flow through was centrifuged at 1,500g for 10 min at 4°C. The supernatant representing the cytoplasmic fraction was transferred to a new tube and centrifuged at 10,000g for 10 min at 4°C to remove any residual membranes, then the supernatant was carefully transferred to a new tube for protein gel blot analysis. The pellet from the 1,500g spin was dissolved with 10 ml nuclei resuspension buffer 1 (20 mM Tris-HCl, pH7.4, 2.5 mM $MgCl_2$, and 0.2% Triton X-100) and then centrifuged at 1,500g for 10 min to collect nuclei. This step was repeated 8 times to wash the nuclei. After the final wash, the pellet was resuspended with 500 μl nuclei resuspension buffer 2 (20 mM Tris-HCl, pH7.5, 250 mM sucrose, 10 mM $MgCl_2$, 0.5% Triton X-100, 5 mM 2-mercaptoethanol, and cOmplete Protease Inhibitor Cocktail (Roche)), then carefully loaded onto 500 μl nuclear resuspension buffer 3 (20 mM Tris-HCl, pH7.5, 1.7 M sucrose, 10 mM $MgCl_2$, 0.5% Triton X-100, 5 mM 2-mercaptoethanol, and cOmplete Protease Inhibitor Cocktail (Roche)) without disturbing the bottom layer, and centrifuged at 16,000g for 45 min at 4°C. The nuclear pellet was resuspended in 1XSDS loading buffer and boiled at 95°C for 10 min for protein gel blot analysis.

Multiple sequence alignment

Protein sequences of AGOs were retrieved from Uniprot (https://www.uniprot.org/). Amino acid alignments were generated using MUSCLE [74] (https://www.ebi.ac.uk/Tools/msa/muscle/) with default settings, and alignments were edited with ESPript3 (http://espript.ibcp.fr/ESPript/ESPript/).

Structure prediction

The structure of human AGO2 associated with a 21-nt guide RNA (PDB, ID 4W5N) was used for the construction of the Arabidopsis AGO1 model[48]. The Arabidopsis AGO1 amino acid sequence was aligned to human AGO2 by MUSCLE, with the amino acids 1-168 and 1010-1048 of Arabidopsis AGO1 lacking a template from human AGO2 being removed from modeling. Three-dimensional models of Arabidopsis AGO1 were generated using UCSF-Chimera (https://www.cgl.ucsf.edu/chimera/), and the one with the best score from 20 models was selected for this study.

Plasmid construction of GFP-AGO1 and *MIR165A*

35S::MIR165A has been described previously[75]. To construct *35S::GFP-AGO1,* the *GFP-AGO1* fragment was cloned from *pAGO1::GFP-AGO1*[76] and moved into pEarleyGate 100[62] (predigested by XbaI and XhoI) using the NEBuilder HiFi DNA Assembly Cloning Kit (NEB). Phospho mutations of AGO1 were introduced by PCR amplification of *GFP-AGO1* with primers carrying the mutations. Sequences of the primers used are listed in Supplementary Table 2.

Transient expression of proteins and RNA in *Nicotiana benthamiana*

Transient expression of protein and RNA in *N. benthamiana* was performed as described[77]. The *A. tumefaciens* strain GV3101 carrying *35S::GFP-AGO1*, phospho-mutated *35S::GFP-AGO1* and *35S::MIR165A* were infiltrated into the leaves of four-week-old *N. benthamiana.* Three grams of leaves were collected four days post inoculation followed by IP as described above, except that GFP-Trap_MA (ChromoTek) was used to precipitate GFP-tagged proteins.

***In vitro* RISC assembly**

mRNA preparation. *3×FLAG-AGO1* mRNA and its mutants (S253A, S253D, Y255A, Y255D, S253A/Y255A, S253D/Y255D) were *in vitro* transcribed from NotI-linearized *pBYL-3×FLAG-AGO1*[78] and *pBYL-3×FLAG-AGO1-S253A*, *-S253D*, *-Y255A*, *-Y255D*, - *S253A/Y255A*, and *-S253D/Y255D*, respectively, by AmpliScribe T7 High Yield Transcription Kit (Lucigen). These transcripts were then capped with ScriptCap m^7G Capping System (Cell Script). Information regarding all primers used in this study is included in Supplementary Table 2.

Preparation of small RNA duplexes. Synthetic RNA oligonucleotides (Ajinomoto Bio-Pharma Services) were phosphorylated by T4 Polynucleotide Kinase (Takara) in the presence of [γ-^{32}P]ATP or non-radioactive ATP, purified with MicroSpin G-25 Columns (Cytiva), and annealed.

Passenger strand ejection assay. Generally, 5 µl of the BY-2 lysate, 2.5 µl of substrate mixture (3 mM ATP, 0.4 mM GTP, 100 mM creatine phosphate, 200 µM each of 20 amino acids, 320 µM spermine, 0.4 U/µl creatine phosphokinase

(Calbiochem)), and 0.5 µl of 300 nM mRNAs carrying 3×FLAG-tagged AGO1 or its mutants were mixed and incubated at 25°C for 90 min. To assemble RISCs, 2.0 µl of 10 nM radiolabeled small RNA duplexes were added to the reaction mixture and incubated at 25°C for 90 min. The reaction was mixed with anti-FLAG M2 antibody (Sigma) immobilized on 5 µl of Dynabeads protein G (Invitrogen) and incubated for 30 min on ice. After incubation, the beads were washed three times with 1×lysis buffer (30 mM HEPES (pH 7.4), 100 mM KOAc and 2 mM $Mg(OAc)_2$) containing 0.1% Triton X-100 and 200 mM NaCl, and treated with 10 µl 1 × lysis buffer containing 0.6 U proteinase K at 25°C for 30 min. The samples were resuspended in 10 µl of 2 × native loading dye (50% glycerol, 4 mM MgCl2, 0.02% bromophenol blue, 0.02% xylene cyanol, 0.04% tartrazine and 0.5 × TBE), and 5 µl aliquots were separated in a 12% acrylamide native gel at 4°C. Gels were analyzed by PhosphorImager (Typhoon FLA 7000, Cytiva) and quantified using the MultiGauge software (Fujifilm Life Sciences). Equimolar amounts of non-radiolabeled small RNA duplexes were used for western blotting of immunoprecipitated AGO1 proteins.

Western blotting. Western blotting was performed as previously described with modifications[79]. The membrane was blocked in TBST (25 mM Tris–HCl (pH 7.4), 150 mM NaCl, 0.1% (v/v) Tween) containing 1.0% nonfat dried milk (w/v) for 30 min. Anti-DDDDK-tag mAb (Medical & Biological Laboratories, #M185-3S; 1:5000 dilution) and anti-α-tubulin mAb (Sigma, #T6074; 1:10,000 dilution) were used as

primary antibodies. Anti-IgG (H+L) (Mouse) pAb-HRP (Medical & Biological Laboratories, #330; 1:10,000 dilution) was used as a secondary antibody.

Data availability

Raw sequence data and processed data generated in this study were deposited in the NCBI GEO database under the accession number GSE176568. Proteomic data is available via MassIVE with the identifier MSV000088221. Other supporting data is available from the corresponding authors upon request. Source data are provided with this paper.

Figures and Tables

Fig. 3.1. Arabidopsis AGO1 can be phosphorylated *in vivo*.

(a) Schematic representation of the domain organization of Arabidopsis AGO1. The identified phosphorylation sites are marked by red asterisks.

(b) Alignments showing the conservation or lack of conservation of AGO1 phosphorylation sites in the Arabidopsis AGO family. The red color denotes identity of residues in all proteins. Yellow denotes similar residues. The phosphorylation sites are marked by red asterisks.

(c) Alignments showing the conservation or lack of conservation of Arabidopsis AGO1 phosphorylation sites in AGOs from 13 species including *Arabidopsis thaliana* (*At*), *Arabidopsis lyrate* (*Al*), *Brassica napus* (*Bn*), *Glycine max* (*Gm*), *Oryza sativa* (*Os*), *Zea mays* (*Zm*), *Physcomitrella patens* (*Pp*), *Chlamydomonas reinhardtii* (*Cr*), *Schizosaccharomyces pombe* (*Sp*), *Drosophila melanogaster* (*Dm*), *Muc musculus* (*Mm*), *Homo sapiens* (*Hs*), and *Thermus thermophilus* (*Tt*). Red denotes identity of residues in all proteins. Yellow denotes similar residues. The Arabidopsis AGO1 phosphorylation sites are marked by red asterisks.

(d) A predicted structure of Arabidopsis AGO1−siRNA complex based on the structure of human AGO2 (PDB, ID 4W5N). The positions of AGO1 S253 and Y255 are highlighted in red. The 21-nt guide strand is in orange.

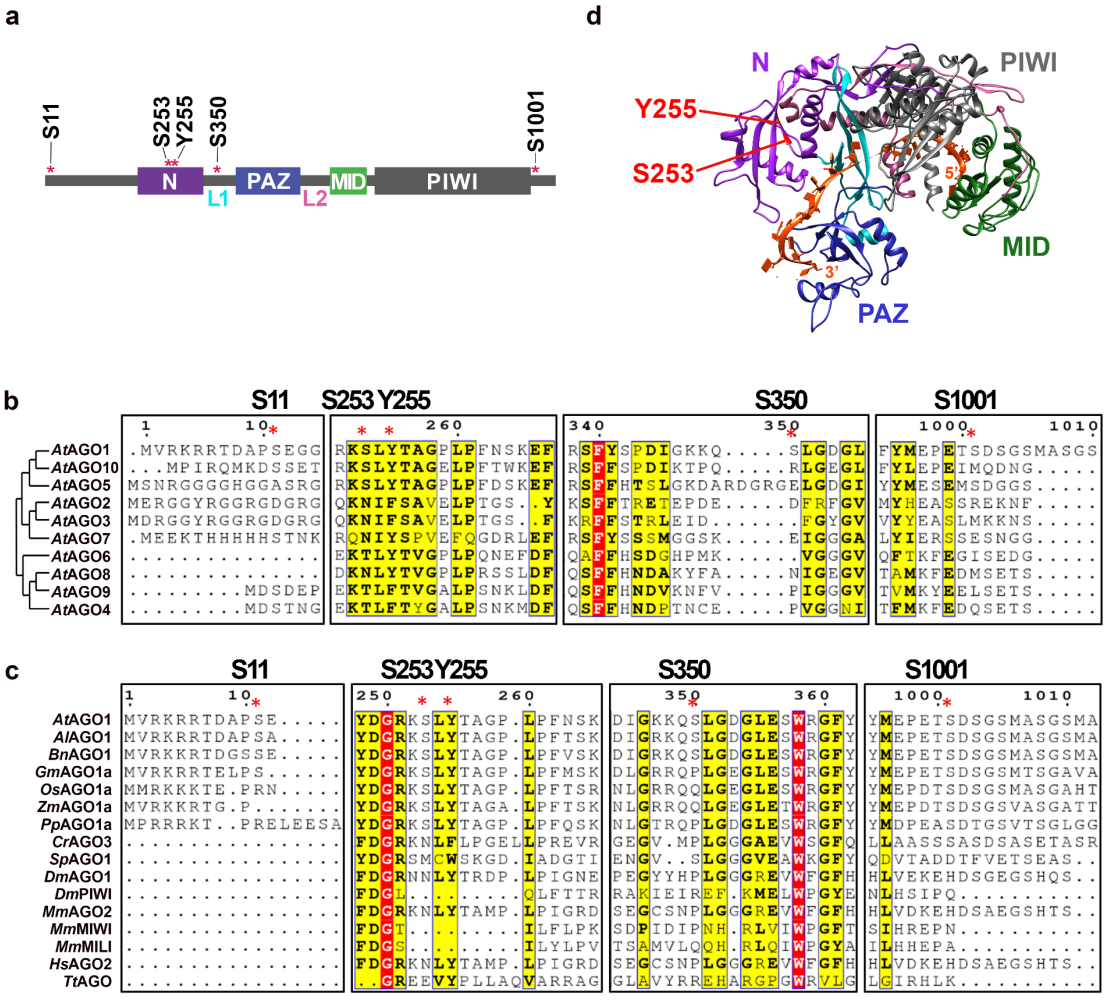
a
S11
S253
Y255
S350
S1001
N
PAZ
MID
PIWI
L1
L2
d
N
PIWI
Y255
S253
MID
PAZ
5'
3'
b
S11
S253 Y255
S350
S1001
AtAGO1
AtAGO10
AtAGO5
AtAGO2
AtAGO3
AtAGO7
AtAGO6
AtAGO8
AtAGO9
AtAGO4
c
S11
S253Y255
S350
S1001
AtAGO1
AlAGO1
BnAGO1
GmAGO1a
OsAGO1a
ZmAGO1a
PpAGO1a
CrAGO3
SpAGO1
DmAGO1
DmPIWI
MmAGO2
MmMIWI
MmMILI
HsAGO2
TtAGO

Fig. 3.2. Arabidopsis *AGO1* phospho-mutants cannot fully rescue the developmental phenotypes of *ago1-36.*

(a) Six-week-old plants of *HA-AGO1 ago1-36*, *HA-AGO1 5A ago1-36, HA-AGO1 5D ago1-36*, *HA-AGO1 2A ago1-36*, *HA-AGO1 2D ago1-36*, *HA-AGO1 S253A ago1-36*, *HA-AGO1 S253D ago1-36*, *HA-AGO1 Y255A ago1-36*, *HA-AGO1 Y255D ago1-36,* and *ago1-36*. Scale bar, 2cm.

(b) Leaves of 4-week-old plants of *HA-AGO1 ago1-36*, *HA-AGO1 5A ago1-36, HA-AGO1 5D ago1-36*, *HA-AGO1 2A ago1-36*, *HA-AGO1 2D ago1-36*, *HA-AGO1 S253A ago1-36*, *HA-AGO1 S253D ago1-36*, *HA-AGO1 Y255A ago1-36*, and *HA-AGO1 Y255D ago1-36*. Scale bar, 2cm.

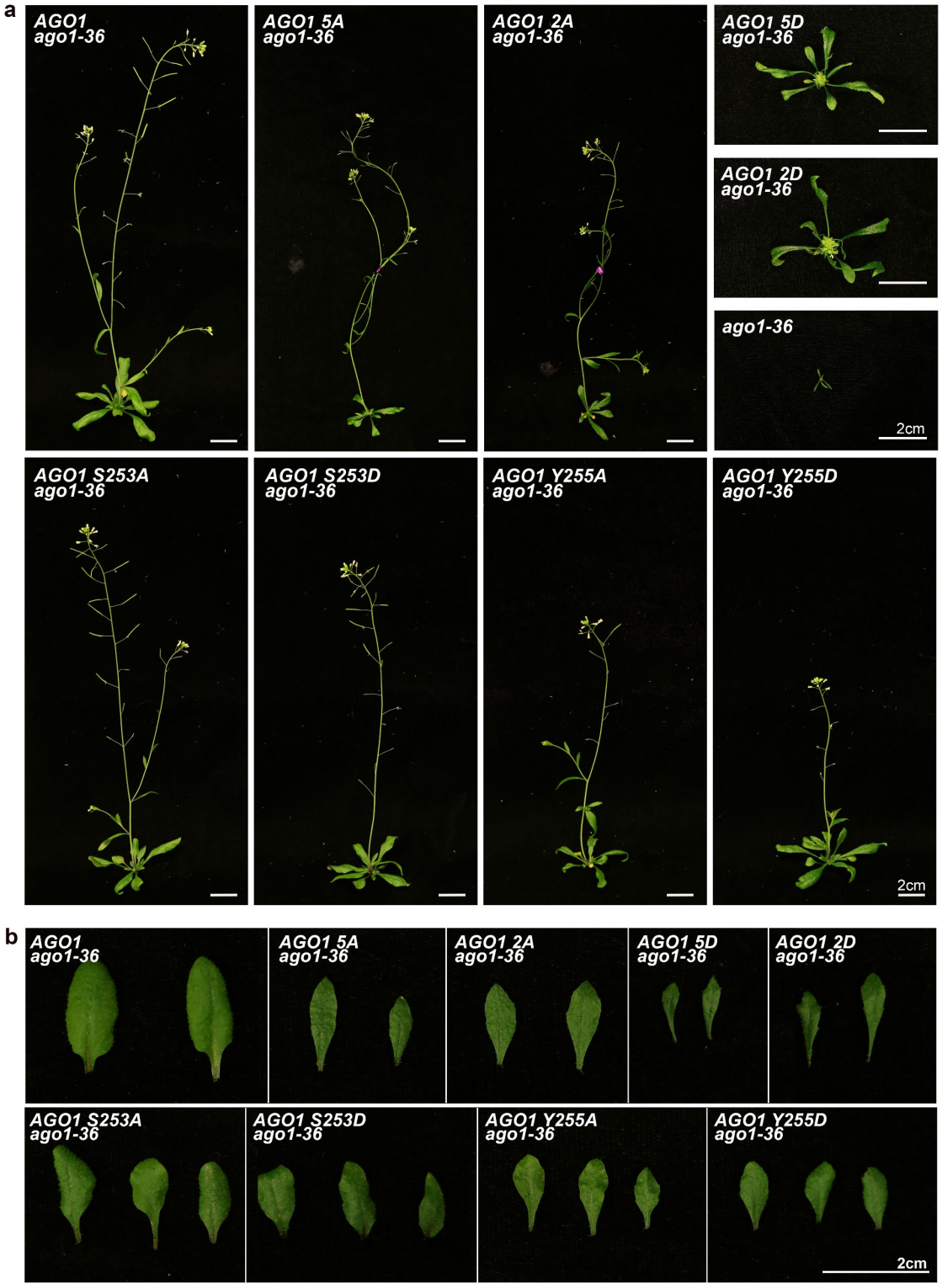
a
AGO1
ago1-36
AGO1 5A
ago1-36
AGO1 2A
ago1-36
AGO1 5D
ago1-36
AGO1 2D
ago1-36
ago1-36
2cm
AGO1 S253A
ago1-36
AGO1 S253D
ago1-36
AGO1 Y255A
ago1-36
AGO1 Y255D
ago1-36
2cm
b
AGO1
ago1-36
AGO1 5A
ago1-36
AGO1 2A
ago1-36
AGO1 5D
ago1-36
AGO1 2D
ago1-36
AGO1 S253A
ago1-36
AGO1 S253D
ago1-36
AGO1 Y255A
ago1-36
AGO1 Y255D
ago1-36
2cm

Fig. 3.3. The accumulation of miRNAs is affected by AGO1 phosphorylation.

(a) Northern blots to detect the accumulation of three miRNAs in *ago1-36,* and *ago1-36* expressing wild-type AGO1 (WT) or various AGO1 phospho-mutants. The numbers represent relative abundance of the miRNAs among the different genotypes. The U6 blots serve as a loading control for the miRNA blots above. Note that all genotypes were analyzed on the same gel, but the *ago1-36* lane was not next to the other lanes in the original gel.

(b to d) Small RNA-seq of *ago1-36* and transgenic lines expressing wild-type AGO1 or AGO1 phospho-mutants in the *ago1-36* background. Three biological replicates of each genotype were included in the analysis.

(b) Volcano plots showing miRNAs and miRNA*s with significantly different expression (fold change > 1.5 and adjusted *P* value < 0.01) between *AGO1* mutants and *AGO1*. Red dots denote miRNAs or miRNA*s with increased accumulation, while blue dots denote miRNAs or miRNA*s with reduced accumulation.

(c) Heatmap showing differential expression of miRNAs and miRNA*s between *AGO1* mutants and *AGO1*.

(d) Heatmap showing levels of miRNAs and the corresponding miRNA*s in *AGO1* mutants relative to *AGO1*.

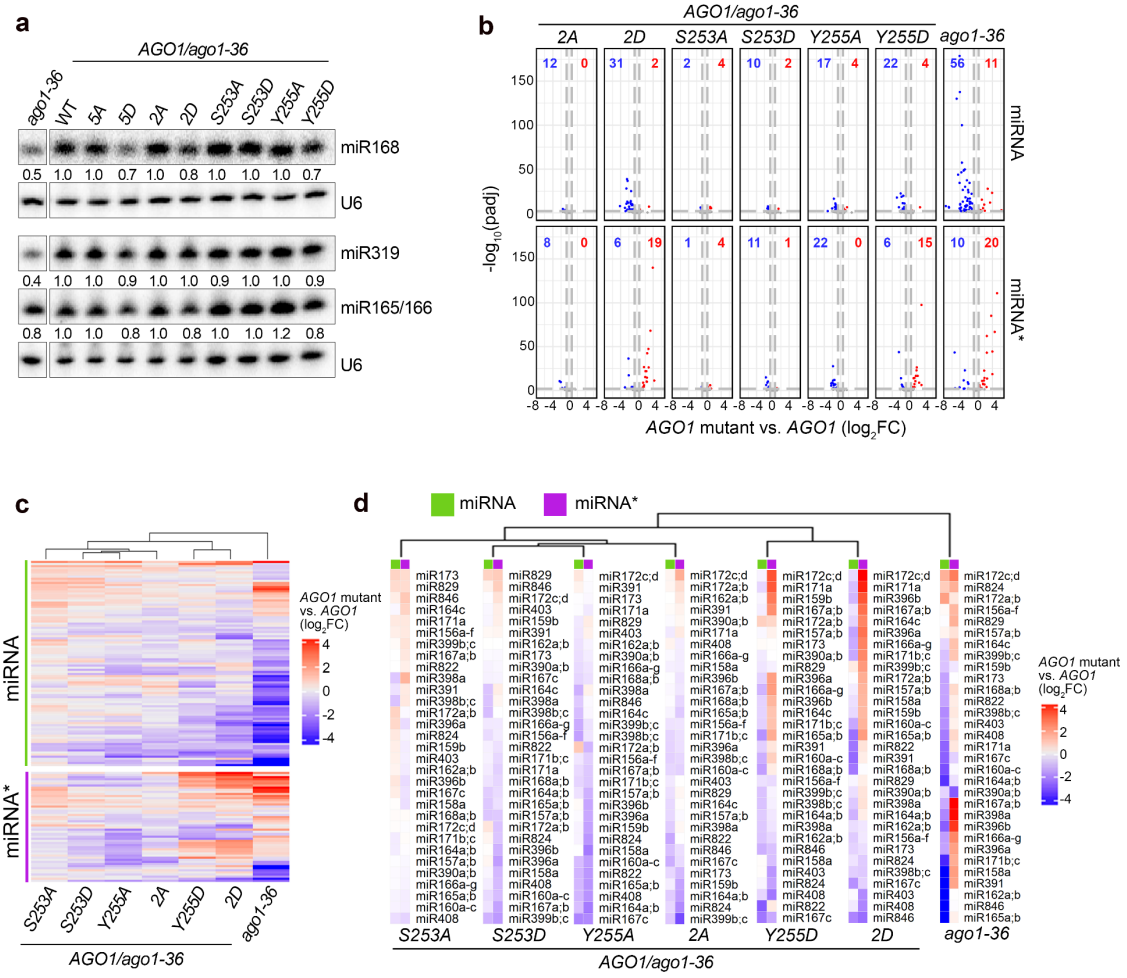
a
AGO1/ago1-36
ago1-36
WT
5A
5D
2A
2D
S253A
S253D
Y255A
Y255D
miR168
0.5 1.0 1.0 0.7 1.0 0.8 1.0 1.0 1.0 0.7
U6
miR319
0.4 1.0 1.0 0.9 1.0 1.0 0.9 1.0 1.0 0.9
miR165/166
0.8 1.0 1.0 0.8 1.0 0.8 1.0 1.0 1.2 0.8
U6
b
AGO1/ago1-36
2A
2D
S253A
S253D
Y255A
Y255D
ago1-36
miRNA
miRNA*
-log10(padj)
AGO1 mutant vs. AGO1 (log2FC)
c
miRNA
miRNA*
AGO1 mutant vs. AGO1 (log2FC)
S253A
S253D
Y255A
2A
Y255D
2D
ago1-36
AGO1/ago1-36
d
miRNA
miRNA*
AGO1 mutant vs. AGO1 (log2FC)
S253A
S253D
Y255A
2A
Y255D
2D
ago1-36
AGO1/ago1-36

Fig. 3.4. Assays of miRNA loading for AGO1 phospho-mutants.

(a) Scheme for the RISC assembly assay in tobacco BY-2 lysate. FLAG-AGO1 and phospho-mutated FLAG-AGO1 were translated in the lysate and subjected to the RISC assembly assay. Then, AGO1 proteins were immunoprecipitated and the associated small RNAs were analyzed.

(b) Sequences of miR156/miR156*, miR398/ miR398* and miR173/miR173* duplexes. The Upper and bottom strands represent the guide and passenger strands, respectively. The 5′ end of the guide strand was radiolabeled with ^{32}P. “M” indicates the 2′-*O*-methyl modification at the 3′ terminal ribose.

(c) Western blotting of wild-type (WT) and phospho-mutant FLAG-AGO1 proteins expressed in BY-2 lysate before (left) and after (right) immunoprecipitation with anti-FLAG antibody. The gel at the bottom shows the tubulin protein as an internal control.

(d) Native gel analysis of RISC assembly for wild-type AGO1 (WT) and its phosphorylation mutants (Y255A and Y255D) using miR156, miR398, miR173 duplexes. ‘ds’ and ‘ss’ denote double-stranded miRNAs (pre-RISC) and single-stranded miRNAs (mature RISC), respectively.

(e) Quantification of duplex loading efficiency in (d). Mean values ± s.d. from three independent experiments are shown.

(f) Quantification of passenger strand ejection efficiency in (d). Mean values ± s.d. from three independent experiments are shown.

(g to i) Analysis of small RNA-seq data of AGO1-associated small RNAs. Wild-type AGO1 was in the *ago1-36* background, while all AGO1 phospho-mutants were in the *ago1-36/+* background. Two biological replicates of each genotype were included in the analysis.

(g) Size (in nucleotides (nt)) distribution depicting the abundance of 18- to 26-nt small RNAs and miRNAs from IP-ed HA-AGO1 or HA-AGO1 phospho-mutants. RPM, reads per million (see Methods).

(h) Scatter plots showing the abundance of miRNAs and miRNA*s (RPM>2) in IPs of HA-AGO1 vs HA-AGO1 phospho-mutants.

(i) Volcano plots showing miRNAs and miRNA*s with significantly different levels (fold change > 1.5 and adjusted *P* value < 0.01) between IP-ed AGO1 phospho-mutants and AGO1. Red dots denote miRNAs or miRNA*s with significantly higher levels, while blue dots denote miRNAs or miRNA*s with significantly lower levels.

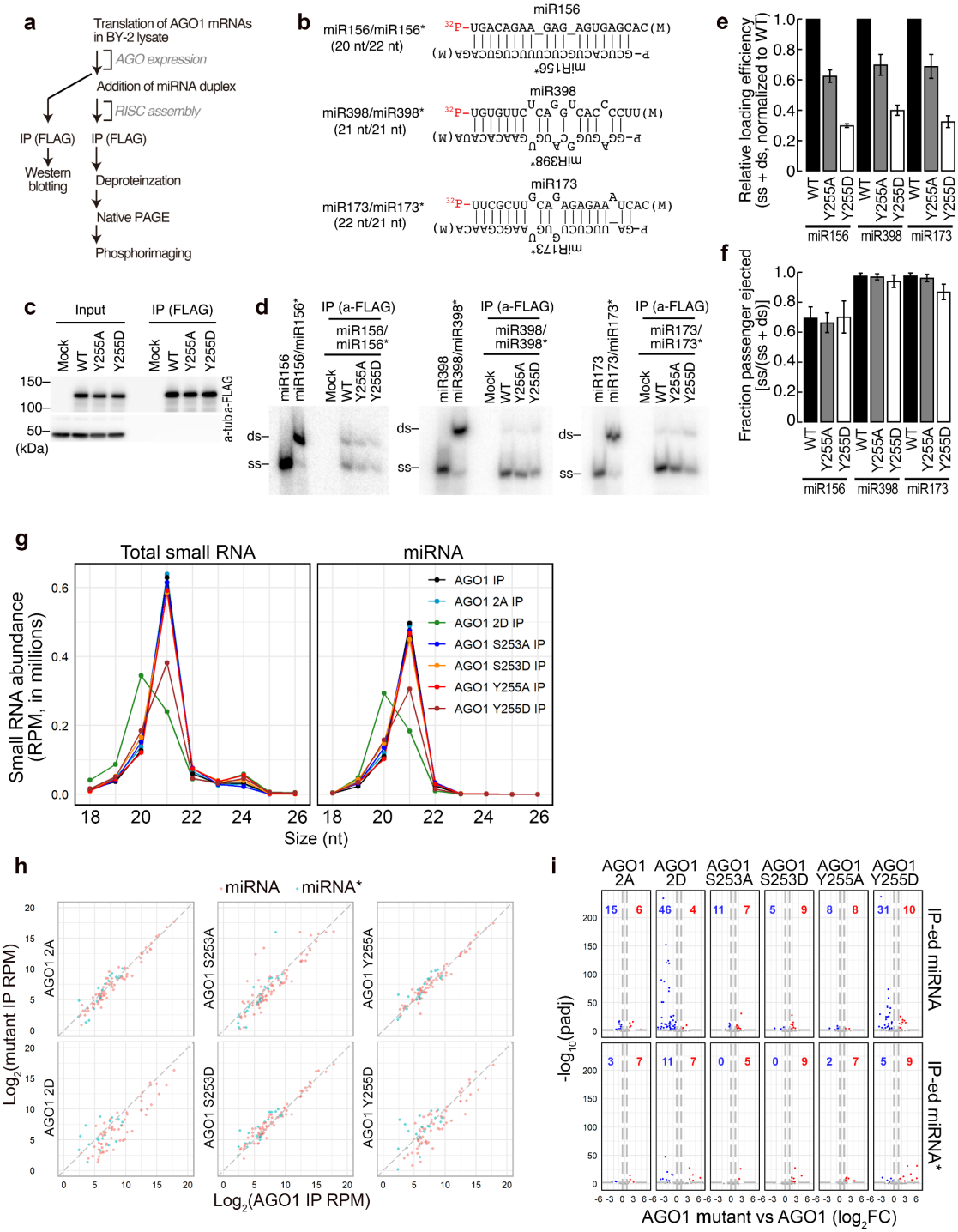
a
Translation of AGO1 mRNAs in BY-2 lysate
AGO expression
Addition of miRNA duplex
RISC assembly
IP (FLAG)
IP (FLAG)
Western blotting
Deproteinization
Native PAGE
Phosphorimaging
b
miR156
miR156/miR156*
(20 nt/22 nt)
miR398
miR398/miR398*
(21 nt/21 nt)
miR173
miR173/miR173*
(22 nt/21 nt)
c
Input
IP (FLAG)
Mock
WT
Y255A
Y255D
150–
100–
50–
(kDa)
a-tub
a-FLAG
d
IP (a-FLAG)
miR156/
miR156*
miR398/
miR398*
miR173/
miR173*
ds–
ss–
e
Relative loading efficiency
(ss + ds, normalized to WT)
f
Fraction passenger ejected
[ss/(ss + ds)]
miR156
miR398
miR173
g
Total small RNA
miRNA
Small RNA abundance
(RPM, in millions)
Size (nt)
AGO1 IP
AGO1 2A IP
AGO1 2D IP
AGO1 S253A IP
AGO1 S253D IP
AGO1 Y255A IP
AGO1 Y255D IP
h
miRNA
miRNA*
Log2(mutant IP RPM)
Log2(AGO1 IP RPM)
AGO1 2A
AGO1 S253A
AGO1 Y255A
AGO1 2D
AGO1 S253D
AGO1 Y255D
i
AGO1 2A
AGO1 2D
AGO1 S253A
AGO1 S253D
AGO1 Y255A
AGO1 Y255D
IP-ed miRNA
IP-ed miRNA*
-log10(padj)
AGO1 mutant vs AGO1 (log2FC)

Fig. 3.5. AGO1 Y255D is defective in siRNA duplex loading and passenger strand ejection.

(a) Sequences of a 21-nt siRNA duplex. The 5′ end of the guide strand was radiolabeled with ^{32}P. “M” indicates the 2′-*O*-methyl modification at the 3′ terminal ribose. The 5′ terminal nucleotide of the passenger strand bears a C6-amino modified linker (N6) to promote unidirectional loading.

(b) (Top) Native gel analysis of RISC assembly for wild-type AGO1 (WT) and its phospho-mutants (S253A, S253D, Y255A, Y255D, 2A and 2D) using the siRNA duplex shown in (a). (Bottom) Western blotting of FLAG-AGO1 and FLAG-AGO1 phospho-mutant proteins expressed in tobacco BY-2 lysate after immunoprecipitation with anti-FLAG antibody.

(c) Quantification of duplex loading efficiency in (b). Mean values ± s.d. from three independent experiments are shown.

(d) Quantification of passenger strand ejection efficiency in (b). Mean values ± s.d. from three independent experiments are shown.

(e to g) Analysis of small RNA-seq from RNA in AGO1 immunoprecipitates. Wild-type AGO1 (WT) was in the *ago1-36* background while all AGO1 phospho-mutants were in the *ago1-36/+* background. Two biological replicates of each genotype were included in the analysis.

(e) Size (in nucleotides (nt)) distribution depicting the abundance of 18- to 26-nt ta-siRNAs from AGO1 IP and AGO1 phospho-mutants IP. RPM, reads per million.

(f) Composition of small RNAs in 20-, 21-, and 22-nt classes in AGO1 IP and AGO1 phospho-mutants IP. Each column represents a biological replicate.

(g) Ratios of siRNA and siRNA* for the duplexes containing TAS1_siR255 and TAS3_5D7 in various AGO1 IPs. TAS1_siR255 and TAS3_5D7 were considered the siRNA strands in the duplexes with their corresponding siRNA*s. Mean values ± s.d. from two biological replicates are shown.

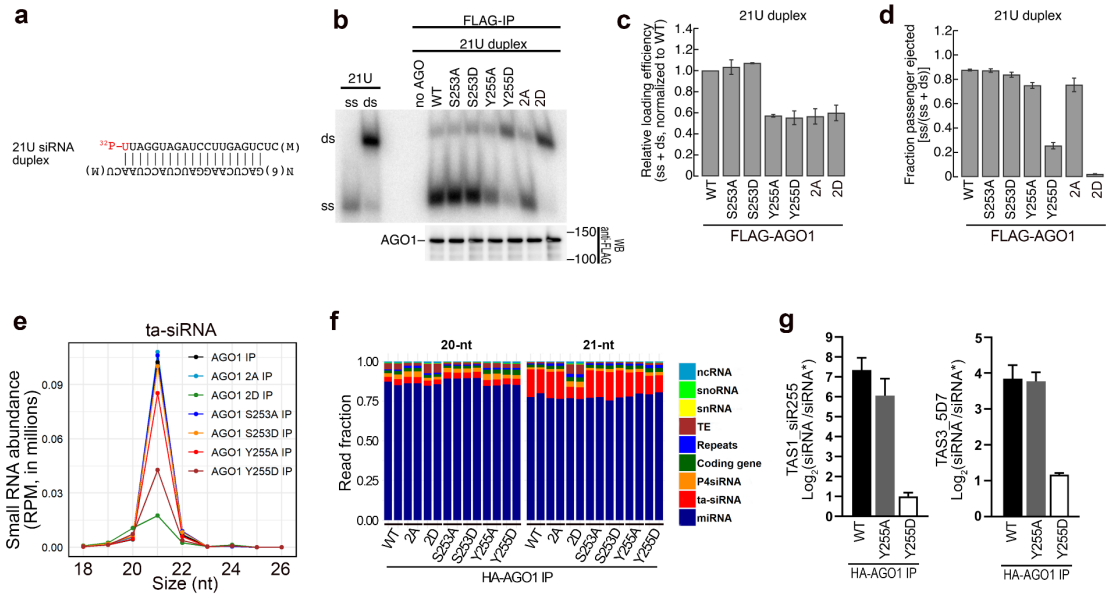
a
21U siRNA duplex
b
FLAG-IP
21U duplex
21U
ss ds
no AGO
WT
S253A
S253D
Y255A
Y255D
2A
2D
ds
ss
AGO1
150
100
WB: anti-FLAG
c
21U duplex
Relative loading efficiency (ss + ds, normalized to WT)
FLAG-AGO1
d
21U duplex
Fraction passenger ejected [ss/(ss + ds)]
FLAG-AGO1
e
ta-siRNA
Small RNA abundance (RPM, in millions)
Size (nt)
AGO1 IP
AGO1 2A IP
AGO1 2D IP
AGO1 S253A IP
AGO1 S253D IP
AGO1 Y255A IP
AGO1 Y255D IP
f
20-nt
21-nt
Read fraction
ncRNA
snoRNA
snRNA
TE
Repeats
Coding gene
P4siRNA
ta-siRNA
miRNA
HA-AGO1 IP
g
TAS1_siR255 Log2(siRNA/siRNA*)
TAS3_5D7 Log2(siRNA/siRNA*)
HA-AGO1 IP

Fig. 3.6. miRNA target repression requires AGO1 Y255 phosphorylation.

RNA-seq and small RNA-seq were performed with RNA isolated from 12-day-old seedlings. All lines containing *pAGO1:3XHA-AGO1* or *pAGO1:3XHA-AGO1* phospho-mutants were in the *ago1-36* background. Three biological replicates of each genotype were included in the analysis.

(a) Volcano plots showing miRNA target genes with significantly different expression (fold change > 1.5 and adjusted *P* value < 0.05) between *AGO1* mutants and *AGO1*. Red dots denote genes with significantly higher expression, while blue dots denote genes with significantly lower expression.

(b) Heatmap showing differential expression of 130 experimentally verified miRNA target genes between *ago1-36* or *AGO1* phospho-mutants in *ago1-36* and *AGO1 ago1-36*.

(c) Heatmap depicting significantly derepressed miRNA target genes in (a) and their corresponding miRNAs. Relative miRNA or mRNA levels between *ago1-36* and *AGO1 ago1-36* or between *AGO1* phospho-mutants in *ago1-36* and *AGO1 ago1-36* are shown.

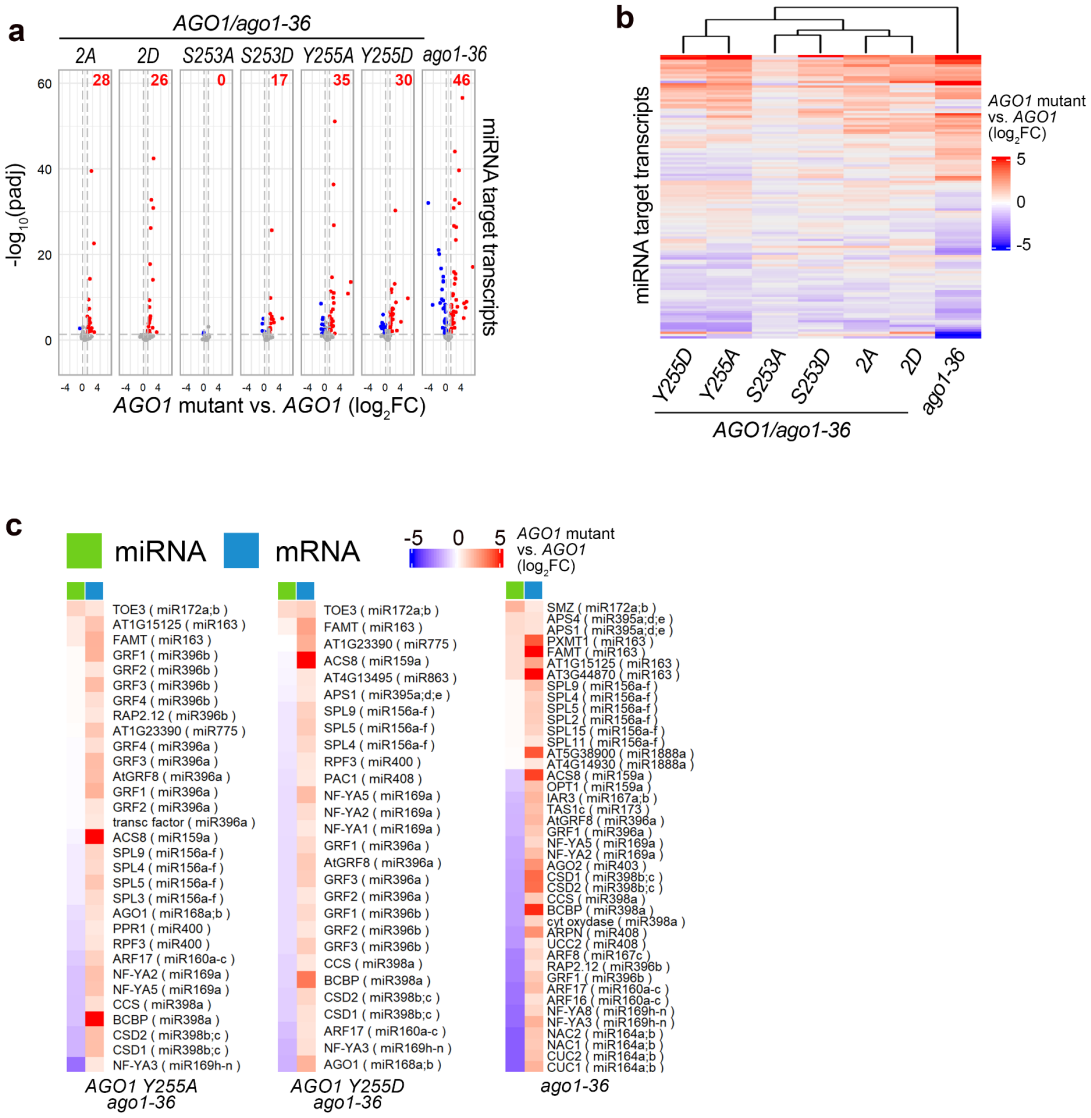
a
AGO1/ago1-36
2A
2D
S253A
S253D
Y255A
Y255D
ago1-36
28
26
0
17
35
30
46
-log10(padj)
miRNA target transcripts
AGO1 mutant vs. AGO1 (log2FC)
b
miRNA target transcripts
AGO1 mutant vs. AGO1 (log2FC)
5
0
-5
Y255D
Y255A
S253A
S253D
2A
2D
ago1-36
AGO1/ago1-36
c
miRNA
mRNA
-5 0 5
AGO1 mutant vs. AGO1 (log2FC)
TOE3 (miR172a;b)
AT1G15125 (miR163)
FAMT (miR163)
GRF1 (miR396b)
GRF2 (miR396b)
GRF3 (miR396b)
GRF4 (miR396b)
RAP2.12 (miR396b)
AT1G23390 (miR775)
GRF4 (miR396a)
GRF3 (miR396a)
AtGRF8 (miR396a)
GRF1 (miR396a)
GRF2 (miR396a)
transc factor (miR396a)
ACS8 (miR159a)
SPL9 (miR156a-f)
SPL4 (miR156a-f)
SPL5 (miR156a-f)
SPL3 (miR156a-f)
AGO1 (miR168a;b)
PPR1 (miR400)
RPF3 (miR400)
ARF17 (miR160a-c)
NF-YA2 (miR169a)
NF-YA5 (miR169a)
CCS (miR398a)
BCBP (miR398a)
CSD2 (miR398b;c)
CSD1 (miR398b;c)
NF-YA3 (miR169h-n)
AGO1 Y255A ago1-36
TOE3 (miR172a;b)
FAMT (miR163)
AT1G23390 (miR775)
ACS8 (miR159a)
AT4G13495 (miR863)
APS1 (miR395a;d;e)
SPL9 (miR156a-f)
SPL5 (miR156a-f)
SPL4 (miR156a-f)
RPF3 (miR400)
PAC1 (miR408)
NF-YA5 (miR169a)
NF-YA2 (miR169a)
NF-YA1 (miR169a)
GRF1 (miR396a)
AtGRF8 (miR396a)
GRF3 (miR396a)
GRF2 (miR396a)
GRF1 (miR396b)
GRF2 (miR396b)
GRF3 (miR396b)
CCS (miR398a)
BCBP (miR398a)
CSD2 (miR398b;c)
CSD1 (miR398b;c)
ARF17 (miR160a-c)
NF-YA3 (miR169h-n)
AGO1 (miR168a;b)
AGO1 Y255D ago1-36
SMZ (miR172a;b)
APS4 (miR395a;d;e)
APS1 (miR395a;d;e)
PXMT1 (miR163)
FAMT (miR163)
AT1G15125 (miR163)
AT3G44870 (miR163)
SPL9 (miR156a-f)
SPL4 (miR156a-f)
SPL5 (miR156a-f)
SPL2 (miR156a-f)
SPL15 (miR156a-f)
SPL11 (miR156a-f)
AT5G38900 (miR1888a)
AT4G14930 (miR1888a)
ACS8 (miR159a)
OPT1 (miR159a)
IAR3 (miR167a;b)
TAS1c (miR173)
AtGRF8 (miR396a)
GRF1 (miR396a)
NF-YA5 (miR169a)
NF-YA2 (miR169a)
AGO2 (miR403)
CSD1 (miR398b;c)
CSD2 (miR398b;c)
CCS (miR398a)
BCBP (miR398a)
cyt oxydase (miR398a)
ARPN (miR408)
UCC2 (miR408)
ARF8 (miR167c)
RAP2.12 (miR396b)
GRF1 (miR396b)
ARF17 (miR160a-c)
ARF16 (miR160a-c)
NF-YA8 (miR169h-n)
NF-YA3 (miR169h-n)
NAC2 (miR164a;b)
NAC1 (miR164a;b)
CUC2 (miR164a;b)
CUC1 (miR164a;b)
ago1-36

Fig. 3.7. AGO1 phosphorylation in RISC formation and RISC activity.

(a) Phospho-mimetic AGO1 Y255D and AGO1 S253D Y255D (2D) inhibit miRNA and siRNA duplex loading, and siRNA passenger strand ejection. AGO1 2D also mildly affects miRNA passenger strand ejection. Non-phosphorylatable AGO1 Y255A is compromised in target repression.

(b) A proposed model of AGO1 Y255 phosphorylation/dephosphorylation on AGO1's activities. Proper RISC assembly, including duplex loading and passenger strand ejection, requires non-phosphorylated Y255. However, optimal target repression may require Y255 phosphorylation.

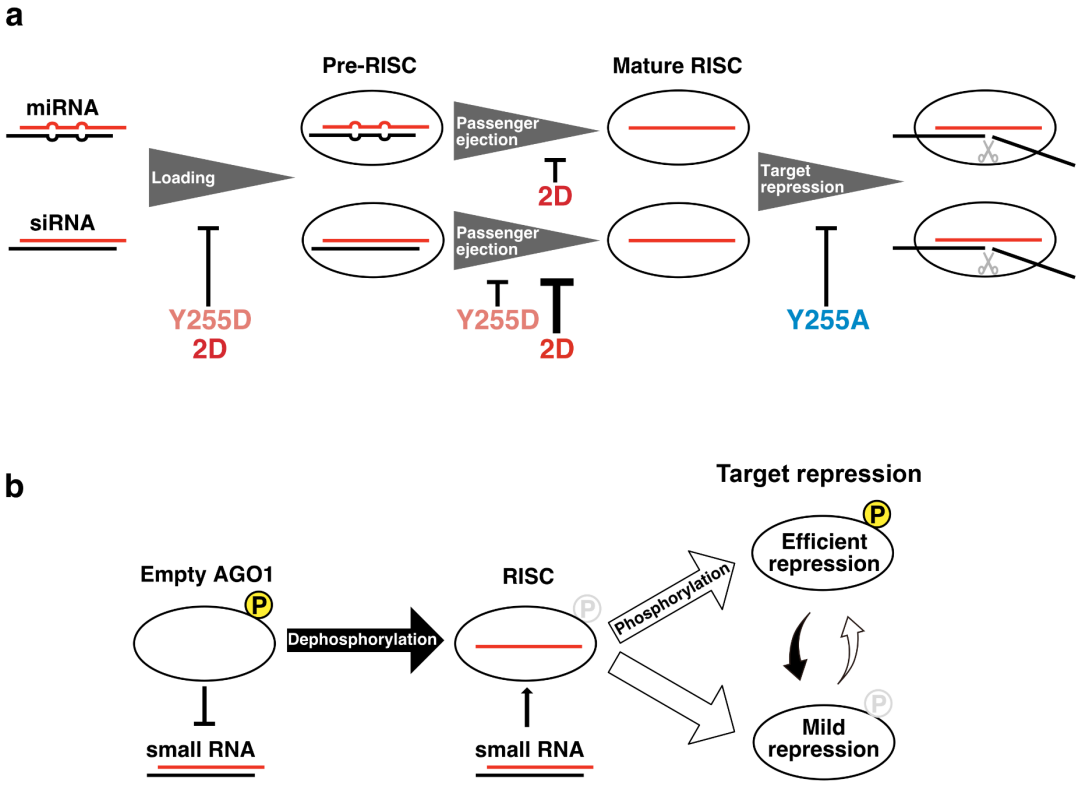
a
Pre-RISC
Mature RISC
miRNA
siRNA
Loading
Passenger ejection
2D
Passenger ejection
Target repression
Y255D
2D
Y255D
2D
Y255A
b
Target repression
Empty AGO1
P
Dephosphorylation
RISC
Phosphorylation
Efficient repression
P
Mild repression
P
small RNA
small RNA

Fig. S3.1. Four phospho-peptides of Arabidopsis AGO1 were identified by IP-MS/MS.

(a) MS/MS spectra showing phosphorylation of endogenous AGO1 at S11. The red circle denotes the phosphorylation site. Fragments with neutral loss were denoted with “–H3PO4”.

(b) MS/MS spectra showing phosphorylation of endogenous AGO1 at S350. The red circle denotes the phosphorylation site. Fragments with neutral loss were denoted with “–H3PO4”.

(c) MS/MS spectra showing phosphorylation of endogenous AGO1 at S1001. The red circle denotes the phosphorylation site. Fragments with neutral loss were denoted with “–H3PO4”.

(d) MS spectra showing the monophosphorylated peptide 253SLYTAGPLPFNSK265 of AGO1, $[M+2H]^{2+}$ =737.85.

(e) MS/MS spectra showing phosphorylation of endogenous AGO1 at Y255. The red circle denotes the phosphorylation site. The peaks marked by y2, y3, etc. represent the C-terminal fragments resulting from breakage at the indicated positions in the peptide sequence. Y11 is of the mass consistent with an additional phospho group.

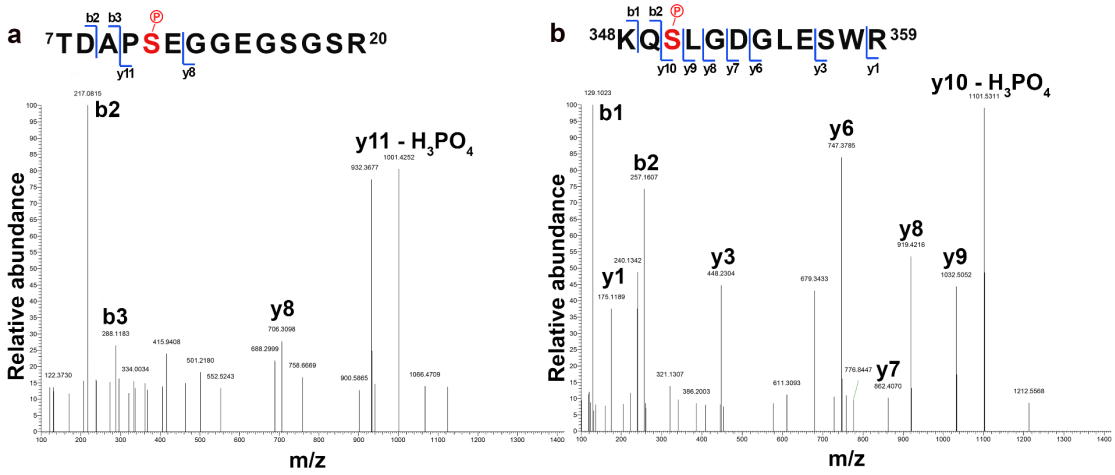
a
7TDAPSEGGEGSGSR20
b2 b3
y11
y8
b2
b3
y11 - H3PO4
y8
Relative abundance
m/z
b
348KQSLGDGLESWR359
b1 b2
y10 y9 y8 y7 y6 y3 y1
b1
b2
y1
y3
y6
y8
y9
y7
y10 - H3PO4
Relative abundance
m/z

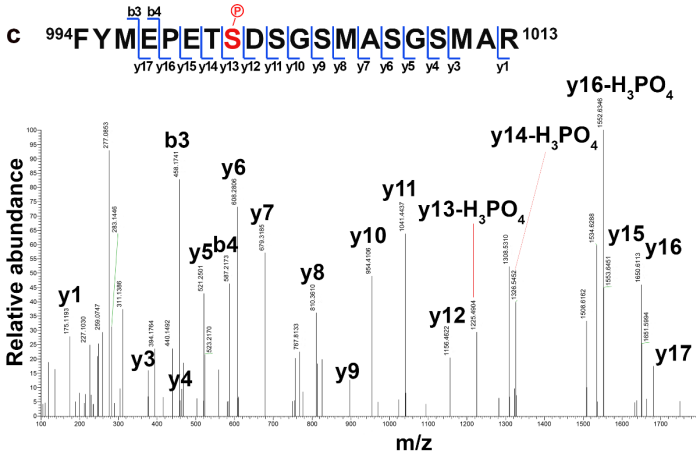
c
994FYMEPETSDSGSMASGSMAR1013
b3 b4
y17 y16 y15 y14 y13 y12 y11 y10 y9 y8 y7 y6 y5 y4 y3 y1
y16-H3PO4
y14-H3PO4
b3
y6
y7
y11
y13-H3PO4
y10
y15
y16
y5
b4
y8
y1
y12
y3
y4
y9
y17
Relative abundance
m/z

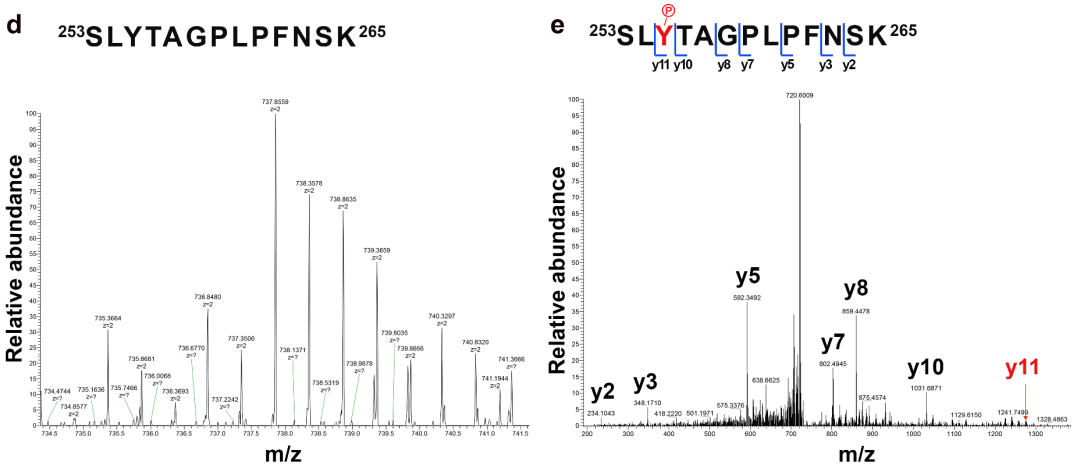
d
253SLYTAGPLPFNSK265
Relative abundance
m/z
e
253SLYTAGPLPFNSK265
y11 y10 y8 y7 y5 y3 y2
y5
y8
y7
y10
y11
y2
y3
Relative abundance
m/z

Fig. S3.2. Northern blots to detect the accumulation of three miRNAs in *ago1-36, ago1-3,* and *ago1-36* expressing wild-type *AGO1*. The numbers represent relative abundance of the miRNAs among the different genotypes. The U6 blots serve as a loading control for the miRNA blots above. Note that all genotypes were analyzed on the same gel, but the *AGO1 ago1-36* lane was not next to the other lanes in the original gel.

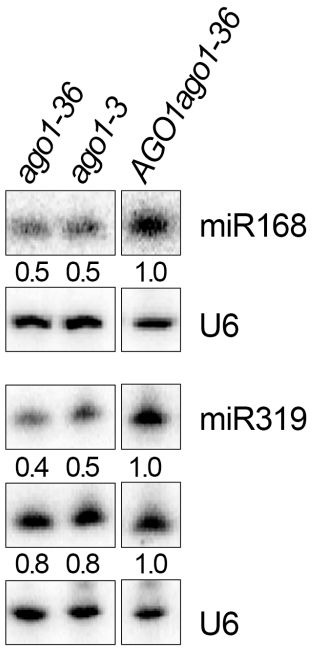
ago1-36
ago1-3
AGO1ago1-36
miR168
0.5 0.5 1.0
U6
miR319
0.4 0.5 1.0
0.8 0.8 1.0
U6

Fig. S3.3. AGO1 phosphorylation mutants exhibit pleiotropic developmental defects.

(a) Twelve-day-old seedlings of Col (wild type), *ago1-36, HA-AGO1 ago1-36*, *HA-AGO1 5A ago1-36, HA-AGO1 5D ago1-36*, *HA-AGO1 2A ago1-36*, *HA-AGO1 2D ago1-36*, *HA-AGO1 S253A ago1-36*, *HA-AGO1 S253D ago1-36*, *HA-AGO1 Y255A ago1-36*, and *HA-AGO1 Y255D ago1-36*. Scale bar, 1cm.

(b) Inflorescences of *HA-AGO1 ago1-36*, *HA-AGO1 5A ago1-36, HA-AGO1 5D ago1-36*, *HA-AGO1 2A ago1-36*, *HA-AGO1 2D ago1-36*, *HA-AGO1 S253A ago1-36*, *HA-AGO1 S253D ago1-36*, *HA-AGO1 Y255A ago1-36*, and *HA-AGO1 Y255D ago1-36.*

(c) Siliques of the indicated genotypes. Siliques were opened to show the lack of a full set of seeds in all mutants. Scale bar, 1mm.

(d) Four-week-old plants of *HA-AGO1 S1001A ago1-36* (left) and *HA-AGO1 3D ago1-36* (right).

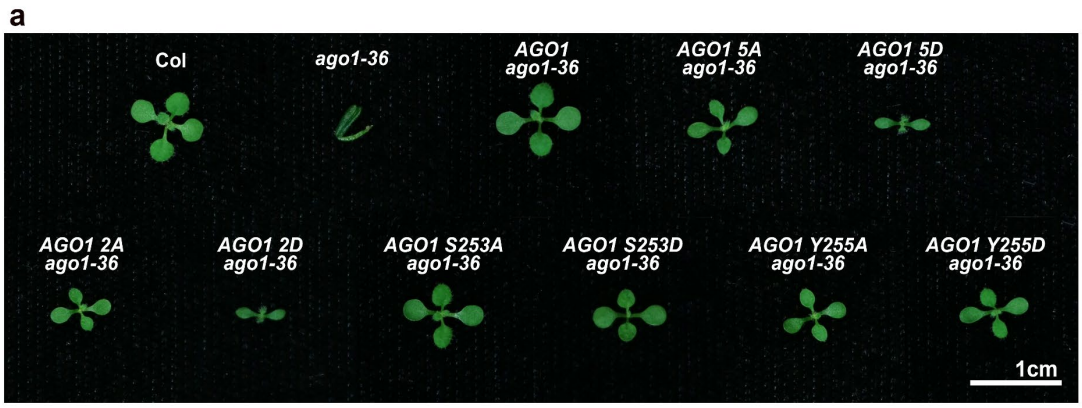
a
Col
ago1-36
AGO1 ago1-36
AGO1 5A ago1-36
AGO1 5D ago1-36
AGO1 2A ago1-36
AGO1 2D ago1-36
AGO1 S253A ago1-36
AGO1 S253D ago1-36
AGO1 Y255A ago1-36
AGO1 Y255D ago1-36
1cm

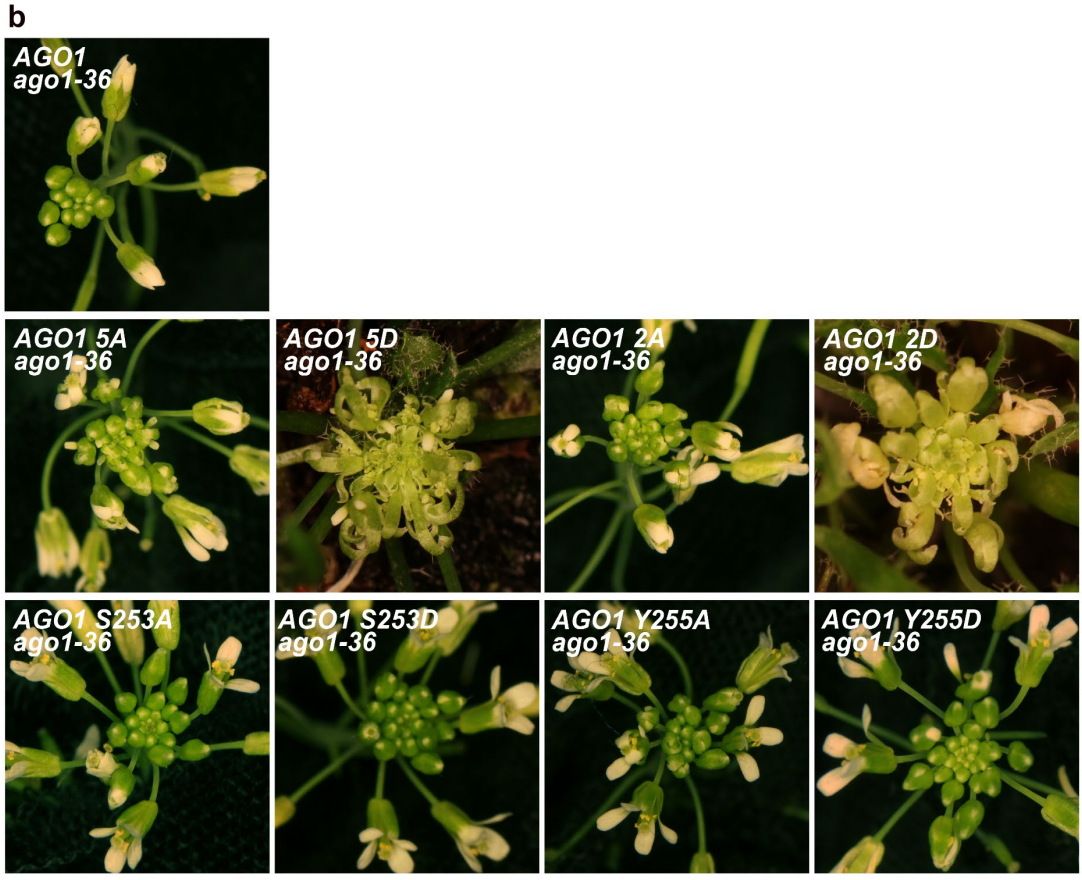
b
AGO1 ago1-36
AGO1 5A ago1-36
AGO1 5D ago1-36
AGO1 2A ago1-36
AGO1 2D ago1-36
AGO1 S253A ago1-36
AGO1 S253D ago1-36
AGO1 Y255A ago1-36
AGO1 Y255D ago1-36

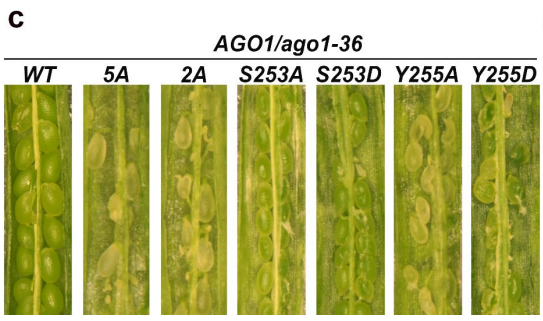
c
AGO1/ago1-36
WT
5A
2A
S253A
S253D
Y255A
Y255D

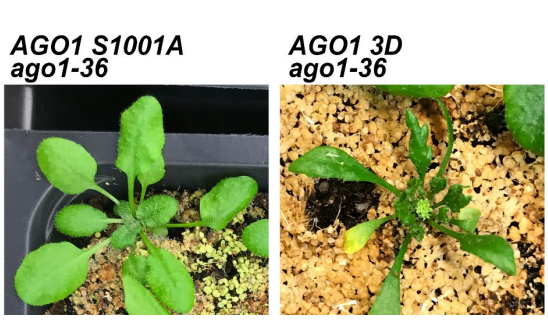
d
AGO1 S1001A ago1-36
AGO1 3D ago1-36

Fig. S3.4. Small RNA-seq of *AGO1 ago1-36*, *AGO1 5A ago1-36* and *AGO1 5D ago1-36*.

Three biological replicates of each genotype were included in the analysis.

(a) PCA showing the reproducibility of the three replicates.

(b) Size (in nucleotides (nt)) distribution depicting the abundance of 18- to 26-nt small RNAs. RPM, reads per million (see Methods).

(c) Volcano plots showing miRNAs and miRNA*s with significantly different levels (Fold change > 1.5 and adjusted *P* value < 0.01) between *AGO1* phospho-mutants and *AGO1*. Red dots denote miRNAs or miRNA*s with significantly higher accumulation, while blue dots denote miRNAs or miRNA*s with significantly reduced levels. Adjusted *P* values were calculated using the Wald test corrected with the Benjamini and Hochberg method.

(d) Heatmap depicting levels of miRNAs and the corresponding miRNA*s in *AGO1* phospho-mutants relative to *AGO1* (all in the *ago1-36* background).

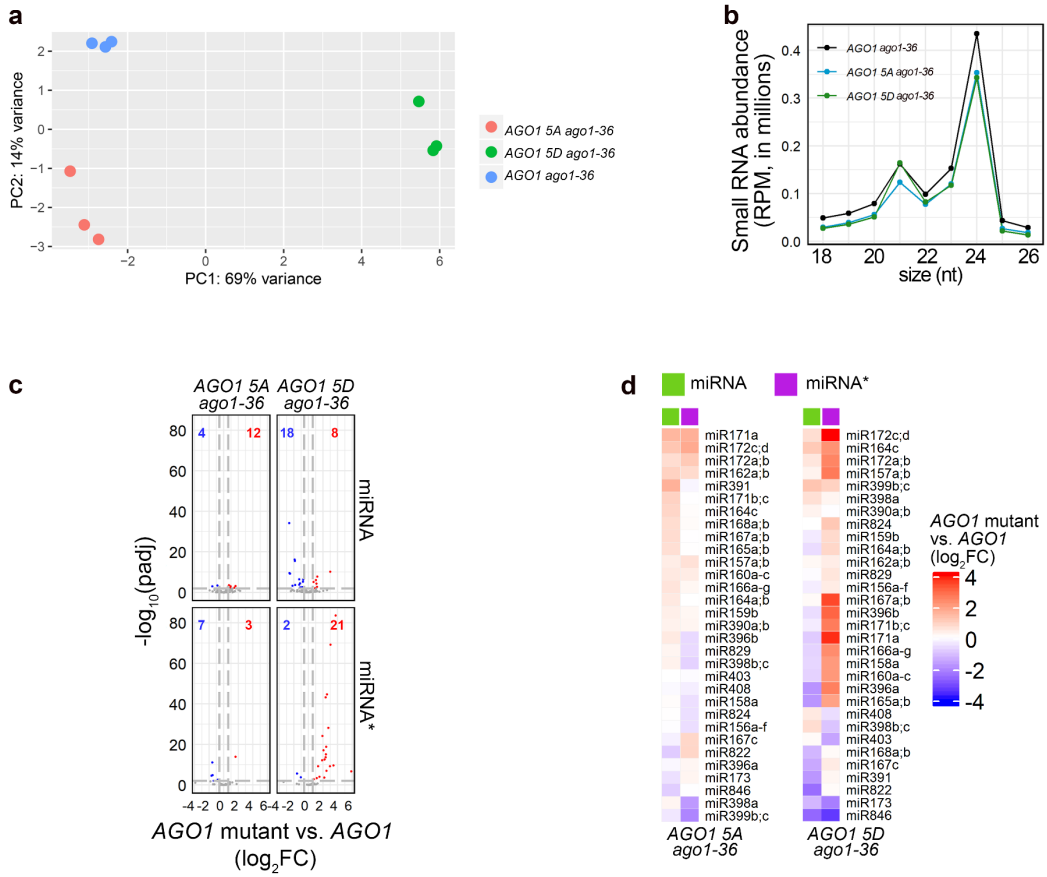
a
PC2: 14% variance
PC1: 69% variance
AGO1 5A ago1-36
AGO1 5D ago1-36
AGO1 ago1-36
b
Small RNA abundance (RPM, in millions)
size (nt)
AGO1 ago1-36
AGO1 5A ago1-36
AGO1 5D ago1-36
c
AGO1 5A ago1-36
AGO1 5D ago1-36
-log10(padj)
miRNA
miRNA*
AGO1 mutant vs. AGO1 (log2FC)
d
miRNA
miRNA*
AGO1 5A ago1-36
AGO1 5D ago1-36
AGO1 mutant vs. AGO1 (log2FC)

Fig. S3.5. Profiling of AGO1 5A- and AGO1 5D-associated small RNAs.

(a to c) and (e to g), analysis of small RNA-seq data from RNA in AGO1 immunoprecipitates (IPs). Wild-type AGO1 (WT) was IP-ed from *HA-AGO1 ago1-36* while AGO1 5A and AGO1 5D were IP-ed from *HA-AGO1-5A ago1-36/+* and *HA-AGO1-5D ago1-36/+*, respectively. Two biological replicates of each genotype were included in the analysis.

(a) PCA showing that the biological replicates were reproducible.

(b) Size (in nucleotides (nt)) distribution depicting the abundance of 18- to 26-nt small RNAs in IPs from AGO1 and AGO1 phospho-mutants. Both total small RNAs and miRNAs only are shown. RPM, reads per million (see Methods).

(c) Composition of small RNAs in the 21-nt and 22-nt classes in IPs from wild-type AGO1 (WT) and AGO1 phospho-mutants. Each column represents a biological replicate.

(d) Northern blots to detect the accumulation of two miRNAs and a *TAS1*-originated ta-siRNA in *HA-AGO1 ago1-36*, *HA-AGO1 5A ago1-36*/+ and *HA-AGO1 5D ago1-36*/+. The U6 blots serve as a loading control for the miRNA blots above. The HA western blot shows the amounts of IP-ed HA-AGO1 and HA-AGO1 phospho-mutants. cFBPase serves as the loading control for the input samples.

(e) Scatter plots showing miRNA and miRNA* abundance (RPM>2) in IPs from AGO1 vs. AGO1 phospho-mutants.

(f) Volcano plots showing miRNAs and miRNA*s with significantly different levels (Fold change > 1.5 and adjusted *P* value < 0.01) between IP-ed AGO1 phospho-

mutants and AGO1. Red dots denote miRNAs or miRNA*s with significantly higher abundance, while blue dots denote miRNAs or miRNA*s with significantly lower abundance. Adjusted *P* values were calculated using the Wald test corrected with the Benjamini and Hochberg method.

(g) Heatmap depicting the levels of miRNAs and the corresponding miRNA*s in IPs from AGO1 phospho-mutants relative to AGO1.

(h) Western blots to determine the nuclear-cytoplasmic partitioning of AGO1 in *AGO1 ago1-36*, *AGO1 5A ago1-36*, and *AGO1 5D ago1-36*. Blots were probed using HA, cFBPase, and H3 antibodies, respectively. H3 is a nuclear marker and used to quantify HA-AGO1 in the total lysate (T) and nuclear fraction (N). cFBPase is a cytoplasmic marker and used to quantify HA-AGO1 in the total lysate (T) and the cytoplasmic fraction (C). This experiment was repeated two times with similar results.

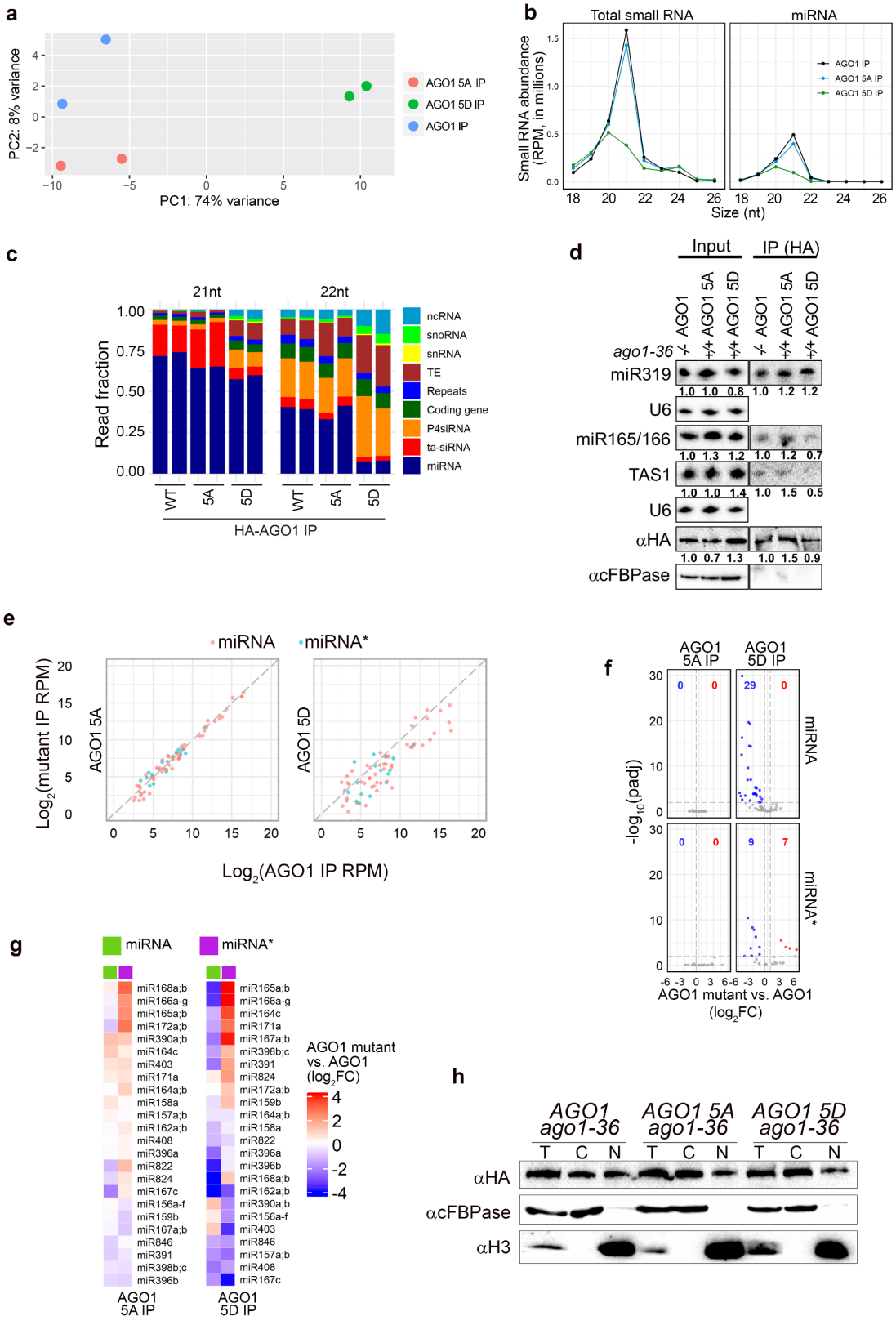
a
PC2: 8% variance
PC1: 74% variance
AGO1 5A IP
AGO1 5D IP
AGO1 IP
b
Total small RNA
miRNA
Small RNA abundance (RPM, in millions)
Size (nt)
AGO1 IP
AGO1 5A IP
AGO1 5D IP
c
21nt
22nt
Read fraction
ncRNA
snoRNA
snRNA
TE
Repeats
Coding gene
P4siRNA
ta-siRNA
miRNA
WT
5A
5D
HA-AGO1 IP
d
Input
IP (HA)
ago1-36
AGO1
AGO1 5A
AGO1 5D
miR319
U6
miR165/166
TAS1
αHA
αcFBPase
e
miRNA
miRNA*
Log2(mutant IP RPM)
AGO1 5A
AGO1 5D
Log2(AGO1 IP RPM)
f
AGO1 5A IP
AGO1 5D IP
-log10(padj)
AGO1 mutant vs. AGO1 (log2FC)
g
miRNA
miRNA*
AGO1 mutant vs. AGO1 (log2FC)
AGO1 5A IP
AGO1 5D IP
h
AGO1 ago1-36
AGO1 5A ago1-36
AGO1 5D ago1-36
T
C
N
αHA
αcFBPase
αH3

Fig. S3.6. Profiling of small RNAs in AGO1 single and double phospho-mutants.

(a) Western blots to determine the protein levels of wild-type AGO1 (WT) and AGO1 phospho-mutants from transgenic lines expressing various *HA-AGO1* transgenes in *ago1-36*. The HA antibody was used to detect HA-AGO1 and HA-AGO1 mutants. cFBPase is a loading control. MW, molecular weight.

(b to c) Analysis of small RNA-seq data from total RNA isolated from 12-day-old seedlings. All lines containing *pAGO1:3XHA-AGO1* or *pAGO1:3XHA-AGO1* phospho-mutants were in the *ago1-36* background. Three biological replicates of each genotype were analyzed.

(b) PCA showing the reproducibility of the three biological replicates of each genotype.

(c) Size (in nucleotides (nt)) distribution depicting the abundance of 18- to 26-nt small RNAs in various genotypes. RPM, reads per million (see Methods).

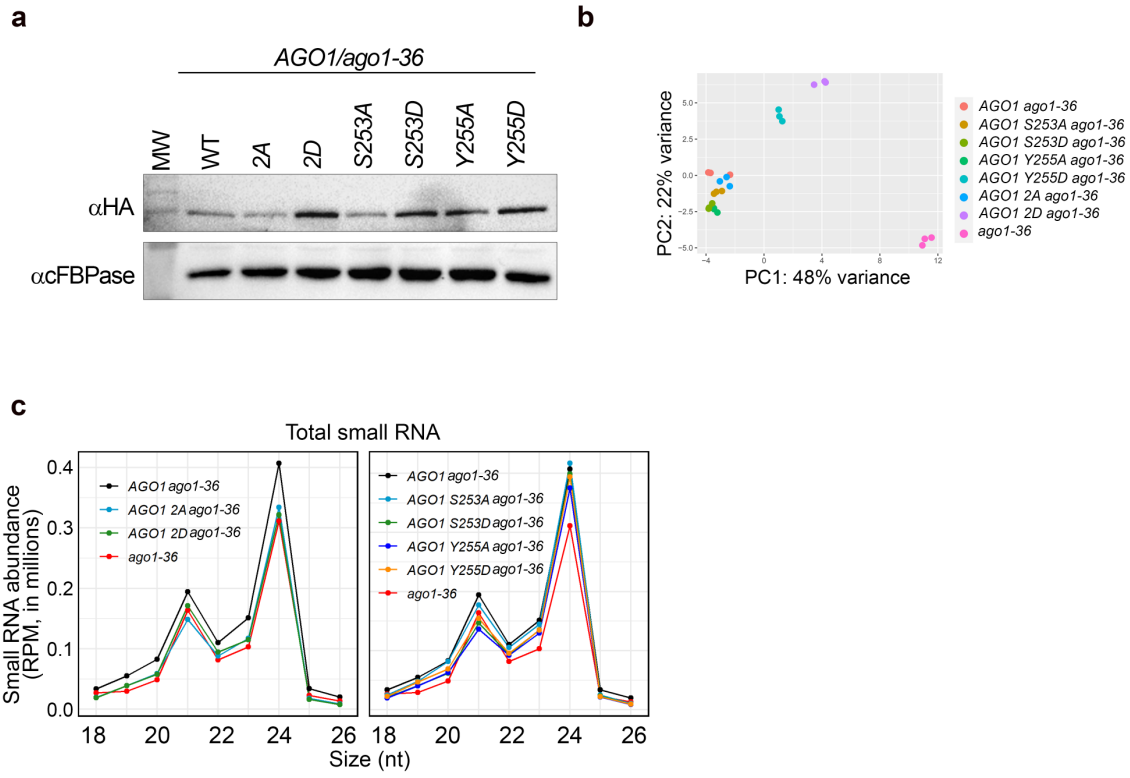
a
AGO1/ago1-36
MW
WT
2A
2D
S253A
S253D
Y255A
Y255D
αHA
αcFBPase
b
PC2: 22% variance
PC1: 48% variance
AGO1 ago1-36
AGO1 S253A ago1-36
AGO1 S253D ago1-36
AGO1 Y255A ago1-36
AGO1 Y255D ago1-36
AGO1 2A ago1-36
AGO1 2D ago1-36
ago1-36
c
Total small RNA
Small RNA abundance (RPM, in millions)
Size (nt)
AGO1 ago1-36
AGO1 2A ago1-36
AGO1 2D ago1-36
ago1-36
AGO1 ago1-36
AGO1 S253A ago1-36
AGO1 S253D ago1-36
AGO1 Y255A ago1-36
AGO1 Y255D ago1-36
ago1-36

Fig. S3.7. *In vitro* RISC assembly assays to determine the duplex loading and passenger strand ejection efficiencies of AGO1 mutants.

'ds' and 'ss' denote double-stranded miRNAs (pre-RISC) and single-stranded miRNAs (mature RISC), respectively. "M" indicates the 2′-*O*-methyl modification at the 3′ terminal ribose.

(a) (Top) Native gel analysis of RISC assembly for wild-type AGO1 (WT) and phosphorylation mutants (S253A, S253D, Y255A, Y255D, 2A and 2D) using the miR398/miR398* duplex. (Bottom) Western blotting of AGO1 proteins expressed in the tobacco BY-2 lysate after immunoprecipitation with anti-FLAG antibody.

(b) Quantification of duplex loading (left) and passenger strand ejection (right) efficiency. Mean values ± s.d. from three independent experiments are shown.

(c) Sequences of 20–22 nt siRNA duplexes. The inserted base-pairs are highlighted in pink and orange. The 5′ end of the guide strand was radiolabeled with ^{32}P. The 5′ terminal nucleotide of the passenger strand bears a C6-amino modified linker (N6) to promote unidirectional loading.

(d) Native gel analysis of RISC assembly for wild-type AGO1 (WT) and phospho-mutants (Y255A and Y255D) using siRNA duplexes shown in (c).

(e) Quantification of duplex loading efficiency in (d). Mean values ± s.d. from three independent experiments are shown.

(f) Quantification of passenger strand ejection efficiency in (d). Mean values ± s.d. from three independent experiments are shown.

(g) Sequences of siRNA duplexes that bear A, U, G or C at the 5′ end of the guide strand. The 5′ end of the guide strand was radiolabeled with ^{32}P. The 5′ terminal nucleotide of the passenger strand bears a C6-amino modified linker (N6) to promote unidirectional loading.

(h) Native gel analysis of RISC assembly for wild-type AGO1 (WT) and phospho-mutants (Y255A and Y255D) using siRNA duplexes shown in (g).

(i) Quantification of duplex loading efficiency in (h). Mean values ± s.d. from three independent experiments are shown.

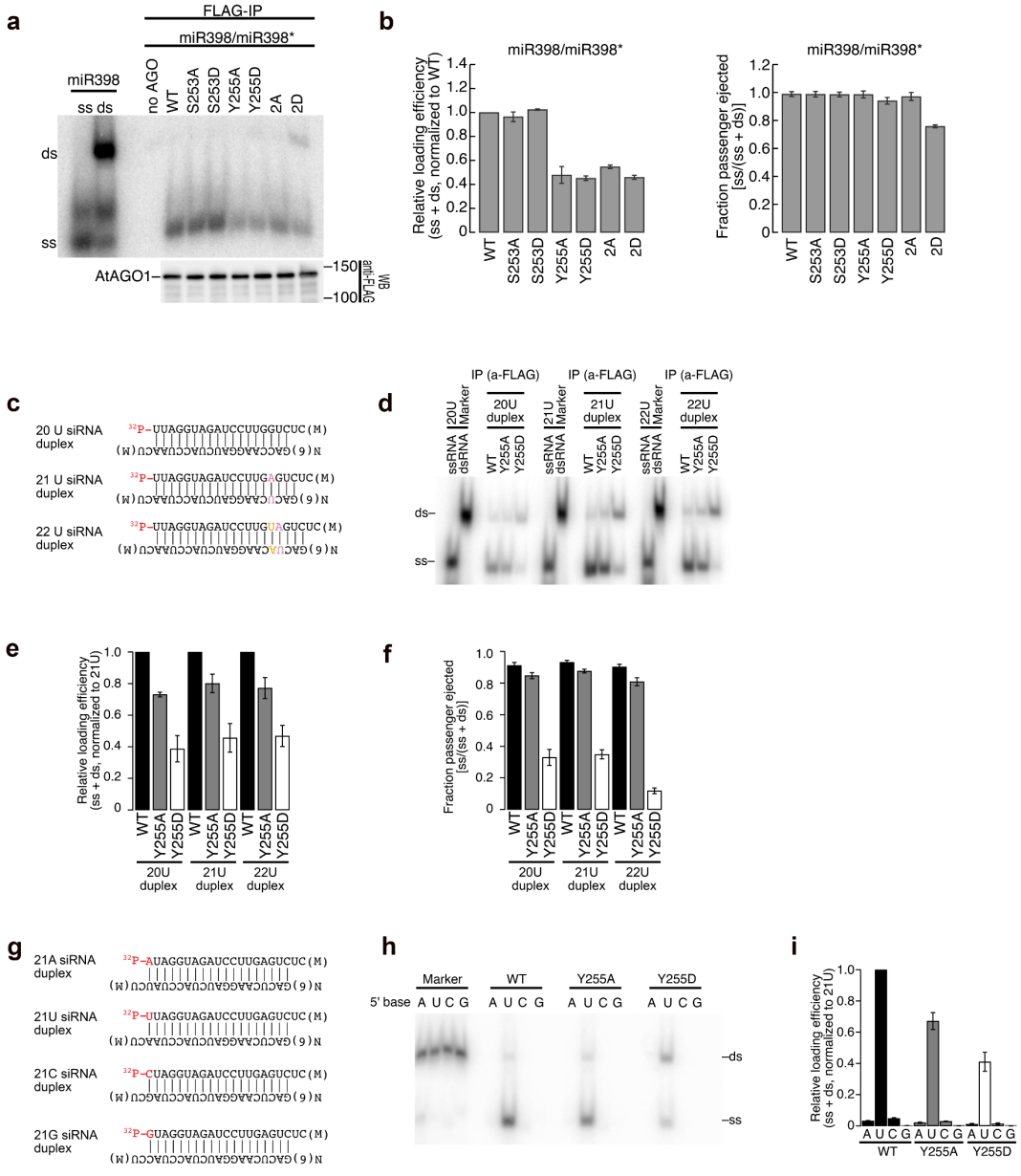
a
FLAG-IP
miR398/miR398*
miR398
ss ds
no AGO
WT
S253A
S253D
Y255A
Y255D
2A
2D
ds
ss
AtAGO1
–150
–100
WB anti-FLAG
b
miR398/miR398*
Relative loading efficiency (ss + ds, normalized to WT)
Fraction passenger ejected [ss/(ss + ds)]
c
20 U siRNA duplex
21 U siRNA duplex
22 U siRNA duplex
d
IP (a-FLAG)
ssRNA
dsRNA
Marker
20U duplex
21U duplex
22U duplex
WT
Y255A
Y255D
ds–
ss–
e
Relative loading efficiency (ss + ds, normalized to 21U)
f
Fraction passenger ejected [ss/(ss + ds)]
g
21A siRNA duplex
21U siRNA duplex
21C siRNA duplex
21G siRNA duplex
h
Marker
WT
Y255A
Y255D
5' base
A U C G
–ds
–ss
i
Relative loading efficiency (ss + ds, normalized to 21U)

Fig. S3.8. Profiling of AGO1-associated small RNAs for wild-type AGO1 and single and double phospho-mutants.

Small RNA-seq was performed with RNA from AGO1 IP from *ago1-36* expressing *pAGO1:3XHA-AGO1* or *ago1-36*/+ expressing *pAGO1:3XHA-AGO1* phospho-mutants. Two biological replicates of each genotype were included in the analysis.

(a) PCA showing that the biological replicates were reproducible.

(b) Heatmap depicting the levels of miRNAs and the corresponding miRNA*s in IPs of AGO1 phospho-mutants relative to AGO1.

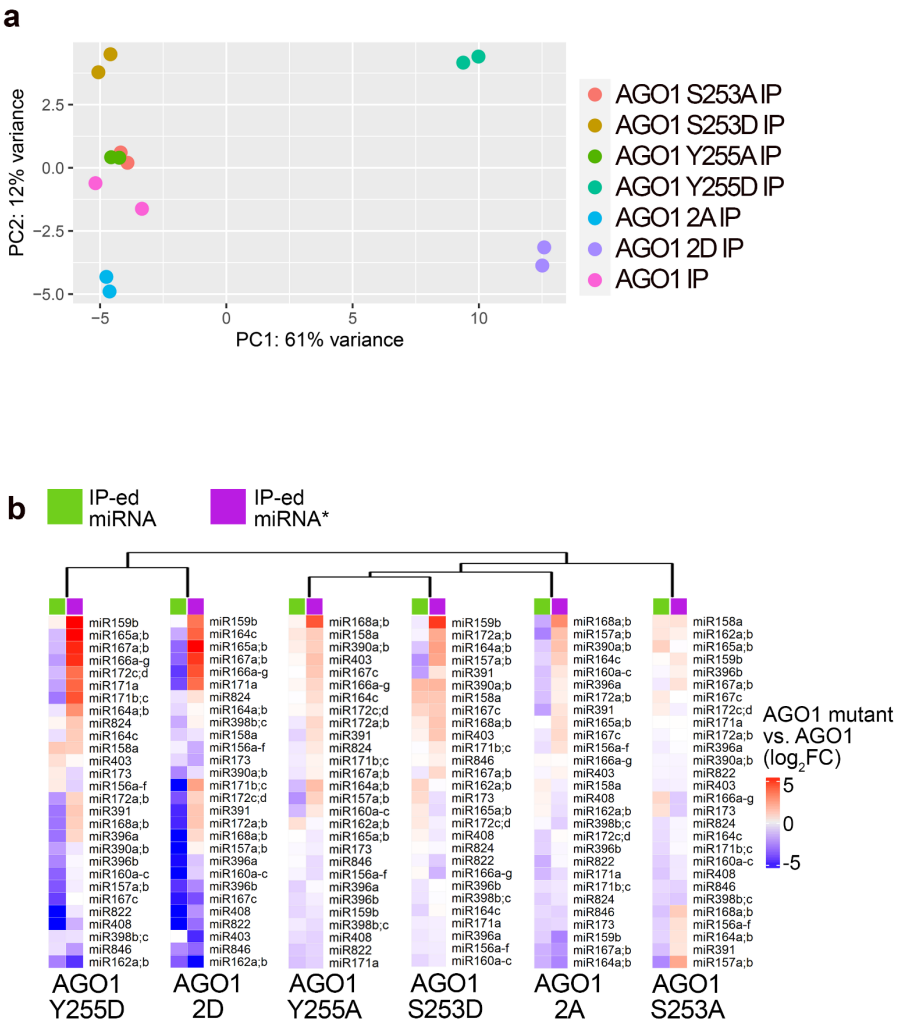
a
PC2: 12% variance
PC1: 61% variance
AGO1 S253A IP
AGO1 S253D IP
AGO1 Y255A IP
AGO1 Y255D IP
AGO1 2A IP
AGO1 2D IP
AGO1 IP
b
IP-ed miRNA
IP-ed miRNA*
AGO1 mutant vs. AGO1 (log2FC)
AGO1 Y255D
AGO1 2D
AGO1 Y255A
AGO1 S253D
AGO1 2A
AGO1 S253A

Fig. S3.9. Most AGO1 2D-loaded miRNAs are 1-nt shorter at the 3' ends.

Small RNA-seq was performed with RNA from AGO1 IP from wild-type AGO1 or AGO1 phospho-mutants. Wild-type AGO1 was in the *ago1-36* background while all AGO1 phospho-mutants were in the *ago1-36/+* background. Two biological replicates of each genotype were included in the analysis.

(a) Bar plots showing the composition of 18- to 24-nt miRNA reads in AGO1 IPs according to their direction and length of truncation relative to the annotated miRNAs. Reads mapping to miRNA*s were excluded from this analysis. Most 20-nt reads associated with AGO1 2D were 21-nt miRNAs with 1-nt truncation at the 3' ends.

(b) Bar plots showing the composition of reads corresponding to annotated 20-, 21-, 22- and 24-nt miRNAs in AGO1 IPs. Reads mapping to miRNA*s were excluded from this analysis. Annotated 21-nt miRNAs showed dramatically increased 3' truncation in AGO1 2D as compared to wild type AGO1, and most truncation was by 1-nt at the 3' end.

(c) Scatter plots showing the ratio of 21-nt vs. 20-nt isoforms of annotated 21-nt miRNAs and miRNA*s in AGO1 IP. Most AGO1 2D-associated miRNAs annotated as 21-nt long showed a reduced 21-nt/20-nt ratio compared to AGO1-associated miRNAs.

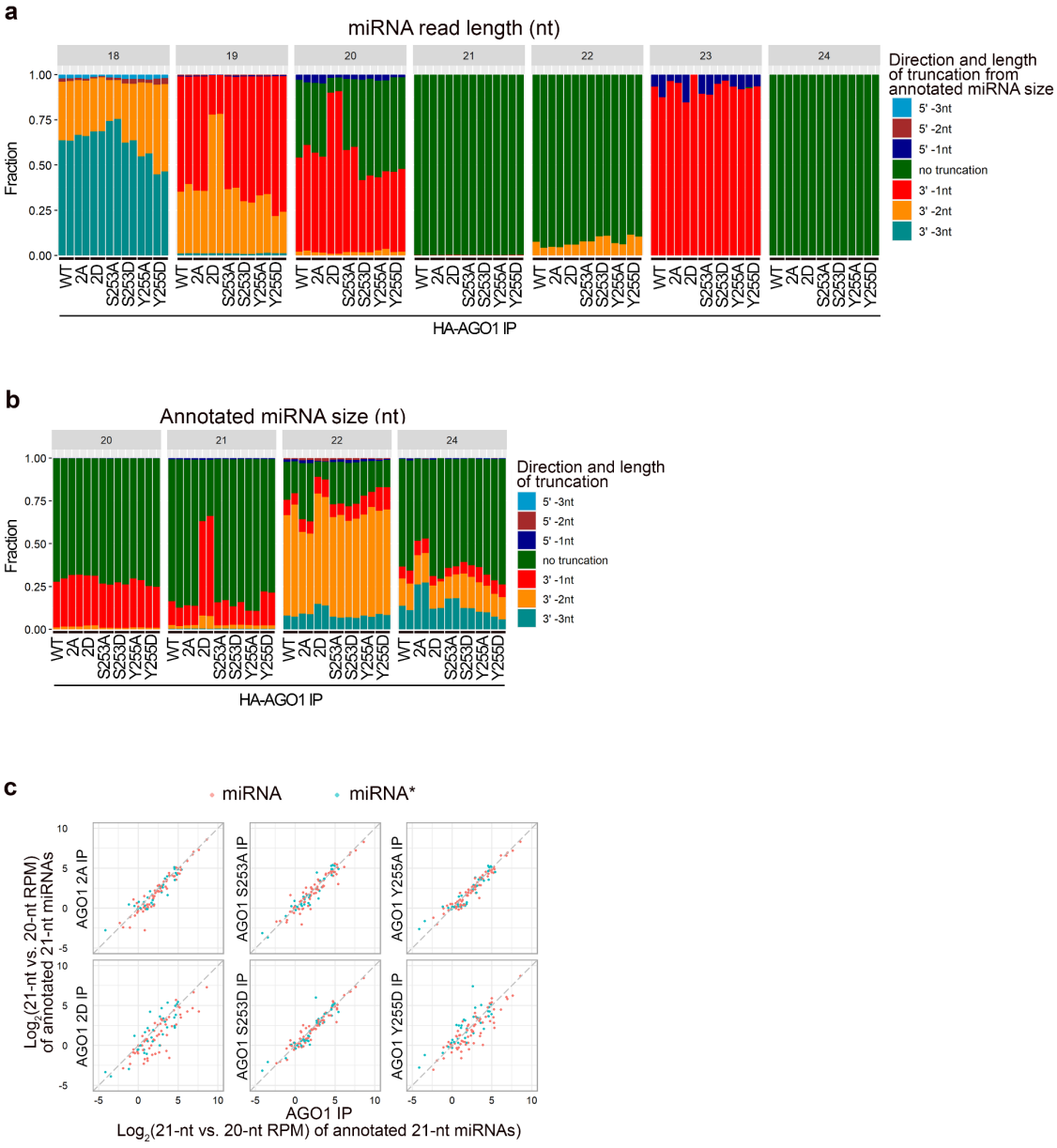
a
miRNA read length (nt)
18
19
20
21
22
23
24
Fraction
1.00
0.75
0.50
0.25
0.00
WT
2A
2D
S253A
S253D
Y255A
Y255D
HA-AGO1 IP
Direction and length of truncation from annotated miRNA size
5' -3nt
5' -2nt
5' -1nt
no truncation
3' -1nt
3' -2nt
3' -3nt
b
Annotated miRNA size (nt)
20
21
22
24
Direction and length of truncation
c
miRNA
miRNA*
AGO1 2A IP
AGO1 S253A IP
AGO1 Y255A IP
AGO1 2D IP
AGO1 S253D IP
AGO1 Y255D IP
Log2(21-nt vs. 20-nt RPM) of annotated 21-nt miRNAs
AGO1 IP
Log2(21-nt vs. 20-nt RPM) of annotated 21-nt miRNAs)

Fig. S3.10. PCA analysis of RNA-seq. All lines containing *pAGO1:3XHA-AGO1* or *pAGO1:3XHA-AGO1* phospho-mutants were in the *ago1-36* background. Three biological replicates of each genotype were analyzed.

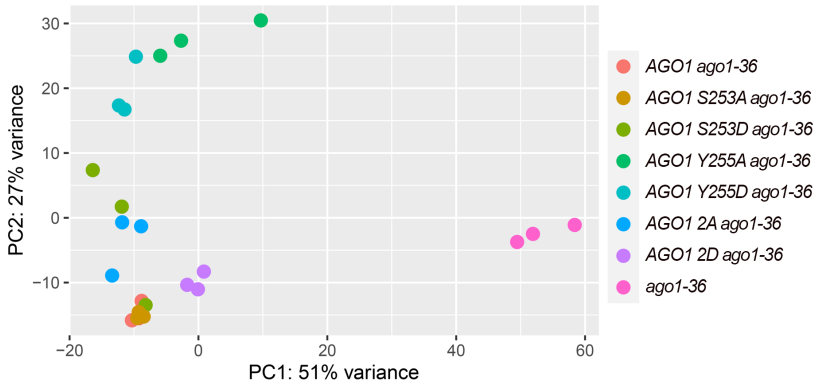
30
20
10
0
−10
PC2: 27% variance
−20
0
20
40
60
PC1: 51% variance
AGO1 ago1-36
AGO1 S253A ago1-36
AGO1 S253D ago1-36
AGO1 Y255A ago1-36
AGO1 Y255D ago1-36
AGO1 2A ago1-36
AGO1 2D ago1-36
ago1-36

Fig. S3.11. Immunoprecipitation (IP) of GFP-AGO1 and phospho-mutated GFP-AGO1 followed by RNA gel blot analysis of miR165 association. The levels of miR165 in the immunoprecipitate were quantified against those of the respective GFP-AGO1 proteins and shown in red. U6 and cFBPase serve as the RNA and protein loading controls, respectively, for the input samples. Two independent replicates (rep) are shown.

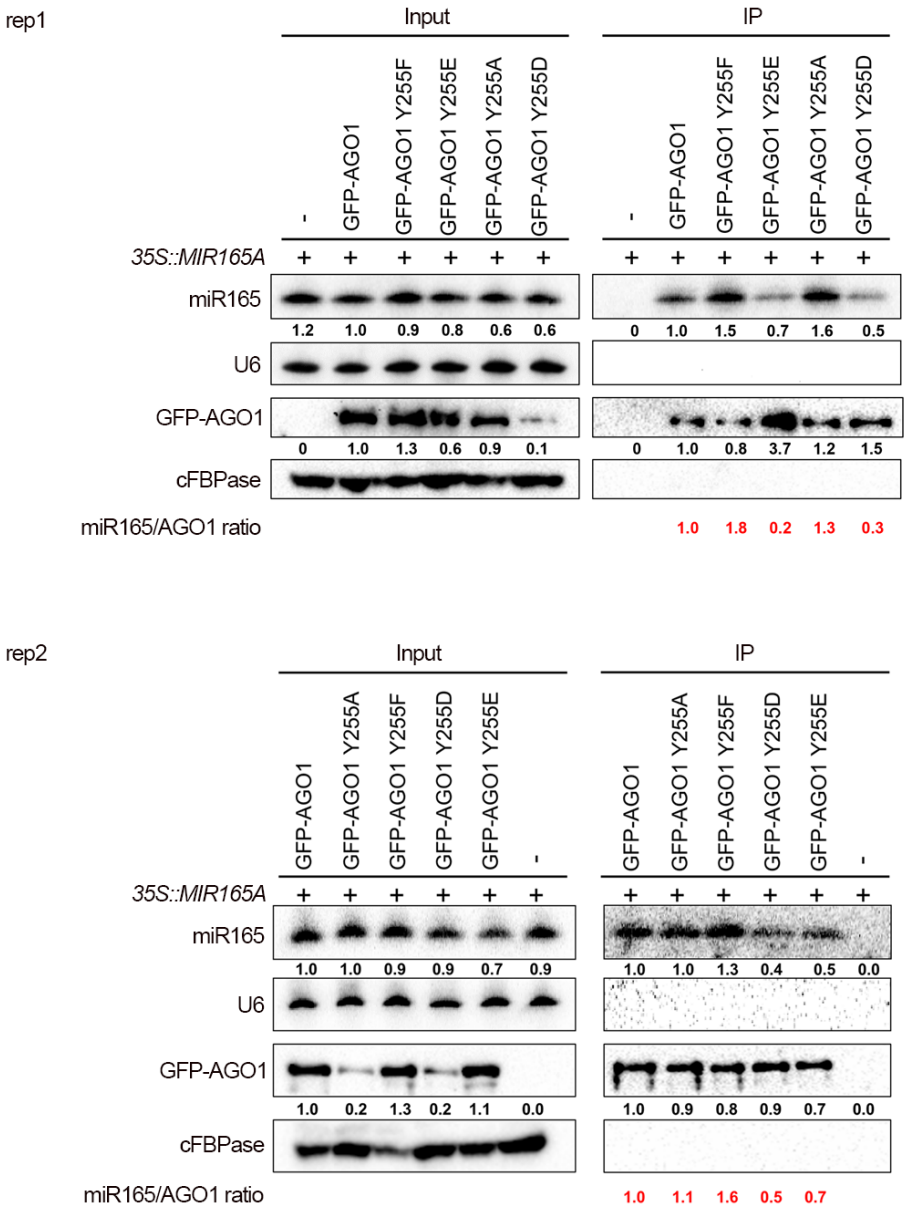
rep1
Input
IP
-
GFP-AGO1
GFP-AGO1 Y255F
GFP-AGO1 Y255E
GFP-AGO1 Y255A
GFP-AGO1 Y255D
35S::MIR165A
miR165
1.2 1.0 0.9 0.8 0.6 0.6
0 1.0 1.5 0.7 1.6 0.5
U6
GFP-AGO1
0 1.0 1.3 0.6 0.9 0.1
0 1.0 0.8 3.7 1.2 1.5
cFBPase
miR165/AGO1 ratio
1.0 1.8 0.2 1.3 0.3
rep2
Input
IP
GFP-AGO1
GFP-AGO1 Y255A
GFP-AGO1 Y255F
GFP-AGO1 Y255D
GFP-AGO1 Y255E
-
35S::MIR165A
miR165
1.0 1.0 0.9 0.9 0.7 0.9
1.0 1.0 1.3 0.4 0.5 0.0
U6
GFP-AGO1
1.0 0.2 1.3 0.2 1.1 0.0
1.0 0.9 0.8 0.9 0.7 0.0
cFBPase
miR165/AGO1 ratio
1.0 1.1 1.6 0.5 0.7

Supplementary table 3.1. Expression of 130 miRNA target genes as determined by RNA sequencing

Target Gene ID	Target Gene	log2FC ago1-36 vs AGO1	Padj ago1-36 vs AGO1	log2FC AGO1 5A vs AGO1	Padj AGO1 5A vs AGO1	log2FC AGO1 5D vs AGO1	Padj AGO1 5D vs AGO1
AT1G01040	DCL1	0.154183	0.445879	0.469052	0.000454	0.366204	0.005741
AT1G06580	PPR1	-0.31069	0.277571	0.199481	0.546508	0.311883	0.257008
AT1G08830	CSD1	3.707329	5.03E-141	1.414421	1.58E-31	2.173388	1.06E-75
AT1G10120	AT1G10120	0.078664	0.715339	0.52265	7.46E-06	0.402852	0.000551
AT1G12520	CCS	1.375499	1.45E-31	0.471982	1.59E-05	1.638539	8.20E-65
AT1G12820	IPS1	-0.5124	0.000291	0.200451	0.13581	0.110043	0.425361
AT1G15125	AT1G15125	2.312012	1.66E-08	-0.00625	0.992682	0.196801	0.720074
AT1G17590	NF-YA8	1.078189	4.04E-11	0.337121	0.115492	0.898697	2.21E-07
AT1G23390	AT1G23390	0.493236	0.191632	-1.76695	1.36E-34	-2.49664	4.25E-69
AT1G27340	F-box	0.432897	1.86E-06	0.539735	5.12E-05	0.628859	6.57E-07
AT1G27360	SPL11	0.667763	0.012308	0.625465	0.013651	0.480194	0.056665
AT1G27370	SPL10	1.8119	3.60E-16	0.517314	0.000298	0.974824	3.75E-14
AT1G30210	TCP24	-0.18789	0.338072	0.42026	0.000132	0.245093	0.031587
AT1G30490	PHV/ATHB-15	0.446495	0.02487	0.474119	0.002475	0.447873	0.002962
AT1G31280	AGO2	2.778997	2.21E-40	-0.61175	2.31E-05	-0.13506	0.428907
AT1G48410	AGO1	-4.74673	6.51E-174	1.366796	6.44E-38	2.032197	5.34E-85
AT1G50055	TAS1b	-0.6238	0.032383	0.375124	0.085824	0.718769	0.000102
AT1G51760	IAR3	1.898652	4.35E-24	0.122475	0.482062	0.251727	0.068865
AT1G53160	SPL4	1.221504	1.56E-11	1.050451	9.65E-17	0.814569	2.42E-10
AT1G53230	TCP3	-0.17854	0.6912	1.186783	4.10E-22	0.661011	1.93E-07
AT1G53290	AT1G53290	-0.34838	0.01258	-0.05889	0.804796	-0.21499	0.21143
AT1G53780	AT1G53780	-0.11293	0.703947	0.426021	0.00142	0.607191	7.48E-07

Target Gene ID	Target Gene	log2FC ago1-36 vs AGO1	Padj ago1-36 vs AGO1	log2FC AGO1 5A vs AGO1	Padj AGO1 5A vs AGO1	log2FC AGO1 5D vs AGO1	Padj AGO1 5D vs AGO1
AT1G53910	RAP2.12	0.750705	6.54E-09	0.178477	0.124305	0.118484	0.303345
AT1G54160	NF-YA5	1.034267	1.26E-05	0.236493	0.31098	0.381206	0.052461
AT1G56010	NAC1	1.411516	1.25E-16	-0.0399	0.858836	0.369713	0.007167
AT1G62720	PPR2	-0.24579	0.634125	0.027593	0.970905	0.308408	0.534776
AT1G62930	RPF3	0.069602	0.768702	0.339618	0.075544	0.251883	0.183814
AT1G63080	PPR	-0.49075	0.038556	0.740111	6.10E-05	0.730937	4.56E-05
AT1G63130	TPR-like	0.737572	4.18E-07	0.235579	0.127123	0.220136	0.129073
AT1G64580	AT1G64580	0.202109	0.479143	-0.00446	0.98951	0.300732	0.176742
AT1G66690	AT1G66690	-0.88963	0.046284	0.032332	0.969235	-0.00736	0.991667
AT1G66700	PXMT1	4.031762	7.46E-06	0.35754	0.72956	2.60192	7.64E-05
AT1G69170	SPL6	-0.10515	0.702709	0.355657	0.047174	0.530821	0.000861
AT1G72230	Cu binding protein	-2.21501	2.14E-09	-0.21855	0.380816	-0.58546	0.003268
AT1G72830	NF-YA3	2.000357	4.40E-27	0.239786	0.167696	1.13263	1.27E-17
AT1G77850	ARF17	1.703825	1.75E-33	1.440948	3.51E-33	1.305816	2.54E-27
AT2G02850	ARPN	2.814185	1.18E-32	0.418002	0.144932	-0.09511	0.78002
AT2G22840	GRF1	1.418311	1.96E-27	1.516739	9.23E-43	1.279853	1.04E-30
AT2G27400	TAS1a	-1.00091	3.89E-05	0.481081	0.008643	0.980649	7.53E-10
AT2G28190	CSD2	3.624761	2.52E-57	1.057841	4.06E-15	2.030312	2.99E-56
AT2G28350	ARF10	-0.76136	2.38E-07	0.347163	0.009402	0.505505	2.96E-05
AT2G28550	TOE1	-1.33789	1.49E-15	-0.38724	0.015389	-0.77683	3.62E-08
AT2G29130	LAC2	-4.18635	6.38E-09	0.214417	0.726203	-1.381	0.002451
AT2G30210	LAC3	-1.90845	1.99E-17	0.18823	0.474659	-0.34773	0.107184
AT2G31070	TCP10	-0.66033	0.015634	-0.09063	0.587815	-0.069	0.654022
AT2G33770	PHO2	0.534583	0.013005	0.642364	4.07E-08	0.063963	0.682783
AT2G33810	SPL3	0.415996	0.110153	1.229236	1.18E-18	1.633703	2.21E-33

Target Gene ID	Target Gene	log2FC ago1-36 vs AGO1	Padj ago1-36 vs AGO1	log2FC AGO1 5A vs AGO1	Padj AGO1 5A vs AGO1	log2FC AGO1 5D vs AGO1	Padj AGO1 5D vs AGO1
AT2G34010	MRG1	-0.41935	0.435249	-1.02357	0.078474	-1.10628	0.044117
AT2G34710	PHB	-1.37361	2.38E-14	0.181729	0.330183	-0.16185	0.350903
AT2G36400	GRF3	-0.1443	0.693322	0.476515	0.002133	0.533364	0.000255
AT2G38080	IRX12 LAC4	-1.80929	3.03E-10	-0.0957	0.732881	-0.53865	0.004963
AT2G38950	AT2G38950	0.774643	6.22E-07	0.113916	0.572749	0.260943	0.09595
AT2G39250	SNZ	-5.29238	9.70E-33	-0.51943	0.173197	-2.41533	4.34E-14
AT2G39675	TAS1c	1.63566	7.03E-14	0.356294	0.034056	0.906609	1.29E-10
AT2G39681	TAS2	0.405334	0.010892	0.577763	4.24E-06	1.219106	1.26E-26
AT2G42200	SPL9	1.790328	3.78E-15	-0.3525	0.061359	-0.06387	0.77501
AT2G44790	UCC2	0.76817	0.001985	0.14052	0.571413	0.192481	0.357732
AT2G45160	SCL6 II	-0.01746	0.92836	0.527419	1.18E-05	0.14084	0.319988
AT2G45480	GRL9	-1.36286	5.47E-10	0.749231	0.000114	0.835631	6.44E-06
AT2G45720	AT2G45720	-0.55359	5.38E-05	0.13234	0.505519	0.05569	0.779297
AT2G47020	AT2G47020	-1.07308	2.88E-08	0.256963	0.253634	0.612277	0.0007
AT3G02200	AT3G02200	0.011737	0.938046	0.207406	0.125964	0.59464	6.22E-08
AT3G05690	NF-YA2	1.721791	9.54E-45	1.62615	2.01E-40	1.487604	3.09E-34
AT3G09220	LAC7	-0.50725	0.10432	0.2917	0.11301	-0.25879	0.143354
AT3G11440	MYB65	-0.16068	0.60312	0.030568	0.943413	0.382872	0.149703
AT3G14110	FLU	0.314966	0.044991	0.142791	0.314427	0.17708	0.154625
AT3G14770	AT3G14770	-1.35423	4.31E-08	-0.86714	0.000312	-0.19601	0.486301
AT3G15030	TCP4	-0.48881	0.148681	1.181938	1.90E-10	0.721702	0.000147
AT3G15170	CUC1	1.968584	2.94E-07	1.80755	8.76E-06	2.424624	1.26E-10
AT3G15270	SPL5	1.369607	2.01E-07	1.603437	1.59E-19	0.903022	1.89E-06
AT3G15640	cyt oxydase	1.160396	2.31E-11	0.284984	0.014153	0.282271	0.010395
AT3G17185	TAS3a	-2.59978	9.44E-22	0.331673	0.103675	0.567334	0.0012

Target Gene ID	Target Gene	log2FC ago1-36 vs AGO1	Padj ago1-36 vs AGO1	log2FC AGO1 5A vs AGO1	Padj AGO1 5A vs AGO1	log2FC AGO1 5D vs AGO1	Padj AGO1 5D vs AGO1
AT3G22110	PAC1	0.549758	0.000205	-0.05783	0.741387	-0.17732	0.167033
AT3G22890	APS1	0.749533	3.03E-05	-0.633	3.10E-11	-0.55922	3.02E-09
AT3G23690	bHLH DNA-binding	0.1367	0.391081	-0.20529	0.236246	-0.38287	0.00849
AT3G26810	AFB2	-0.47597	0.004552	0.350348	0.002149	0.515357	8.02E-07
AT3G27200	plastocyanin-like	-1.72314	1.61E-12	-0.22286	0.424619	-0.08945	0.751827
AT3G44860	FAMT	6.372987	8.91E-18	-1.58356	0.08183	-2.21389	0.006664
AT3G52910	GRF4	-0.43684	0.058754	0.633549	0.000141	0.712665	6.66E-06
AT3G54990	SMZ	0.594589	0.017428	-0.2552	0.569987	-0.37343	0.328209
AT3G57920	SPL15	1.148788	0.000171	0.326671	0.310908	0.329754	0.264622
AT3G58030	zinc finger prot	-0.00107	0.994839	0.223729	0.097468	0.179598	0.168513
AT3G60250	PROTEIN KINASE CK2	-0.47532	0.032183	0.306018	0.018411	0.562365	8.19E-07
AT3G60630	SCL6 III	0.276261	0.177515	0.838372	1.03E-12	0.330163	0.010079
AT3G62980	TIR1	-0.53801	0.007985	0.642675	1.38E-07	0.715824	1.14E-09
AT4G00150	SCL6 IV	-0.8389	0.002298	0.352168	0.116949	0.305355	0.153514
AT4G03190	GRH1	-0.31357	0.147942	-0.00151	0.994753	0.129972	0.46569
AT4G13495	AT4G13495	-0.79392	1.16E-05	-1.05047	4.95E-10	-0.12517	0.567333
AT4G14930	AT4G14930	0.650312	0.004424	-0.52621	8.45E-05	-0.29068	0.035395
AT4G18390	TCP2	-0.96448	8.50E-05	-0.32012	0.023537	-0.56745	6.29E-06
AT4G24150	AtGRF8	1.833514	5.01E-15	1.79248	2.41E-11	1.565468	6.00E-09
AT4G30080	ARF16	0.799076	1.07E-08	0.249498	0.136245	0.439948	0.002045
AT4G32880	ATHB-8	-1.0519	4.88E-08	0.048238	0.846305	-0.13241	0.482428
AT4G36920	AP2	-0.07346	0.775663	0.240221	0.159822	0.433458	0.002723

Target Gene ID	Target Gene	log2FC ago1-36 vs AGO1	Padj ago1-36 vs AGO1	log2FC AGO1 5A vs AGO1	Padj AGO1 5A vs AGO1	log2FC AGO1 5D vs AGO1	Padj AGO1 5D vs AGO1
AT4G37740	GRF2	0.387273	0.040568	0.540805	0.001015	0.446888	0.005933
AT4G37770	ACS8	4.456999	2.83E-08	-0.77119	0.07406	-0.97556	0.015018
AT5G02350	AT5G02350	-1.0484	0.061381	-0.26799	0.673306	-0.52043	0.318108
AT5G06100	MYB33	-0.61469	8.05E-05	0.429975	0.003289	0.549637	4.97E-05
AT5G06510	NF-YA10	-1.05046	0.019362	0.506329	0.072473	-0.40615	0.167607
AT5G07130	LAC13	-0.97962	0.010179	0.069029	0.87529	-0.30538	0.330109
AT5G07680	ANAC079/ANAC080	-0.35175	0.377655	0.315608	0.235254	0.212045	0.42407
AT5G08310	AT5G08310	-0.9204	0.007228	0.546004	0.112265	0.241705	0.517805
AT5G08415	AT5G08415	0.212512	0.309781	0.224215	0.255552	0.153105	0.428798
AT5G10180	SULTR2;1	0.017313	0.946034	0.10773	0.467274	-0.3695	0.000827
AT5G10950	AT5G10950	-0.22159	0.667855	-0.40403	0.008043	-0.30375	0.043699
AT5G12840	NF-YA1	-0.85828	5.16E-09	-0.25396	0.075662	-0.41538	0.001037
AT5G16480	ATPFA-DSP5	-2.43775	8.71E-21	-0.26912	0.226041	0.008229	0.976034
AT5G18100	CSD3	-0.5512	0.003805	-0.12161	0.510947	0.216403	0.147934
AT5G20230	BCBP	4.759254	1.10E-09	0.047379	0.958794	0.032901	0.965163
AT5G21930	PAA2	-0.61324	0.006262	0.175759	0.201678	-0.02141	0.896086
AT5G23480	AT5G23480	0.39625	0.401815	0.507926	0.269196	0.847434	0.026976
AT5G37020	ARF8	1.101416	1.70E-06	0.155033	0.397027	0.807828	8.27E-10
AT5G38550	AT5G38550	-1.49294	0.001432	-0.79898	0.007652	-0.89105	0.001838
AT5G38900	AT5G38900	4.090565	2.51E-09	-0.47861	0.316874	0.083189	0.874391
AT5G39610	NAC2	1.477766	8.48E-05	-1.18104	1.33E-07	-0.12181	0.662867
AT5G43060	MMG4.7	0.024975	0.915109	-0.1925	0.239397	-0.4348	0.001149
AT5G43270	SPL2	1.308129	1.52E-06	0.062606	0.799256	0.599039	7.43E-05
AT5G43740	CC-NBS-LRR	-0.40549	0.176768	0.042892	0.879221	-0.10315	0.633457

Target Gene ID	Target Gene	log2FC ago1-36 vs AGO1	Padj ago1-36 vs AGO1	log2FC AGO1 5A vs AGO1	Padj AGO1 5A vs AGO1	log2FC AGO1 5D vs AGO1	Padj AGO1 5D vs AGO1
AT5G43780	APS4	0.772483	2.50E-08	0.345252	0.00526	0.207809	0.099941
AT5G50570	SPL13	1.984044	4.40E-10	-0.21411	0.560374	-0.27741	0.380263
AT5G51270	AT5G51270	-0.82508	0.272952	-0.53084	0.552752	-1.51104	0.0469
AT5G53660	AtGRF7	0.72373	0.182369	2.064288	1.65E-11	2.464591	7.02E-17
AT5G53950	CUC2	1.573522	0.001306	1.048447	0.037252	1.773138	4.02E-05
AT5G55930	OPT1	1.606179	7.03E-14	-0.32668	0.148108	1.061304	1.23E-09
AT5G60020	LAC17	-1.35667	1.71E-14	-0.00894	0.978167	-0.11529	0.61372
AT5G60120	TOE2	-0.83222	1.49E-05	-0.44327	0.000444	0.178601	0.187144
AT5G60690	REV	-0.09433	0.749295	0.460363	0.003536	0.616538	2.11E-05
AT5G61430	ANAC100	0.244742	0.467116	0.286801	0.361227	0.528199	0.039079
AT5G67180	TOE3	-0.03547	0.910013	-0.33135	0.221522	-0.69973	0.002419
AT5G05390	LAC12	NA	NA	-0.7159	0.544724	-1.03926	0.319555

Target Gene ID	Target Gene	log2FoldChange AGO1 2A vs AGO1	Padj AGO1 2A vs AGO1	log2FoldChange AGO1 2D vs AGO1	Padj AGO1 2D vs AGO1
AT1G01040	DCL1	0.02279	0.963044	0.180055	0.614777
AT1G06580	PPR1	0.25885	0.569609	-0.18708	0.755281
AT1G08830	CSD1	1.28384	5.08E-15	2.098895	3.55E-43
AT1G10120	AT1G10120	0.13187	0.702629	-0.01684	0.978745
AT1G12520	CCS	0.6405	3.27E-06	1.309926	6.98E-27
AT1G12820	IPS1	0.13702	0.604876	-0.0543	0.890226
AT1G15125	AT1G15125	0.16857	0.865221	0.413144	0.645449
AT1G17590	NF-YA8	0.38809	0.11506	1.024609	2.07E-08
AT1G23390	AT1G23390	1.22265	0.002527	-0.57138	0.323691
AT1G27340	F-box	-0.0726	0.699274	0.049077	0.840211
AT1G27360	SPL11	0.38924	0.354636	0.212687	0.723611
AT1G27370	SPL10	0.69008	0.019802	0.691128	0.026664
AT1G30210	TCP24	-0.55012	0.009653	-0.08594	0.850701
AT1G30490	PHV/ATHB-15	0.1219	0.762522	-0.06802	0.902573
AT1G31280	AGO2	-0.44328	0.182893	-0.14444	0.796054
AT1G48410	AGO1	0.14163	0.686215	2.007017	1.32E-31
AT1G50055	TAS1b	0.19782	0.719827	0.464513	0.300304
AT1G51760	IAR3	-0.03468	0.949496	0.045995	0.940224
AT1G53160	SPL4	1.10365	4.41E-08	-0.2548	0.486884
AT1G53230	TCP3	-1.32955	0.001762	-0.1638	0.866928
AT1G53290	AT1G53290	0.09168	0.735166	-0.12486	0.66405
AT1G53780	AT1G53780	0.0435	0.946215	-0.31138	0.485507
AT1G53910	RAP2.12	-0.00108	0.99802	0.030818	0.940224
AT1G54160	NF-YA5	0.97235	0.000432	1.191641	9.01E-06
AT1G56010	NAC1	0.11543	0.764003	0.102987	0.824952
AT1G62720	PPR2	0.06082	0.95883	0.239415	0.817446

Target Gene ID	Target Gene	log2FoldChange AGO1 2A vs AGO1	Padj AGO1 2A vs AGO1	log2FoldChange AGO1 2D vs AGO1	Padj AGO1 2D vs AGO1
AT1G62930	RPF3	0.40597	0.111178	0.387011	0.162665
AT1G63080	PPR	0.19266	0.649551	0.49294	0.117326
AT1G63130	TPR-like	0.22254	0.365297	0.513096	0.006271
AT1G64580	AT1G64580	-0.1744	0.729129	0.033053	0.970462
AT1G66690	AT1G66690	0.07049	0.947216	-0.06103	0.964978
AT1G66700	PXMT1	1.26014	0.410535	2.881639	0.014624
AT1G69170	SPL6	0.27605	0.461985	0.104247	0.859549
AT1G72230	Cu binding protein	0.24903	0.727955	0.117094	0.908662
AT1G72830	NF-YA3	0.69529	0.003523	0.917595	5.81E-05
AT1G77850	ARF17	0.89058	5.29E-08	1.000173	4.79E-10
AT2G02850	ARPN	-0.07846	0.911147	0.544777	0.189007
AT2G22840	GRF1	0.92392	3.39E-10	1.220382	1.92E-18
AT2G27400	TAS1a	-0.09457	0.867174	0.174867	0.75863
AT2G28190	CSD2	1.13421	2.96E-05	1.925927	8.64E-15
AT2G28350	ARF10	0.3402	0.087178	0.457188	0.014624
AT2G28550	TOE1	-0.29907	0.251252	0.510341	0.022623
AT2G29130	LAC2	-0.91126	0.190005	-1.22442	0.069423
AT2G30210	LAC3	0.07419	0.89229	-0.3952	0.287515
AT2G31070	TCP10	-0.28887	0.542775	-0.03469	0.971453
AT2G33770	PHO2	0.04864	0.928959	-0.14215	0.779192
AT2G33810	SPL3	1.17677	8.98E-06	-0.24563	0.628208
AT2G34010	MRG1	0.50443	0.50044	0.089183	0.948804
AT2G34710	PHB	0.15949	0.656258	-0.31042	0.317956
AT2G36400	GRF3	0.56108	0.189975	0.320365	0.590851
AT2G38080	IRX12 LAC4	-0.40158	0.393281	-0.22301	0.737474
AT2G38950	AT2G38950	0.22776	0.386536	0.266369	0.322099

Target Gene ID	Target Gene	log2FoldChange AGO1 2A vs AGO1	Padj AGO1 2A vs AGO1	log2FoldChange AGO1 2D vs AGO1	Padj AGO1 2D vs AGO1
AT2G39250	SNZ	0.6	0.095247	0.351991	0.470614
AT2G39675	TAS1c	0.11258	0.828409	0.44417	0.221733
AT2G39681	TAS2	0.21633	0.399965	0.453296	0.026509
AT2G42200	SPL9	0.84624	0.003794	1.262583	2.65E-06
AT2G44790	UCC2	0.06981	0.908802	0.124163	0.84908
AT2G45160	SCL6 II	0.53058	0.001697	0.012552	0.981134
AT2G45480	GRL9	0.31655	0.287696	0.643712	0.006097
AT2G45720	AT2G45720	-0.52843	0.001012	-0.04011	0.918233
AT2G47020	AT2G47020	-0.25735	0.428728	-0.20395	0.605954
AT3G02200	AT3G02200	0.20862	0.205154	0.08779	0.736484
AT3G05690	NF-YA2	1.67512	3.13E-40	1.531536	1.69E-33
AT3G09220	LAC7	-0.04701	0.953127	0.246516	0.702997
AT3G11440	MYB65	0.28675	0.515332	0.378514	0.377261
AT3G14110	FLU	0.09858	0.751065	0.221029	0.405447
AT3G14770	AT3G14770	0.89971	0.002055	0.02697	0.975902
AT3G15030	TCP4	-0.51223	0.285662	-0.22446	0.763136
AT3G15170	CUC1	1.30697	0.008246	1.168795	0.031256
AT3G15270	SPL5	0.98971	0.002016	0.31555	0.570024
AT3G15640	cyt oxydase	0.27684	0.340028	0.325943	0.268521
AT3G17185	TAS3a	-0.59267	0.118798	-0.39119	0.423664
AT3G22110	PAC1	0.14799	0.59866	0.065386	0.872752
AT3G22890	APS1	0.46103	0.054252	0.353113	0.214924
AT3G23690	bHLH DNA-binding	-0.01864	0.9625	-0.24498	0.284015
AT3G26810	AFB2	-0.12814	0.694737	-0.17416	0.604325
AT3G27200	plastocyanin-like	-0.4158	0.234307	-0.27484	0.539481

Target Gene ID	Target Gene	log2FoldChange AGO1 2A vs AGO1	Padj AGO1 2A vs AGO1	log2FoldChange AGO1 2D vs AGO1	Padj AGO1 2D vs AGO1
AT3G44860	FAMT	-0.16872	0.941135	0.266264	0.911354
AT3G52910	GRF4	0.97666	2.95E-05	0.937503	0.000117
AT3G54990	SMZ	-0.4452	0.270861	0.513918	0.160606
AT3G57920	SPL15	1.33608	9.59E-05	1.04467	0.006793
AT3G58030	zinc finger prot	0.04329	0.867174	-0.01123	0.977605
AT3G60250	PROTEIN KINASE CK2	0.00728	0.990926	-0.33724	0.35461
AT3G60630	SCL6 III	0.29213	0.322869	0.268399	0.424687
AT3G62980	TIR1	-0.0189	0.973639	-0.21449	0.594501
AT4G00150	SCL6 IV	-0.55136	0.152263	-0.49789	0.251108
AT4G03190	GRH1	0.2271	0.518579	-0.00019	0.999995
AT4G13495	AT4G13495	0.09807	0.805593	0.489192	0.05128
AT4G14930	AT4G14930	0.66711	0.016963	-0.00026	0.999939
AT4G18390	TCP2	-0.20093	0.676704	0.032648	0.97077
AT4G24150	AtGRF8	2.38011	2.73E-23	0.880751	0.0065
AT4G30080	ARF16	-0.4378	0.019949	0.164089	0.574396
AT4G32880	ATHB-8	-0.10962	0.792356	-0.26918	0.447358
AT4G36920	AP2	-0.57272	0.028937	-0.13877	0.777493
AT4G37740	GRF2	0.43409	0.073633	0.789767	0.000121
AT4G37770	ACS8	1.80858	0.146227	1.993284	0.115477
AT5G02350	AT5G02350	0.0389	0.97827	-0.37808	0.749494
AT5G06100	MYB33	0.07561	0.822061	0.052348	0.904887
AT5G06510	NF-YA10	0.53855	0.406756	0.329455	0.710496
AT5G07130	LAC13	-0.0835	0.929049	-0.36301	0.632169
AT5G07680	ANAC079/ANAC080	-0.89209	0.056868	-0.49596	0.42977
AT5G08310	AT5G08310	-0.26451	0.676275	-0.17886	0.825986

Target Gene ID	Target Gene	log2FoldChange AGO1 2A vs AGO1	Padj AGO1 2A vs AGO1	log2FoldChange AGO1 2D vs AGO1	Padj AGO1 2D vs AGO1
AT5G08415	AT5G08415	-0.47688	0.053794	-0.28341	0.386986
AT5G10180	SULTR2;1	-0.17909	0.617206	-0.16509	0.693242
AT5G10950	AT5G10950	0.13939	0.89114	0.013387	0.993116
AT5G12840	NF-YA1	0.34522	0.079769	0.127214	0.695406
AT5G16480	ATPFA-DSP5	-0.19378	0.707296	-0.48027	0.243242
AT5G18100	CSD3	0.10563	0.790052	-0.34809	0.241116
AT5G20230	BCBP	2.44182	0.014867	1.658811	0.181423
AT5G21930	PAA2	-0.0994	0.841076	-0.57476	0.058694
AT5G23480	AT5G23480	-0.09246	0.933832	0.587427	0.418255
AT5G37020	ARF8	0.22344	0.619035	0.747046	0.013479
AT5G38550	AT5G38550	-0.80257	0.230517	-0.53877	0.524822
AT5G38900	AT5G38900	0.75202	0.570239	1.049569	0.412582
AT5G39610	NAC2	1.32767	0.003131	0.213995	0.8271
AT5G43060	MMG4.7	-0.51307	0.022067	-0.25406	0.426839
AT5G43270	SPL2	0.03156	0.968304	-0.19924	0.766813
AT5G43740	CC-NBS-LRR	-0.44395	0.298063	-0.07753	0.922546
AT5G43780	APS4	-0.03432	0.926149	0.176981	0.520296
AT5G50570	SPL13	0.30496	0.63941	0.215338	0.795245
AT5G51270	AT5G51270	-0.86289	0.458558	-1.49019	0.177987
AT5G53660	AtGRF7	1.76881	0.001489	1.275893	0.055397
AT5G53950	CUC2	1.5757	0.007736	1.855991	0.001266
AT5G55930	OPT1	0.69624	0.012894	1.100914	1.57E-05
AT5G60020	LAC17	-0.30176	0.254535	0.118808	0.774151
AT5G60120	TOE2	-0.57449	0.017457	0.765692	0.000641
AT5G60690	REV	-0.22934	0.603758	0.262217	0.573314
AT5G61430	ANAC100	-0.71145	0.090606	0.297032	0.614543

Target Gene ID	Target Gene	log2FoldChange AGO1 2A vs AGO1	Padj AGO1 2A vs AGO1	log2FoldChange AGO1 2D vs AGO1	Padj AGO1 2D vs AGO1
AT5G67180	TOE3	0.93639	0.000232	0.263018	0.57016
AT5G05390	LAC12	NA	NA	NA	NA

Target Gene ID	Target Gene	log2FoldChange AGO1 253A vs AGO1	Padj AGO1 253A vs AGO1	log2FoldChange AGO1 253D vs AGO1	Padj AGO1 253D vs AGO1
AT1G01040	DCL1	-0.28463	0.427891	-0.23366	0.32559167
AT1G06580	PPR1	0.295888	0.604691	0.215529	0.56395186
AT1G08830	CSD1	0.304881	0.326166	0.886718	7.17E-07
AT1G10120	AT1G10120	-0.06372	0.906915	-0.07371	0.79528519
AT1G12520	CCS	0.561003	0.000867	1.321607	2.07E-26
AT1G12820	IPS1	0.055418	0.900187	0.323019	0.06347891
AT1G15125	AT1G15125	-0.10062	0.945296	0.750316	0.16895306
AT1G17590	NF-YA8	0.119868	0.819822	0.385424	0.09216141
AT1G23390	AT1G23390	0.821951	0.173092	1.685249	1.42E-05
AT1G27340	F-box	0.16128	0.387308	0.185979	0.12027803
AT1G27360	SPL11	0.379224	0.498225	0.214672	0.58665526
AT1G27370	SPL10	0.188927	0.769631	0.232534	0.49808981
AT1G30210	TCP24	-0.01963	0.975267	-0.08234	0.76865764
AT1G30490	PHV/ATHB-15	-0.37808	0.307117	-0.35124	0.16047691
AT1G31280	AGO2	-0.3239	0.514203	-0.47323	0.10475058
AT1G48410	AGO1	-0.48815	0.093368	0.12125	0.65708381
AT1G50055	TAS1b	0.445885	0.419734	-0.43135	0.24836491
AT1G51760	IAR3	-0.12674	0.828832	0.087508	0.78874521
AT1G53160	SPL4	0.316087	0.42204	0.433029	0.07332188
AT1G53230	TCP3	-0.24648	0.814116	-1.14626	0.00798375
AT1G53290	AT1G53290	0.024312	0.958153	0.097895	0.63633872
AT1G53780	AT1G53780	-0.33653	0.516762	0.050009	0.90659687
AT1G53910	RAP2.12	0.079332	0.842869	0.218843	0.21390232
AT1G54160	NF-YA5	0.273665	0.644617	0.878626	0.0023797
AT1G56010	NAC1	0.126811	0.807782	0.516978	0.01870556

Target Gene ID	Target Gene	log2FoldChange AGO1 253A vs AGO1	Padj AGO1 253A vs AGO1	log2FoldChange AGO1 253D vs AGO1	Padj AGO1 253D vs AGO1
AT1G62720	PPR2	0.079587	0.95638	-0.39364	0.54442628
AT1G62930	RPF3	-0.2736	0.504851	0.37094	0.11816405
AT1G63080	PPR	-0.4442	0.303946	0.176821	0.59639041
AT1G63130	TPR-like	-0.18673	0.598441	-0.07122	0.7769462
AT1G64580	AT1G64580	-0.16489	0.818393	-0.44131	0.180134
AT1G66690	AT1G66690	-0.51074	0.584012	0.249279	0.68643646
AT1G66700	PXMT1	-0.22722	0.943608	1.506814	0.2109178
AT1G69170	SPL6	-0.28128	0.579142	-0.20773	0.5265735
AT1G72230	Cu binding protein	0.13539	0.902954	0.218779	0.69259547
AT1G72830	NF-YA3	-0.04284	0.951989	0.298036	0.27562864
AT1G77850	ARF17	-0.10383	0.822613	0.225866	0.29528149
AT2G02850	ARPN	0.320717	0.616799	0.769233	0.0195421
AT2G22840	GRF1	0.006018	0.992308	0.966754	1.44E-10
AT2G27400	TAS1a	0.10698	0.883851	-0.64757	0.03113853
AT2G28190	CSD2	0.709986	0.071559	1.208599	1.28E-05
AT2G28350	ARF10	-0.1158	0.772653	-0.2678	0.16711633
AT2G28550	TOE1	-0.07046	0.894648	-0.01294	0.96724272
AT2G29130	LAC2	-0.27915	0.837167	0.088836	0.91407693
AT2G30210	LAC3	-0.72825	0.036762	0.581192	0.03379846
AT2G31070	TCP10	-0.34295	0.56462	-1.15071	0.00016004
AT2G33770	PHO2	-0.37277	0.368006	0.207502	0.48653277
AT2G33810	SPL3	0.341617	0.516679	1.051318	0.0001355
AT2G34010	MRG1	-0.07779	0.960385	0.006305	0.9944394
AT2G34710	PHB	-0.33089	0.365416	-0.32856	0.17070474
AT2G36400	GRF3	-0.02842	0.978878	1.007379	0.00350002

Target Gene ID	Target Gene	log2FoldChange AGO1 253A vs AGO1	Padj AGO1 253A vs AGO1	log2FoldChange AGO1 253D vs AGO1	Padj AGO1 253D vs AGO1
AT2G38080	IRX12 LAC4	-0.49268	0.390306	-0.58698	0.10808985
AT2G38950	AT2G38950	-0.01264	0.983084	0.244393	0.2554203
AT2G39250	SNZ	-0.06288	0.945296	0.518218	0.12230031
AT2G39675	TAS1c	0.232195	0.686666	-0.0757	0.84818092
AT2G39681	TAS2	-0.00771	0.989378	-0.28125	0.17326169
AT2G42200	SPL9	0.522324	0.255761	0.908528	0.00174628
AT2G44790	UCC2	-0.11668	0.877836	0.648813	0.03013608
AT2G45160	SCL6 II	-0.04204	0.930167	-0.00353	0.99047189
AT2G45480	GRL9	-0.31455	0.457294	0.218343	0.43482998
AT2G45720	AT2G45720	0.08135	0.836598	0.184779	0.31294978
AT2G47020	AT2G47020	-0.24952	0.568722	-0.203	0.4617404
AT3G02200	AT3G02200	0.029389	0.937899	0.149159	0.3265615
AT3G05690	NF-YA2	0.122789	0.728111	0.499714	0.00163546
AT3G09220	LAC7	-0.11254	0.902284	0.543604	0.14042471
AT3G11440	MYB65	-0.21923	0.747744	0.076429	0.86236548
AT3G14110	FLU	0.290354	0.311892	0.250608	0.1989643
AT3G14770	AT3G14770	0.526082	0.253809	0.926751	0.00141927
AT3G15030	TCP4	-0.10373	0.917165	-0.72527	0.06014061
AT3G15170	CUC1	-0.30094	0.822683	-0.33198	0.66248382
AT3G15270	SPL5	0.132303	0.878442	0.280523	0.49212658
AT3G15640	cyt oxydase	0.145623	0.767773	0.001011	0.99774733
AT3G17185	TAS3a	0.11989	0.885273	-0.55886	0.1054865
AT3G22110	PAC1	0.172445	0.623343	0.032715	0.90202525
AT3G22890	APS1	-0.09439	0.864674	-0.29484	0.21670961
AT3G23690	bHLH DNA-binding	-0.1933	0.529518	-0.08465	0.7015256

Target Gene ID	Target Gene	log2FoldChange AGO1 253A vs AGO1	Padj AGO1 253A vs AGO1	log2FoldChange AGO1 253D vs AGO1	Padj AGO1 253D vs AGO1
AT3G26810	AFB2	-0.03051	0.957307	0.076859	0.77199949
AT3G27200	plastocyanin-like	-0.311	0.54838	-0.21755	0.52271479
AT3G44860	FAMT	-0.96434	0.649607	-0.19962	0.89569848
AT3G52910	GRF4	0.101645	0.877836	0.571315	0.02835276
AT3G54990	SMZ	0.458945	0.332621	-0.05566	0.9064237
AT3G57920	SPL15	0.265605	0.758525	0.116645	0.8348964
AT3G58030	zinc finger prot	-0.01809	0.962679	0.179694	0.21534567
AT3G60250	PROTEIN KINASE CK2	-0.07011	0.917877	0.362958	0.18542544
AT3G60630	SCL6 III	0.018201	0.978878	-0.01111	0.97410461
AT3G62980	TIR1	0.018516	0.979278	0.207359	0.45561086
AT4G00150	SCL6 IV	-0.10918	0.896319	-0.59173	0.0816888
AT4G03190	GRH1	-0.36513	0.346465	0.161562	0.58592727
AT4G13495	AT4G13495	-0.2654	0.500471	-0.92349	9.90E-06
AT4G14930	AT4G14930	-0.03161	0.968963	0.115194	0.75117358
AT4G18390	TCP2	-0.2544	0.668696	-0.24417	0.48566692
AT4G24150	AtGRF8	0.217156	0.771246	1.352281	3.01E-06
AT4G30080	ARF16	-0.05634	0.90358	-0.09026	0.70152546
AT4G32880	ATHB-8	-0.59305	0.05495	-0.60647	0.01028356
AT4G36920	AP2	-0.24291	0.609306	-0.54718	0.030583
AT4G37740	GRF2	-0.09121	0.871093	-0.04692	0.88592515
AT4G37770	ACS8	-0.24059	0.946501	-0.43653	0.81669345
AT5G02350	AT5G02350	-0.33616	0.818393	-0.39018	0.61969346
AT5G06100	MYB33	-0.1714	0.637918	-0.01679	0.95377326
AT5G06510	NF-YA10	-0.13637	0.916463	-0.20104	0.76552472
AT5G07130	LAC13	0.122062	0.915098	-0.13344	0.82454481

Target Gene ID	Target Gene	log2FoldChange AGO1 253A vs AGO1	Padj AGO1 253A vs AGO1	log2FoldChange AGO1 253D vs AGO1	Padj AGO1 253D vs AGO1
AT5G07680	ANAC079/ANAC080	-0.16124	0.879104	-0.35559	0.47678321
AT5G08310	AT5G08310	-0.38001	0.614983	-0.37166	0.4216196
AT5G08415	AT5G08415	0.043506	0.945753	-0.25863	0.30781867
AT5G10180	SULTR2;1	-0.66098	0.016389	-0.34943	0.14811824
AT5G10950	AT5G10950	0.315881	0.786327	1.881304	7.21E-05
AT5G12840	NF-YA1	0.075708	0.864878	0.472684	0.00641996
AT5G16480	ATPFA-DSP5	-0.06378	0.942095	0.223302	0.5541046
AT5G18100	CSD3	0.077124	0.893225	0.396886	0.08837516
AT5G20230	BCBP	-0.14222	0.960248	4.05629	9.02E-06
AT5G21930	PAA2	-0.19388	0.735854	0.051788	0.89253515
AT5G23480	AT5G23480	0.205252	0.871093	-0.22029	0.75671226
AT5G37020	ARF8	-0.38805	0.425765	-0.56437	0.05548109
AT5G38550	AT5G38550	-0.19358	0.884814	0.113981	0.87922475
AT5G38900	AT5G38900	0.273919	0.904489	0.995987	0.30451956
AT5G39610	NAC2	-0.34445	0.732654	0.449373	0.39642119
AT5G43060	MMG4.7	0.031237	0.959983	-0.0889	0.75600347
AT5G43270	SPL2	-0.1461	0.863532	0.141873	0.75184627
AT5G43740	CC-NBS-LRR	-0.04396	0.963962	-0.39358	0.28755155
AT5G43780	APS4	0.050749	0.910562	0.489842	0.00364
AT5G50570	SPL13	-0.43147	0.585896	-0.07564	0.90212188
AT5G51270	AT5G51270	-0.31082	0.874215	-0.13989	0.90496231
AT5G53660	AtGRF7	-0.03604	0.984295	0.421066	0.58540766
AT5G53950	CUC2	0.052929	0.978878	0.309635	0.7220866
AT5G55930	OPT1	-0.0937	0.895806	-0.42481	0.16186976
AT5G60020	LAC17	-0.2469	0.513731	-0.32198	0.15924067

Target Gene ID	Target Gene	log2FoldChange AGO1 253A vs AGO1	Padj AGO1 253A vs AGO1	log2FoldChange AGO1 253D vs AGO1	Padj AGO1 253D vs AGO1
AT5G60120	TOE2	-0.10863	0.851314	-0.08323	0.79103491
AT5G60690	REV	-0.31203	0.552879	-0.0561	0.8908675
AT5G61430	ANAC100	0.586664	0.265328	-0.09058	0.85918888
AT5G67180	TOE3	0.189795	0.765068	0.314844	0.33570724
AT5G05390	LAC12	NA	NA	NA	NA

Target Gene ID	Target Gene	log2FoldChange AGO1 255A vs AGO1	Padj AGO1 255A vs AGO1	log2FoldChange AGO1 255D vs AGO1	Padj AGO1 255D vs AGO1
AT1G01040	DCL1	-0.29041	0.174078	-0.40062	0.043277
AT1G06580	PPR1	0.602714	0.029305	0.336424	0.269269
AT1G08830	CSD1	1.679931	1.60E-27	0.791601	1.47E-06
AT1G10120	AT1G10120	0.609331	0.000859	0.418498	0.029925
AT1G12520	CCS	0.869601	4.46E-12	0.66252	2.83E-07
AT1G12820	IPS1	-0.15222	0.41864	0.244753	0.139861
AT1G15125	AT1G15125	1.552783	0.000517	-1.01859	0.034209
AT1G17590	NF-YA8	0.168425	0.502708	0.313639	0.137999
AT1G23390	AT1G23390	1.460375	4.20E-05	2.081891	1.64E-09
AT1G27340	F-box	-0.39684	7.44E-05	-0.23218	0.028973
AT1G27360	SPL11	-0.6405	0.038239	-0.51135	0.102772
AT1G27370	SPL10	0.200438	0.549426	0.043095	0.908354
AT1G30210	TCP24	0.234371	0.282116	0.029438	0.913538
AT1G30490	PHV/ATHB-15	-0.06839	0.827297	-0.30777	0.185505
AT1G31280	AGO2	-0.44809	0.099393	-0.65249	0.009999
AT1G48410	AGO1	0.814	8.20E-06	1.977427	5.66E-31
AT1G50055	TAS1b	-0.89062	0.004086	-0.53617	0.099137
AT1G51760	IAR3	-0.20717	0.443908	-0.57295	0.009788
AT1G53160	SPL4	0.99464	2.64E-07	1.023535	1.05E-07
AT1G53230	TCP3	-0.57152	0.199985	-0.64499	0.130998
AT1G53290	AT1G53290	0.352449	0.016134	0.123187	0.477707
AT1G53780	AT1G53780	-0.04101	0.920821	-0.56639	0.034854
AT1G53910	RAP2.12	0.645447	2.46E-06	0.249235	0.112084
AT1G54160	NF-YA5	1.526883	1.37E-10	1.745408	6.96E-14
AT1G56010	NAC1	-0.05766	0.849479	-0.13219	0.595422

Target Gene ID	Target Gene	log2FoldChange AGO1 255A vs AGO1	Padj AGO1 255A vs AGO1	log2FoldChange AGO1 255D vs AGO1	Padj AGO1 255D vs AGO1
AT1G62720	PPR2	-0.32693	0.599336	0.101679	0.870654
AT1G62930	RPF3	0.713503	0.000202	0.667596	0.000557
AT1G63080	PPR	0.703829	0.002484	0.418697	0.097524
AT1G63130	TPR-like	0.517221	0.001358	0.375831	0.026107
AT1G64580	AT1G64580	-0.47429	0.11451	-0.43745	0.140076
AT1G66690	AT1G66690	0.217739	0.711872	-0.25133	0.649922
AT1G66700	PXMT1	1.375789	0.229921	-1.74712	0.128086
AT1G69170	SPL6	-0.09729	0.781441	-0.27507	0.325759
AT1G72230	Cu binding protein	-0.37709	0.429401	0.185796	0.706595
AT1G72830	NF-YA3	0.628049	0.004099	0.80256	0.000134
AT1G77850	ARF17	1.196139	2.02E-15	0.733754	4.02E-06
AT2G02850	ARPN	-0.54778	0.129603	-0.39767	0.271319
AT2G22840	GRF1	1.983582	8.07E-52	0.988879	1.24E-12
AT2G27400	TAS1a	-1.16633	5.67E-06	-1.24573	1.09E-06
AT2G28190	CSD2	1.657277	9.36E-12	1.080261	2.10E-05
AT2G28350	ARF10	-0.52665	0.001086	-0.04187	0.848917
AT2G28550	TOE1	-0.04405	0.878767	0.494262	0.00819
AT2G29130	LAC2	-0.75848	0.196298	-1.85954	0.000728
AT2G30210	LAC3	-0.70421	0.00464	-0.46388	0.076019
AT2G31070	TCP10	-0.49655	0.114421	-0.28947	0.389254
AT2G33770	PHO2	0.27353	0.307398	0.052138	0.867237
AT2G33810	SPL3	0.958423	0.000153	-0.1533	0.645553
AT2G34010	MRG1	0.113648	0.880003	0.355623	0.537598
AT2G34710	PHB	-0.23841	0.317916	-0.06241	0.817764
AT2G36400	GRF3	1.754159	2.34E-09	1.310883	1.54E-05

Target Gene ID	Target Gene	log2FoldChange AGO1 255A vs AGO1	Padj AGO1 255A vs AGO1	log2FoldChange AGO1 255D vs AGO1	Padj AGO1 255D vs AGO1
AT2G38080	IRX12 LAC4	-0.47814	0.172135	-0.41157	0.239571
AT2G38950	AT2G38950	0.370225	0.043224	0.34342	0.061248
AT2G39250	SNZ	-0.80741	0.006903	0.069339	0.860462
AT2G39675	TAS1c	-0.21189	0.517928	0.009605	0.979807
AT2G39681	TAS2	-0.30005	0.112616	-0.24168	0.206128
AT2G42200	SPL9	1.105926	1.17E-05	1.200295	1.46E-06
AT2G44790	UCC2	-0.76927	0.004227	-0.82772	0.001846
AT2G45160	SCL6 II	0.572165	0.000163	0.383033	0.017089
AT2G45480	GRL9	0.552678	0.008779	0.200575	0.424459
AT2G45720	AT2G45720	-0.14866	0.415269	-0.37449	0.0139
AT2G47020	AT2G47020	-0.51689	0.018165	-0.50759	0.019479
AT3G02200	AT3G02200	0.139207	0.337154	0.04036	0.804644
AT3G05690	NF-YA2	1.612796	4.40E-37	0.908099	7.79E-12
AT3G09220	LAC7	-0.83216	0.009723	-0.86027	0.00695
AT3G11440	MYB65	0.418252	0.167953	0.483416	0.090883
AT3G14110	FLU	0.363575	0.031252	0.472659	0.003418
AT3G14770	AT3G14770	-0.42588	0.163535	0.298828	0.340979
AT3G15030	TCP4	-0.09953	0.845735	-0.07509	0.871864
AT3G15170	CUC1	0.427262	0.474979	0.043086	0.953561
AT3G15270	SPL5	1.485482	6.03E-08	1.367233	8.11E-07
AT3G15640	cyt oxydase	0.437241	0.033354	0.138832	0.569545
AT3G17185	TAS3a	-1.66214	3.23E-09	-1.05961	0.000254
AT3G22110	PAC1	0.306757	0.078086	0.597992	0.000123
AT3G22890	APS1	-0.02463	0.938225	0.621931	0.00139
AT3G23690	bHLH DNA-binding	0.242691	0.147327	0.387794	0.010635

Target Gene ID	Target Gene	log2FoldChange AGO1 255A vs AGO1	Padj AGO1 255A vs AGO1	log2FoldChange AGO1 255D vs AGO1	Padj AGO1 255D vs AGO1
AT3G26810	AFB2	-0.35432	0.06301	-0.2475	0.214485
AT3G27200	plastocyanin-like	-0.93779	0.000246	-0.79606	0.001933
AT3G44860	FAMT	1.992408	0.026206	2.369473	0.006028
AT3G52910	GRF4	0.857662	0.000107	0.537145	0.023506
AT3G54990	SMZ	-0.78585	0.011356	-0.84486	0.005314
AT3G57920	SPL15	0.531931	0.174688	0.263802	0.541717
AT3G58030	zinc finger prot	0.075097	0.641162	0.113763	0.420941
AT3G60250	PROTEIN KINASE CK2	0.240095	0.390492	-0.10086	0.738676
AT3G60630	SCL6 III	0.171779	0.506563	0.145472	0.562318
AT3G62980	TIR1	0.068227	0.832463	-0.17132	0.511083
AT4G00150	SCL6 IV	-1.22052	1.56E-05	-0.76638	0.010262
AT4G03190	GRH1	0.384369	0.100611	0.252296	0.306939
AT4G13495	AT4G13495	0.061123	0.838602	0.67956	0.000433
AT4G14930	AT4G14930	-0.07198	0.846718	0.493871	0.053706
AT4G18390	TCP2	0.221355	0.511496	0.146307	0.663753
AT4G24150	AtGRF8	1.693518	1.01E-11	1.393629	5.09E-08
AT4G30080	ARF16	-0.26606	0.140429	-0.13167	0.500038
AT4G32880	ATHB-8	-0.33209	0.162215	0.027977	0.928087
AT4G36920	AP2	-0.50207	0.030988	-0.74346	0.000734
AT4G37740	GRF2	0.711407	0.000158	0.646172	0.000704
AT4G37770	ACS8	6.159492	2.75E-14	5.260977	1.71E-10
AT5G02350	AT5G02350	-1.38727	0.028834	-0.8408	0.182152
AT5G06100	MYB33	-0.1134	0.610708	0.082054	0.700385
AT5G06510	NF-YA10	1.37998	0.000666	1.099004	0.009013
AT5G07130	LAC13	-0.54607	0.233949	-0.58299	0.185542

Target Gene ID	Target Gene	log2FoldChange AGO1 255A vs AGO1	Padj AGO1 255A vs AGO1	log2FoldChange AGO1 255D vs AGO1	Padj AGO1 255D vs AGO1
AT5G07680	ANAC079/ANAC080	-1.42052	0.000226	-1.49733	9.04E-05
AT5G08310	AT5G08310	-0.32016	0.470514	-0.84549	0.024174
AT5G08415	AT5G08415	0.21515	0.378509	0.15199	0.537662
AT5G10180	SULTR2;1	-0.17627	0.495333	-0.19353	0.425207
AT5G10950	AT5G10950	0.221974	0.727543	0.150488	0.80504
AT5G12840	NF-YA1	0.392043	0.01562	0.593296	9.12E-05
AT5G16480	ATPFA-DSP5	-0.21064	0.562285	-0.2969	0.362707
AT5G18100	CSD3	0.144949	0.583703	0.003557	0.990454
AT5G20230	BCBP	5.431203	1.41E-11	3.394854	5.64E-05
AT5G21930	PAA2	0.433501	0.092536	0.003578	0.991814
AT5G23480	AT5G23480	-0.11696	0.870986	-0.61215	0.263357
AT5G37020	ARF8	-0.37661	0.197893	-0.48667	0.075675
AT5G38550	AT5G38550	-1.54512	0.002526	-1.56848	0.001943
AT5G38900	AT5G38900	0.557731	0.588716	-0.33701	0.748476
AT5G39610	NAC2	-0.12937	0.838062	-0.19327	0.723691
AT5G43060	MMG4.7	-0.49669	0.011535	-0.68516	0.000264
AT5G43270	SPL2	-0.16627	0.68921	-0.10272	0.80019
AT5G43740	CC-NBS-LRR	-0.34346	0.33377	-0.56027	0.077727
AT5G43780	APS4	-0.28641	0.090958	-0.43175	0.005953
AT5G50570	SPL13	1.009296	0.005719	0.643063	0.100555
AT5G51270	AT5G51270	-1.45334	0.101623	-1.61261	0.06211
AT5G53660	AtGRF7	-0.17694	0.840604	-0.46411	0.51837
AT5G53950	CUC2	0.98452	0.101258	0.243976	0.750128
AT5G55930	OPT1	0.552797	0.032168	-0.00995	0.978893
AT5G60020	LAC17	-0.319	0.131289	-0.0945	0.697489

Target Gene ID	Target Gene	log2FoldChange AGO1 255A vs AGO1	Padj AGO1 255A vs AGO1	log2FoldChange AGO1 255D vs AGO1	Padj AGO1 255D vs AGO1
AT5G60120	TOE2	-0.47257	0.031128	0.152589	0.54894
AT5G60690	REV	-0.54531	0.041848	-0.44907	0.100164
AT5G61430	ANAC100	-1.01173	0.003898	-1.28217	0.00021
AT5G67180	TOE3	0.718828	0.003946	1.234749	3.78E-08
AT5G05390	LAC12	NA	NA	NA	NA

Supplementary table 3.2. Primers and probes

Primers used for genotyping	**Sequence (5’ -> 3’)**
Y23 LBb1.3	ATTTTGCCGATTTCGGAAC
Y135 ago1-36 SALK_087076 F	AATCAGGTATATTCCGGTGGG
Y136 ago1-36 SALK_087076 R	CAATGAGGCTTTATCACCAGC
Primers used for plasmid construction (Arabidopsis transgenic plant)	**Sequence (5’ -> 3’)**
Y25 AGO1 CDS DTOPO F	CACCATGGTGAGAAAGAGAAGA
Y26 AGO1 CDS R	TCAGCAGTAGAACATGACACGC
Y249 AGO1 NP OL 3XHA R	ttaacccgctcatGATGATTCCTGTGAAAATAACACAAC
Y250 AGO1 NP OL 3XHA F	cacaggaatcatcATGAGCGGGTTAATTAAC
Y267 AGO1 CDS OL 3'UTR R	agggtgaatcaacTCAGCAGTAGAACATGAC
Y268 AGO1 CDS OL 3'UTR F	gttctactgctgaGTTGATTCACCCTCTATCTATCTTTATG
Y245 PEG301 NcoI OL AGO1NP 1.6K F	acaacttcttcgcccccgttttcacACGTGATGACAGCCACCA
Y269 AGO1 3'UTR OL PEG301/100 XbaI R	ctagtcccgggtcttaattaactctTTTAGGCATTTTCCACGC
Y70 AGO1 P S11D t31g_c32a_F	GAGAAGAACGGATGCTCCAGATGAAGGAGGTGAAGGC
Y71 AGO1 P S11D t31g_c32a_R	GCCTTCACCTCCTTCATCTGGAGCATCCGTTCTTCTC
Y74 AGO1 P S253D a757g_g758a_F	TCCAGCGTATGATGGTCGAAAAGATCTTTACACTGCTGGTC
Y75 AGO1 P S253D a757g_g758a_R	GACCAGCAGTGTAAAGATCTTTTCGACCATCATACGCTGGA
Y78 AGO1 P Y255D t763g_F	CGTATGATGGTCGAAAAAGTCTTGACACTGCTGGTCCAC
Y79 AGO1 P Y255D t763g_R	GTGGACCAGCAGTGTCAAGACTTTTTCGACCATCATACG
Y82 AGO1 P S350D t1054g_c1055a_a1056t_F	CCTTTTATTCCCCTGATATAGGAAAAAAACAAGATTTGGGGGATGGCTTGGA
Y83 AGO1 P S350D t1054g_c1055a_a1056t_R	TCCAAGCCATCCCCCAAATCTTGTTTTTTTCCTATATCAGGGGAATAAAAGG
Y86 AGO1 P S1001D t3007g_c3008a_a3009t_F	TCTACATGGAGCCAGAGACAGATGACAGTGGCTCAATGGCTAG
Y87 AGO1 P S1001D t3007g_c3008a_a3009t_R	CTAGCCATTGAGCCACTGTCATCTGTCTCTGGCTCCATGTAGA
Y314 AGO1 P S253D Y255D F a757g_g758a_t763g_ F	tcttccagcgtatgatggtcgaaaagatcttgacactgctggtcc
Y315 AGO1 P S253D Y255D R a757g_g758a_t763g_ R	ggaccagcagtgtcaagatcttttcgaccatcatacgctggaaga
Y121 AGO1 P S11A t31g F	aagaacggatgctccagctgaaggaggtgaagg
Y122 AGO1 P S11A t31g R	ccttcacctccttcagctggagcatccgttctt

Y123 AGO1 P S253A a757g_g758c F	tccagcgtatgatggtcgaaaagctctttacactgctggtc
Y124 AGO1 P S253A a757g_g758c R	gaccagcagtgtaaagagcttttcgaccatcatacgctgga
Y125 AGO1 P Y255A t763g_a764c F	cagcgtatgatggtcgaaaaagtcttgccactgctggtccac
Y126 AGO1 P Y255A t763g_a764c R	gtggaccagcagtggcaagacttttttcgaccatcatacgctg
Y127 AGO1 P S350A t1048g F	cccctgatataggaaaaaaacaagcattgggggatggctt
Y128 AGO1 P S350A t1048g R	caagccatcccccaatgcttgttttttttcctatatcagggg
Y129 AGO1 P S1001A t3001g F	catggagccagagacagcagacagtggctcaat
Y130 AGO1 P S1001A t3001g R	attgagccactgtctgctgtctctggctccatg
Y311 AGO1 P S253A Y255A F a757g_g758c_t763g_a764c_ F	tcgtcttccagcgtatgatggtcgaaaagctcttgccactgctggtcc act
Y312 AGO1 P S253A Y255A R a757g_g758c_t763g_a764c_ R	agtggaccagcagtggcaagagcttttcgaccatcatacgctgga agacga
Y581 PEG100 XhoI OL GFP F	ttcatttggagaggacacgcATGAGTAAAGGAGAAGAA C
Y624 AGO1 Y255F F	tgatggtcgaaaaagtcttttcactgctggtccact
Y625 AGO1 Y255F R	agtggaccagcagtgaaaagacttttcgaccatca
Y626 AGO1 Y255E F	cgtatgatggtcgaaaaagtcttgagactgctggtccactt
Y627 AGO1 Y255E R	aagtggaccagcagtctcaagacttttcgaccatcatacg
1094 pBYL_3xFLAG_AtAGO1 R	CCAAAAGTCTCAAGCTGGCGCGCCTCAGCAG TAGAACATGACAC
1235 pBYL_3xFLAG_AtAGO1 F	GACTCACTATAGGGAGACCCAAGCTGGCGCG CCATGGACTACAAAGACCATGACGG
1332 pBYL_3xFLAG_AtAGO1_Y255A F	AAAAGTCTTGCCACTGCTGGTCCACTTCCCT
1333 pBYL_3xFLAG_AtAGO1_Y255A R	CCAGCAGTGGCAAGACTTTTTCGACCATCAT
1334 pBYL_3xFLAG_AtAGO1_Y255D F	AAAAGTCTTGACACTGCTGGTCCACTTCCC
1335 pBYL_3xFLAG_AtAGO1_Y255D R	CAGCAGTGTCAAGACTTTTTCGACCATCAT
1358 pBYL_3xFLAG_AtAGO1_S253D_Y255D F	TGATGGTCGAAAAGACCTTGACACTGCTGGTC CACTTCCC
1359 pBYL_3xFLAG_AtAGO1_S253D_Y255D R	CAAGGTCTTTTCGACCATCATACGCTGGAAG
1360 pBYL_3xFLAG_AtAGO1_S253A_Y255A F	TGGTCGAAAAGCCCTTGCCACTGCTGGTCCA CTTCCCTTT
1361 pBYL_3xFLAG_AtAGO1_S253A_Y255A R	GCAGTGGCAAGGGCTTTTCGACCATCATACG CTG
1362 pBYL_3xFLAG_AtAGO1_S253A F	ATGGTCGAAAAGCCCTTTACACTGCTGGTCCA CT
1363 pBYL_3xFLAG_AtAGO1_S253A R	GTGTAAAGGGCTTTTCGACCATCATACGCTG
1364 pBYL_3xFLAG_AtAGO1_S253D F	GATGGTCGAAAAGACCTTTACACTGCTGGTCC ACT
1365 pBYL_3xFLAG_AtAGO1_S253D R	GTAAAGGTCTTTTCGACCATCATACGCTG

Northern blot probes	**Sequence (5’ -> 3’)**
U6 probe	AGGGGCCATGCTAATCTTCTC
miR168-AS probe	TTCCCGACCTGCACCAAGCGA
miR165/166-AS probe	GGGGAATGAAGCCTGGTCCGA
miR319-AS probe	AGGGAGCTCCCTTCAGTCCAA
TAS1-siR480(+) ASRP255 -AS probe	TACGCTATGTTGGACTTAGAA

References

1. Xie, Z. et al. Expression of Arabidopsis MIRNA genes. Plant Physiol. 138, 2145–2154 (2005).
2. Zheng, B. et al. Intergenic transcription by RNA polymerase II coordinates Pol IV and Pol V in siRNA-directed transcriptional gene silencing in Arabidopsis. Genes Dev. 23, 2850–2860 (2009).
3. Park, W., Li, J., Song, R., Messing, J. & Chen, X. CARPEL FACTORY, a Dicer homolog, and HEN1, a novel protein, act in microRNA metabolism in Arabidopsis thaliana. Curr. Biol. 12, 1484–1495 (2002).
4. Reinhart, B. J., Weinstein, E. G., Rhoades, M. W., Bartel, B. & Bartel, D. P. MicroRNAs in plants. Genes Dev. 16, 1616–1626 (2002).
5. Kurihara, Y. & Watanabe, Y. Arabidopsis micro-RNA biogenesis through Dicer-like 1 protein functions. Proc. Natl. Acad. Sci. U. S. A. 101, 12753–12758 (2004).
6. Dong, Z., Han, M. H. & Fedoroff, N. The RNA-binding proteins HYL1 and SE promote accurate in vitro processing of pri-miRNA by DCL1. Proc. Natl. Acad. Sci. U. S. A. 105, 9970–9975 (2008).
7. Yu, B. et al. Methylation as a crucial step in plant microRNA biogenesis. Science 307, 932–935 (2005).
8. Baumberger, N. & Baulcombe, D. C. Arabidopsis ARGONAUTE1 is an RNA slicer that selectively recruits microRNAs and short interfering RNAs. Proc. Natl. Acad. Sci. U. S. A. 102, 11928–33 (2005).
9. Qi, Y., Denli, A. M. & Hannon, G. J. Biochemical specialization within Arabidopsis RNA silencing pathways. Mol. Cell 19, 421–428 (2005).
10. Iki, T. et al. In vitro assembly of plant RNA-induced silencing complexes facilitated by molecular chaperone HSP90. Mol. Cell 39, 282–291 (2010).
11. Llave, C., Xie, Z., Kasschau, K. D. & Carrington, J. C. Cleavage of scarecrow-like mRNA targets directed by a class of Arabidopsis miRNA. Science 297, 2053–2056 (2002).
12. Chen, X. A microRNA as a translational repressor of APETALA2 in Arabidopsis flower development. Science 303, 2022–2025 (2004).
13. Brodersen, P. et al. Widespread translational inhibition by plant miRNAs and siRNAs. Science 320, 1185–1190 (2008).
14. Mi, S. et al. Sorting of small RNAs into Arabidopsis Argonaute complexes is directed by the 5’ terminal nucleotide. Cell 133, 116–127 (2008).

15. Chen, X. Small RNAs and their roles in plant development. Annu. Rev. Cell Dev. Biol. 25, 21–44 (2009).

16. Yu, Y., Zhang, Y., Chen, X. & Chen, Y. Plant noncoding RNAs: hidden players in development and stress responses. Annu. Rev. Cell Dev. Biol. 35, 407–431 (2019).

17. Bohmert, K. et al. AGO1 defines a novel locus of Arabidopsis controlling leaf development. EMBO J. 17, 170–180 (1998).

18. Vazquez, F. et al. Endogenous trans-acting siRNAs regulate the accumulation of arabidopsis mRNAs. Mol. Cell 16, 69–79 (2004).

19. Allen, E., Xie, Z., Gustafson, A. M. & Carrington, J. C. microRNA-directed phasing during trans-acting siRNA biogenesis in plants. Cell 121, 207–221 (2005).

20. Howell, M. D. et al. Genome-wide analysis of the RNA-DEPENDENT RNA POLYMERASE6/DICER-LIKE4 pathway in Arabidopsis reveals dependency on miRNA- and tasiRNA-directed targeting. Plant Cell 19, 926–942 (2007).

21. Peragine, A., Yoshikawa, M., Wu, G., Albrecht, H. L. & Poethig, R. S. SGS3 and SGS2/SDE1/RDR6 are required for juvenile development and the production of trans-acting siRNAs in Arabidopsis. Genes Dev. 18, 2368–2379 (2004).

22. Yoshikawa, M., Peragine, A., Park, M. Y. & Poethig, R. S. A pathway for the biogenesis of trans-acting siRNAs in Arabidopsis. Genes Dev. 19, 2164–75 (2005).

23. Williams, L., Carles, C. C., Osmont, K. S. & Fletcher, J. C. A database analysis method identifies an endogenous trans-acting short-interfering RNA that targets the Arabidopsis ARF2, ARF3, and ARF4 genes. Proc. Natl. Acad. Sci. U. S. A. 102, 9703–9708 (2005).

24. Fahlgren, N. et al. Regulation of AUXIN RESPONSE FACTOR3 by TAS3 ta-siRNA affects developmental timing and patterning in Arabidopsis. Curr. Biol. 16, 939–944 (2006).

25. Hunter, C. et al. Trans-acting siRNA-mediated repression of ETTIN and ARF4 regulates heteroblasty in Arabidopsis. Development 133, 2973–2981 (2006).

26. Lingel, A., Simon, B., Izaurralde, E. & Sattler, M. Nucleic acid 3′-end recognition by the Argonaute2 PAZ domain. Nat. Struct. Mol. Biol. 11, 576–577 (2004).

27. Ma, J. B., Ye, K. & Patel, D. J. Structural basis for overhang-specific small interfering RNA recognition by the PAZ domain. Nature 429, 318–322 (2004).

28. Frank, F., Sonenberg, N. & Nagar, B. Structural basis for 5′-nucleotide base-specific recognition of guide RNA by human AGO2. Nature 465, 818–822 (2010).

29. Frank, F., Hauver, J., Sonenberg, N. & Nagar, B. Arabidopsis Argonaute MID domains use their nucleotide specificity loop to sort small RNAs. EMBO J. 31, 3588–95 (2012).

30. Song, J. J., Smith, S. K., Hannon, G. J. & Joshua-Tor, L. Crystal structure of argonaute and its implications for RISC slicer activity. Science 305, 1434–1437 (2004).

31. Liu, J. et al. Argonaute2 is the catalytic engine of mammalian RNAi. Science 305, 1437–1441 (2004).

32. Ma, J. B. et al. Structural basis for 5′ -end-specific recognition of guide RNA by the A. fulgidus Piwi protein. Nature 434, 666–670 (2005).

33. Boland, A., Huntzinger, E., Schmidt, S., Izaurralde, E. & Weichenrieder, O. Crystal structure of the MID-PIWI lobe of a eukaryotic argonaute protein. Proc. Natl. Acad. Sci. U. S. A. 108, 10466–10471 (2011).

34. Bologna, N. G. et al. Nucleo-cytosolic shuttling of ARGONAUTE1 prompts a revised model of the plant microRNA pathway. Mol. Cell 69, 709-719.e5 (2018).

35. Tsuboyama, K., Tadakuma, H. & Tomari, Y. Conformational activation of Argonaute by distinct yet coordinated actions of the Hsp70 and Hsp90 chaperone systems. Mol. Cell 70, 722–729 (2018).

36. Iwasaki, S. et al. Hsc70/Hsp90 chaperone machinery mediates ATP-dependent RISC loading of small RNA duplexes. Mol. Cell 39, 292–299 (2010).

37. Carbonell, A. et al. Functional analysis of three Arabidopsis ARGONAUTES using slicer-defective mutants. Plant Cell 24, 3613–3629 (2012).

38. Kwak, P. B. & Tomari, Y. The N domain of Argonaute drives duplex unwinding during RISC assembly. Nat. Struct. Mol. Biol. 19, 145–152 (2012).

39. Wang, Y. et al. Nucleation, propagation and cleavage of target RNAs in Ago silencing complexes. Nature 461, 754–761 (2009).

40. Champion, A., Kreis, M., Mockaitis, K., Picaud, A. & Henry, Y. Arabidopsis kinome : after the casting. Funct. Integr. Genomics 4, 163–187 (2004).

41. Lopez-Orozco, J. et al. Functional analyses of phosphorylation events in human Argonaute 2. RNA 21, 2030–2038 (2015).

42. Rüdel, S. et al. Phosphorylation of human Argonaute proteins affects small RNA binding. Nucleic Acids Res. 39, 2330–2343 (2011).

43. Golden, R. J. et al. An Argonaute phosphorylation cycle promotes microRNA-mediated silencing. Nature 542, 197–202 (2017).

44. Zeng, Y., Sankala, H., Zhang, X. & Graves, P. R. Phosphorylation of Argonaute 2 at serine-387 facilitates its localization to processing bodies. Biochem. J. 413, 429–436 (2008).

45. Quévillon Huberdeau, M. et al. Phosphorylation of Argonaute proteins affects mRNA binding and is essential for microRNA- guided gene silencing in vivo. EMBO J. 36, 2088–2106 (2017).

46. Horman, S. R. et al. Akt-mediated phosphorylation of argonaute 2 downregulates cleavage and upregulates translational repression of MicroRNA targets. Mol. Cell 50, 356–367 (2013).

47. Li, Z. et al. Origin, evolution and diversification of plant ARGONAUTE proteins. Plant J. 1–12 (2021). doi:10.1111/tpj.15615

48. Schirle, N. T., Sheu-Gruttadauria, J. & MacRae, I. J. Structural basis for microRNA targeting. Science 346, 608–613 (2014).

49. Arribas-Hernández, L., Kielpinski, L. J. & Brodersen, P. mRNA decay of most Arabidopsis miRNA targets requires slicer activity of AGO1. Plant Physiol. 171, 2620–2632 (2016).

50. Vaucheret, H., Vazquez, F., Crété, P. & Bartel, D. P. The action of ARGONAUTE1 in the miRNA pathway and its regulation by the miRNA pathway are crucial for plant development. Genes Dev. 18, 1187–1197 (2004).

51. Li, S. et al. Biogenesis of phased siRNAS on membrane-bound polysomes in Arabidopsis. Elife 5, e22750 (2016).

52. Tang, X. et al. MicroRNA-mediated repression of the seed maturation program during vegetative development in Arabidopsis. PLoS Genet. 8, 20–22 (2012).

53. Morel, J. B. et al. Fertile hypomorphic ARGONAUTE (ago1) mutants impaired in post-transcriptional gene silencing and virus resistance. Plant Cell 14, 629–639 (2002).

54. Dai, X., Zhuang, Z. & Zhao, P. X. PsRNATarget: A plant small RNA target analysis server (2017 release). Nucleic Acids Res. 46, W49–W54 (2018).

55. Dephoure, N., Gould, K. L., Gygi, S. P., Kellogg, D. R. & Drubin, D. G. Mapping and analysis of phosphorylation sites : a quick guide for cell biologists. Mol. Biol. Cell 24, 535–542 (2013).

56. Schirle, N. T. & MacRae, I. J. The crystal structure of Human Argonaute2. Science 336, 1037–1040 (2012).

57. Nakanishi, K., Weinberg, D. E., Bartel, D. P. & Patel, D. J. Structure of yeast Argonaute with guide RNA. Nature 486, 368–374 (2012).

58. Elkayam, E. et al. The structure of human argonaute-2 in complex with miR-20a. Cell 150, 100–110 (2012).

59. Yu, B., Pletka, C. C. & Iwahara, J. NMR observation of intermolecular hydrogen bonds between protein Tyrosine side-chain OH and DNA phosphate groups. J. Phys. Chem. B 124, 1065–1070 (2020).

60. Li, S. et al. MicroRNAs inhibit the translation of target mRNAs on the endoplasmic reticulum in Arabidopsis. Cell 153, 562–574 (2013).

61. Nakamura, S. et al. Gateway binary vectors with the bialaphos resistance gene, bar, as a selection marker for plant transformation. Biosci. Biotechnol. Biochem. 74, 1315–1319 (2010).

62. Earley, K. W. et al. Gateway-compatible vectors for plant functional genomics and proteomics. Plant J. 45, 616–629 (2006).

63. Clough, S. J. & Bent, A. F. Floral dip : a simplified method for Agrobacterium-mediated transformation of Arabidopsis thaliana. Plant J. 16, 735–743 (1998).

64. Kurihara, Y., Takashi, Y. & Watanabe, Y. The interaction between DCL1 and HYL1 is important for efficient and precise processing of pri-miRNA in plant microRNA biogenesis. RNA 12, 206–212 (2006).

65. Craig, R. & Beavis, R. C. TANDEM : matching proteins with tandem mass spectra. Bioinformatics 20, 1466–1467 (2004).

66. Craig, R., Cortens, J. P. & Beavis, R. C. Open source system for analyzing, validating, and storing protein identification data. J. Proteome Res. 3, 1234–1242 (2004).

67. Beavis, R. C. Using the global proteome machine for protein identification. Methods Mol. Biol. 328, 217–228 (2006).

68. Martin, M. Cutadapt removes adapter sequences from high-throughput sequencing reads. EMBnet.journal 17, 10 (2011).

69. Johnson, N. R., Yeoh, J. M., Coruh, C. & Axtell, M. J. Improved placement of multi-mapping small RNAs. G3 Genes, Genomes, Genet. 6, 2103–2111 (2016).

70. Love, M. I., Huber, W. & Anders, S. Moderated estimation of fold change and dispersion for RNA-seq data with DESeq2. Genome Biol. 15, (2014).

71. Arribas-Hernández, L. et al. The slicer activity of ARGONAUTE1 is required specifically for the phasing, not production, of trans-acting short interfering RNAs in Arabidopsis. Plant Cell 28, 1563–1580 (2016).

72. Dobin, A. et al. STAR: Ultrafast universal RNA-seq aligner. Bioinformatics 29, 15–21 (2013).

73. Liao, Y., Smyth, G. K. & Shi, W. FeatureCounts: An efficient general purpose program for assigning sequence reads to genomic features. Bioinformatics 30, 923–930 (2014).

74. Edgar, R. C. MUSCLE : a multiple sequence alignment method with reduced time and space complexity. BMC Bioinformatics 5, (2004).

75. Fan, L. et al. Microtubules promote the non-cell autonomy of MicroRNAs by inhibiting their cytoplasmic loading into ARGONAUTE1 in Arabidopsis. bioRxiv (2021).

76. Wang, W. et al. An importin beta protein negatively regulates microRNA activity in Arabidopsis. Plant Cell 23, 3565–3576 (2011).

77. Kathleen Martin et al. Transient expression in Nicotiana benthamiana fluorescent marker lines provides enhanced definition of protein localization, movement and interactions in planta. Plant J. 59, 150–162 (2009).

78. Endo, Y., Iwakawa, H. O. & Tomari, Y. Arabidopsis ARGONAUTE7 selects miR390 through multiple checkpoints during RISC assembly. EMBO Rep. 14, 652–658 (2013).

79. Tomari, Y., Iwakawa, H. & Carbonell, A. In vitro analysis of ARGONAUTE-mediated target cleavage and translational repression in plants. Methods Mol. Biol. 1640, 55–71 (2017).

Conclusions and Perspectives

microRNA (miRNA)-mediated gene silencing requires the association between miRNA and an ARGUNAUTE (AGO) protein to form a miRNA-induced silencing complex, or miRISC. The formation of miRISC entails two major steps: first the miRNA/miRNA* duplex is loaded into an AGO protein, then the AGO unwinds the duplex and selectively retains one strand (guide strand or miRNA), which guides AGOs to target genes, whereas the other strand (passenger strand or miRNA*) is ejected[1]. In plants, the majority of miRNAs preferentially associate with AGO1[2]. Previous studies have reported that the assembly of AGO1 miRISC is facilitated by the molecular chaperone HEAT SHOCK PROTEIN 90 (HSP90) and the importin-beta family protein TRANSPORTIN 1 (TRN1), while negatively regulated by another importin-beta family protein ENHANCED MIRNA ACTIVITY 1 (EMA1)[3–6]. A study on AGO1 with the nuclear export signal (NES) mutated hinted that miRNA loading into AGO1 takes place in the nucleus[7]. In my dissertation research, I seek to understand detailed mechanisms that regulate AGO1-miRISC formation in plants. Two novel mechanisms that regulate this process and beyond were identified and reported in chapters two and three. In chapter two, we reported that the N-terminal extension (NTE) region of Arabidopsis AGO1 is essential for miRNA association. As the NTE region is highly conserved in plant AGO1s, but not other plant AGOs or animal AGOs, this mechanism may be unique to plant AGO1s. However, the broader implication is that the NTEs of other plant AGOs or animal AGOs assist in RISC formation through interactions with similar

chaperones using structural features that maybe conserved with plant AGO1, or assist in other processes such as the nuclear-cytoplasmic partitioning of AGOs or target gene regulation. In chapter three, we showed that phosphorylation and de-phosphorylation of AGO1 at Y255 regulates its miRNA loading and target repression activities, respectively. As AGO1 Y255 is not only conserved in many plant AGO1s but also in animal AGO proteins, such as human AGO2, drosophila AGO1, and mouse AGO2, phosphorylation/dephosphorylation at this residue could regulate miRISC formation and target repression in other species.

In chapter two, we showed that the NTE (a.a. 1-189) region of Arabidopsis AGO1, particularly a.a. 91-189, is essential for rescuing the developmental phenotype of an *ago1* null allele. Through global analyses of AGO1-associated small RNAs, we showed that a.a. 91-189 of AGO1 are required for the association with miRNAs and trans-acting small interfering RNAs (ta-siRNAs), and thus critical for miRNA- and ta-siRNA- mediated gene silencing. Furthermore, we showed that a.a. 91-189 of AGO1 regulate miRNA loading independently of a role in the nuclear-cytoplasmic shuttling of AGO1. 91-to-189 of AGO1 may affect protein-protein interactions, such as between AGO1 and HSP90 and TRN1, which should be tested in the future. On the other hand, a.a. 1-90 of AGO1 are dispensable for rescuing the developmental defects of an *ago1* null allele or for miRNA and ta-siRNA loading, however, we found it can facilitate target repression and ta-siRNA biogenesis. We further showed that the a.a. 1-90 and a.a. 91-189 regions of the NTE redundantly promote the activities of AGO1 in the biogenesis of ta-siRNAs.

Some of our findings were unexpected, and we discuss the implications below. miRNAs are nearly depleted in the AGO1 mutant with the truncation of a.a. 91-189, but ta-siRNA biogenesis is unaffected in this mutant. This surprising result led us to suspect that only a small amount of AGO1-miR173 is required to trigger the biogenesis of ta-siRNAs. Another surprising finding is that the truncation of a.a. 91-189 does not affect the nuclear-cytoplasmic partitioning of AGO1 while mutation of the NES (a.a. 149-158) results in exclusive nuclear localization of the protein[7]. This implies that, besides the previously reported NLS (a.a. 2-6), there must be other NLSs or mechanisms directing AGO1's nucleus importation. We predicted a new NLS (a.a. 102-111) residing in the NTE region, and the function of this potential NLS should be tested in the future. The subcellular locations of AGO1 RISC formation pertain to the non-cell autonomous activities of miRNAs and remain to be better understood[8,9]. To test whether miRNA loading into AGO1 occurs exclusively in the nucleus or the cytoplasm, or in both locations, AGO1 mutants that reside in the nucleus only and cytoplasm only are required. Further studies to test the nuclear-cytoplasmic partitioning of AGO1 mutated in both NLSs (a.a. 2-6 and a.a.102-111) might lead to a cytoplasmic-only AGO1 mutant and help answer the question of where miRNA loading happens. The 10 Arabidopsis AGO family members contain NTEs with various lengths and variable sequences, suggesting that the NTEs of AGOs might provide AGO-specific functions. Future studies to investigate the functions of the NTEs of other AGOs could reveal unknown regulatory mechanisms.

In chapter three, we reported that Arabidopsis AGO1 is phosphorylated at multiple amino acids *in vivo*, and the phosphorylation status of the tyrosine residue Y255, which resides in the functionally less understood N domain, impacts RISC assembly and RISC activity. *In vivo* profiling of small RNA association and *in vitro* RISC formation assays showed that phospho-mimetic AGO1 is defective in the loading of both miRNA and siRNA duplexes and in passenger strand ejection of siRNA but not miRNA duplexes. In contrast, non-phosphorylatable AGO1 is largely normal in miRISC and siRISC formation but is compromised in target RNA repression. Together, these findings indicate that phosphorylation and dephosphorylation of AGO1 at Y255 regulate the efficiency of RISC formation and RISC activities. The phosphorylation of AGO1 could affect the motion of the N domain thus preventing small RNA loading and unwinding. Our current understanding of Arabidopsis AGO1 structure is mainly based on structural modeling using human AGO2 and bacterial AGOs as guides, however, their preference towards small RNAs and their activities in target regulation are distinct from AGO1. Future studies to unveil the structure of plant AGO1 and AGO1 with different phosphorylation stature are necessary. In addition to Y255, we also identified three other phosphorylation sites on AGO1. However, a non-phosphorylatable mutation on any of the three sites does not cause development phenotypes under normal growth conditions. As plant AGO1 is also essential for antiviral immunity[10], future studies could test whether phosphorylation on these sites affects plant immunity. Fourteen-day-old Arabidopsis seedlings were used to

detect the phosphorylation of AGO1 in this study, whether phosphorylation/ dephosphorylation of AGO1 only takes place at certain developmental stages or only in certain tissues or subcellular compartments should be further investigated.

References

1. Baumberger, N. & Baulcombe, D. C. Arabidopsis ARGONAUTE1 is an RNA slicer that selectively recruits microRNAs and short interfering RNAs. Proc. Natl. Acad. Sci. U. S. A. 102, 11928–33 (2005).
2. Mi, S. et al. Sorting of small RNAs into Arabidopsis Argonaute complexes is directed by the 5' terminal nucleotide. Cell 133, 116–127 (2008).
3. Iki, T. et al. In vitro assembly of plant RNA-induced silencing complexes facilitated by molecular chaperone HSP90. Mol. Cell 39, 282–291 (2010).
4. Iwasaki, S. et al. Hsc70/Hsp90 chaperone machinery mediates ATP-dependent RISC loading of small RNA duplexes. Mol. Cell 39, 292–299 (2010).
5. Wang, W. et al. An importin beta protein negatively regulates microRNA activity in Arabidopsis. Plant Cell 23, 3565–3576 (2011).
6. Cui, Y., Fang, X. & Qi, Y. TRANSPORTIN1 promotes the association of microRNA with ARGONAUTE1 in Arabidopsis. Plant Cell 28, 2576–2585 (2016).
7. Bologna, N. G. et al. Nucleo-cytosolic shuttling of ARGONAUTE1 prompts a revised model of the plant microRNA pathway. Mol. Cell 69, 709-719.e5 (2018).
8. Brioudes, F. et al. HASTY, the Arabidopsis EXPORTIN5 ortholog, regulates cell-to-cell and vascular microRNA movement. EMBO J. 1–22 (2021). doi:10.15252/embj.2020107455
9. Fan, L. et al. Microtubules promote the non-cell autonomy of MicroRNAs by inhibiting their cytoplasmic loading into ARGONAUTE1 in Arabidopsis. bioRxiv (2021).
10. Morel, J. B. et al. Fertile hypomorphic ARGONAUTE (ago1) mutants impaired in post-transcriptional gene silencing and virus resistance. Plant Cell 14, 629–639 (2002).